An Anion Pathway in the Sarcoplasmic Reticulum of Skeletal Muscle

TREVOR M. LEWIS

Thesis submitted for the degree of
Doctor of Philosophy
in
The University of Adelaide
(Faculty of Science)

Department of Physiology

December 1993

Dedicated to the memory of my grandfather,
Phillip Alfred Lewis,
(1897-1989)
who would have been proud.

CONTENTS

PART I.
PATCH CLAMP STUDIES OF THE ANION CHANNEL IN SARCOBALLS

2. PREPARATION OF SARCOBALLS

3. ELEMENTARY PROPERTIES

4. KINETIC ANALYSIS

PART II.
STRUCTURE AND COMPOSITION OF SARCOBALLS

5. GLIMPSES OF SARCOBALL STRUCTURE

6. ANTIBODY LABELLING OF MEMBRANES

PART III.
GENERAL DISCUSSION

7. A FAMILY OF HIGH CONDUCTANCE ANION CHANNELS

SUMMARY

Since identifying the sarcoplasmic reticulum (SR) as both the source and sink for the Ca^{2+} which activates a muscle contraction, the Ca^{2+} conductance of this membrane has been the prime subject of study. As new techniques were developed, further characteristics of the Ca^{2+} conductance and transport system could be investigated. However, even from the early work with radio-isotope flux or osmotic swelling measurements, other accompanying conductances were identified. Both an anion and a cation conductance were found and were proposed as necessary "counter-ion" pathways to balance the movement of Ca^{2+} across the sarcoplasmic reticulum. While the counter-cation conductance, a K^+ channel, has been well investigated, it has not been until more recent times that the secrets of the counter-anion conductance have been explored at a single channel level. This study contributes to the further characterisation of the SR anion channel.

The close association of the SR with the myofilaments has meant that SR has generally been isolated as vesicles for study. The sarcoball technique provided a novel opportunity to gain direct access to what was proposed to be mainly SR membrane. With the sarcoball technique, the sarcolemma of single skeletal muscle fibres is mechanically peeled away, leaving the internal membranes, which are extruded to the surface of the skinned fibre during a contraction of the myofibrils. Hemispherical blebs form at the surface which are able to be patch clamped. Previous studies with this preparation investigated a Ca^{2+} channel which, on the basis its pharmacological behaviour, was identified as the Ca^{2+}

release channel of the SR. This was evidence that the preparation contained SR, although the presence of other internal membranes could not be excluded. A large conductance anion channel was also found in this preparation and it has been substantially investigated by Hals et al. (1989, 1990).

A significant characteristic of this channel is that in symmetrical ionic conditions, the channel exhibits a high open probability centred on 0 mV and closes at small positive or negative potentials. This steep, bell-shaped voltage dependence raised two issues which were addressed during the present study; (i) what is the kinetic basis for this bell-shaped voltage dependence, and (ii) the possibility that the anion channel was in fact the voltage dependent anion channel (VDAC) from mitochondrial outer membrane and that differences between the behaviour seen in the earlier bilayer studies compared to sarcoballs could be due to isolation or membrane effects.

As a modification of the original technique was required to form sarcoballs easily from skeletal muscle fibres of *Bufo marinus*, the elementary properties of the channel were studied briefly to identify that the same channel was being observed in this preparation compared with Hals et al. (1989). Patch clamping of excised sarcoball membrane identified an anion channel with conductance properties and a voltage dependence very similar to that previously reported. A number of subconductance states are also a part of the channel behaviour.

Using a combination of steady-state and non-stationary kinetic analysis methods, the underlying mechanism of the voltage dependent gating was investigated. The prevalence of multi-channel patches and the voltage-dependence of the channel meant that non-stationary analysis was more suitable. Non-stationary analysis suggested a separate closed state for positive and negative potentials, and that movement between these two closed states was mainly via open states. In the steady state analysis carried out on the few patch clamp recordings containing a single channel, dwell times indicated at least three open states and three closed states. Autocorrelation analysis of the open and closed durations revealed at least three entry/exit pathways between the open and closed aggregates. Three

kinetic schemes are proposed, each with three open and three closed states. By appropriate placement of voltage-dependent and voltage-independent rate constants, and taking account of the kinetic restrictions, each of these schemes successfully predict a bell-shaped voltage-dependence.

Electron microscopy was utilised to investigate the structure and membrane content of the sarcoball preparation from *Bufo marinus* and *Xenopus laevis*. Observations indicated that vesiculated internal membranes are extruded from within the spaces between the bundles of myofilaments to the surface of the skinned fibre. At the surface, the internal structure of the extruded sarcoball was most reminiscent of a foam-like structure. Other features of the structure strongly suggested that mitochondrial and T-tubule membrane may be contributing to the structure. Immunogold labelling with specific antibodies was used to identify some of the membranes within the structure. The predominance of SR membrane, which was previously suspected, was confirmed by specific labelling with an antibody to the Ca^{2+}/Mg^{2+}-ATPase and separately with an antibody to the ryanodine receptor/Ca^{2+} release channel complex. An antibody to the voltage dependent anion channel (VDAC) of mitochondrial outer membrane labelled membrane structures of sarcoballs, but was also found to label the SR *in situ* within the myofibrils. This important result suggests a protein present in the SR which is identified by the VDAC antibody.

The anion channel investigated here is most likely to originate from the SR membrane. It is one of a growing number of large conductance anion channels which exhibit a bell-shaped voltage dependence. From protein sequence analysis and immunogenic identity, there is evidence that VDAC-like channels are present in a variety of different membranes, and this study contributes new evidence to include the SR in this family. The present study also contributes a new understanding of the voltage-dependent kinetics of the SR anion channel. In the future, this knowledge should help in understanding the role this anion channel may play in the regulation of Ca^{2+} release and uptake by the SR.

ABBREVIATIONS AND GLOSSARY

Constants

F	Faraday's constant; 9.648×10^4 C mol^{-1}
k	Boltzmann's constant; 1.381×10^{-23} V C K^{-1}
R	gas constant; 8.314 V C K^{-1} mol^{-1}
T	absolute temperature

Planar bilayer systems

cis	By definition, *cis* is the side of planar bilayer recording systems to which the vesicles or solubilised protein was added to fuse with the membrane. It is also the side of the bilayer on which the membrane potential is specified, relative to the *trans* side.
trans	Describes the side of the membrane opposite the *cis* side in planar bilayer recording systems.

Abbreviations

4-AP	4-Aminopyridine
A-9-C	Anthracene-9-carboxylic acid
a.c.f.	autocorrelation function
ACh	Acetylcholine
APb	Alkaline Protease b, a serine protease specific for arginine and lysine residues.
BZD	Benzodiazepine
cDNA	Complimentary deoxyribonucleic acid. Produced by using messenger ribonucleic acid (mRNA) as a template.
DIDS	4,4'-Diisothiocyano-stilbene 2,2'-disulfonic acid
$GABA_A$	γ-Aminobutyric acid receptor protein type A
I-V	Current-voltage relation
MOPS	3-Morpholino-propanesulfonic acid
NK1	Neurokinin 1
NMDA	N-Methyl-D-aspartate
p.a.c.f.	partial autocorrelation function

p.d.f.	probability density function
PBS	Phosphate buffered saline
PVP	Polyvinylpyrrolidone
SIF	Synthetic interstitial fluid
SITS	4-Acetamido, 4'-isothiocyano-stilbene 2,2'-disulfonic acid
SPIT	3-Sulfophenyl isothiocyanate
SR	Sarcoplasmic reticulum
TES	N-Tris(hydroxymethyl)-methyl-2-aminoethane-sulphonic acid
TNBS	Trinitrobenzene sulfonic acid
TrisCl	Tris-hydroxymethyl-aminomethane hydrochloride
VDAC	Voltage-dependent anion-selective channel from mitochondrial outer membrane

PUBLICATIONS

Refereed publication

LEWIS, T.M., A.F. DULHUNTY, P.R. JUNANKAR, AND C. STANHOPE (1992) The ultrastructure of sarcoballs on the surface of skinned amphibian skeletal muscle fibres. *Journal of Muscle Research and Cell Motility* **13**, 640-653.

Abstracts presented at conferences

LEWIS, T.M., M.L. ROBERTS AND A.H. BRETAG (1992) Kinetic analysis of a high conductance, voltage dependent anion channel from the sarcoplasmic reticulum of amphibian skeletal muscle. *Proceedings of the Australian Physiological and Pharmacological Society* **24(2)**, 142P

LEWIS, T.M., M.L. ROBERTS AND A.H. BRETAG (1992) Is the SR anion channel a member of the VDAC family? *Proceedings of the Australian Physiological and Pharmacological Society* **23(2)**, 203P

LEWIS, T.M., A.F. DULHUNTY, P.R. JUNANKAR, AND C. STANHOPE (1991) Ultrastructure and membrane content of sarcoballs. *Proceedings of the Australian Physiological and Pharmacological Society* **22(2)**, 161P

LEWIS, T.M. AND A.H. BRETAG (1991) A large conductance anion channel in a sarcoplasmic reticulum preparation from the semitendinosus muscle of the cane toad. *Proceedings of the Australian Physiological and Pharmacological Society* **22(1)**, 19P

DECLARATION

This work contains no material which has been accepted for the award of any other degree or diploma in any university or other tertiary institution and, to the best of my knowledge and belief, contains no material previously published or written by another person, except were due reference has been made in the text.

I give consent to this copy of my thesis, when deposited in the University Library, being available for loan and photocopying.

DATE: 17 December 1993

ACKNOWLEDGEMENTS

During this study, I was a recipient of an Australian Postgraduate Research Award from January 1989 to August 1992.

I wish to acknowledge the guidance and support of my supervisors Associate Professor Allan Bretag and Dr Michael Roberts. They provided an environment to broaden my thinking and to develop my skills.

Thanks to Dr Greg Pike who provided a valuable sounding board and could always bring a smile to my face to maintain my sanity. Very special thanks to Kimberley McPherson for the friendship we shared as students in the same laboratory. I wish to thank Stan Flavel and Greg Powell for their technical assistance from time to time. Particular thanks to David Bryant for continuing technical assistance and support, and to Ruth Woodland for administrative support and friendship. Additional thanks to Janet Fewsdale and Loreen Treloar for administrative support; to the laboratory manager Graham Langsford and to Brian Purdell from the Medical School Workshop, for provision of material support during my candidature.

I wish to thank Dr Angela Dulhunty, Muscle Research Group, John Curtin School of Medical Research, for a continuing interest in my work and for the opportunity to go to Canberra and learn the post-embedding antibody-labelling technique as well as use of the D12 antibody to the SR Ca^{2+}/Mg^{2+}-ATPase. Thanks also to Dr Pauline Junankar for spirited discussions and for the opportunity of labelling sarcoballs with the junctional ryanodine receptor protein antibody. Particular thanks to the technical support from Caroline Stanhope for training me in the antibody labelling technique. General thanks to the John Curtin School of Medical Research electron microscopy centre staff for expert assistance and photography.

Thanks to Dr Derek Laver, also of the Muscle Research Group, John Curtin School of Medical Research, for his valuable assistance in "talking kinetics" and for the use of the EVPROC software which he developed. Additional thanks to Dr Steve Tyerman, School of Biological Sciences, Flinders University of S.A., for contributing to my understanding of kinetic analysis.

I gratefully acknowledge the assistance of the staff of the Centre for Electron Microscopy and Microstructural Analysis (CEMMSA) at The University of Adelaide, and in particular Dr Marilyn Henderson for advice on immunolabelling, Debbie Smith for expertly sectioning the material and Ken Crocker for training and technical assistance on the electron microscopes. Additional thanks to Dr John Power for helpful discussions on appropriate methods; Chris Leigh, Department of Anatomy, for sectioning material, discussions on methods and assistance with photography; Dale Caville,

Department of Pathology, for assistance with the production of photographic prints.

Thanks to the Muscular Dystrophy Association of South Australia for generous financial support on a number of occasions, making it possible to attend conferences to present my work and to travel to Canberra to complete work at the John Curtin School of Medical Research. Without this support much of the work would not have been possible.

Finally, to my parents Rosalie and Murray, my brother Christopher, sister Vicki and brother-in-law Bernard who were right behind me all the way, and to Beverley Veasey who stood beside me at the end.

1. INTRODUCTION

Although the anion conductance of the sarcoplasmic reticulum (SR) has been recognised for some time, it has attracted less attention than the cation conductances. Whereas the Ca^{2+} release channel and, to a lesser extent, the K^+ channel have been well characterised even at the single channel level, this has been lacking for the anion conductance. What is becoming apparent, is that an integrated view of the SR function and processes is not possible without an understanding of the contribution the anion conductance makes to the system. It has previously been assumed that the anion conductance plays a role in balancing the Ca^{2+} fluxes across the SR. There is inconsistent evidence for this role, however, and it has yet to be functionally demonstrated. The recent renewed interest in the SR anion conductance is providing a fundamental understanding at the single channel level which will hopefully allow these issues to be addressed.

1.1 Historical perspective of sarcoplasmic reticulum function

Skeletal muscle has attracted a vast array of physiological and biochemical approaches to investigate the contraction process. The SR has been shown to be an essential element in this, though to begin with, the only clue in the puzzle had been something much simpler: the regular striations of muscle fibres. The regular repeating units (sarcomeres) of actin and myosin filaments which are longitudinally arranged in a hexagonal array, have been established as the physical structures responsible for contraction. The sliding filament theory

proposed independently by both A.F. Huxley and Niedergerke (1954) and by H.E. Huxley and Hanson (1954) describes the arrangement of the myosin and actin filaments, such that they move past each other within each sarcomere, to produce the muscular contraction. The generation of contractile force is now known to be due to the formation and cycling of cross-bridges between the myosin heads and the actin filaments (for a review see Ashley et al., 1991), though the exact nature of the molecular mechanism is still not clear (Rayment et al., 1993a, b). Actomyosin cross-bridge cycling is dependent upon ATP and is triggered by a rapid rise in myoplasmic Ca^{2+} levels. Calcium binds to troponin and removes the inhibition which, in the absence of Ca^{2+}, the troponin-tropomyosin complex has upon the formation of cross-bridges between actin and myosin.

This mediating role of Ca^{2+} in the contraction process was recognised at an early stage in the history of muscle, thought not without controversy. Isolated contractile proteins and "thoroughly dead" muscle both contract upon exposure to KCl (Szent-Györgyi, 1949), as do intact muscle fibres. When injected directly into the interior of a muscle fibre, however, KCl did not produce a contraction and neither did NaCl. (Heilbrunn & Wiercinski, 1947). Yet, when $CaCl_2$ was injected, a contraction was produced. Calcium was known to be present in the myoplasm and was known to be involved in blood clotting. In an imaginative step, contraction was compared to clotting of proteins (Heilbrunn & Wiercinski, 1947). It was also recognised that a substance applied to the exterior of a muscle fibre to produce a contraction might not be the same substance having the effect upon the interior. After all, Ca^{2+} applied externally to a skeletal muscle fibre did not produce a contraction. Instead, it was proposed that a stimulus applied to the outside would cause release of Ca^{2+} at the surface or outer region of the cell which would then enter the myoplasm to produce the contraction. The calculations of A. V. Hill (1948, 1949), however, demonstrated that the time required for any mediator of the contraction to enter the cell and sufficiently

penetrate the myoplasm by diffusion alone is far greater than the time taken to reach maximal twitch tension.

This was reconciled by Huxley and Taylor (1958) with their perceptive interpretation of the localised contractions which were dramatically demonstrated in skeletal muscle. By applying a small depolarising current to the surface membrane with a pipette in register with a Z-line of the myofilaments in frog skeletal muscle, a contraction was produced which was confined to the corresponding I-band. If the pipette was shifted to other sites within the same sarcomere, no contraction was observed. With crab muscle, however, the sensitive sites were in register with the A-I boundary of the myofilaments. Structural information from electron microscopy on the internal membranes of muscle fibres was emerging at about the same time (Porter & Palade, 1957), which described the "triad" arrangement of transverse tubules (T-tubules) with lateral membrane sacs, at the time collectively termed "sarcoplasmic reticulum". These triads were identified at the level of the Z-line in amphibian muscle and at each of the A-I boundaries in mammalian muscle. Huxley and Taylor (1958) recognised that these triads corresponded with the sensitive sites capable of producing local contractions in amphibian muscle, and inspired by mammalian muscle, investigated the location of triads in crab muscle which proved to be at the A-I boundaries where the sensitive sites were. Thus, they proposed that the T-tubules conducted the surface membrane depolarisation into the fibre interior, therefore circumventing the problem of diffusion posed by A. V. Hill (1948, 1949). At the time, it still hadn't been shown that the T-tubules were continuous with the surface membrane, and neither had the function of the SR been identified, although the stage had now been set for the investigation of these structures in the coupling of excitation at the surface membrane to contraction of the myofibrils.

The relationship between the SR and Ca^{2+} began with the description of a "relaxing factor", extracted from muscle, having the ability to dissociate the actin-

myosin complex in the presence of ATP (Marsh, 1951, 1952). The microsomal fraction containing the "relaxing factor" was found to consist of membrane vesicles. These membrane vesicles, thought to originate from the SR, possessed a Mg^{2+}-dependent ATPase activity capable of accumulating Ca^{2+} from the surrounding medium (Ebashi, 1961; Ebashi & Lipmann, 1962).

The accumulation of Ca^{2+} by SR vesicles was found to be enhanced in the presence of anions such as orthophosphate, pyrophosphate, oxalate and fluoride (Hasselbach, 1964). It was proposed that SR vesicles were permeable to these anions, which would precipitate Ca^{2+} inside the vesicles and greatly increase the capacity for further accumulation of Ca^{2+} (De Meis et al., 1974). This suggested that the Ca^{2+}/Mg^{2+}-ATPase activity was regulated by free Ca^{2+} levels in the SR lumen (Inesi & de Meis, 1989), but did little more than emphasise the presence of the anion permeability.

Subsequently, the SR Ca^{2+}/Mg^{2+}-ATPase protein was isolated (MacLennan, 1970) and successfully reconstituted into membranes (Racker, 1972) with Ca^{2+} accumulating behaviour. The energetic characteristics and mechanism of Ca^{2+} translocation by this protein have been extensively investigated (see reviews by Tada et al., 1978; Jencks, 1989). The isolation of the protein lead to probing its structure and sequencing (Allen, 1980a, b; Allen et al., 1980a, b). From the cDNA sequence, the complete primary sequence of the protein has been deduced, with predictions of secondary and tertiary structures (MacLennan et al., 1985). At this molecular level, the ATP binding site in a domain on the cytoplasmic surface and a high affinity Ca^{2+} binding site in a predicted transmembrane domain have been identified (Clarke et al., 1989).

At about the same time as the initial findings of Ca^{2+}/Mg^{2+}-ATPase activity, it was also established that the Ca^{2+} which elicited a physiological muscle contraction was released from the SR (Hasselbach, 1964; Sandow, 1965). The autoradiographic studies of Winegrad (1965, 1968, 1970) provided evidence that

the Ca^{2+} was primarily released from the terminal cisternae of the SR. The relationship between structure and function was beginning to be neatly unfolded. Close apposition of the T-tubules and terminal cisternae of the SR excited imaginations about the link between surface membrane depolarisation and release of Ca^{2+} for contraction.

How Ca^{2+} release could be brought about was investigated in SR vesicles and skinned fibres (described below) using a wide range of agents (reviewed by Endo, 1977). Physiological agents such as Ca^{2+} and ATP triggered release, while Mg^{2+} reduced the release. Other useful agents included caffeine which elicited a maximal release, ruthenium red which blocked the release and ryanodine which was found to produce a sustained contracture in intact fibres.

This descriptive profile of the Ca^{2+} release process, while useful in identifying the characteristics, is incapable of shedding light on the mechanism. A clue to the mechanism was provided by the rapid rate of Ca^{2+} release, which could only be reconciled as a free diffusion pathway; it was too fast to be an active transport mechanism. So it was logical to go looking for a Ca^{2+} channel in the SR membrane. Incorporation of SR membrane into planar bilayers provided the best opportunity to look for the Ca^{2+} channel and indeed it was found (Smith et al., 1985). The channel was identified by the same descriptive profile of the agents that modify Ca^{2+} release in intact SR. Since then, the biophysical characterisation of the Ca^{2+} release channel has been very successful, and has been taken to yet another level of understanding with the isolation and purification of the channel protein (Inui et al., 1987). The purified protein was identified by its ability to bind ryanodine and by characteristic Ca^{2+} channel behaviour when the protein was reconstituted into planar bilayers (Hymel et al., 1988; Lai et al., 1988). Electron microscopy of the purified protein (Lai et al., 1988; Liu et al., 1989) indicated that this was the "foot protein", previously observed by others to occur in the gap between the T-tubule and the SR (Ferguson et al., 1984). The three

dimensional architecture of the protein is described as a quatrefoil structure (Wagenknecht et al., 1989). Having isolated the protein, partial sequencing and subsequent probing of a cDNA library has lead to determination of the complete amino acid sequence of the Ca^{2+} release channel (Takeshima et al., 1989).

Despite this intense attack, understanding the process by which electrical events on the surface membrane result in the release of Ca^{2+} from the SR remains incomplete (reviewed by Dulhunty, 1992). Perhaps the most fundamental reason for this situation is the inaccessibility of the SR membrane to studies which could immediately provide information of the events that occur during Ca^{2+} release. If only the *in situ* SR membrane could be voltage clamped, then the ionic basis for the conductance of the membrane and the influence of T-tubule depolarisation upon these conductances could be determined. This would take us much closer towards an understanding of excitation-contraction coupling. Unfortunately, the small dimensions of the SR have meant that direct measurements of the SR membrane electrical conductances have not been possible.

1.2 Principles of counter-ion currents

With the SR established as the membrane compartment responsible for the uptake and release of Ca^{2+}, the majority of research on SR has focused on the mechanisms by which these processes occur. The Ca^{2+} permeability of the SR membrane changes with the physiological state of the muscle fibre during contraction and relaxation. At rest, the SR is relatively impermeable to Ca^{2+}, but upon the appropriate physiological signal, there is a rapid increase in permeability for the release of Ca^{2+} to trigger the contraction (Endo, 1977). Regulation of the amount of Ca^{2+} released from the SR is an important factor in regulating the force of contraction.

For the required Ca^{2+} fluxes across the SR membrane to occur, it has been generally speculated that there is a passive counter-flux of cations or,

equivalently, a co-flux of anions to balance the movement of Ca^{2+}. This is well illustrated by the calculations of Oetliker (1982), which show that if the efflux of Ca^{2+} from the SR during a single muscle twitch was to occur without any compensating ion movements, the Ca^{2+} equilibrium potential would be reached after only 4.5% of the required Ca^{2+} (210 nmol Ca^{2+} per gram muscle; Endo, 1977) had been released. At the equilibrium potential, the driving force for Ca^{2+} is zero and no further release of Ca^{2+} would occur. It has also been suggested that these counter-ion movements may not be a simple electrical shunt to balance Ca^{2+}, but may be more active in influencing the development of any potential across the SR membrane with the Ca^{2+} release (Hals et al., 1989). In this way, by controlling the developing membrane potential, the release of Ca^{2+} can be regulated and consequently the contraction is regulated. Consideration must also be given to the nature of balancing ion movements which must occur during re-uptake of Ca^{2+} by the Ca^{2+}/Mg^{2+}-ATPase in the SR.

An additional aspect to be considered is the change in osmolarity which may occur with the efflux of Ca^{2+} from the SR. A redistribution of anions across the SR membrane might occur to re-establish the Donnan equilibrium, once the Ca^{2+} has been released from the SR, leaving behind the large anionic binding proteins. These binding proteins may well be protonated as Ca^{2+} leaves, as there is an alkalinization of the myoplasm associated with the release of Ca^{2+} which is thought to be due to protons moving into the SR (Hollingworth & Baylor, 1990; Pape et al., 1990). Conversely, the re-uptake of Ca^{2+} by the SR Ca^{2+}/Mg^{2+}-ATPase is associated with an extrusion of protons, thought to be produced as Ca^{2+} takes up sites on the binding proteins in the SR (Haynes, 1982; Madeira, 1982).

The only certain thing, is that there are likely to be a number of facets to the counter-ion system, which address the wider issues of Ca^{2+} release and uptake by the SR. There has been no evidence that any one ion-flux predominates in the

counter-ion movement. The electron-probe studies of Somlyo et al. (1981) have shown that during a tetanus in frog skeletal muscle, apart from the expected shift of Ca^{2+} from the SR to the myoplasm, there is no major redistribution of any single ion to balance the shift in Ca^{2+}. There were significant increases in the amount of K^+ and Mg^{2+} present in the SR, but as calculated by Oetliker (1982), these shifts are insufficient to balance the efflux of Ca^{2+}. There were no changes in the distribution of Cl^- between the SR and the myoplasm. The apparent ion deficit may be carried by organic ions or protons, since molecules made up of elements below Na in the periodic table are not detectable with the electron-probe system used (Somlyo et al., 1981).

So, although the initial emphasis was the Ca^{2+} permeability of the SR, it was soon apparent that the permeability of the membrane to other ions was also important. It was necessary to determine what these permeabilities were and then ask what influences they have upon the Ca^{2+} release or uptake process. In this manner possible candidates for counter- or co-ions may be identified. Determining the permeability characteristics of the SR, however, was not a simple task and was very much dependent upon the techniques available.

1.3 SR membrane permeability

One very successful approach to investigating the SR permeability has been to remove the membrane from the *in situ* setting and produce isolated membrane vesicles. SR vesicles are prepared by homogenising skeletal muscle tissue followed by removal of the contractile proteins and other unwanted organelles by centrifugation. Further purification of SR vesicles by centrifugation on a sucrose gradient reveals sub-populations of vesicles with different buoyant densities, described as "light" and "heavy" SR vesicles (Meissner, 1975). Within the light vesicles, the Ca^{2+}/Mg^{2+}-ATPase protein accounted for 90% of the protein present. Between 55% and 65% of the protein in heavy vesicles was identified as Ca^{2+}/Mg^{2+}-ATPase and a significant portion of the remaining protein was Ca^{2+}

binding proteins. Accordingly, it was thought that the light vesicles were mainly from longitudinal SR and heavy vesicles were mainly from terminal cisternae (Meissner, 1975). Despite this difference between vesicle fractions, the majority of studies on monovalent ion permeability have used unfractionated SR vesicles. The few exceptions are McKinley and Meissner (1978) who specifically wanted to observe monovalent ion fluxes during Ca^{2+} accumulation by heavy SR vesicles, and Labarca et al. (1980) who examined the distribution of the SR K^+ channel in the different fractions.

Several independent methods have been employed to investigate the permeability of SR membranes. These are radioisotope flux measurements, the response of vesicles to an osmotic stress, and changes of an imposed membrane potential (reviewed by Meissner, 1983).

Radioisotope flux measurements

The first direct measurements of SR permeability were made by Duggan and Martonosi (1970) using radioisotope exchange. SR vesicles were incubated in the presence of a radioactive ion or solute. After centrifugation for one hour, the fraction of radiolabel contained in the pelleted vesicles compared to that remaining in the supernatant can be used to determine the "excluded volume". The excluded volume is a measure of the SR membrane permeability to the solute of interest. Larger molecules such as inulin (MW 5000-5500) and dextran (MW 15000-17000) were entirely excluded, indicating the SR vesicles were impermeable to these molecules. Smaller anions such as acetate, Cl^- and citrate were fully equilibrated across the vesicle membranes, indicating a high permeability. As the centrifugation step took one hour, it was not possible to discriminate between the permeabilities of the smaller anions since they had fully equilibrated within this time period. This problem was overcome by diluting vesicles pre-loaded with radioisotope tracer into unlabelled medium, then collecting samples of vesicles on Millipore filters at subsequent time intervals (Meissner & McKinley, 1976). In

this assay, the radioactivity retained by the vesicles on the filters is an indication of the efflux rate of the tracer and the internal vesicle space. With this technique, the limit of the time resolution was reduced to the 15 to 30 seconds it took to execute the Millipore filtration step.

Even with the improved time resolution of the Millipore filtration technique, the high permeability of the SR vesicles to Cl^- was unable to be resolved, as the efflux occurred entirely within the 15 to 30 seconds of the filtration step (Meissner & McKinley, 1976). Other solutes such as sucrose, divalent cations Ca^{2+} and Mg^{2+}, and large monovalent ions such as $Tris^+$, $choline^+$ and $gluconate^-$ were all found to be impermeant (Meissner & McKinley, 1976). The permeability to small monovalent cations identified two populations of SR vesicles. Type I vesicles, comprising approximately 70% of vesicles, are permeable to K^+, Na^+ and Rb^+ and Type II vesicles, the remaining 30%, are relatively impermeable to these same cations (McKinley & Meissner, 1977, 1978).

The permeability of Type I vesicles to small cations is not due to leaky vesicles, as the vesicle membranes are still selectively permeable to small anions (McKinley & Meissner, 1977, 1978). It is thought that the differences arise from a limited number of K^+/Na^+ channels present in the SR membrane, such that many vesicles will contain one to a few such channels (Type I vesicles) and some will contain none (Type II vesicles). Evidence for this is inferred from an increase in the fraction of K^+/Na^+ impermeable vesicles (Type II vesicles) which occurs when vesicle suspensions are sonicated, producing homogeneous vesicles of smaller surface area, (McKinley & Meissner, 1978). Furthermore, the relative fraction of Type I and Type II vesicles was similar for crude SR vesicle preparations as for "heavy" and "light" vesicles, suggesting a uniform distribution of the K^+/Na^+ channels throughout the SR membrane.

Permeabilities determined from osmotic gradients

The development of a light scattering measurement of membrane permeability (Selser et al., 1976) made significant improvements on the time resolution (on a time scale of 2 to 3 seconds) over radioisotope tracer methods. The technique monitors the changes in light scattering due to osmotically induced changes in vesicle size and shape. Vesicles mixed with a solution of higher osmolarity initially shrink due to efflux of water and then re-swell at a rate dependent upon the ability of the membrane to allow the net movement of the salt ions into the vesicle to counter the osmotic stress. The less permeant ion of this pair will be the dominant factor in limiting the rate of the reswelling process. The permeation time of an ion is defined as the time taken to reach the half-maximal change in light-scattering intensity.

A good account of the SR anion permeability has been provided by Kasai's laboratory using the light scattering technique. It has been shown that the relative permeability of SR vesicles to Cl^- is about 50 times greater than to K^+ (Kometani & Kasai, 1978). Other anions such as methane sulphonate, phosphate and oxalate all had a permeation time similar to that of K^+. Small monovalent cations also had a similar permeation time to K^+, with a permeability sequence of $Rb^+ > K^+ > Na^+ > Li^+$. The vesicles are relatively impermeable to Ca^{2+} and Mg^{2+}, to the large monovalent cations $Tris^+$ and $choline^+$, and to glucose, which is exactly the same selectivity as shown by the radioisotope measurements. The general conclusion reached by Komentani and Kasai (1978) was that the SR membrane was anion selective, because of the overwhelming permeability to Cl^-.

Disulphonic acid stilbene derivatives SITS, DIDS and H_2DIDS were used to inhibit anion permeability in SR vesicles (Kasai & Kometani, 1979; Kasai & Taguchi, 1981). In an attempt to identify the protein responsible for the anion permeability, [^{3}H]H_2DIDS was used in binding studies, which showed some of the inhibitor bound to a 100 kDa protein suggested to be the Ca^{2+}/Mg^{2+}-ATPase,

though 90% of the labelled inhibitor was found associated with low molecular weight proteins on an SDS polyacrylamide gel (Kasai & Taguchi, 1981). It was suggested that the anion pathway in SR membranes is possibly a small molecular weight protein which binds [^{3}H]H_2DIDS tightly, but reversibly.

There has been some doubt as to whether the light scattering technique detects only changes in vesicle volume. The ionophore melittin, from bee venom, forms non-selective pores which are large enough for Ca^{2+} and glucose to move across the membrane. When a glucose osmotic stress is applied to SR vesicles in the presence of melittin, no change in light scattering was observed, as might be expected for a membrane made freely permeable to glucose. An osmotic stress imposed by KCl, however, produced similar changes in light scattering in both the presence and absence of melittin. Since melittin would make the vesicles freely permeable to K^+, it is thought that the changes in light scattering may be due to changes in the membrane refractive index, altered by ionic strength (Garcia & Miller, 1984). So although the work of Kasai and colleagues has heightened the awareness of the SR anion permeability, the work by Garcia and Miller (1984) may invalidate some of the conclusions drawn from the light scattering technique.

Permeabilities determined from electrochemical gradients

Permeability of the SR has also been determined by measuring changes in membrane potential due to an imposed concentration gradient. These potentials, however, have been produced exclusively by cation gradients in the presence of impermeable anions, and so no information regarding anions has been produced with this technique.

Recordings of membrane potentials are made using potential sensitive dyes such as 3,3'-dipentyl-2,2'-oxadicarbocyanine (McKinley & Meissner, 1978; Meissner & Young, 1980) which characteristically decrease in fluorescence when vesicles become negatively charged inside. A change in fluorescence is therefore

dependent upon the magnitude of the developed potential across the vesicle membrane and, considering the differences in permeability of Type I and Type II vesicles, it is also dependent upon the fraction of vesicles that are polarised (McKinley & Meissner, 1978; Meissner & Young, 1980). Indeed, a larger fluorescence signal was recorded in the presence of the K^+ ionophore, valinomycin, suggesting the presence of a vesicle fraction (equivalent to Type II vesicles) with no intrinsic K^+ permeability, now rendered permeable and able to develop a K^+ diffusion potential. Comparison of the fluorescence signals in the presence and absence of valinomycin produce estimates of the fraction of Type I and Type II vesicles present which are in close agreement with those obtained from radioisotope tracer methods (McKinley & Meissner, 1977, 1978).

The rate at which the fluorescence signals returned to baseline levels is a measure of the rate at which the diffusion potential dissipates. It is interesting to note that the rate at which K^+ diffusion potentials dissipate increases in a non-linear fashion with more negative membrane potentials (McKinley & Meissner, 1978), indicating that the K^+/Na^+ permeability pathway in SR vesicles may be altered by membrane potential. This behaviour is entirely consistent, being of the same polarity, with the voltage-dependent K^+ channel behaviour as has been described in planar bilayers (see below).

A proton permeability pathway was also demonstrated in SR vesicles using this technique (Meissner & Young, 1980). Application of H^+ gradients produced transient changes in fluorescent signals. Both Type I and Type II vesicles were shown to have very similar H^+ permeabilities, which suggests a high number of H^+ permeable pathways in the SR. Large potentials were generated when H^+ and K^+ diffusion potentials were in the same direction, while a transient signal indicating rapid H^+ and K^+ exchange occurred with opposing H^+ and K^+ diffusion gradients. The evidence suggests that the H^+ permeability is independent of the K^+/Na^+ channel (Meissner & Young, 1980).

All of the studies discussed above used skeletal muscle SR vesicles. Similar ion permeabilities have also been demonstrated in cardiac SR vesicles (Meissner & McKinley, 1982), using the same three techniques described above.

While each of the techniques used to measure permeabilities in SR vesicles has its failings, they also complement each other in the nature of the information provided as they measure different vesicle parameters. Radioisotope tracer methods have been useful in isolated vesicle preparations to determine the exchange or efflux of larger solutes and relatively impermeable ions. Similar information is provided by the light scattering technique, with the advantage of improved time resolution but is limited to net movement of salt ions. Use of imposed membrane potentials allowed measurement of free cation permeabilities, although the fraction of vesicles which can be polarised needed to taken into account. Collectively, they present evidence for three independent, passive permeabilities in the SR membrane for monovalent ions: 1) an anion conductance, 2) a K^+/Na^+ conductance, and 3) a H^+ conductance. It is also apparent that the Cl^- permeability is approximately 50 times greater than the K^+ permeability. Each of these conductances are possible counter-ion pathways which may contribute during Ca^{2+} release and uptake by the SR.

1.4 Incorporation of ion channels into planar bilayers

The artificial bilayer technique of Mueller and Rudin (1969a) has proved to be very useful in the investigation of ion channel proteins, particularly for the SR which is not accessible *in situ* for electrophysiological investigation. Bilayers were first used to investigate a range of water soluble channel formers, or ionophores, from micro-organisms. Thus, gramicidin A and B, valinomycin, nystatin, amphotericin and others, were incorporated into bilayers (Mueller & Rudin, 1969b; Haydon & Hladky, 1972). As the function of these ionophores is to attack other micro-organisms by incorporation into the target cell membrane, they posed few problems for incorporation into artificial bilayers. The study of ion

transport mechanisms, including ion channels, from higher organisms (reviewed by Miller, 1983) has required a more sophisticated understanding for the insertion of these pathways into artificial bilayers. Although some conductance pathways had been successfully inserted into artificial bilayers by solubilizing the proteins in detergents (Shamoo & Eldefrawi, 1975; Bradley et al., 1976), it was a rather harsh treatment of the protein. The fusion of membrane vesicles to bilayers presented a much more gentle way of reconstituting conductance pathways, and the conditions required for fusion of SR vesicles were well described by the study of Miller et al. (1976). Incorporation of SR vesicles into bilayers allowed distinction of individual cation and anion pathways for the first time (Miller, 1978). Fusion of SR vesicles to the bilayer is proposed to proceed such that the outer surface of the vesicles, equivalent to the myoplasmic surface, faces into the *cis* chamber and the SR luminal surface faces into the *trans* chamber.

SR calcium release channel

A key aspect to the characterisation of the Ca^{2+} release channel in planar bilayers has been the strong pharmacological profile which has been established for the Ca^{2+} release process using SR vesicles and skinned fibres. Thus, when vesicles were incorporated into bilayers, there were a number of tools ready to identify behaviour that would implicate the channel as being involved in the Ca^{2+} release process.

Using SR vesicles enriched for the terminal cisternae fraction, a large conductance Ca^{2+} channel (100 pS with 53 mM Ca^{2+} on the *trans* side) was found with rapid gating kinetics (Smith et al., 1985, 1986b). This channel was activated from the *cis* side by addition of free Ca^{2+} in the micromolar range and also by addition of millimolar ATP. Together at optimal concentrations, they had additive effects and the channel was maximally activated, occupying the open state with a much greater frequency but without changing the open state lifetimes. Ruthenium red (1 μM on the *cis* side) irreversibly blocked channels which had previously been

activated by ATP. Channel activity was also modulated by Mg^{2+} on the *cis* side, in a competitive manner opposing the activation by Ca^{2+}. The presence of Mg^{2+} on the *trans* side had no effect upon the channel behaviour.

Another important agent in the characterisation of the Ca^{2+} release channel has been the plant alkaloid ryanodine. This high affinity ligand has been useful in localising the Ca^{2+} release channel in the terminal cisternae of SR (Fleischer et al., 1985) and in purification of the channel protein (Pessah et al., 1986). When ryanodine was applied to Ca^{2+} channels from SR vesicles incorporated into bilayers, two characteristic effects were initially reported (Rousseau et al., 1987). Firstly, the channel became insensitive to activation by Ca^{2+} and ATP, and the blockers Mg^{2+} and ruthenium red were less effective. Secondly, ryanodine interacted with the open channel, locking it into a substate of lower conductance but the open probability was greatly increased. At even lower concentrations, ryanodine (10 nM) activated the channel by increasing the open probability without any changes in conductance (Bull et al., 1989).

The behaviour of the purified ryanodine receptor protein, reconstituted into bilayers, is essentially the same as the native Ca^{2+} release channel from SR vesicles. The purified protein maintains the regulatory sites for modulation by Ca^{2+}, ATP, Mg^{2+} and ruthenium red (Hymel et al., 1988; Lai et al., 1988). While the ryanodine receptor channel exhibits a main conductance of 91 pS (50 mM Ca^{2+} on the *trans* side) which is similar to the native channel (Lai et al., 1988), in most cases it displays multiple subconductance states which are often flickery and less well defined (Hymel et al., 1988). It has been proposed that these multiple conductance states may represent intrinsic conductances of the protein subunits that comprise the channel protein, and that they are normally coupled to gate cooperatively, giving the characteristic 100 pS conductance of the native Ca^{2+} channel (Liu et al. 1989).

SR potassium channel

Since the first description of the SR K^+ channel in planar bilayers by Miller (1978), the channel has been extensively characterised (for review see Miller et al., 1984). Most of the work published on the SR K^+ channel has been from rabbit SR vesicles incorporated into planar bilayers, though there is one study on frog SR vesicles (Labarca & Miller, 1981). The SR K^+ channels from these two species display qualitatively similar behaviour.

At the macroscopic level, the K^+ current exhibits a rectifying behaviour, with the current becoming larger at positive potentials (Miller, 1978). At the single channel level, only two conductance states are observed: open and closed. The voltage dependent behaviour of the K^+ channel is able to be described by an exceptionally simple kinetic scheme, consisting of a single open state and a single closed state (Labarca et al., 1980). From observations of single exponential macroscopic current relaxations, which directly reflect the rate constants measured from single channel recordings, this model was further confirmed (Labarca et al., 1980). The voltage dependence of this two state model is able to be described by a Boltzmann relation with an effective gating charge of +1.1 (Miller & Rosenberg, 1979a; Labarca et al., 1980). Modification of the voltage dependence is possible with the application of Alkaline Proteinase b (APb), which is a serine protease specific for arginine and lysine residues. When APb applied to the *trans* side, the channel becomes much less sensitive to voltage, changing the channel from a rectifier to a linear conductor. Single channels are still observed to open and close but the effect of APb uncouples the channel behaviour from the intramembrane electric field, reducing the effective gating charge to approximately +0.1 (Miller & Rosenberg, 1979a). Changing the lipid environment of the bilayer to which the channel is inserted also alters the voltage dependence. Increasing the proportion of negatively charged lipids shifts the voltage dependence curve to the right, and positively charged lipids shifts the curve to the left (Miller et al., 1984).

The K^+ channel has a high unitary conductance of 142 pS in symmetrical 100 mM K^+. With increasing K^+ concentration, the conductance saturates in a Michaelis-Menten manner, reaching a maximum conductance of 214 pS at 1 M K^+. From these properties, a model of the channel pore has been proposed such that the pore can bind at most one ion at a time (Coronado et al., 1980). The pore is highly selective for small monovalent cations, with a conductance sequence $K^+ > NH_4^+ > Rb^+ > Na^+ > Li^+ > Cs^+$ (Coronado et al., 1980). Both Li^+ and Cs^+ have an extremely low conductance, but whereas Li^+ seems relatively inert, Cs^+ exerts a voltage dependent blockade of the channel, reducing the conductance at positive potentials (Coronado et al., 1980). The effect of Cs^+ can be explained in terms of an open channel block at a site which is accessible only from the *cis* side (Coronado & Miller, 1979). Increasing the K^+ concentration relieves the Cs^+ block, indicating Cs^+ competes for a binding site within the channel's K^+ conduction pathway (Coronado et al., 1980). Long chain ammonium derivatives, decamethonium and hexamethonium, are much more potent blockers than Cs^+, however, they are effective only from the *trans* side of the membrane (Coronado & Miller, 1980).

SR anion channel

It is surprising, given the early interest in anions enhancing the accumulation of Ca^{2+} and the large permeability to anions found in SR vesicles, that when vesicles were fused to bilayers the anion conductance was left in the background. Originally there were doubts as to whether the anion conductance was due to an ion channel or a non-specific leak. Initially this issue was not addressed directly, as it was the cation conductance that was of interest and the comparison of behaviour with the anion conductance was only to establish the cation conductance as a specific and independent pathway. Unlike the K^+ channel, the anion conductance was not voltage dependent and it was not sensitive to low pH (Miller, 1978). The conductance was not sensitive to transition metals (Miller &

Rosenberg, 1979b) or modified by APb (Miller & Rosenberg, 1979a). Only in more recent times has the anion conductance attracted a little more attention and been established as an independent anion selective channel.

Rabbit skeletal muscle SR vesicles incorporated into planar bilayers exhibit an anion channel with high unitary conductance of 200 pS in 100 mM choline Cl (Tanifuji et al., 1987). The channel conductance saturates with increasing Cl^- concentrations, reaching an estimated maximum conductance of 700 pS. This channel has at least four or five subconductance levels and fast flickering events between the open and closed levels. In contrast to the early work on bilayers by Miller (1978), the macroscopic current shows a voltage dependence at positive potentials where the averaged current is reduced. Inspection of single channel records show that while the fully open conductance is not reduced, the channel tends to occupy subconductance levels with greater frequency at more positive potentials. The channel is only weakly selective for anions over cations and does not select between monovalent anions, although SO_4^{2-} is almost impermeable. Addition of SO_4^{2-} to the *cis* side of the bilayer membrane produces a voltage dependent block, reducing the Cl^- conductance at negative potentials in a simple competitive fashion.

Anion channels have also been reported by Rousseau et al. (1988) from rabbit and trout skeletal muscle SR vesicles. These channels were of smaller conductance compared to the report of Tanifuji et al. (1987), but still displayed several subconductance states which seem to be a consistent feature of the SR anion channel. The rabbit SR channel had a conductance of 70 pS in symmetrical 125 mM choline Cl^-, and although the conductance did saturate in a concentration dependent manner, the maximal conductance was only 154 pS. A slight voltage dependence was also reported for these channels, with the open probability relationship being described as an attenuated bell-shaped curve with the P_O ranging from 0.60 to 0.90, centred about 0 mV. A voltage dependent block is also

produced by SO_4^{2-} from the *cis* side of the membrane. No regulating function for Ca^{2+} was found, as a range of concentrations (5 mM down to 0.1 μM) applied to either the *cis* or *trans* chambers produced no appreciable affect on the anion channel conductance or gating behaviour. Like the studies of Kasai's laboratory where SR vesicle anion permeability was blocked with stilbenes (Kasai & Kometani, 1979; Kasai & Taguchi, 1981), these anion channels were blocked efficiently and irreversibly by DIDS at submillimolar concentrations.

Planar bilayers have been very successful in describing the biophysical characteristics of the individual channel proteins. The presence of the K^+ channel in the SR membrane and its voltage dependent behaviour suggests that it might play a role in balancing the Ca^{2+} fluxes across the SR membrane. The anion channel is similarly implicated, even though it is less well characterised.

1.5 Access to native SR membrane

While the SR vesicle and planar bilayer techniques provide valuable information about the nature of SR conductances, there is always the concern as to whether they truly reflect the behaviour *in vivo*. Isolating SR vesicles may alter the membrane properties. Fusion of vesicles to planar bilayers may be selective, and represent only a fraction of the vesicle population (Meissner, 1983; Miller et al., 1984). Ideally, investigation of the SR membrane would be pursued while it remained in its native state. This has only been possible in one exceptional situation, in lobster antenna muscle, where there is an large volume fraction of SR membrane (Tang et al., 1987). After mechanically removing the sarcolemma, recordings were able to be made directly from the SR using the patch clamp technique.

A novel technique of assembling bilayer membranes at the tip of a patch pipette has been described by Coronado and Latorre (1983). This "tip dip" method has been used to investigate a Ca^{2+} channel from native SR membrane (Suárez-Isla et

al., 1986). The channel was activated by caffeine and inhibited by dantrolene, however the unitary conductance was only 5 pS in symmetrical 200 mM $CaCl_2$ solutions, compared to 100 pS for the Ca^{2+} release channel described in bilayers. No work on SR anion channels, however, has been reported that utilises this technique.

The techniques which offer the most promise are the skinned fibre and the sarcoball preparations in vertebrate muscle. As it is not possible to demonstrate a physiological function of SR vesicle ion channels in planar bilayers, the skinned fibre preparation offers an opportunity for such a functional demonstration of the role of these channels. This is not possible, however, without specific agents to modify the conductance of interest. Such agents are best investigated and demonstrated in the isolated membrane patch. Thus, the bilayer and sarcoball techniques offer complimentary and supporting information to that obtained from skinned fibres.

Skinned skeletal muscle fibres

There are actually a range of preparations which come under the category of skinned fibres. The original preparation by Natori (1954) describes stripping the sarcolemma away from a muscle fibre immersed in oil, to leave the underlying myofibrils and SR intact. This allows access and control of the myofibrillar environment. Others have chemically "removed" the sarcolemma by permeabilising the membrane with glycerol, EGTA or saponin (Stephenson, 1981). In the Natori type skinned fibre, the T-tubules are thought to be sealed over and the SR to be intact, while chemically permeabilised fibres have T-tubules and SR membranes in various states of function (Stephenson, 1981).

These skinned fibre preparations have been valuable in mechanical studies of the contractile apparatus and the process of Ca^{2+} activation, using the contractile apparatus as a sensitive assay for the free Ca^{2+} concentration. In the Natori

skinned fibre, the time course of force transients is a reflection of the Ca^{2+} release and uptake kinetics. Taking advantage of the maximal release of Ca^{2+} elicited by caffeine to empty the SR, buffered Ca^{2+} solutions can then be used for controlled loading of the SR (Endo et al., 1970). The effects of releasing agents or modifiers can then be assessed from a known starting point and checked by a subsequent caffeine release to determine the residual Ca^{2+} in the SR. By maintaining the functional relationship between the T-tubules, the SR and the contractile filaments, this *in situ* preparation has structural and diffusional elements which are not a part of isolated SR membrane systems. This also means that there are more variables which need to be considered and controlled.

The use of this preparation to investigate the role and effects of monovalent ions upon the function of the skinned fibre has been limited. Initial attempts were motivated by the belief that there may be a potential across the SR membrane in much the same way as there is across the surface membrane. Ionic substitution was used to impose a change in potential across the SR membrane in an attempt to trigger the release of Ca^{2+}. One way this was attempted was by replacing a less permeant anion with the more permeant Cl^-, the so called "Cl^- stimulated release". In SR vesicles, such ionic substitution produced a Ca^{2+} release which was later found to be an artefact due to osmotic stress (Meissner & McKinley, 1976). To avoid this osmotic artefact, Cl^- substitution was performed while maintaining a constant product of $[K^+][Cl^-]$ in solutions bathing skinned fibres (Mobley, 1979; Donaldson, 1985; Stephenson, 1985). While the intention of these ionic substitution experiments was to release Ca^{2+} by depolarising the SR membrane, it was found that the release of Ca^{2+} that did occur was in fact due to depolarisation of the T-tubules coupled to the SR by the normal physiological pathway. When a muscle fibre is mechanically skinned, the T-tubules remain, seal over and repolarise due to the Na^+/K^+-ATPase in the T-tubule membrane (Ikemoto et al., 1989). By incubating the skinned fibre in ouabain specifically to inhibit the

Na^+/K^+-ATPase, the "Cl^- stimulated release" could be abolished (Donaldson, 1985).

Subsequently, the role of anions in the uptake and release of Ca^{2+} from the SR has either been ignored or tacitly accepted as a part of the system when using skinned fibres. In most cases, when investigating the contractile responses in skinned fibres, the major anion present in the bathing solutions is impermeant to the SR. Yet Ca^{2+} uptake and release is still able to occur (Ford & Podolsky, 1970), which means either anions do not make a major contribution to the counter-ion fluxes, or other ions make up for the deficit of anion movement. As mentioned earlier, there is no evidence from electron-probe analysis for an asymmetric distribution of Cl^- across the SR at rest or after a 2 s tetanus (Somlyo et al., 1981). If other anions, not detected by the electron-probe, were to provide a counter-ion flux, then the anion channel would have to be selective for these anions over Cl^-. This is inconsistent with the weak selectivity between monovalent anions and poor permeability of divalent anions demonstrated with SR vesicles in bilayers (see above). At the present moment there are no specific blockers of the SR anion conductance which might be able to be used to test the functional role of anions by blocking the anion conductance in skinned fibres. Although the stilbenes, DIDS and SITS have been used to inhibit the anion conductance in SR vesicles, the problem with these protein modifiers is that they act upon many different SR proteins, including the Ca^{2+}/Mg^{2+}-ATPase (Byers & Meissner, 1986).

The only studies in skinned fibres which are directly concerned with the influence of counter-ions upon the movement of Ca^{2+} across the SR have both used pharmacological blockers to modify the K^+ conductance. In both studies caffeine was used to cause release of Ca^{2+} from the SR, so as to by-pass the normal coupling process between the T-tubules and the SR.

Fink and Stephenson (1987) found that the amount of Ca^{2+} able to be released was markedly increased when loading took place in the presence of 4-aminopyridine

(4-AP), tetraethylammonium, decamethonium, and procaine, all of which are known to block the SR K^+ channel (Coronado & Miller, 1980, 1982). Similar results were also obtained when the K^+ in the Ca^{2+} loading solution was partially replaced with the less permeant Na^+ ion. The K^+ channel blockers were not present in the release solution, so as to avoid complications which may arise from interaction of the blockers with the contractile apparatus or directly on the Ca^{2+} release channel. The results obtained are somewhat unanticipated, as perhaps a decrease in Ca^{2+} loading may be expected with the reduced charge compensation available when the K^+ conductance is blocked. The interpretation offered is that with the K^+ conductance blocked, there is a compensating increase in the H^+ efflux from the SR during Ca^{2+} uptake. As a consequence, the SR lumen becomes more alkaline and increases the apparent Ca^{2+}-binding affinity of the SR Ca^{2+}-binding proteins. The free Ca^{2+} concentrations of the SR lumen are therefore much lower for a longer period of time, allowing the Ca^{2+}/Mg^{2+}-ATPase to pump in more Ca^{2+} before it is eventually inhibited by rising SR Ca^{2+} levels.

Using the SR K^+ channel blocker 1,10-*bis*-guanidino-*n*-decane (bisG10) Abramcheck and Best (1989) investigated the role of the SR K^+ channel during Ca^+ release in skinned fibres. The blocker bisG10 has been demonstrated to be a potent inhibitor of the SR K^+ channel incorporated into planar bilayers (Garcia & Miller, 1984). Abramcheck and Best found bisG10 produced a decrease in the Ca^{2+} release rate in a dose dependent manner, indicated by a decrease in the force transient and a decrease in the Ca^+ transient recorded using the Ca^{2+} sensitive metallochromic dye antipyrylazo III. In contrast to the experiments by Fink and Stephenson described above, bisG10 was only present during the caffeine stimulated release of Ca^{2+} from the SR. The loading of the SR was carried out under normal conditions. To test if the reduced Ca^{2+} release in the presence of bisG10 is actually due to a reduced K^+ counter-ion flux, releases were also stimulated in solutions where choline was partially substituted for K^+. In this

case a reduced Ca^{2+} release was also observed, strongly suggesting a regulatory role of the K^+ conductance.

The results of Fink and Stephenson and those of Abramcheck and Best appear to be diametrically opposed. It is difficult to reconcile these differences without performing the appropriate experiments to determine the effects of 4-AP and bisG10 on both the Ca^{2+} release and uptake processes. It is possible, however, that these results reflect real differences in the contribution of the K^+ channel conductance in these two processes.

Sarcoball technique

The development of the sarcoball technique by Stein and Palade (1988) provided a simple preparation that allows access to the SR with the minimum amount of intervention. The preparation is described with more detail in Chapter 2. Briefly, sarcoballs are produced by allowing mechanically skinned skeletal muscle fibres to contract unrestrained, causing the extrusion of internal membranes to the fibre surface where the hemispherical blebs of membrane form. Patch clamp techniques were used to investigate the nature of the conductances present in the membrane.

a) Calcium release channel

A voltage-dependent Ca^{2+} channel described in this preparation was identified as the Ca^{2+} release channel of the SR on the basis of its activation by caffeine (5 mM) and block by ruthenium red (1 μM) (Stein & Palade, 1988). The channel exhibited two open levels of relatively high conductance (80-100 pS and 120-160 pS) and had limited selectivity for Ca^{2+} over K^+ (P_{Ca}/P_K=6.5), which are similar to the characteristics reported for the Ca^{2+} release channel isolated from rabbit SR and incorporated into bilayers (Smith et al., 1985). It was also found that the Ca^{2+} channel was consistently asymmetrically oriented in the membrane, such that ruthenium red blocked the Ca^{2+} channel activity when present in the pipette,

while 10 μM ruthenium red on the bath side of the membrane had no effect. This was confirmed by forming outside-out patches, whereupon 2 μM ruthenium red in the bath rapidly blocked channel activity. On the basis of this result, it was proposed that inside-out patches formed from the sarcoball surface had the myoplasmic surface facing into the pipette and the SR luminal surface facing the bath. Others have also used the same preparation and report similar Ca^{2+} channels, which are additionally activated by micromolar ryanodine (Kwok & Best, 1990) and inactivated by an endogenous protein kinase (Wang & Best, 1992).

In contrast, another Ca^{2+} channel recorded by Wang et al. (1992) in sarcoballs was not sensitive to ryanodine, ruthenium red or caffeine. This strongly suggested that it was not the Ca^{2+} release channel. This channel was affected by vanadate, AlF_4^-, reactive red 120 and cyclopiazonic acid, all of which are known inhibitors of the Ca^{2+}/Mg^{2+}-ATPase. It was proposed that the channel activity was instead a form of the Ca^{2+}/Mg^{2+}-ATPase behaving as a Ca^{2+} conducting channel.

The ability to record the Ca^{2+} release channel in sarcoballs was posed as physiological evidence that this preparation comprised mainly SR membrane. No morphological studies had been performed on this preparation, however, to identify directly the nature of the membranes. It was not ruled out that there might be other internal membranes, such as T-tubules and mitochondria, contributing to the structure.

b) Sarcoball K^+ channel

Brief information has been presented by several independent groups for a K^+ channel. Stein et al. (1989) report a K^+ channel from mammalian SR with a conductance of 100 pS, which is highly selective for K^+ over Ca^{2+} (P_K/P_{Ca}>1000) but only weakly sensitive to potential. The K^+ channel reported by Vivaudou et al. (1989) from frog skeletal muscle is very similar in all respects except for the smaller conductance of 52 pS, which is of a similar level to the subconductance

state of 60 pS reported by Stein et al. (1989). A similar conductance of 61 pS is reported by Wang et al. (1992) for a K^+ selective channel, with a second conductance level of 82 pS which is seldom seen. This channel is blocked by decamethonium and hexamethonium in a voltage dependent manner. In general, these results are similar to those recorded from SR K^+ channels reconstituted into bilayers, although in bilayers the channel exhibits a much more prominent voltage dependence.

c) Sarcoball anion channel

The anion channel described in the sarcoball preparation, using excised inside-out patch clamp techniques, has a high conductance of 505 pS in symmetrical 200 mM TrisCl (Hals et al., 1989). With increasing Cl^- concentration, the conductance saturates in a Michaelis-Menten manner reaching an estimated maximum conductance of 617 pS and a half-maximal conductance occurring at 77 mM TrisCl. Despite the large conductance, the channel maintains a high selectivity for anions over cations, with a permeability ratio P_{Cl}/P_K = 45, determined from the shift in reversal potential with a KCl salt gradient. Selectivity among anions favours smaller monovalent anions and the channel is impermeable to larger anions such as gluconate. A voltage-dependent effect is observed in the presence of divalent anions SO_4^{2-} and PO_4^{2-} in the bath solution which reduces the probability of open channel events at positive pipette potentials, without any effect upon the unitary conductance. No change in the channel conductance or gating is observed when altering the free Ca^{2+} within physiological ranges on either side of the patched membrane.

Recordings of the anion channel show numerous subconductance states, of which two are prominent enough to be further characterised. A fast flickering substate (S1) with a conductance of approximately half the main open state is found in most recordings. It exhibits bursts of flickering behaviour while still attached to the sarcoball surface, but these decrease in activity immediately upon excising the

patch. The other substate (S2) described is of smaller conductance (125 pS) which is seen to open in addition to the main open state and also from the closed state.

The most striking feature of the anion channel is the steep voltage dependence of the channel open probability which is bell-shaped, centred about 0 mV such that the channel closes with shifts in potential away from zero, in symmetrical ionic solutions (Hals et al., 1989). This is initially surprising, as bilayer studies generally describe a voltage-independent anion conductance in SR vesicles (Miller, 1978; Miller & Rosenberg, 1979b; Tanifuji et al., 1987). When a direct comparison was made between the anion conductances from SR membrane fused into liposomes and that from sarcoball membrane, the liposome anion channels were also found to be voltage-independent (Hals et al., 1989).

Since the bell-shaped voltage-dependence of the sarcoball anion channel is similar to that of mitochondrial VDAC, which might also be present in the preparation, their biophysical properties were compared. It was suggested that there were sufficient differences to distinguish the sarcoball anion channel as a separate channel to the mitochondrial VDAC (Hals et al., 1989).

The involvement of positive charged residues in the channel protein structure being responsible for the voltage-dependence and conductance of the anion channel were investigated using a range of stilbene derivatives Hals & Palade, 1990). The reactive isothiocyano groups of the stilbenes are capable of covalently linking amino groups. An irreversible modification by SPIT and TNBS reduced the channel conductance at all membrane potentials. As the reagents were applied to only one side of the membrane, it suggests that the effect is not due to modification of charged groups within a vestibule to the channel pore, as this would predict a change in conductance in only one direction. Instead, they thought that the modification occurs in the narrow part of the channel pore.

Separate modification by DIDS applied via the bath solution significantly reduced the maximal open probability and shifted the bell-shaped voltage-dependence curve to more negative potentials, so that it was centred about -30 mV. These results suggest that positively charged amino groups which are able to be accessed and modified by specific stilbenes, are associated with the voltage-dependence and separately the conductance of the anion channel. Both SITS and DIDS have been used previously to inhibit anion permeability in rabbit SR vesicles (Kasai & Kometani, 1979; Campbell & MacLennan, 1980; Kasai & Taguchi, 1981).

1.6 Summary and aims

The focus of this study is the anion channel found in the sarcoball preparation from amphibian skeletal muscle. This channel has been described for skeletal muscle of the frog *Rana catesbeiana* but, in this study, muscle from the cane toad, *Bufo marinus*, was to be used. Consequently, the first aim of this study was to establish the presence of the anion channel in sarcoballs prepared from *Bufo marinus*.

The sarcoball anion channel has a distinctive bell-shaped voltage-dependence, and naturally this has influenced hypotheses regarding the role the channel might play in the SR membrane. During Ca^{2+} release, the potential that develops across the SR membrane might cause the anion channel to close, limiting the counter-ion flux and acting like a brake to further release of Ca^{2+} (Hals et al,. 1989). Alternatively, the anion channel might be a very effective shunt, since it is maximally open at 0 mV and it has a large conductance, so that a potential may be unable to develop during Ca^{2+} release. Although the sarcoball preparation is unable to address directly the question of what role the anion channel is plays in the SR membrane, it provides a good means of investigating the voltage-dependent behaviour of the channel and so can contribute to the overall understanding of the behaviour of the SR membrane. A second aim of this study

was, therefore, to investigate the mechanism underlying the voltage-dependent behaviour of the channel.

Previously, the voltage-dependence of the channel has been described in terms of its steady-state characteristics, although during the course of this study a brief report on the dynamic behaviour appeared (Zahradnik et al., 1990). A third aim of this study was, therefore, to investigate further the dynamic behaviour of the sarcoball anion channel.

The sarcoball itself also warranted further investigation, as there had been only one electron micrograph published of the preparation (Stein & Palade, 1988). A fourth aim of this study was to describe the sarcoball preparation at the electron microscope level.

What internal membranes are present in the sarcoball preparation is not known with certainty, though it was thought to be mainly SR membrane (Stein & Palade, 1988). Knowledge of the membrane in which the anion channel occurs is an important part of the characterisation of the channel. A part of this description was the need to distinguish between the sarcoball anion channel and the VDAC from mitochondrial outer membrane. Rather than rely just on a biophysical comparison of these two channels, it was thought that a direct probing for the presence of mitochondrial VDAC was warranted. The fifth aim of this study was, therefore, to establish what membranes; that is SR or, indeed, membranes from any other source, contributed to its structure.

PART I.
PATCH CLAMP STUDIES OF THE ANION CHANNEL IN SARCOBALLS

2. PREPARATION OF SARCOBALLS

2.1 Introduction

"Sarcoballs" is the term first introduced by Stein and Palade (1988) to describe a preparation of internal membranes from skeletal muscle fibres of the frog, *Rana catesbeiana*. Individual muscle fibres were mechanically skinned in a Ca^{2+} containing saline solution, whereupon small blebs of membrane appeared at the fibre surface immediately following removal of the sarcolemma. These blebs coalesced to form the larger hemispherical sarcoballs as the fibre contracted. When the fibres were skinned in relaxing solution, no blebs were observed until a contracture of the fibre was triggered by the addition of Ca^{2+}. It has been proposed that the free Ca^{2+} concentration and the degree of shortening are critical factors involved in the formation of sarcoballs (Stein & Palade, 1988). It is shown here, however, that sarcoballs can also be formed by mechanically skinning muscle fibres in a solution of CsF (200 mM), which then contract without the need for the addition of Ca^{2+} to the solution.

By using this technique, direct access is obtained for patch-clamp recording from internal membranes which are normally inaccessible *in situ*. In particular, it provides access to native SR membranes, which are thought to be the major component of sarcoballs. An investigation into the morphology of this preparation is presented in Part II.

2.2 Method of preparation

Cane toads, *Bufo marinus*, or clawed toads, *Xenopus laevis*, were double pithed and the semitendinosus muscle was removed and placed into synthetic interstitial fluid (SIF) of composition (in mM): 107.7 NaCl, 26.2 $NaHCO_3$, 9.64 NaGluconate, 1.67 NaH_2PO_4, 3.48 KCl, 1.53 $CaCl_2$, 0.69 $MgSO_4$, 5.55 glucose, 7.6 sucrose, 280 mOsM, pH 7.40 maintained by bubbling with a 95%/5% O_2/CO_2 gas mixture (Bretag, 1969). SIF has been shown to be most suitable for the maintenance and well being of muscle tissue from mammalian and toad species (Bretag, 1969). The muscle was pinned out at *in vivo* length and bundles of fibres were dissected intact from tendon to tendon. The bundles of fibres were placed in a solution of 200 mM CsF, 10 mM TES, pH 7.40, adjusted with KOH. Single fibres were isolated and then mechanically skinned using fine forceps. The process of skinning a skeletal muscle fibre involves holding one end of the fibre steady while a few myofibrils are teased away from the end of the fibre. In one action, these few myofibrils are held and pulled away from the fibre, moving down along the length of the fibre. During this action, the sarcolemma was observed to be rolling up like a cuff in front of where the myofibrils were being pulled away from the rest of the fibre. The skinned fibres were allowed to undergo an unrestrained contracture in the CsF solution, whereupon many sarcoballs appeared at the fibre surface.

Alternatively, sarcoballs could also be produced by mechanically skinning single fibres in SIF or in the amphibian Ringer used by Stein et al. (1988) (in mM, 117 NaCl, 4.7 KCl, 1.2 $CaCl_2$, 5.0 TES, pH 7.4, adjusted with KOH). Again, the skinned fibres were allowed to contract unrestrained in these solutions. As will be described in the following Chapter, anion channels with the same characteristics could be recorded in sarcoballs produced by either of these methods. It was found, however, to be much easier to mechanically skin and form sarcoballs in the CsF solution and so this was the method of choice.

Observations of the formation of sarcoballs

Hemispherical blebs of extruded membrane can be observed to form at the surface of amphibian skeletal muscle fibres as they are allowed to contract unrestrained after being mechanically skinned. When the fibres are skinned in CsF solution, the contracture develops over several seconds, while fibres skinned in SIF contract immediately as the sarcolemma is removed. The hemispherical blebs of membrane, or sarcoballs, appear and enlarge as the contracture develops. Sarcoballs appear on all exposed surfaces of the mechanically skinned fibre. An example of a skinned fibre is shown in Figure 2.1, with sarcoballs ranging in size from 10 μm to >100 μm in diameter. In CsF, where the contracture is slower, the formation process can be followed and small blebs are observed to merge with neighbouring blebs as they grow to form the larger blebs. There continues to be some extrusion of membranes and merging of adjacent blebs even after the shortening of the muscle fibre segment is complete. This activity, however, is nowhere as vigorous as that which occurs during the contracture and may reflect an elastic component within the myofilament lattice exerting an effect upon the internal membranes. The contracture that produces sarcoballs is complete and irreversible, perhaps indicating the fibre is in a rigor state. This state is maintained even after a number of different solution changes.

2.3 What is caesium fluoride doing?

Caesium fluoride has previously been used as a relaxing solution when cutting fibres for the Vaseline gap recording technique and as an internal replacement solution in the same cut fibre preparation (Hille & Campbell, 1976). Caesium fluoride was used in the present study to allow muscle fibres to be mechanically skinned without the associated problems of fibres contracting during the skinning process, as occurred in Ringer's or SIF solutions. Originally it was planned to transfer the skinned fibres to a Ca^{2+} buffered solution to cause the fibre to contract and form the sarcoballs. It was soon observed, however, that this was not

necessary, as fibres skinned in the CsF solution underwent a slow contracture soon after the skinning process was completed. It was not expected that the fibres should contract in the CsF solution. This reasoning was based on knowing F^- is an avid binder of Ca^{2+} (solubility product K_{so}=-10.4, Sillén & Martell, 1964) and Cs^+ has been reported to have a low conductance and a voltage-dependent blocking action on isolated K+ channels from the SR (Coronado & Miller, 1979). With Cs^+ as the only monovalent cation present, the release of Ca^{2+} from the SR might be expected to be limited because of the reduced counter ion conductance through the K^+ channel. Evidence from skinned muscle fibres, however, shows Cs^+ had a small or no effect upon the Ca^{2+} release from the SR (Palade & Vergara, 1982; Abramcheck & Best, 1989).

Since the skinned fibres do contract in CsF, and it seems unlikely that CsF would directly activate the myofibrils, it is a reasonable assumption that sufficient Ca^{2+} has been released from the SR to activate the contracture.

The information on F^- suggests several possible actions, some which would prevent contracture and others that would induce contracture. Fluoride is a known inhibitor of SR membrane associated protein phosphatase. When rabbit SR vesicles are preincubated with NaF to inhibit the phosphatase, subsequent addition of ATP promotes the phosphorylation of two SR proteins (a 160 kDa and a 150 kDa protein). This results in an inhibition of Ca^{2+} accumulation and a stimulation of Ca^{2+} efflux from the vesicles (Orr et al., 1991). A stimulated Ca^{2+} efflux such as this may also be occurring with skeletal muscle fibres skinned in CsF and produce the contracture observed. The inhibition of Ca^{2+} accumulation appears to be due to F^- interacting with the ground state (or E conformation) of the SR Ca^{2+}/Mg^{2+}-ATPase before the ATP is added, which precludes any subsequent binding of ATP and therefore preventing any activity of this pump protein (Narayanan et al., 1991).

Figure 2.1 A skinned fibre with sarcoballs
An isolated single fibre from the semitendinosus muscle of *Bufo marinus* was mechanically skinned and allowed to contract unrestrained in CsF solution. Hemispherical blebs of membrane, which ranged in size from 10 µm to 100 µm in diameter, can be seen along the surface of the skinned fibre. Clear striations have been obscured because of the extent of the contracture. Photographed with Nomarski optics; magnification x200.

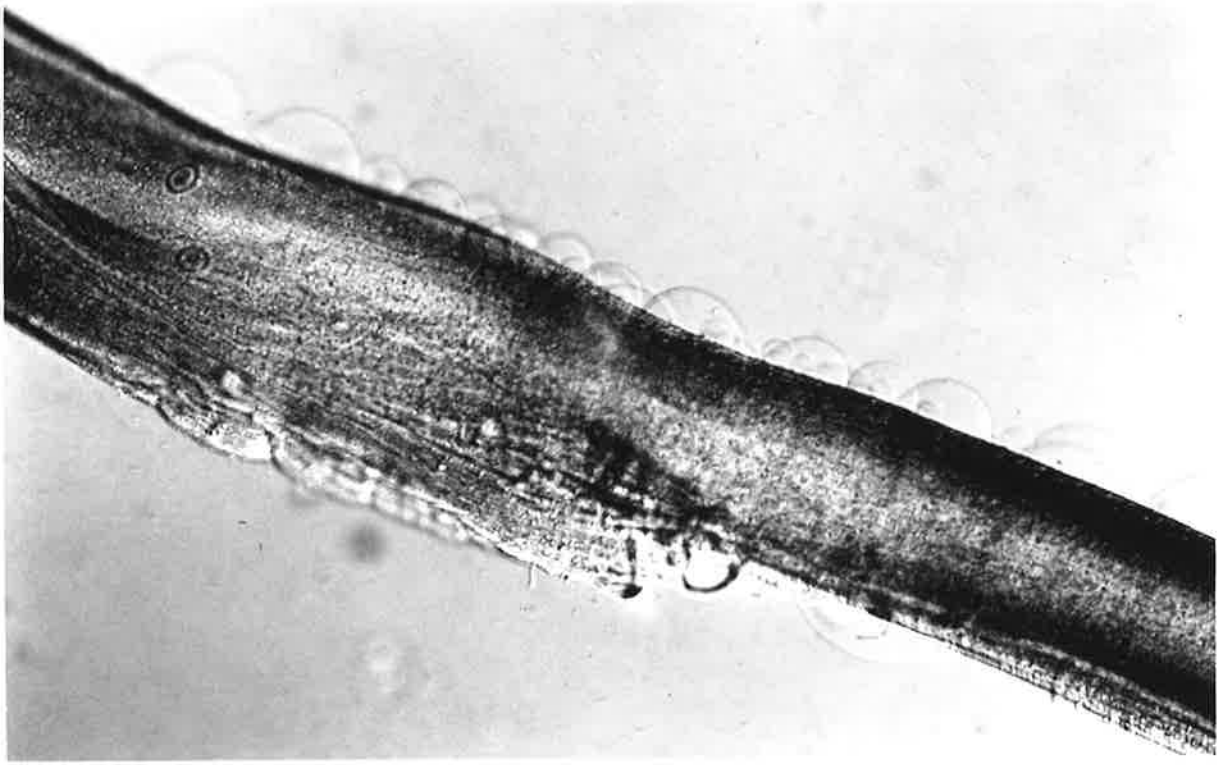

If F^- is as permeant through the SR membrane as has been indicated (Meissner, 1986), then it might be expected that an influx of F^- would cause the precipitation of Ca^{2+} inside the SR and prevent subsequent release. This has been proposed as a mechanism to account for the increase in Ca^{2+} accumulation seen with canine cardiac SR vesicles in the presence of F^- (Narayanan et al., 1991). In this case, the ATP is initially present and so the inhibition of Ca^{2+}/Mg^{2+}-ATPase by F^-, described above, does not occur. The precipitation of CaF_2 maintains a lower free Ca^{2+} concentration inside the SR vesicles, allowing the Ca^{2+}/Mg^{2+}-ATPase to continue accumulating Ca^{2+} for a longer period of time before being inhibited by increasing Ca^{2+} levels inside the vesicles.

To reconcile the avid binding of Ca^{2+} by F^- and the increase in free $[Ca^{2+}]$ which must occur to produce the contracture, it may be possible that the CsF_2 is not uniformly distributed in the skinned muscle preparation. It has been shown that there is a Donnan equilibrium between the myofibrilar and extra-myofibrilar regions of skeletal muscle due to the anionic contractile proteins (Stephenson et al., 1981). A non-uniform distribution of F^- such that it is partitioned to the extra-myofibrilar regions, may allow sufficient free Ca^{2+} to be released into the myofibrilar region to cause the slow contracture observed. This is entirely speculative, however, and it provides no information as to the mechanism which triggers the Ca^{2+} release in CsF solution. So it remains that sarcoball formation occurs easily in CsF solution by an uncertain mechanism and that ion channels can be recorded from the membrane.

3. ELEMENTARY PROPERTIES

3.1 Aims and Introduction

The anion channel from the sarcoball preparation has been investigated previously (Hals et al., 1989; Hals & Palade, 1990). In the present study, however, a modification of the original techniques was required to enable easy formation of sarcoballs from skeletal muscle of the cane toad, *Bufo marinus*. It was essential, therefore, to establish whether the same anion channel could be observed under these conditions. This channel also needed to be distinguished from any other anion channels that may be present from other internal membranes, as there is the possibility that the sarcoball preparation was not purely SR membrane. For example, the voltage-dependent anion selective channel (VDAC) from mitochondrial outer membrane (Colombini, 1986), the sarcolemmal anion channel (Blatz & Magleby, 1983; Woll et al., 1987; Stein & Palade, 1989) or the nuclear envelope anion channel (Tabares et al., 1991).

Characteristics useful in identifying the sarcoball anion channel include, (i) a large conductance of 505 pS in symmetrical 200 mM TrisCl, (ii) saturation of the channel conductance with increasing anion concentration, (iii) a bell-shaped voltage-dependence of the channel open probability, and (iv) a high selectivity for anions over cations (Hals et al., 1989). In addition, several blocking agents and protein modifiers were utilised to identify the anion channel. The stilbenes DIDS and SITS have been shown to have some interesting effects upon the sarcoball anion

channel, in particular DIDS modifies the voltage dependent gating of the channel (Hals & Palade, 1990).

3.2 Methods

Preparation

Sarcoballs were prepared from muscle fibres of *Bufo marinus*, as described in the previous Chapter. Skeletal muscle fibres were mechanically skinned in either CsF solution or in SIF. When skinned in the CsF solution, single fibres were obtained only from bundles of fibres placed freshly in CsF solution. These skinned fibres with sarcoballs were rinsed in nominally Ca^{2+} free TrisCl solution (100 mM, pH 7.4) to remove any CsF which would cause the precipitation of the Ca^{2+} that was normally present in the bath solution to aid seal formation. Sarcoball preparations were never kept longer than thirty minutes in the recording chamber before a seal was formed for recording. All experiments were conducted at room temperature (20-25°C).

Patch clamp recording techniques

Patch clamp pipettes were manufactured from borosilicate glass haematocrit capillaries (Modulohm IS) with a taper and tip diameter determined by a two stage process on a vertical pipette puller (model 720; David Kopf Instruments). Pipettes were coated with Sylgard (Dow Corning Corp.) and the tips then fire-polished to give a bubble number of between 3.2 and 4.2 (Corey & Stevens, 1983). With symmetrical 100 mM TrisCl solutions, the pipettes had tip resistances between 10 and 25 MΩ. The high resistance electrodes were used to increase the probability of obtaining patches containing a single anion channel.

Pipettes were passed through the air-solution interface with a positive pressure (20 cm H_2O) to prevent blockage of the pipette tip, after which the pressure was reduced. High resistance (10-80 GΩ) seals were able to be formed at the surface

of the sarcoball with the application of minimal suction; normally -4 cm of H_2O. All recordings were made on excised patches in the inside-out configuration of the patch clamp technique (Hamill et al., 1981). This configuration was used because (i) the sarcoball interior is of an unknown composition, and (ii) it allowed the inner surface of the patch to be exposed to various bath solutions. As the orientation of the patch membrane cannot be definitively related to its native position, all potentials are described as pipette potentials with the reference potential on the bath side. In many cases, the patch of membrane excised by the pipette was still connected to the sarcoball surface by a fine tether. These tethers could be disrupted by running a droplet of bath solution down the outside of the barrel of the pipette. Usually, rather than removing the patch pipette from the sarcoball surface and then disrupting any tether that may have formed, a droplet of solution was run down the pipette barrel while still attached to the sarcoball surface to produce an excised patch.

Single channel currents were recorded using a List EPC-7 patch-clamp amplifier (List Medical). The combined random background noise from the recording apparatus and the detached patch was within the range of 260 to 320 fA RMS, with the channel in the closed state, at a bandwidth of 10 kHz (-3dB). Steady state recordings were taken from the 10 kHz low pass filtered output of the EPC-7, passed through a pulse code modulator (VR-10, Instrutech Corporation) and the signal stored using a video cassette recorder (National VCR) for off-line analysis at a later stage. During play-back for inspection or analysis, current signals were filtered at 1 kHz (-3dB) with an eight-pole Bessel filter (AI 2040, Axon Instruments) and collected at a sampling frequency of 5 kHz.

Single channel current-voltage (I-V) relations were routinely determined by a voltage stepping protocol. Recordings were made using pCLAMP software (version 5.5.1, Axon Instruments) with a LABMASTER TL-1 interface to generate voltage-step waveforms and simultaneously collect data on a microcomputer

(80286, IBM compatible). From a holding of 0 mV, six episodes of voltage steps were applied to the patch. Each voltage step episode was 900 ms in duration and began at ±10 mV, incrementing by 10 mV each episode to reach ±60 mV, returning to the holding potential for 200 ms between episodes. Current traces were filtered at 500 Hz (-3dB) and collected at a sampling frequency of 1 kHz.

Patch clamp recordings were made in a chamber within a central well of volume 150 µl, which could be flooded from an outer concentric ring of volume 1 ml to effect rapid solution changes. Both the Ag/AgCl wire of the patch electrode and the Ag/AgCl pellet for the ground reference electrode were exposed to the same solution (generally 100 mM TrisCl). An agar bridge of 100 mM TrisCl was used to make the electrical connection between the Ag/AgCl ground reference electrode and the bath solution. In some cases where recordings were made continuously in solutions of a constant composition, a simple Ag/AgCl wire inserted directly into the bath was used as the ground electrode. Junction potentials were calculated from the generalised Henderson liquid junction potential equation, as modified by Barry and Diamond (1970), using the JPCalc software (P.H. Barry, School of Physiology and Pharmacology, University of New South Wales, Sydney, Australia). All current-voltage relationships and reversal potentials were corrected for any junction potential offsets.

Selectivity of the channel

The selectivity of the channel for anions against cations was determined from reversal potential (E_{rev}) measurements made with KCl solutions. The protocol used was to form patches in symmetrical 100 mM KCl solutions and then exchange the bath solution to either 30 mM KCl or 200 mM KCl. The ground reference electrode in these experiments was electrically connected to the bath via 100 mM KCl and a 100 mM KCl agar bridge. Permeability ratios were calculated using the equation:

$$E_{rev} = RT/F \ln\{(P_{Cl}[Cl^-]_b + P_K[K^+]_p)/(P_{Cl}[Cl^-]_p + P_K[K^+]_b)\} \qquad (3.1)$$

where E_{rev} is the reversal potential, R is the gas constant, T is the temperature in degrees Kelvin, F is Faraday's constant, P_{Cl} is the permeability to Cl^-, P_K is the permeability to K^+, and the subscripts b and p indicate the concentrations in the bath and pipette, respectively. A value of 25.4 mV for RT/F at 22°C was used in all calculations.

Solutions

At the beginning of this study, recordings were made with symmetrical 200 mM TrisCl solutions, pH 7.4, with 2 mM Ca^{2+} (as Ca MOPS; 3-morpholino-propanesulfonic acid) added to the bath solution to aid giga-ohm seal formation. Under these conditions, results could be directly compared with those of Hals et al. (1989, 1990). For the major part of this study, the standard recording solutions were symmetrical 100 mM TrisCl, pH 7.4, again with the bath containing an additional 2 mM Ca MOPS. The free Ca^{2+} concentration within the pipette solution was not controlled, and is considered nominally Ca^{2+}-free.

Chemicals

MOPS and anthracene-9-carboxylic acid (A-9-C) were purchased from Aldrich Chemical Co. Tris base, $ZnCl_2$, DIDS and SITS were purchased from Sigma Chemical Co. Sodium perrhenate was purchased from Koch-Light Laboratories Ltd. Niflumic acid was kindly provided by Squibb. Meclofenamic acid and flufenamic acid were kindly provided by Parke-Davis Co.. All other chemicals were of analytical grade.

A 10 mM aqueous stock was made up for both DIDS and SITS, neutralised with NaOH, which were protected from the light. Niflumic, meclofenamic and flufenamic acids and A-9-C were made up as aqueous stocks neutralised with NaOH.

Analysis of results

Single channel amplitudes were measured manually from currents resulting from the voltage-step protocol and were used to produce I-V relationships, from which the slope conductance was determined. Mean current relaxation traces were obtained from ensemble averages of 15 trials for each episode, which were then corrected for the seal leakage conductance and expressed in terms of the channel open probability. The open probability, P_O, was determined from the mean ensemble current, I, using $P_O = I/(i \,.\, N)$, where N is the number of functional channels in the patch and i is the unitary conductance. The number of functional channels in the patch was estimated from the peak current at the beginning of the voltage step. Initially, this was checked against the binomial estimation from the variance of the averaged current (data not presented). Both methods agreed very well, and so for simplicity and ease, the peak current estimate was routinely used..

An estimate of the steady-state open-probability was obtained from the average P_O in the last 50 ms of each episode. These values were plotted against the episode potential to give the voltage-dependent open-probability, (V), curve. A Boltzmann equation of the form

$$P_O(V) = 1/\{1+\exp[(zF/RT)(V-V_0)]\} \qquad (3.2)$$

could be fitted to each half of the $P_O(V)$ curve, where R, T and F have their usual values as for Equation (3.1), V is the applied potential and V_0 is the potential at which half the channels are open (ie. $P_O(V) = 0.5$). From this fit, an estimate of the effective gating charge, z, can be obtained from the steepness of the curve. Curve fitting was performed by the InPlot software (GraphPad Inc., version 4.03) which utilises the Levenberg-Marquardt algorithm for the method of non-linear least-squares, assessed by the chi-squared statistic. All appropriate numerical data are given as mean ± standard error of the mean (SEM).

3.3 Results

Sarcoballs on the surface of mechanically skinned muscle fibres ranged in size from 10 to 150 µm in diameter. Generally, the larger ones of approximately 80 to 100 µm were selected for patch clamping. They present a very fluid surface when touched by microelectrodes for patch clamp recordings and, unlike sarcolemmal vesicles, the structure does not collapse when it is punctured by a microelectrode.

Channel activity

A large conductance anion channel was found in 94% of all detached patches formed in symmetrical 100 mM TrisCl. The number of channels present in a patch ranged from 1 to 9 and an example of a multi-channel recording in shown in Figure 3.1. The activity of the channel recorded in excised patches remained similar throughout the recording period. The lifetime of patches was as short as 5 minutes, and in very few cases as long as 1.5 hours, though typically patches lasted 30 minutes, under constant conditions. The anion channel exhibited a linear I-V relationship, with a slope conductance of 558 ± 22 pS (n=6) in symmetrical 200 mM TrisCl, which is similar to the conductance of 505 pS reported by Hals et al. (1989) under the same conditions. Since patches generally contained more than one channel, recordings made in symmetrical 200 mM TrisCl would often overload the patch-clamp amplifier. To avoid this, standard recordings were made in symmetrical 100 mM TrisCl. Under these conditions, the channel also exhibited a linear I-V relationship, with a slope conductance of 274 ± 5 pS (n=25). An example of I-V relationships obtained in symmetrical 200 and 100 mM TrisCl are shown in Figure 3.2A. The same behaviour was observed for sarcoball membranes prepared by mechanically skinning in SIF (data not shown) as for those prepared by mechanically skinning in CsF. All results presented here are from sarcoballs formed by mechanically skinning in CsF.

Channel activity could often be seen at a test potential of +10 mV, immediately after formation of a seal onto the surface of the sarcoball. Frequently, upon

detaching the patch, the channel activity would no longer be present at +10 mV. This appeared to be associated with the presence of a tether or a small vesicle at the pipette tip, and by switching the recording to current clamp mode, a potential was recorded which drifted between -20 to -110 mV (always a negative potential). Consistent with this, when the pipette potential was driven in voltage clamp mode to a potential greater than +20 mV, channel activity was observed. This was interpreted as driving the patch to an effective membrane potential near 0 mV, where channel openings are more frequent. Shifting the pipette potential to greater than +40 mV would often result in a large burst of activity which would then persist after returning to 0 mV and was not inactivated by time spent at large negative pipette potentials. In these cases, individual single channel events could not be distinguished, possibly because there were large numbers of active channels in the patch. The patch also exhibited less voltage dependent behaviour, as assessed by the fraction of channels open at the end of a 900 ms voltage step (see section on voltage dependence). In other cases, shifting to a potential greater than +40 mV would result in a burst of activity, closely followed by losing the giga-ohm seal on the patch of membrane. All results presented here are from patches where there was no obvious tether present during the recording.

Conductance and selectivity

The selectivity of the anion channel for Cl^- over K^+ ions was determined from the shift in reversal potential measured from patches initially formed in symmetrical 100 mM KCl and the bath solution then exchanged to either 30 mM KCl or to 200 mM KCl (Figure 3.2B). The reversal potentials recorded for this channel were +22.3 mV (range 21.8 mV to 22.7 mV, n=3) for 30 mM KCl and -16.9 mV (range -16.3 mV to -17.3 mV, n=3) for 200 mM KCl. The potentials calculated from the Nernst equation for Cl^-, are +30.6 mV and -17.6 mV for 30 mM and 200 mM KCl respectively. Solving the Goldman-Hodgkin-Katz equation with the measured

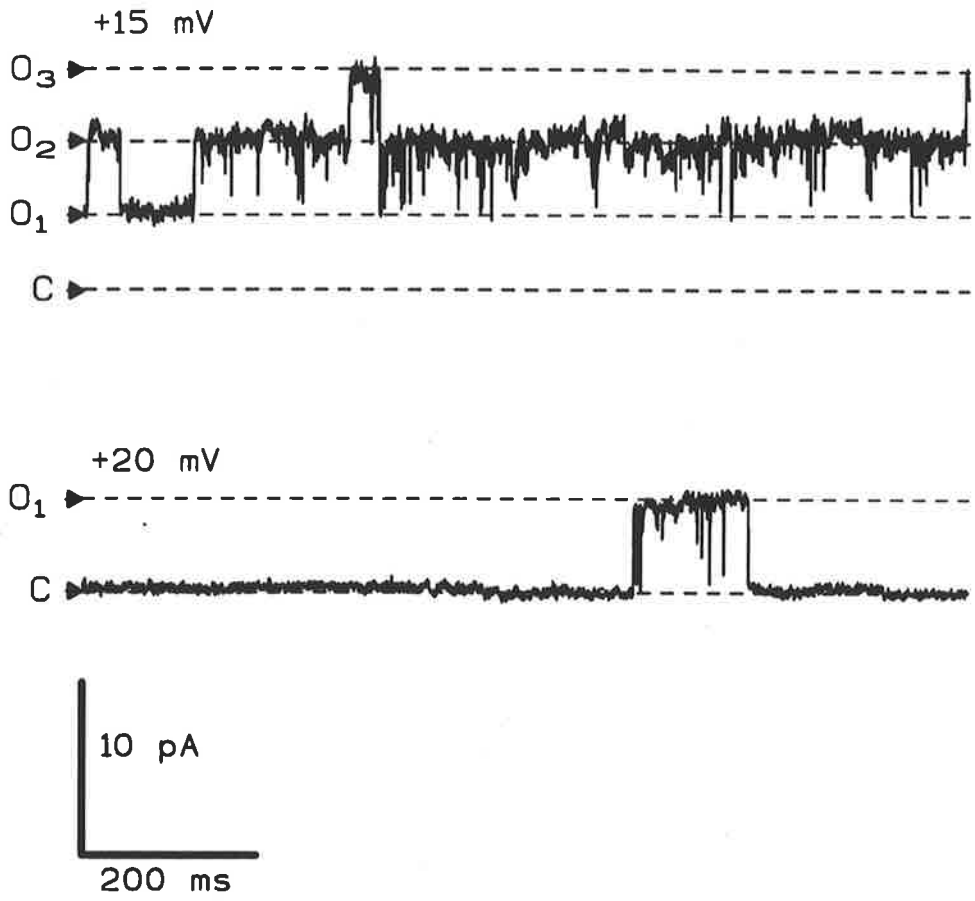

Figure 3.1 Multi-channel recording of sarcoball anion channels.
The majority of patches formed on sarcoball membrane contained more than one channel. The current recordings shown here were from a patch where three channels could be distinguished. The dashed lines are spaced at equal intervals, equivalent to the unitary current predicted from the slope conductance of 280 pS. The voltage dependent nature of the channel meant that at small potentials most of the channels were open at any one time and very rarely were complete closures observed, where no channels were open. This is illustrated by the recording made at +15 mV. The contribution of substate activity from each of the channels present meant that in some parts of the recording the current amplitude was less than that expected from the unitary conductance. With an increase in the potential, the activity was significantly reduced and open events were briefer resulting in recordings like that shown for +20 mV. Since the openings are shorter, there were fewer channels open simultaneously, and so although three channels were still present, only one unitary conductance level could be distinguished at +20 mV.

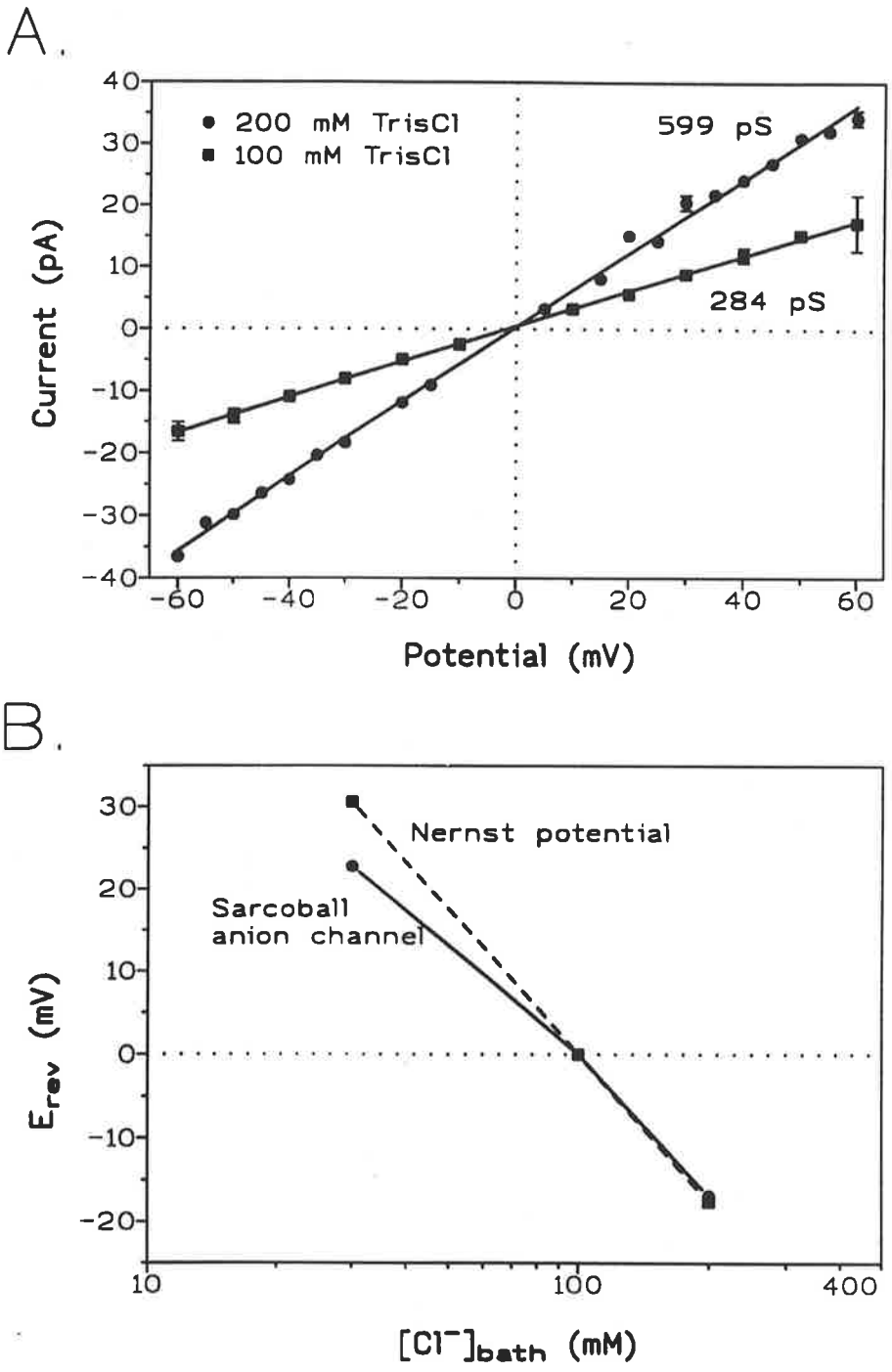

Figure 3.2 Anion channel conductance and selectivity.
A. Examples of I-V relations recorded from two separate patches, one in symmetrical 200 mM TrisCl with a slope conductance of 599 pS, the other in symmetrical 100 mM TrisCl with a slope conductance of 284 pS. B. The anion/cation selectivity of the channel was determined from the shift in reversal potential in the presence of a KCl gradient, with 100 mM KCl in the pipette. The reversal potential is plotted here against the Cl^- concentration in the bath solution. For a comparison, the Nernst potential for Cl^- ions at each concentration is also plotted on the same axes.

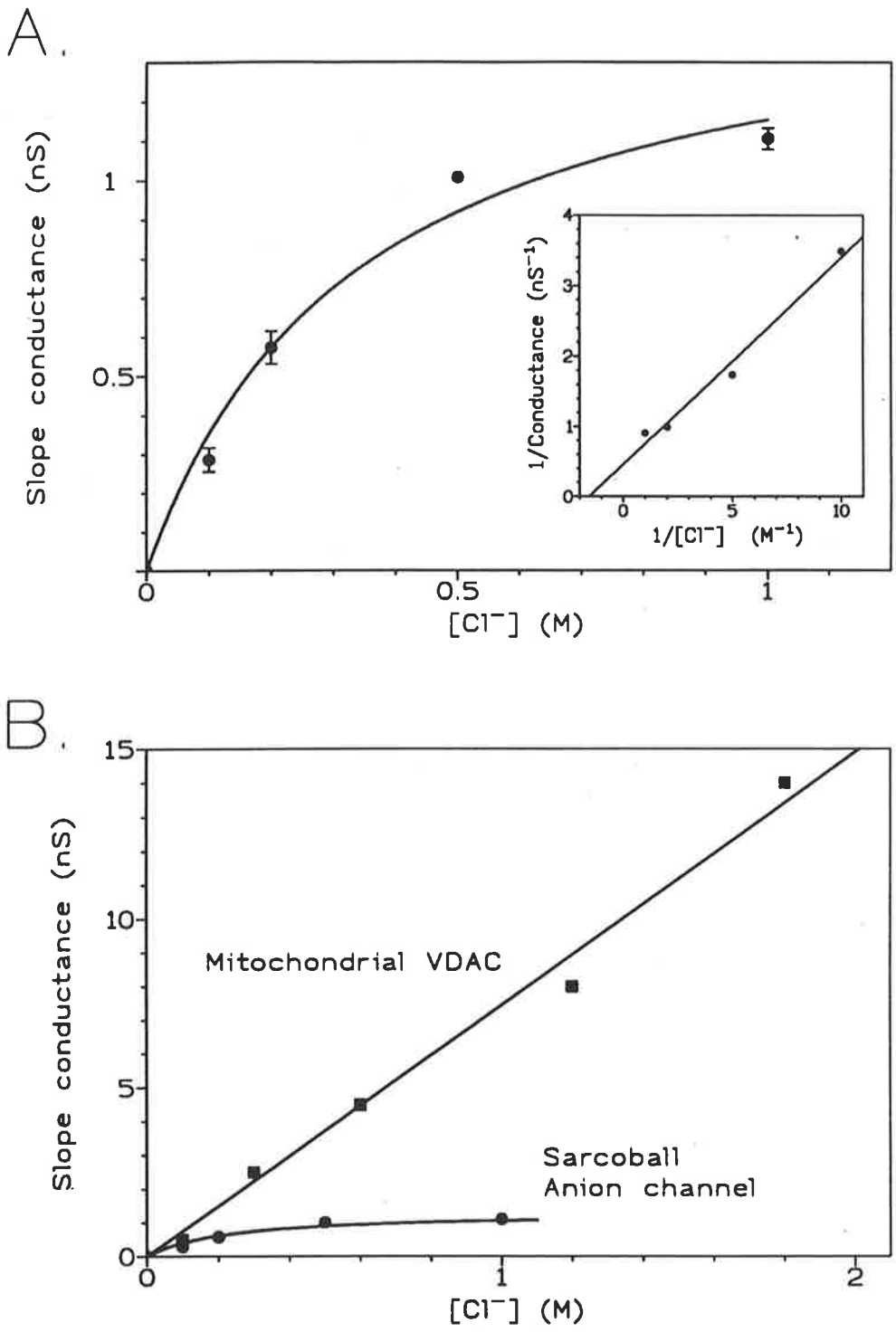

Figure 3.3 Saturation of the anion channel conductance.
The sarcoball anion channel conductance saturates with increasing chloride ion concentration. **A.** The conductance values recorded from symmetrical 100, 200, 500 and 1000 mM TrisCl are plotted along with the Michaelis-Menten curve fit which gave a maximum conductance of 1545 pS and an apparent K_m of 385 mM. The inset shows the linear nature of the data as a double reciprocal plot. **B.** For comparison, the same saturating conductance data of the anion channel recorded here is plotted on the same axes along with data for the VDAC recorded in planar bilayers (data taken from Colombini, (1986), Figure 1). The mitochondrial VDAC conductance continues to increase in a linear fashion with increasing chloride concentration.

reversal potentials gives an estimated P_{Cl}/P_K of 7.5 for 30 mM KCl and 53 for 200 mM KCl.

The slope conductance was determined from measurements of the I-V relation at a range of symmetrical TrisCl concentrations: 100 mM (274±5.2 pS, n=25), 200 mM (558±22 pS, n=6), 500 mM (1008±16 pS, n=3) and 1000 mM (1105±26.7 pS, n=3). A Michaelis-Menten equation was able to be fitted to these mean values, which saturated at 1545 pS, with an apparent K_m value of 385 mM (Figure 3.3A). A comparison between the concentration dependence of conductance for the mitochondrial voltage-dependent anion channel (VDAC) and the anion channel recorded here, is presented in Figure 3.3B to illustrate the differences between these two channels.

Voltage dependence

A step potential protocol was run at the beginning of each experiment to determine both the slope conductance and the voltage dependence. In multi-channel patches, step changes in potential from 0 mV resulted in a peak current corresponding to the total number of active channels present in the patch, with channels then closing in a staircase-like manner over the 900 ms duration of the pulse (Figure 3.4). Channel closure was voltage dependent, with the staircase-like closure becoming more pronounced for positive and negative potentials greater than ±20 mV (Figure 3.4). Sequential recordings from the same patch were used to produce mean ensemble currents for each step potential (Figure 3.5A). Ensemble currents were then expressed as time-dependent open probability plots (Figure 3.5B and C). From data such as this, voltage-dependent open-probability, $P_O(V)$, curves were obtained (Figure 3.6). These $P_O(V)$ curves were generally bell-shaped and centred about 0 mV in symmetrical solutions. The $P_O(V)$ decreases with larger steps in potential away from 0 mV, via a "switching region", where there is a transition from a high P_O to low P_O. It was found that patches containing many channels produced a broader $P_O(V)$ curve

which was less voltage-dependent compared to those obtained with fewer channels present (Figure 3.6A). Although, this was not always the case, as some patches with only one or two channels also had a broader $P_O(V)$ curve. A Boltzmann equation was fitted to each half of the $P_O(V)$ curves obtained from 10 individual experiments. The steepness of the $P_O(V)$ curve is indicated by the gating charge value, z, and the width of the curve is indicated by the potential, V_0, at which half of the channels are open. At positive potentials, the z values ranged from 1.3 to 12.2, while the values for V_0 ranged from 11.7 mV to 48.3 mV. Similarly, at negative potentials, the z values ranged from -1.1 to -10.2 and the V_0 values from -10.4 mV to -43.8 mV. The $P_O(V)$ curves obtained from individual patches were generally symmetrical, though there were some which were less voltage-dependent on one half of the curve compared to the other. Among those cases where this asymmetrical behaviour was observed, skew occurred toward positive potentials as frequently as it did toward negative potentials. The data from 10 individual patches is shown as the mean $P_O(V)$ curve in Figure 3.6B.

Subconductance states

Numerous subconductance states (substates) were observed in the behaviour of the anion channel. The most active of these was a small substate which was entered from the main open state of the channel, reducing the conductance to 235 pS, approximately 85% of the main conductance level. A second prominent substate was also observed at approximately 60% of the main conductance level. Figure 3.7 highlights sections of single channel traces with substate behaviour from a representative patch. The majority of substate activity appeared to be entered with transitions from the main open conductance level and exited with transitions back to the same open level. Some transitions between the closed state and substates were also observed.

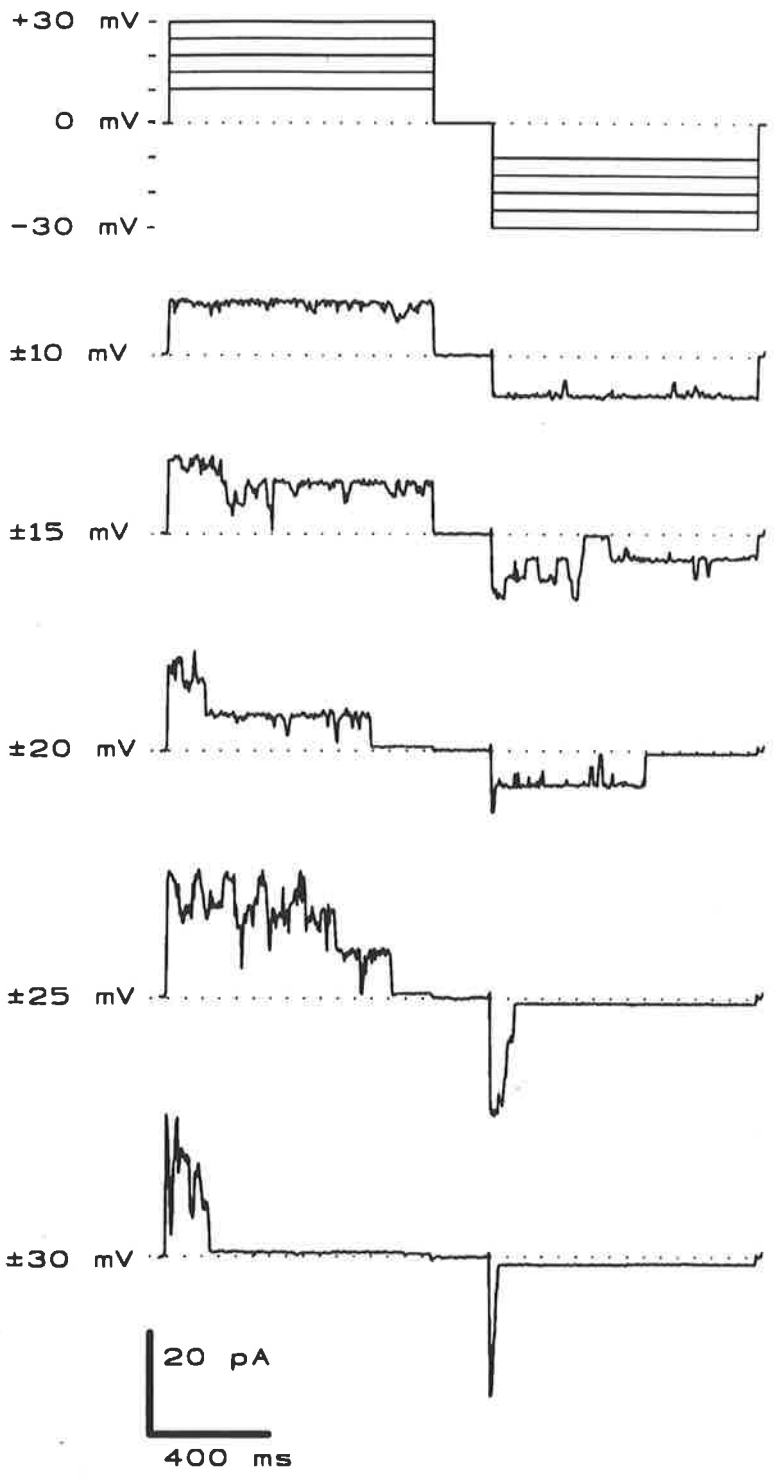

Figure 3.4 Multi-channel recordings from applied voltage steps.
Examples of current recordings made from multi-channel patches in response to the voltage-step protocol routinely applied to membrane patches. At the onset of the step potential, all active anions channels in the patch are open and at small potentials remain open for most of the 900 ms voltage-step. With an increase in the magnitude of the step potentials (both positive and negative), the channels begin to close more frequently. At large potentials, the channels are open at the beginning of the voltage-step and then close in a staircase-like manner.

Figure 3.5 Ensemble currents and open-probability plots.
Current recordings were made from an excised patch in standard solutions in response to the step-potential protocol. **A**. Mean ensemble currents were obtained from 15 sequential recordings at each potential, from a patch containing two channels. Each ensemble current was then expressed as an open-probability plot, according to $Po=(I)/(i \cdot N)$, where I is the mean current, i is the unitary conductance, N is the number of active channels in the patch and Po is the open probability. These are shown in **B**. for the positive potential steps and in **C**. for the negative potential steps. At small potentials, the open-probability remains near 0.8 to 0.9 for the entire duration of the step potential. As the magnitude of the step potential increases, there is a relaxation in the open-probability plots. For all relaxations, the initial level of open-probability is similar, although slightly less for larger potentials, indicating a similar level of activation while at the holding potential immediately before the onset of the voltage step.

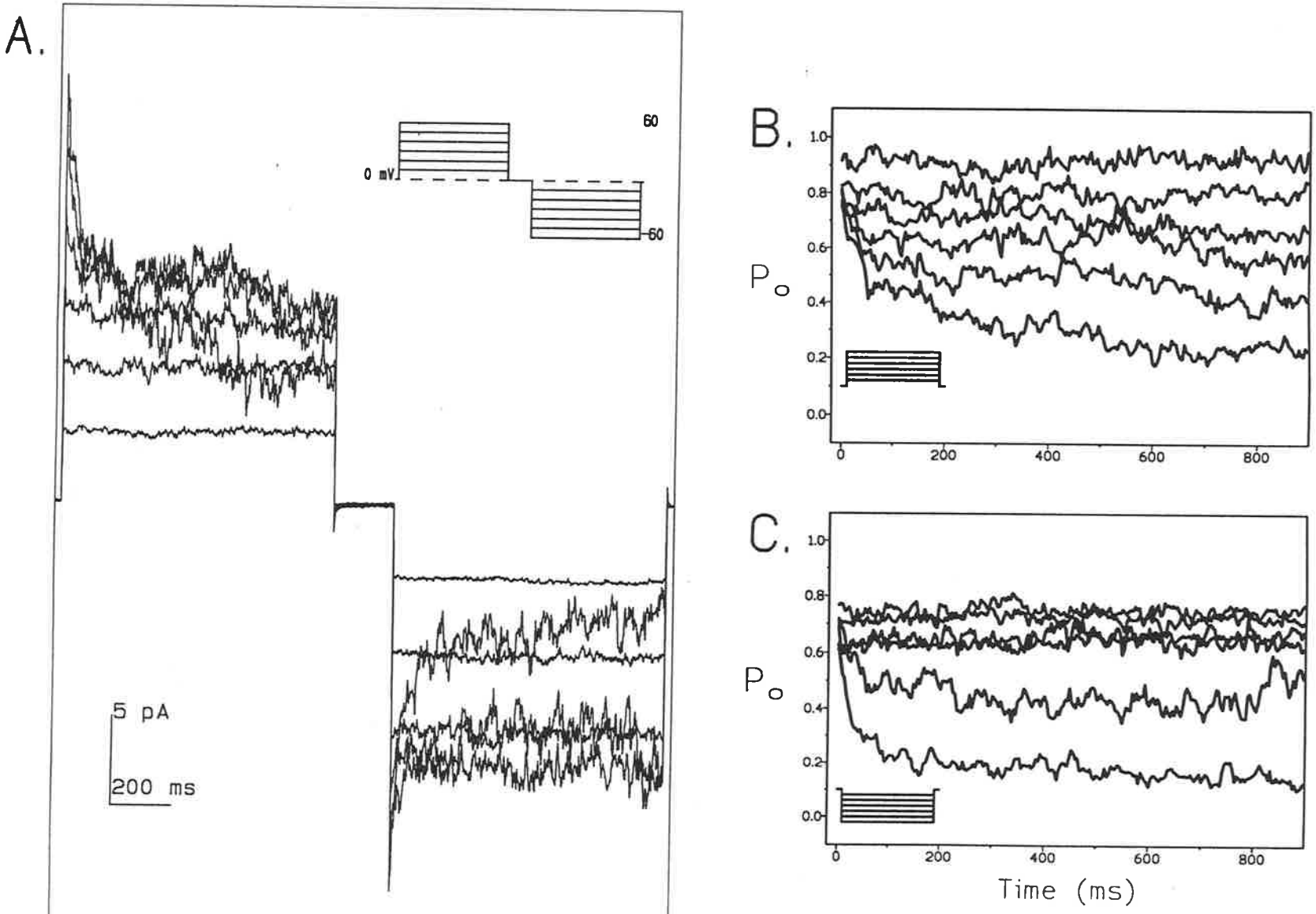
A.
60
0 mV
-60
5 pA
200 ms
B.
Po
1.0
0.8
0.6
0.4
0.2
0.0
0
200
400
600
800
C.
Po
1.0
0.8
0.6
0.4
0.2
0.0
0
200
400
600
800
Time (ms)

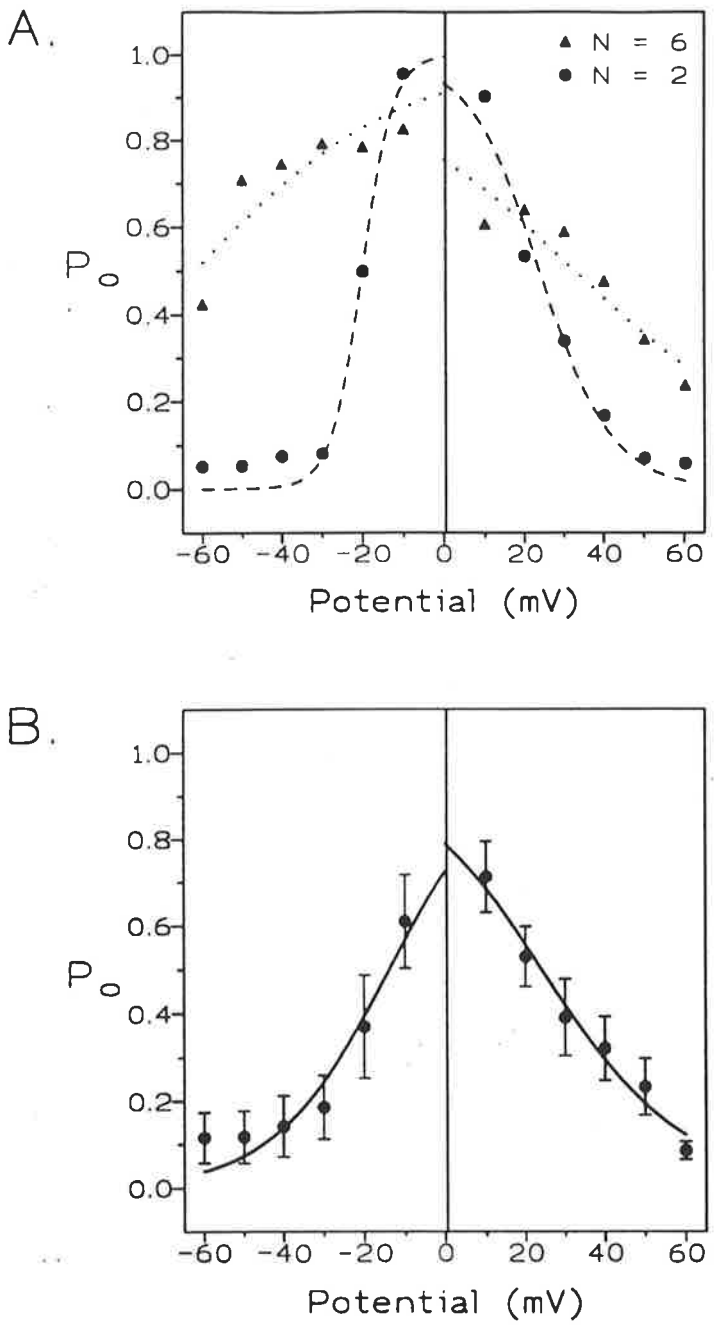

Figure 3.6 Voltage dependent behaviour of the anion channel.
The estimated pseudo-steady-state open-probability in the last 50 ms of each step potential were used to produce *Po(V)* curves. **A.** A comparison is made between the broader *Po(V)* curve obtained from a patch containing 6 channels (triangles) to that obtained with only two channels in the patch (circles). A Boltzmann fit was obtained for each set of data, and with 6 channels in the patch (dotted line) the gating charge values, z, were -0.94 and 0.87, with V_0 values of -62.1 mV and 32.9 mV for negative and positive potentials, respectively. With only two channels present (dashed line), z values were -6.5 and 2.2 with V_0 values of -20.1 mV and 21.7 mV for negative and positive potentials, respectively. **B.** Mean *Po(V)* curve obtained from 10 patches. A Boltzmann equation fit was obtained for each half of the mean *Po(V)* curve and the value of z obtained from the fit was -1.8 ± 0.3 and 1.4 ± 0.1, with V_0 values of -13.9 ± 2.4 mV and 24.1 ± 1.5 mV for negative and positive potentials, respectively.

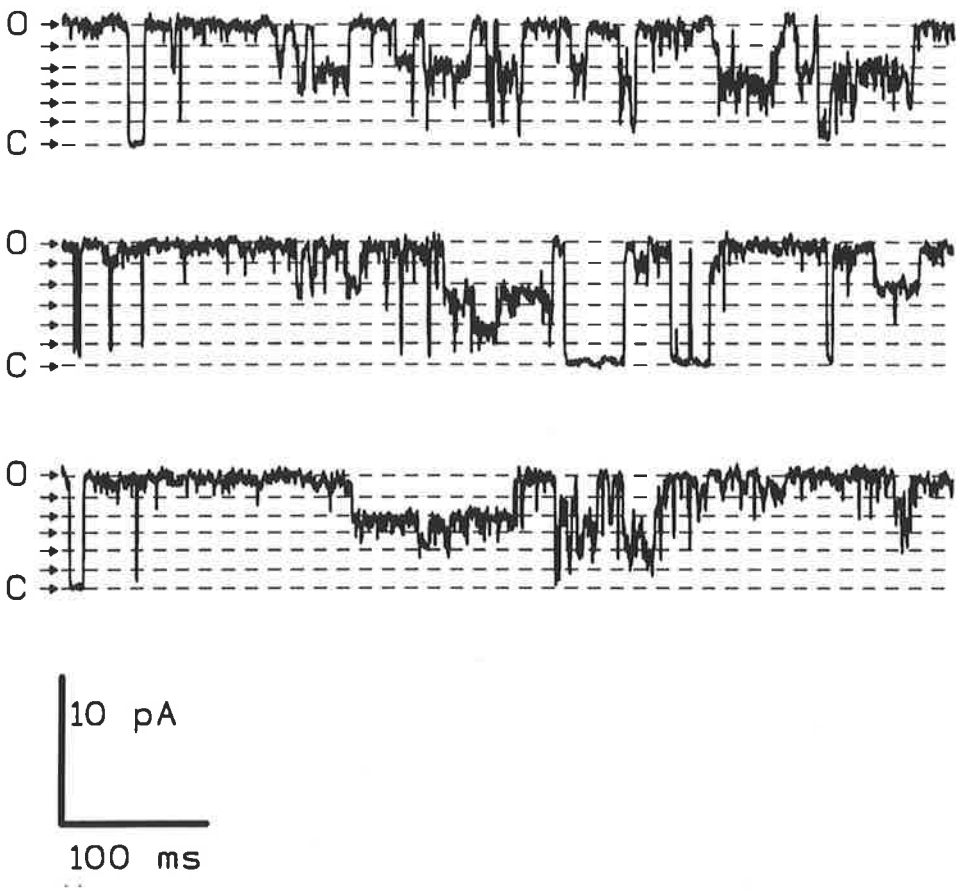

Figure 3.7 Numerous subconductance states of the anion channel.
Numerous subconductance states were observed in the channel recordings. Here, examples are shown of transitions to 5 different subconductance levels, indicated by the dashed lines, between the fully open (O) and fully closed (C) levels. The dashed lines were drawn by eye and approximate the levels at which substate events could be discerned in each individual panel.

Modifiers of channel behaviour

a) Stilbene derivatives

Figure 3.8A shows currents recorded before, during and after a multi-channel patch was exposed to 1 mM DIDS in 100 mM TrisCl. Upon exchanging to the DIDS solution, the open events were shorter, less frequent and often had a flickering appearance. There was also a significant decrease in the channel conductance (Figure 3.8B), with the mean conductances from 3 individual experiments decreasing from 253±12 pS (range 232 to 273 pS) to a conductance of 92.7 ±17pS (range 64 to 124 pS). The voltage dependence of the open probability was shifted such that the bell-shaped curve was centred over -40 mV (Figure 3.9) and the maximal P_O was reduced to only 0.37. While the flickering behaviour was reversible upon washing out the DIDS, the changes in the voltage-dependent open probability and slope conductance (85.8±17 pS; range 56 to 114 pS) were not reversible (n=3 out of 3), even washing with three complete exchanges of the bath volume.

Figure 3.10A shows currents recorded from a different multi-channel patch before, during and after the application of 1 mM SITS in 100 mM TrisCl. A flicker block of the channel open events was observed immediately upon exchanging to SITS. There was a decrease in the slope conductance from 265±15 pS (range 236 to 286 pS) to 145±22 pS (range 107 to 183 pS) and there were fewer channels open at all potentials. Unlike the effect of DIDS, the slope conductance of the channel recovered (n=3 out of 3), to 251±23 pS (range 208 to 283 pS) upon removal of SITS from the bath. Figure 3.10B shows an example of the effects upon conductance. In only 2 out of the 3 patches did the open-probability of the channels fully recover.

b) Negative results

Several agents known to block the sarcolemmal anion channel or other types of large conductance anion channels from other membranes were tried on the

sarcoball anion channel here. The aromatic acids, A-9-C (2.25 mM, n=3), and niflumate (n=3), flufenamate (n=4) and meclofenamate (n=3), each at 50 μM, had no effect upon the slope conductance or voltage dependence of the anion channel. Cationic zinc (as $ZnCl_2$; 5 mM, n=4) and anionic perrhenate (as $NaReO_4$; 10 mM, n=3) also had no effect upon the channel.

The free Ca^{2+} concentration in the bath solution was varied between nominally Ca^{2+} free, up to 2 mM and no change in the anion channel conductance or gating was observed. The presence of 2 mM Ca^{2+} in the pipette solution also had no effect.

Application of a specific antibody to the mitochondrial VDAC (a gift from Dr V. DePinto) at a dilution of 1:200 (the same dilution used in immunogold labelling studies; see Chapter 6) in 100 mM TrisCl had no observable affect upon the anion channel activity (n=3).

3.4 Discussion

The large conductance voltage-dependent anion channel, described here, exhibits characteristics which indicate that it is a similar anion channel to that previously recorded by Hals et al. (1989, 1990). The presence of tethers or small vesicles at the tip of patch electrodes has not been previously reported with respect to sarcoballs. The large burst of activity that occurred upon applying large positive pipette potentials to silent patches is not thought to be due to induction of dormant channels. Rather, the evidence suggests that in these cases, it is due to a vesicle at the tip of the pipette and that one of the membranes of the vesicle breaks down at the high pipette potential, so that either channel activity appears or the giga-ohm seal is broken. Comparison with other reports of channel induction supports these ideas. For example, induction of anion channels is observed in the surface membrane of single, enzymatically isolated frog toe muscles (Woll et al., 1987) and of cultured rat myotubes (Blatz & Magleby, 1983). In these

Figure 3.8 Irreversible modification of conductance by DIDS.
Application of 1 mM DIDS to the bath surface of sarcoball patches had irreversible effects upon the conductance and voltage dependent behaviour of the anion channel. **A.** Examples of current recordings from a patch containing two channels, before, during and after the application of DIDS, in response to a ±30 mV step protocol. Open events were less frequent and shorter in the presence of DIDS. As shown by the I-V relations in **B**, the conductance was substantially reduced, from 274 pS to 64 pS

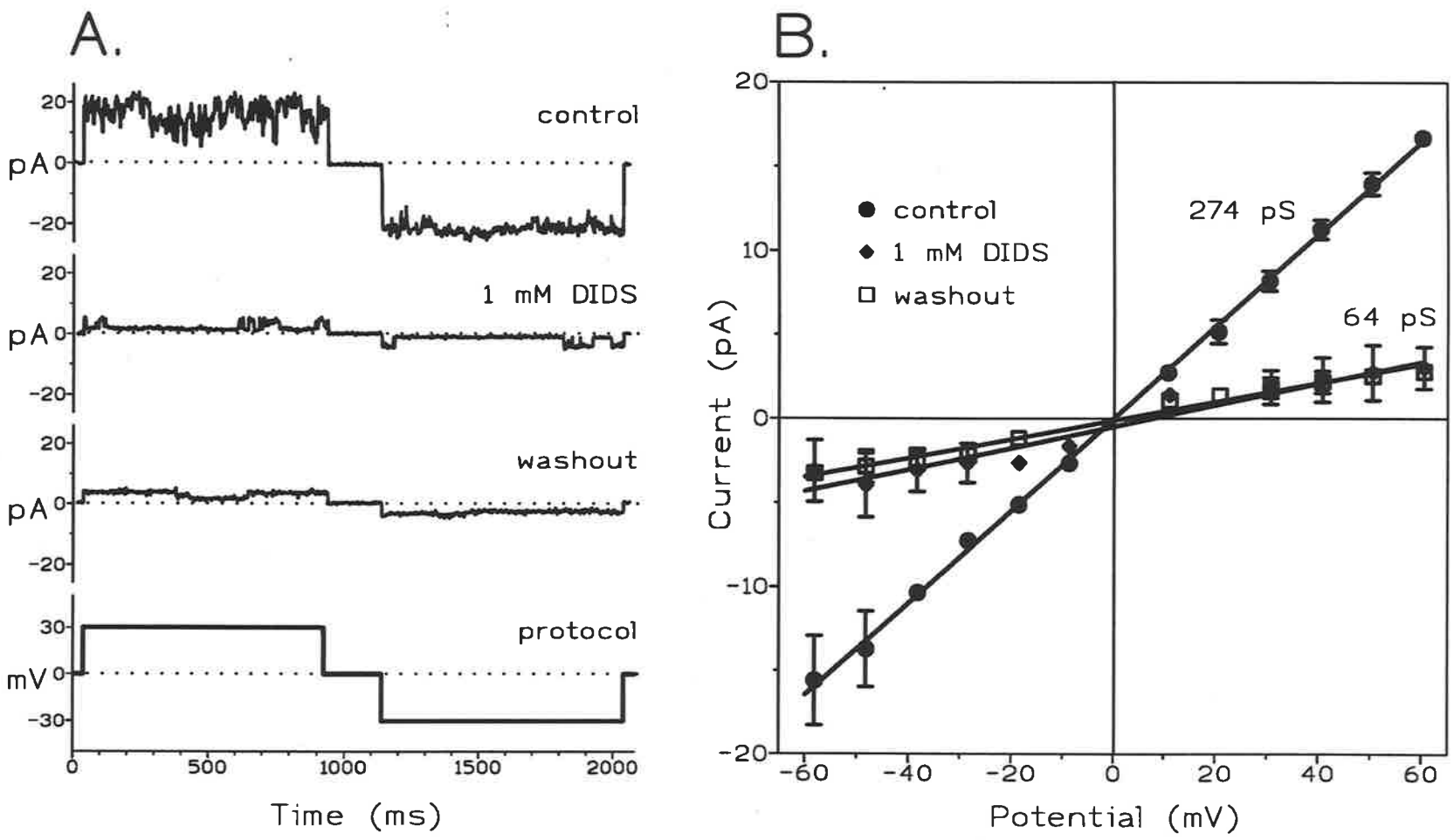
A.
control
1 mM DIDS
washout
protocol
pA
mV
20
0
-20
30
-30
0
500
1000
1500
2000
Time (ms)
B.
control
1 mM DIDS
washout
274 pS
64 pS
Current (pA)
Potential (mV)
20
10
0
-10
-20
-60
-40
-20
0
20
40
60

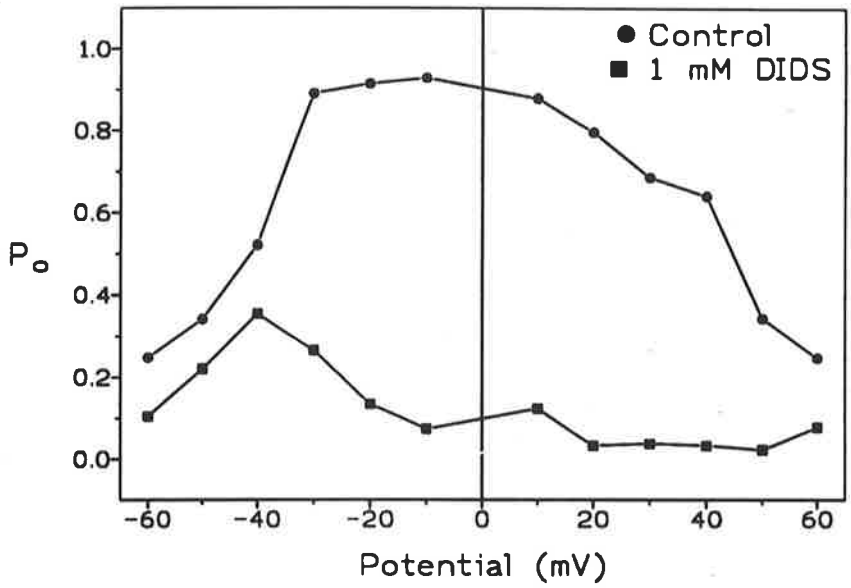

Figure 3.9 DIDS shifts the channel open probability.
The voltage-dependent open-probability of the anion channel was irreversibly modified by the application of 1 mM DIDS. The example shown here has a broad *Po(V)* curve in the control situation, which was often the case for multi-channel patches. In the presence of 1 mM DIDS the *Po(V)* curve was shifted to the left (more negative potentials) and the maximum *Po* was considerably reduced from a control value of 0.92, to a value of 0.37.

Figure 3.10 Reversible reduction of conductance by SITS.
Immediately upon the application of 1 mM SITS to the bath surface of a sarcoball membrane patch, flicker block behaviour of the anion channel was observed, which was reversible upon removal of SITS from the bath. **A.** Examples of current recordings from a patch containing two channels, before, during and after the application of SITS, in response to a ±30 mV step protocol. The reversible effects upon the channel conductance are shown by the I-V relations in **B.** The single channel conductance is reduced to 148 pS in the presence of SITS and returns to the control conductance of 274 pS upon wash-out from the bath.

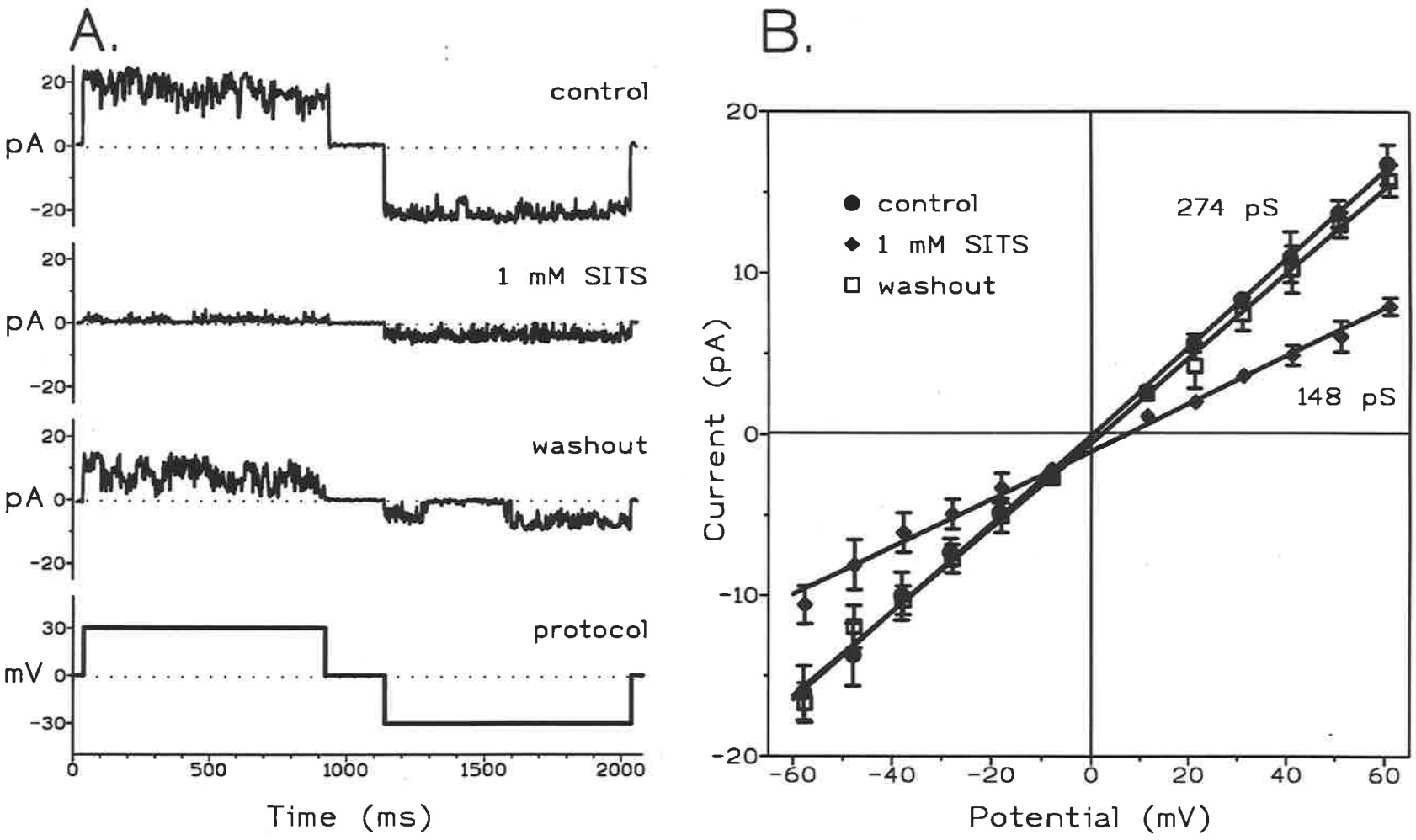
A.
control
1 mM SITS
washout
protocol
pA
mV
20
0
-20
30
-30
0
500
1000
1500
2000
Time (ms)
B.
control
1 mM SITS
washout
274 pS
148 pS
Current (pA)
Potential (mV)
20
10
0
-10
-20
-60
-40
-20
0
20
40
60

preparations, induction occurs upon depolarising the surface membrane to +50 mV for the cultured myotubes and >+20 mV for the toe muscles. The length of time required for induction varied from seconds to minutes. The phenomenon was found to be reversible by holding the patch at hyperpolarising potentials more negative than -70 mV. The burst of activity observed here was not reversible by hyperpolarising, which argues against induction occurring in this case.

Conductance and selectivity

The channel conductance was found to be higher at all anion concentrations compared to Hals et al. (1989). Whereas Hals et al. (1989) found the conductance to saturate at concentrations greater than 500 mM TrisCl, reaching an estimated maximum conductance of 617 pS with a K_m value of 77 mM, here the conductance continued to increase, reaching an estimated maximum conductance of 1545 pS and a K_m value of 385 mM. A saturable conductance is thought to be due to movement of ions through the channel pore occurring in a single file manner, with possibly either a single or multiple binding sites (Hille, 1984). The movement of an ion through a channel pore can be considered in terms of an energy profile, with the binding sites represented as energy wells separated by energy barriers which must be overcome for permeation. The depth of the energy wells is reflected in the K_m value and the magnitude of the largest energy barrier is reflected in the maximum conductance value (Labarca et al., 1980; Hille, 1984). Thus, the behaviour of the anion channel recorded here suggests that the pore has shallower energy wells and smaller energy barriers, allowing the anions to permeate the pore more rapidly, and saturate at larger concentrations in comparison to the anion channel recorded by Hals et al. (1989). These differences might be due to species differences between the frog, *Rana catesbeiana*, and the cane toad, *Bufo marinus*. Alternatively, if the channel is regulated in some manner in the SR, it may represent differences in the pore properties that are

dependent upon the regulated state of the anion channel, which might be different in these two studies.

The values obtained for the P_{Cl}/P_K permeability ratio are consistent with an anion selective channel. The reduced selectivity ratio with 30 mM KCl in the bath and 100 mM KCl in the pipette might reflect a concentration dependence of the permeability ratio. Sodium channels from the squid axon exhibit a concentration dependence of permeability ratios under biionic conditions at low ion concentrations (Begenisich & Cahalan, 1980). In the present case, the reduced permeability ratio seen with 30 mM KCl in the bath may either be due to K^+ blocking the exit site of the channel pore or to K^+ actually permeating the channel pore in the opposite direction to Cl^-. In terms of pore theory, K^+ may bind to a site in a pore but face a very large energy barrier which may not be able to be traversed. It may also indicate a mechanism of anion permeation in conjunction with a cation in a similar manner to that proposed by Franciolini and Nonner (1987) for an anion channel in hippocampal neurones.

Voltage Dependence

The open probability of the anion channel recorded here exhibits a steep voltage dependence with a high P_O near unity centred around 0 mV and decreasing for both positive and negative potentials. This same bell-shaped voltage-dependence was observed in sarcoball anion channels by Hals et al. (1989) and is a distinctive characteristic of many other high conductance anion channels recorded in other tissues (Schein et al., 1976; Blatz & Magleby, 1983; Schneider et al., 1985; Schlichter et al., 1990; Groschner & Kukovetz, 1992). An estimate of the effective gating charge was obtained by using the Boltzmann equation to fit either the positive or negative shoulder of the bell-shaped curve. Assuming that the gating charge, z, moves across the entire width of the membrane, the charge is 1.4 at positive potentials and -1.8 at negative potentials, from the $P_O(V)$ curve of the pooled data (average of 3.5 ± 0.85 channels per patch, n=10). Individual experiments had

values as large as 12.2 where only two or three channels were present in the patch. The values from the pooled data are smaller than the gating charge of 12 estimated by Hals et al. (1989) and correspond with the broader $P_O(V)$ curve observed here with multiple channels in the patch. These values from the pooled data are small even in comparison to other anion channels or other voltage dependent channels; for example 6 for the Na^+ channel and 4.9 for the K^+ channel from squid axon (Hodgkin and Huxley, 1952), 4.3 for the high conductance sarcolemmal anion channel (Woll et al., 1987).

Some of these differences may be accounted for by the different method utilised here to obtain the $P_O(V)$ curve. Hals et al. (1989) estimated the open probability from steady state recordings of channel activity, while in the present study the open probability was estimated from the mean ensemble current at the end of a 900 ms voltage step. It is possible that in patches containing many channels, a steady state level may not have been reached by the end of the 900 ms voltage step. This would result in an over-estimation of the P_O and a broadening of the $P_O(V)$ bell-shaped curve. Nonetheless, since the estimates of P_O are all taken at the same point in time following the onset of the applied voltage-step, a measure of the voltage-dependent behaviour for the channel is still obtained. Alternatively, the decreased steepness of the voltage-dependent behaviour observed in patches containing many channels may represent a real co-operative effect producing an increase in activity. Unitary conductance steps were, however, difficult to determine in these patches, being masked by overlapping channel events and the numerous subconductance states. Thus, although it seemed that perhaps the channels were operating cooperatively, a check for independence of the channel behaviour, by determining if the number of open channels was binomially distributed, was not attempted because of the difficulty in discriminating the unitary conductance steps.

Alternatively, the variability of the $P_O(V)$ behaviour may be due to the regulated state of the anion channel in the patch membrane. The VDAC from mitochondrial outer membrane generally has a broad bell-shaped voltage-dependence, which becomes much steeper in the presence of a highly conserved soluble protein (Holden & Colombini, 1988; Liu & Colombini, 1991). It is possible that the sarcoball anion channel is regulated in a similar manner, and that in some patches the regulator protein is either not present or only attached to some of the channels. It might be expected, however, that the voltage-dependent behaviour of the sarcoball anion channel would change during the lifetime of the patch, if the regulator protein diffused from the channel, but no change was observed.

Substates

Large conductance anion channels often exhibit many subconductance levels, in a similar way to the channel investigated here. In mouse alveolar cells, Krouse et al. (1986) describe the behaviour in terms of six "co-channels" each of 65 pS which act in concert. Geletyuk and Kazachenko (1985) report 16 equal 12 pS steps in the conductance of single anion channels from molluscan neurones. Other authors also report frequent substates for large conductance anion channels, without a specific commitment to the number of co-channels or equally spaced sub-conductance levels (Schwarze & Kolb, 1984; Tanifuji et al., 1987; Velasco et al., 1989; Tabares et al., 1991). Hals et al. (1989) note numerous substates in their recordings of the sarcoball anion channel and give details of a substate which is approximately 50% of the main conductance level (S1) which gates mainly from the open state, and a smaller substate (S2) which gates from both the open and closed states. The two substates described here are comparable to the S1 and S2 substates, although I am less confident about the smaller substate gating from the open level being the same one which gates from the closed level, because of the large number of substates observed.

Stilbene derivatives

Both DIDS and SITS have two negatively charged sulphonate groups, which are independent of the isothiocyano reactive groups. As protein modifying agents, the isothiocyano groups react with positively charged amino groups (i.e. those of arginine and lysine residues). They are also able to have "flicker block" effects, due to the negatively charged sulphonate groups. The term "flicker block" describes the very rapid binding and unbinding of a charged molecule to a channel. As the molecule transiently binds, the channel is blocked, preventing the conduction of ions. This gives a very characteristic flickery appearance of open events and if the rate at which the molecule binds and unbinds is much faster than the recording bandwidth, then the channel conductance may also appear to be decreased. The decrease in conductance observed with SITS was reversible and is therefore likely to be due to a flicker block, whereas DIDS had an irreversible effect upon conductance suggesting covalent modification. These results were consistent with the findings of Hals et al. (1990) except where they found the action of DIDS upon conductance was reversible in two out of three wash-out attempts.

As previously noted (Hals & Palade, 1990), the I-V relationship of the anion channel remains linear in the presence of DIDS. Since DIDS was only applied from the bath side of the membrane, it might be expected that only exposed positive charges on this side of the membrane would be neutralised by covalent modification with DIDS. Thus, any positive charges around the mouth of the channel which normally would attract a high local concentration of anions would be neutralised and reduce the current flow from this side of the membrane. This would result in a non-linear I-V curve. An alternative explanation is therefore required to account for the linear I-V curve observed. The most likely explanation is that the covalent modification by DIDS has occurred at a site which directly impedes the passage of ions through the channel. It has been suggested that the site could be an amino group within the narrow region of the channel

pore (Hals & Palade, 1990). It is also possible that DIDS is exerting its effect remotely. It might be binding to an accessible region of the channel which has conformational consequences that change the pore environment and thus conductance.

The shift in voltage dependence of the open probability which persisted even after extensive wash-out of DIDS indicates a covalent modification by DIDS of an amino group involved in the voltage dependent behaviour of the channel. Shifts in voltage dependence were also seen by Hals et al. (1990) with covalent modification by DIDS and also with asymmetric replacement of Cl^- ions with a less permeant anion. It is not clear at this stage, however, if these two effects are linked in some way or are separate effects.

Both DIDS and SITS are of limited use to investigate the *in situ* role this anion channel may play in the intact SR, since DIDS and SITS will modify any amino groups exposed on any SR protein. So, although they have been used in the past to block anion permeability in isolated vesicles, the success of the block can not be attributed with certainty to an action upon the anion channel. Indeed, comparison of the limited block observed here on the anion channel may not be sufficient to account for the almost complete inhibition of anion permeability in SR vesicles (Campbell & MacLennan, 1980; Kasai, 1981; Kasai & Taguchi, 1981). The usefulness of these stilbenes is limited to studies at the single channel level, where they have assisted in determining the nature of amino acid residues involved with the voltage gating and conductance behaviour of the anion channel (Hals & Palade, 1990).

Other anion channels which might be present

As the sarcolemma is mechanically removed from the muscle fibre during the preparation of sarcoballs, it seems unlikely that the anion channel observed here is from the sarcolemma, though there are some similarities to the anion channel

described in cultured rat myotubes (Blatz & Magleby, 1983). The biophysical behaviour of the sarcoball anion channel is clearly different, however, from the sarcolemmal anion channels recorded from enzymatically isolated frog toe muscles (Woll et al., 1987). Although both of these channels have a bell-shaped voltage-dependence, the anion channels from the frog toe muscle have a very asymmetric voltage-dependence, quite unlike what is seen here, and the selectivity for anions over cations is much smaller (P_{Cl}/P_{Na} = 3.5).

The negative results obtained with the different blocking agents applied to the sarcoball anion channel provide supporting evidence that this channel is not from the sarcolemma. Application of 2.25 mM A-9-C (the same concentration used here) induced a low Cl^--conductance myotonia in the sartorius muscle from *Bufo marinus* (Bretag et al., 1980), consistent with the sarcolemmal Cl^- conductance blocking action of A-9-C in mammalian muscle (Palade & Barchi, 1977). Perrhenate has also been shown to be a specific blocker of amphibian sarcolemmal Cl^- conductance (Sperelakis, 1969), and at 10 mM approximately 70% of the conductance is blocked. Zinc (0.5 mM) has been shown to reduce the sarcolemmal Cl^- conductance from amphibian toe muscle to 32% of control, as measured by ^{36}Cl radio-isotope efflux (Hutter & Warner, 1967). Similarly, Zn^{2+} (5-10 mM) blocks the voltage-dependent anion channel recorded from sarcolemmal spheres (Stein & Palade, 1989).

The VDAC from mitochondrial outer membrane is another anion channel which might be present in sarcoballs. As mentioned in Chapter 1, it has previously been argued that the sarcoball anion channel is not VDAC on the basis of their biophysical differences (Hals et al., 1989). The results presented here concur with this argument, though there is always the possibility that the behaviour of VDAC is different in the sarcoball preparation. This is further discussed in Chapter 7.

Anion channels from T-tubules might also be present in sarcoballs, however, there is very little information about these channels. The information that is available

comes from rabbit skeletal muscle microsomes, enriched for dihydropyridine binding sites, and incorporated into planar bilayers (Coronado & Affolter, 1986; Hamilton et al., 1989). The anion channel is not commonly seen, and has a conductance of 30 pS (100 mM Cl^- on the *cis* side, 50 mM Cl^- on the *trans* side), which is smaller than that found here (Hamilton et al., 1989). It seems unlikely that the sarcoball anion channel is from T-tubules.

Niflumic acid is a potent and irreversible blocker of anion transport (band 3 protein) in red blood cells (Cousin & Motais, 1979) and also blocks the anion channel found in the nuclear envelope (Tabares et al., 1991). As the nuclei in muscle fibres are peripheral, mechanically removing the sarcolemma presumably exposes the nuclear envelope at the surface of the fibre where the sarcoballs form. The anion channel from sarcoballs was not blocked by niflumic acid (or various derivatives) indicating that it is not the nuclear envelope anion channel. It is also unlikely to be the nuclear envelope channel because the sarcoball anion channel appears far too frequently in patches for the small contribution nuclear membrane is expected to make to the sarcoball structure in relation to the total internal membranes.

Overall, it seems most likely that the sarcoball anion channel originates from the SR membrane. The presence of SR membrane in sarcoballs is demonstrated in Chapter 6.

Other SR anion channels

The majority of studies on anion channels from the SR membrane have used vesicles incorporated into artificial bilayers (Miller, 1978; Smith et al., 1986a) or liposomes (Hals et al., 1989). Generally, these channels are of a smaller conductance than that observed in the sarcoball preparation, and are much less voltage dependent. There have been two reports of anion channels from rabbit skeletal muscle SR vesicles; a 200 pS (100 mM choline Cl) channel (Tanifuji et al.,

1987) and a smaller 70 pS (125 mM choline Cl) channel (Rousseau et al., 1988), both of which were weakly voltage-dependent and had conductances that saturated with increasing anion concentrations.

In comparison, two quite different anion channels have been observed in mammalian cardiac SR vesicles inserted into bilayers. A small conductance (55 pS in 260 mM Cl^-) anion channel has been recorded in canine SR vesicles (Rousseau, 1989). This channel displayed a steep bell-shaped voltage-dependence, being maximally open (P_O = 0.8) at around -10 mV and closing to a P_O = 0.2 at ±60 mV. Such a steep voltage-dependence has not be reported for any other SR anion channel recorded in bilayers. The channel activity was insensitive to changes in free [Ca^{2+}], free [Mg^{2+}] and ATP concentrations. In contrast, an anion channel recorded from porcine SR vesicles was regulated by cAMP-dependent phosphorylation (Kawano et al., 1992). This 116 pS (500 mM Cl^-) channel was voltage-independent and normally inactivated soon after incorporation into bilayers. The inclusion of MgATP (2-5 mM) could prevent the inactivation of channels and previously inactivated channels could be reactivated by addition of the catalytic subunit of protein kinase A.

It is difficult to say whether these anion channels are the same as recorded here from sarcoballs, because bilayer and liposome studies have the inherent problem of inserting the channels into an artificial lipid environment which may well alter the channel behaviour. It has been shown that the conductance of the SR K^+ channel is affected by the lipid environment (Bell & Miller, 1984) as are the single channel kinetics of the Ca^{2+} channel from rat skeletal muscle T-tubules (Coronado, 1987).

There is also the possibility that the channel is regulated in some manner, perhaps by phosphorylation as occurs for the cardiac SR anion channel (Kawano et al., 1992), which is altered between the different preparations. Alternatively, the channel behaviour may be modulated by a soluble factor which is lost when SR

membranes are isolated. Such a soluble protein modulator has been described for the voltage-dependent anion-selective channel (VDAC) from mitochondrial outer membrane (Holden & Colombini, 1988; Liu & Colombini, 1991). In the presence of the soluble protein modulator, the bell-shaped voltage-dependence of the VDAC becomes much steeper.

Conclusions

A high conductance anion channel was able to be recorded here from sarcoball membrane prepared from semitendinosus fibres of the cane toad, *Bufo marinus*, which were mechanically skinned in a CsF solution. The conductance, selectivity and voltage dependent behaviour of this anion channel is very similar to the anion channel recorded in sarcoballs from the frog, *Rana catesbeiana* (Hals et al., 1989). The channels also share a shift in the voltage-dependent open-probability produced by covalent modification of the channel protein with the stilbene DIDS (Hals & Palade, 1990). It is concluded that the anion channels recorded here are essentially the same as those previously recorded in frog sarcoballs.

4. KINETIC ANALYSIS

4.1 Aims and Introduction

Analysis of macroscopic membrane currents in the early 1970's has laid the foundations for the more recent kinetic interpretation of ionic currents obtained using the patch clamp technique. Early work made use of membrane currents induced by the application of drugs or transmitters to determine something of the underlying mechanism which produces the membrane current. Katz and Miledi (1970) demonstrated that potentials from the motor endplate were comprised of a large number of discrete changes in conductance. This was accomplished by analysing the increase in membrane noise that occurs during a maintained depolarisation due to steady application of ACh to the motor endplate. The variance of this increase in membrane noise is an estimate of the number of discrete units contributing to the potential and consequently the unit amplitude could also be estimated. Anderson and Stevens (1973) made further advances in describing the gating kinetics of the ACh receptor by applying non-stationary fluctuation analysis to the relaxation of the motor endplate potential. This non-stationary analysis established that a model with two states, one open and one closed, adequately describes both the relaxation of the endplate potential and the conductance fluctuations during steady application of ACh. Thus, the idea that ion channels exhibit discrete changes in conductance as they open and close in a stochastic manner was proposed, not long before the first single channel recordings were made by Neher and Sakmann (1976).

Relaxation analysis has also contributed to the proposals of single channel kinetic schemes underlying macroscopic membrane currents (Colquhoun & Hawkes, 1977; Schwarze & Kolb, 1984; Maconochie & Knight, 1992). The analysis is based upon the idea that application of a perturbation to the equilibrium condition of a population of channels results in a current relaxation as the population shifts to a new equilibrium. It has been mostly used in relation to receptor operated channels but is also applicable where the channel exhibits voltage dependent behaviour (Schwarze & Kolb, 1984). In this case, the perturbation is effected by the application of voltage steps, which can be rapidly and accurately controlled with voltage-clamp techniques. The time course of the current relaxation observed will depend upon the rate constants and the kinetic path taken by the channel population as it shifts to the new equilibrium. Eigen and De Maeyer (1963) (cited in Maconochie & Knight, 1992) established the basis for exponential relaxations, dependent upon chemical reaction schemes linked by first order kinetics. Colquhoun and Hawkes (1977) developed these ideas and provided a basis by which current relaxations could be accounted for by ion channel behaviour described in terms of chemical reaction schemes. They showed that current relaxations are expected to be described as the sum of a number of exponential terms, which is one less than the total number of states that describe the channel gating mechanism. In practice, the relaxation will be dominated by the rate limiting step and faster components may be missed due to the resolution of the data acquisition process.

The common thread which links the kinetic analysis of macroscopic and single channel currents is the assumption that single channels undergo transitions between kinetic states in a stochastic manner and can be described as a Markov process (Colquhoun & Hawkes, 1981, 1982). Other models have been proposed to describe ion channel activity, such as the fractal (Liebovitch et al., 1987) and diffusion (Millhauser et al., 1988) models, however comparison with experimental

data suggests that Markov models provide a better description (Sansom et al., 1989).

As a Markov process, it is assumed that the channel gating kinetics can be described as a continuous process with a finite number of states. Not all of these states, however, will be able to be distinguished by visual inspection of the current recordings. Clearly, an open and a closed conductance can be distinguished, but more than one state may be contributing to the open or closed condition and so are classified as aggregates. The inferential problem of gating kinetics is to deduce from the behaviour of the aggregates the structure and perhaps the transition rates of the underlying Markov process. This information is extracted from recordings of single ion-channels by analysis of the open or closed dwell-time distributions. Colquhoun and Hawkes (1981) have established a theoretical basis for the interpretation of these distributions. It is shown that the distributions of dwell times have the form of a sum of exponentials, and that the number of exponential terms is a lower bound on the number of states in the corresponding aggregate. It is also shown how the exponential time constants are determined by the kinetic rate constants leading away from each of the states in the aggregate. To work backwards and determine the kinetic rate constants from the exponential time constants is not always possible for a system with more than two states, although some aspects of the structure can be deduced.

The anion channel recorded from the sarcoball preparation exhibits a striking bell-shaped voltage-dependence. By using both non-stationary and steady state data recording techniques, different aspects of the channel gating behaviour can be investigated. The aim of this study was to use the information from non-stationary and steady-state analysis to derive a model of a possible kinetic scheme which describes the bell-shaped voltage-dependence of the sarcoball anion channel. The model is not an end in itself but a beginning. By casting the

information in the simplified form of a model, further testable predictions of the channel behaviour may be made.

4.2 Theoretical framework

Markov processes

The way in which the kinetic behaviour of an ion channel is described needs to have measurable quantities or characteristics which can also be obtained from experimental ion-channel data. Colquhoun and Hawkes (1977, 1981) have described the kinetic behaviour of ion channels in terms of a stationary Markov process in a continuous time domain with a finite state space. This has proven to be a very successful approach, as the theory predicts exponential distributions of both open and closed durations like those obtained from analysis of single ion-channel data. Further, it provides a theoretical basis for extracting the number of kinetically distinct states from the exponential distribution of open and closed times. This is best illustrated by beginning with a simple two state model, consisting of an open or conducting state and a closed or non-conducting state. From this two state model, a direct relation can be made between the open and closed states, and the simple, rectangular current steps of single channel behaviour. The way in which these two states are linked is equivalent to a reversible chemical reaction. As such, there are rate constants that describe the movement from the closed to the open state (β) and from the open state to the closed state (α). This can be represented in the following kinetic scheme.

$$C \underset{\alpha}{\overset{\beta}{\rightleftharpoons}} O \qquad (4.1)$$

These rate constants are appropriate when considered in relation to the collective behaviour of many channels shifting from one state to the other, but single channels are observed to open and close in a random manner. This random behaviour of a single channel means that the rate constant leading away from a

state is better considered as a measure of the probability of leaving that state in unit time. It is not a true probability, as it has dimensions of sec^{-1} and is able to take values greater than unity. The probability of leaving, say, the open state after some time, Δt, is approximately given by:

$$\text{Prob(open channel closes after } \Delta t) \approx \alpha.\Delta t \qquad (4.2)$$

The distribution of the probabilities for every open duration, Δt, is the probability density function (p.d.f.) of the open state. This can be more precisely defined as a differential equation. In general, the p.d.f. of some state, S, is determined by the probability of leaving that state within a time interval Δt, after residing in that state for some period of time t. This function is given by:

$$f(t) = \lim_{\Delta t \to 0} [\text{Prob(Duration in } S \text{ is between } t \text{ and } t+\Delta t) / \Delta t] \qquad (4.3)$$

This differential equation is able to be evaluated in terms of the rate constant leading away from the state. For the simple two state model shown here, the p.d.f. for the open state is:

$$f(t) = \alpha \exp(-\alpha t) \qquad (4.4)$$

where α is the rate constant leading away from the open state. A similar expression describes the p.d.f. of the closed state in terms of the rate constant β. Thus, the open and closed durations are each described by a p.d.f. with a single exponential, reflecting the single rate constant that leads away from the open state or the closed state. The relationship between the predicted p.d.f. and a frequency distribution of open or closed durations obtained from experimental data is simply one of scaling. By definition, the area under the p.d.f. curve is unity. Therefore, the frequency of a particular duration, expressed as a fraction of a sufficiently large number of all durations, provides an estimate of the probability density. A more complete description of this derivation for the two state model is given in Colquhoun and Hawkes (1983).

For the more general case, where there might be more than two kinetic states, the theory still holds true. The observable non-conducting, closed events, for example, might be due to an aggregate of several non-conducting, kinetically-distinct states, and the number of exponential terms which describes the frequency distribution is a lower bound to the number of states. This is also true for an aggregate of several kinetically distinct open states all of the same conductance. A more complete description for the general case can be found in Colquhoun and Hawkes (1981).

Connectivity of kinetic schemes

The Markov process implies that the future behaviour of the channel from any specified state in the reaction mechanism at any time t, is independent of what happened before time t. This means that the lifetimes spent in each state are independent of each other and so are uncorrelated. It has been shown, however, that correlations can occur in experimental records because it is not always possible to distinguish between all the individual kinetic states of the reaction mechanism just from visual inspection of the open- and closed-aggregate behaviour. Fredkin et al. (1985) have determined the conditions which produce correlations in the sequence of successive durations of open or closed aggregates for ion channel reaction schemes which are Markov processes. Correlations are possible only when there are at least two indistinguishable closed states and at least two indistinguishable open states. Whether correlations do occur will depend upon the kinetic paths that connect the open and closed states in the reaction mechanism. Specifically, correlations appear upon the condition that there are at least two distinct kinetic paths which enter/exit the closed aggregate and the open aggregate (Fredkin et al., 1985). An alternative way of describing this condition is the connectivity of the reaction mechanism (Colquhoun, 1987; Colquhoun & Hawkes, 1987). The connectivity is the number of states which would need to be deleted from the mechanism to separate all open states totally

from all closed states. Correlations will be seen for reaction mechanisms with a connectivity of greater than one. So, for the examples of kinetic schemes shown in Figure 4.1, although each has three closed states and two open states, only those schemes with more than one kinetic path connecting the open and closed states (schemes II and IV) will exhibit correlations. The nature of connections between the open states or between the closed states is irrelevant.

The autocorrelation function (a.c.f.) of open or closed durations provides information about the connectivity of the underlying process. The autocorrelation function, as the name suggests, compares each element in a series of successive durations with those durations which follow it in the same series. The lag describes the separation between the durations in the series being compared. For any aggregate of indistinguishable states, let the sequence of durations spent in that aggregate be T_1, T_2, T_3,...T_i. It is assumed that this is a stationary sequence, which means the underlying stochastic process that generated this sequence exhibits no systematic change in mean duration or variance over the time interval described by T_1, T_2, T_3,...T_i. This assumption is entirely reasonable for steady state recordings of ion channel behaviour, in which the stochastic process is at equilibrium. This sequence of successive durations has an autocovariance, G(k), function which may be estimated from:

$$G(k) = \frac{1}{n-k}\sum_{i=1}^{n-k}[T_i - \overline{T}][T_{i+k} - \overline{T}] \qquad (4.5)$$

where k is lag of the covariance function, and:

$$\overline{T} = \frac{1}{n}\sum_{i=1}^{n} T_i \qquad (4.6)$$

which is the mean dwell time for the dwell time sequence, for i = 1,2,...,n. The magnitude of the autocovariance function, G(k), has coefficients which are

dependent upon the units of measurement and so the magnitude of G(k) is dependent upon the units of measurement. By taking the a.c.f., which is estimated from:

$$r(k) = G(k)/G(0) \qquad (4.7)$$

the coefficients are normalised, for easier interpretation, with respect to the autocovariance at lag k=0, which is G(0) (equivalent to the variance of the sequence). Thus, r(k) gives a values between -1 and 1. Short-term correlation is exhibited by initially large values of r(k) which successively decrease and tend toward zero as the lag, k, becomes large.

Fredkin et al. (1985) have developed theory which shows that the correlation can be described as the sum of a number of geometrically decaying components. The number of these components is E-1, where E is a lower bound for the connectivity between the open and closed aggregates. An alternative proof of this is shown by Colquhoun and Hawkes (1987). Explicitly, there exist υ_i and σ_i, $0 \leq \sigma_i < 1$ such that:

$$r(k) = \sum_{i=1}^{E-1} \upsilon_i . \sigma_i^{|k|} \quad , \qquad \text{for } k \neq 0 \qquad (4.8)$$

where r(k) is the a.c.f. of the aggregated dwell time sequence, expressed as the sum of E-1 geometrically decaying components. Each σ_i (i=1,2,...E-1) in Equation 4.8 are the eigenvalues, which are neither zero nor one, of a transition matrix which describes those transitions which enter the aggregate of interest. It is a result of Fredkin et al. (1985) that there are at most E-1 such eigenvalues. The values of υ_i (i=1,2,...E-1) are associated with the component of the spectral decomposition of the transition matrix for each eigenvalue σ_i. Further details of the expressions for υ_i are given elsewhere (Fredkin et al., 1985; Colquhoun & Hawkes, 1987; Ball & Sansom, 1988).

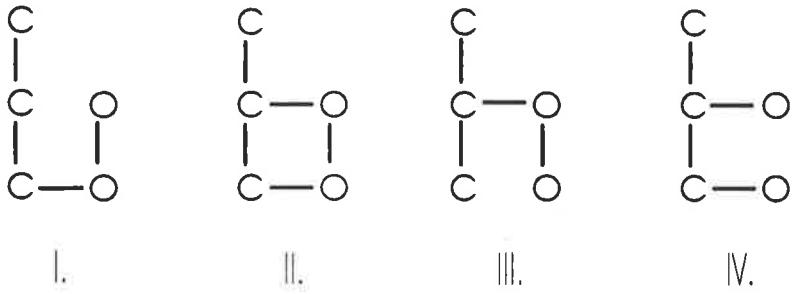

FIGURE 4.1 Connectivity of kinetic schemes.
Each of the above kinetic schemes have three closed states (C) and two open states (O). Adjacent states are linked by reversible transitions. The connections which occur between open states or between closed states are irrelevant to the form of any correlations which may be produced by the scheme. Only the number of connections between the open and closed states matters. Correlations are found in the open or closed durations when the connectivity is greater than one. Schemes I and III have a connectivity of one and so will not show any correlations. Schemes II and IV have a connectivity of two and so will exhibit correlations in the open and closed durations.

4.3 Methods

Preparation and solutions

Sarcoballs were prepared for patch-clamping as detailed previously. All recordings were made from detached patches, under symmetrical ionic conditions; solutions containing 100 mM TrisCl, pH 7.40.

Steady state analysis

Current recordings for steady state analysis were performed as described in Chapter 3, except that recordings were filtered at 5 kHz (-3dB) and digitised at a sampling frequency of 10 kHz (interval of 0.1 ms ≡ 1 *dt*). Any recording which contained double openings consistent with the presence of two or more channels was rejected. Recordings of between 120 and 180 seconds at each potential were typically used for data analysis.

Analysis of the single-channel behaviour was performed using EVPROC software developed by Dr D.R. Laver (Muscle Research Group, John Curtin School of Medical Research, Australian National University, Canberra). The principle by which this software analyses the data is described briefly in Laver (1992) and is based upon the technique developed by Vivaudou et al. (1986). From the raw, digitised data, an events list is obtained which is a series of step-wise current transitions that adequately represents the behaviour of the channel, without the interfering background noise. To obtain the events list, the raw data are first passed through a non-linear digital filter routine which preserves the rapid channel transitions while reducing the noise in regions of constant amplitude (Chung & Kennedy, 1991). The data are then reduced to a number of small steps which maintain an approximately constant current level. Each transition between these levels is then assessed in comparison to a threshold current to determine if the transition is significant above the background noise. The threshold current is

a function of the root mean square of the baseline current, I_{RMS}, and is weighted by the duration of the transition, as described in the following equation:

$$\text{Threshold} = \frac{3.I_{RMS}.\text{Sample frequency}}{\sqrt{n}.\text{Nyquist frequency}} \qquad (4.9)$$

where n is the number of data points (equivalent to the duration) which make up the current level. This algorithm sets the criteria by which abrupt changes in current, which are of sufficient duration, are considered real channel transitions and not noise. Thus, the current levels are accumulated to form an event until a transition of sufficient amplitude and corresponding duration is encountered, which ends that event and begins the next. The duration and average amplitude of each event is stored in the events list.

Once these events lists have been generated, duration or amplitude frequency histograms can be extracted for any type of event. Of great value is the ability to extract information on events which fall within a narrow amplitude discrimination window, by placing either pre- or post-event conditions upon the inclusion of the event in the histogram.

The dead time and the minimum duration for which the amplitude was faithfully detected, was determined empirically from square pulses of varying width, filtered at 5 kHz (-3dB), sampled at 10 kHz and then analysed with EVPROC. This is shown in Figure 4.2. The dead time is estimated to be 0.25 ms, from extrapolating the curve of measured durations to the ordinate axis. The amplitude was detected as being >90% of the original amplitude for durations greater than or equal to 0.3 ms (equivalent to 3 *dt*'s).

a) Duration frequency distributions

The distributions of durations spent in the fully open or closed states were obtained by placing amplitude discrimination windows over the fully open level

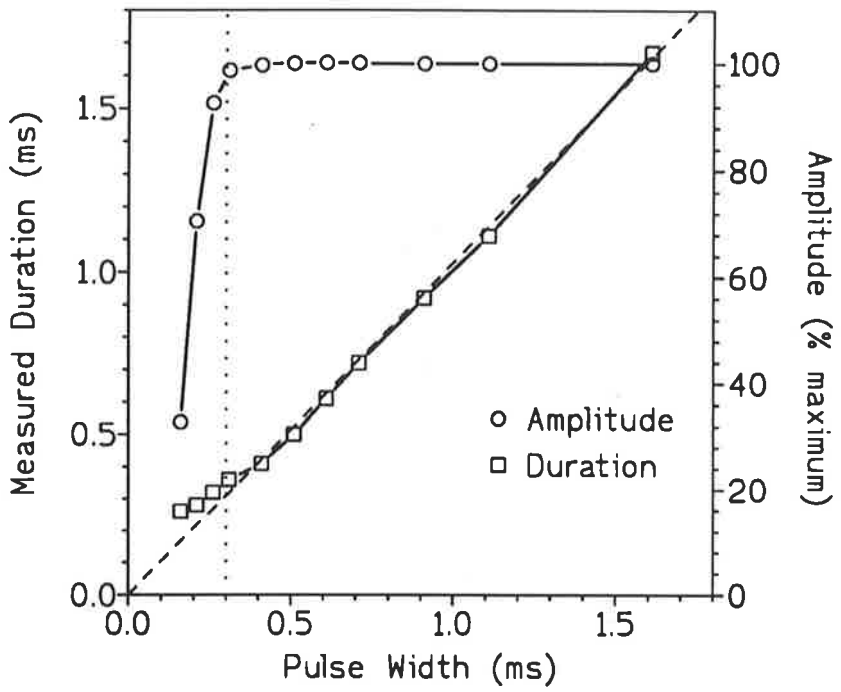

FIGURE 4.2 Dead time of recording and analysis
Recordings of square pulses of different durations were recorded and analysed in the same manner as single channel recordings (filtered at 5 kHz, sampled at 10 kHz, analysed with EVPROC). Pulse durations of 0.3 ms or greater were faithfully represented. Amplitudes were maintained for durations of 0.3 ms or greater. The dead time of the system was estimated to be 0.25 ms, by extrapolating the duration data back to the ordinate axis. Transitions less than the dead time would not be faithfully detected by the system. From these results, the minimum duration criteria for analysis of single channel recordings was set to 0.3 ms.

and the baseline, respectively. An open event was defined as a transition which entered the open state discrimination window, remaining there for at least 3 sampling intervals (3 *dt*'s), until the duration of the event was terminated by a transition to within the baseline discrimination window. Closed events were similarly defined, occurring within the baseline discrimination window for at least 3 *dt*'s and the event duration was terminated by a transition to within the open state discrimination window. This approach allowed separation of open and closed durations from dwell times in substates. The open- and closed-duration frequency distributions were fitted with multi-exponential curves to obtain a lower bound for the number of kinetically distinct open and closed states in the underlying kinetic scheme.

The preponderance of substates, and particularly one near 60% of the single channel conductance, makes the application of a 50% threshold detection protocol inappropriate for the present analysis: numerous transitions are seen to cross the 50% threshold which are apparently transitions between substates and not between the fully open and closed states.

Corrections for the omission of closed or open durations were not made to the duration frequency distributions, however, a lower bound to the number of kinetic states can still be interpreted from the distributions. Event omission does distort the p.d.f.'s of open and closed durations, but spurious additional components are not expected to be introduced as a result (Roux & Sauvé, 1985; Blatz & Magleby, 1986).

b) Autocorrelation analysis

The a.c.f. was estimated according to Equation 4.7. The properties of this estimator are such that r(k) is generally biased, arising from the fact that successive values of G(k) may be highly correlated. By taking the partial autocorrelation function (p.a.c.f.), the excessive correlation between successive

values of G(k) are taken into account, as described by Box and Jenkins (1976). Calculations of the autocorrelation functions and partial autocorrelation functions were performed using Minitab statistical software package (Minitab Inc.) on a VAX 11/785 running VMS.

Non-trivial correlations of aggregate dwell time series data were assessed by comparison to the variation expected from white noise. White noise is a time series of independent events which are identically distributed. For a series of n events, the a.c.f. estimate of white noise is approximately normally distributed about a mean of zero with variance $1/n$, and so $r(k) = 0$ for $k \neq 0$ (Cox & Lewis, 1966). The a.c.f. and p.a.c.f. of a dwell time series of n events were considered significant if the functions were greater than plus or minus twice the approximate standard error ($\pm 2/\sqrt{n}$) expected from a white noise series with the same number of events.

The a.c.f.'s, obtained from the open- and the closed-aggregate dwell times were fitted with the sum of geometrically decaying components of the form shown in Equation 4.8. From these fits, it was possible to obtain an estimate of the number of pathways connecting the open and closed aggregates.

The interpretation of a.c.f.'s to obtain a lower bound to the connectivity of the underlying kinetic scheme has been shown not to be influenced by time interval omission (Ball & Sansom, 1988). For large omitted time intervals, the magnitude of the correlation is reduced but additional components are not artefactually produced. The converse was also found to be true, that is, zero-correlations are an indication of the underlying process having no connectivity and not an artefact of time interval omission (Ball & Sansom, 1988). It is important to realise however, that fitting of a.c.f.'s does not suggest a unique kinetic scheme. Many different stochastic processes may have the same a.c.f.

Non-stationary analysis

Various voltage step protocols were applied to multi-channel patches and the current response was recorded using the pCLAMP software, as described in Chapter 3. Data were stored as individual current traces and ensemble averages were produced from a number of sequential current recordings from the same patch. Except for the ramps protocol, the mean current ensembles were expressed in terms of the channel open probability ,P_O, as described in Chapter 3.

a) Protocol for relaxation kinetics

Ensemble current relaxations were obtained using the voltage-step protocol described in Chapter 3. Fifteen current traces were averaged for each voltage step and expressed as a time-dependent P_O relaxation which was then fitted with an exponential curve.

b) Protocol for reactivation kinetics

The protocol for the reactivation kinetics was devised as a test of independence between the reaction pathways at positive and negative potentials. In this case the membrane patch was held at a potential where the channel was closed for the majority of the time and then stepped to potentials where there is an increased probability of finding the channel in the open state. Thus, from a holding potential of +30 mV, a test-voltage step was made to +15 mV for 220 ms before returning to the holding potential. In this case, the magnitude of the applied electric field was changed but not the sign of the field. This was followed by a 220 ms voltage step to -15 mV, such that both the magnitude and the sign of the applied field altered. Similar reasoning follows for recordings made from a holding potential of -30 mV for voltage steps to ±15 mV. Other recordings were made from a holding potential of -50 mV, stepping to +50 mV for 220 ms before returning to the holding potential. In each case, a period of 4 seconds between each individual recording was allowed for the channel activity to return to the steady-state level at the holding potential. In these protocols the data were

filtered at 1 kHz (-3dB) and collected at a sample frequency of 2 kHz. Ensemble averaged currents were produced from 24 sequential recordings in each patch studied.

c) Ramps protocol

Voltage ramp protocols were applied to membrane patches, beginning at a holding potential of -60 mV, continuing through to +60 mV in 900 ms, pausing for 200 ms and then returning to -60 mV in 900 ms. A period of 4 seconds was allowed between each individual recording for the channel open probability to reach a steady-state level at the holding potential of -60 mV. For this protocol, the data were filtered at 1 kHz (-3dB) and collected at a sample frequency of 2 kHz. Ensemble averages were produced from 18 sequential recordings in each patch studied.

Curve fitting

Curve fitting was executed using the Levenberg-Marquardt algorithm for the method of least-squares assessed by the chi-squared statistic. The fitting routines used were a part of the pSTAT and CLAMPFIT programs of pCLAMP (Axon Instruments) data analysis software for multi-exponentials and the InPlot software (GraphPad Inc.) for other non-liner curves. An F test was used to determine if a more complex curve fitted the data significantly better than a simpler curve, with a significance level of p=0.01.

4.4 Results

Steady state kinetic analysis

The nature of the channel behaviour meant that meaningful steady state recordings could only be made over a limited range of potentials. At small potentials, closures were infrequent and the recording times required to obtain a sufficient number of events were often beyond the limited life time of the patch.

This similarly applies for larger potentials where there are infrequent openings. The most useful recordings were obtained at potentials which correspond to the steepest part of the voltage dependent $P_O(V)$ curve. Different patches exhibited variations in the steepness of the $P_O(V)$ curve, as discussed in Chapter 3 (see Figure 3.6A), and to be cautious, data from recordings at the same potential in different patches were not grouped together. Steady-state recordings were made from four patches where only single channel activity was observed. The results from a single patch are presented here to illustrate the behaviour of the channel.

a) Transition histories

The presence of numerous substates, as seen here with the anion channel, can complicate the interpretation of channel kinetics, depending upon the frequency with which the substates occur and the position of the substates within the kinetic scheme. To assess the contribution of the substates to the underlying kinetic scheme, transition histories were compiled by placing a condition on the type of event which is identified immediately before the events of interest.

For each of the transition histories (Figures 4.3, 4.4 and 4.5), the distribution of all events longer than 1 ms (10 *dt*'s) compiled from the same events lists is included at each recording potential as a comparison, and they show peaks consistent with the open and closed state amplitudes. The peak associated with the open amplitude, has a shoulder which tails off towards the closed amplitude. This distribution is associated with the presence of numerous substates which tend to merge together. There is, however, a small peak in the shoulder distribution that is associated with a predominant substate of an amplitude which is approximately 60% of the fully open state.

At each potential, open events are followed mainly by other events within the open amplitude discrimination window (Figure 4.3). Transitions also occur to substate levels, with a slight peak apparent in the frequency at an amplitude

associated with the 60% substate. The frequency of transitions to substates decreases the further they are away from the open state. The frequency increases again at amplitudes associated with transitions directly to closed events and substate events near the closed events.

Closed events are most frequently followed by transitions directly to the open amplitude, with some transitions to nearby substates (Figure 4.4).

Substate events at approximately 60% of the open state amplitude are followed by transitions to all levels, though there is greater frequency for transitions to open events (Figure 4.5). There is a spread of transitions to nearby substates, which tend to tail off towards the closed amplitude. Transitions to closed events were least frequent.

The results from these transition histories influenced the way in which the remainder of the steady-state data was analysed. The behaviour of the channel was approximated as transitions directly between the fully open and fully closed states, with sojourns to the 60% substate occurring only from the open state. This represents the most frequent transitions observed. Transitions from the open state to the closed state via the 60% substate (and other substates) and transitions from the closed state to the open state via substates occur much less frequently, and so for simplicity are not included in this kinetic treatment.

b) Duration frequency distributions

From visual inspection, the anion channel exhibited a shift from activity dominated by long openings at small potentials, towards activity dominated by long closures at large potentials. To estimate the number of kinetically distinct states responsible for this behaviour, frequency distributions of the open and closed durations were fitted with exponential curves.

FIGURE 4.3 Transitions following open events
The frequency distribution of events longer than 0.5 ms which follow an open event (O) are represented by the circles. Data was obtained from steady-state recordings made at the potentials indicated. The bar at the top of the distribution indicates the amplitude discrimination window used to define an open event. As a comparison, the frequency distribution of all events longer than 1 ms is also displayed (squares). At both +10 mV and +20 mV there is a similar frequency of transitions to substates (S) as to the closed state (C). At -20 mV, most transitions are to substates and few are to the closed state. The frequency of transitions to the closed state increases at -30 mV.

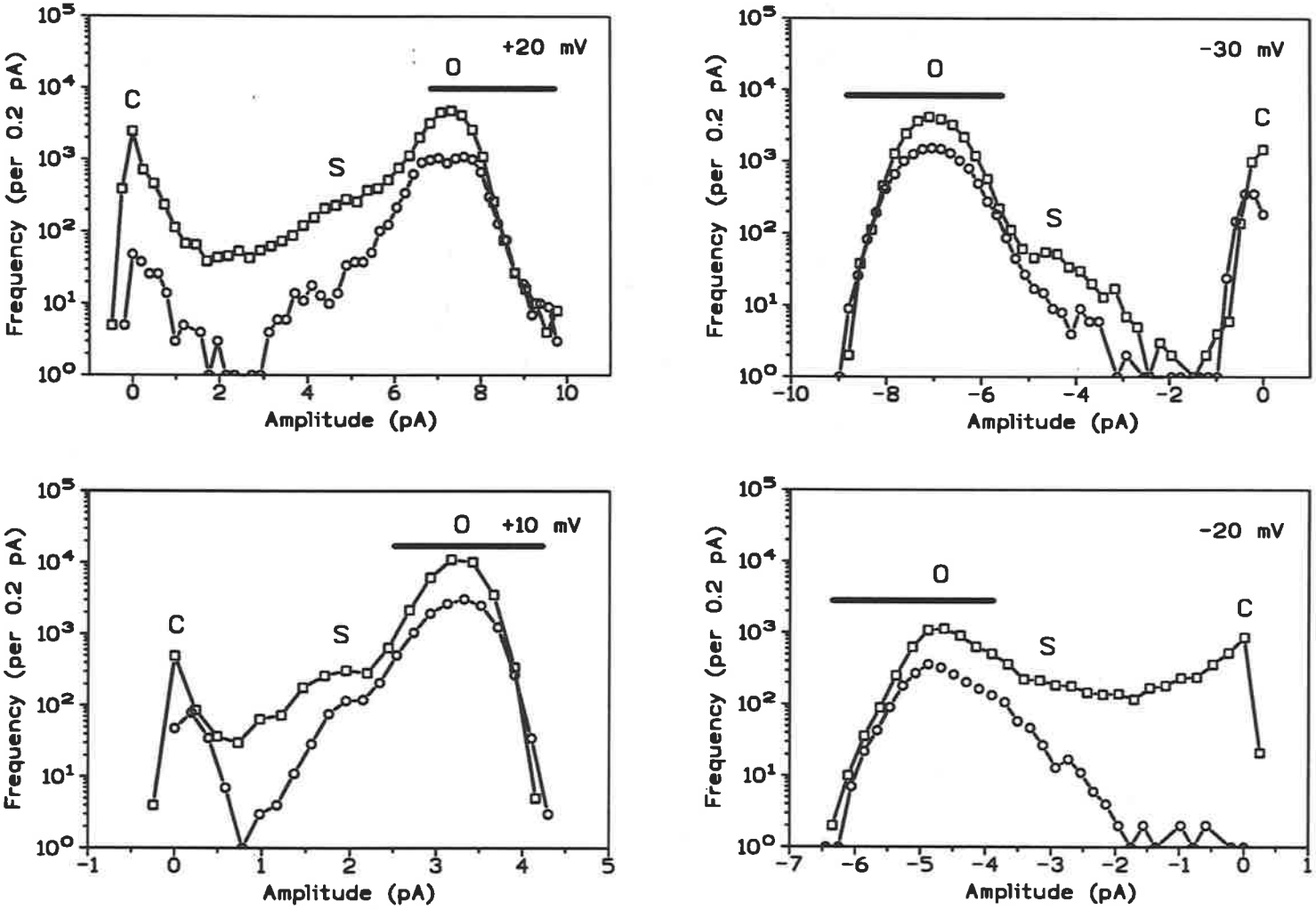
+20 mV
O
C
S
Frequency (per 0.2 pA)
Amplitude (pA)
-30 mV
O
C
S
Frequency (per 0.2 pA)
Amplitude (pA)
O +10 mV
C
S
Frequency (per 0.2 pA)
Amplitude (pA)
-20 mV
O
C
S
Frequency (per 0.2 pA)
Amplitude (pA)

FIGURE 4.4 Transitions following closed events
Frequency distribution of events longer than 0.5 ms which follow a closed event (C) are represented by circles. Data was obtained from steady-state recordings made at the potentials indicated. The amplitude discrimination window used to define a closed event is indicated by the bar. As in Figure 4.3, the frequency distribution of all events longer than 1 ms is also displayed (squares). Transitions were most frequent to the open state, except at -20 mV where transitions to substates (S) were more frequent. Transitions to substates tended to be to those substates nearer to the closed state eg. at +20 mV and -20 mV.

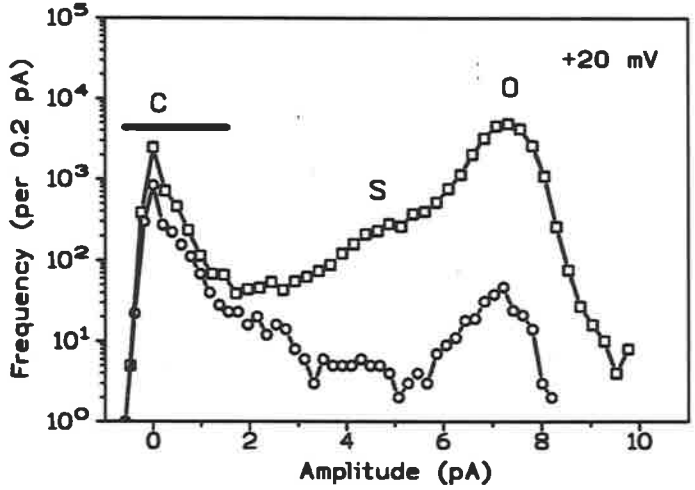
+20 mV
C
O
S
Frequency (per 0.2 pA)
Amplitude (pA)

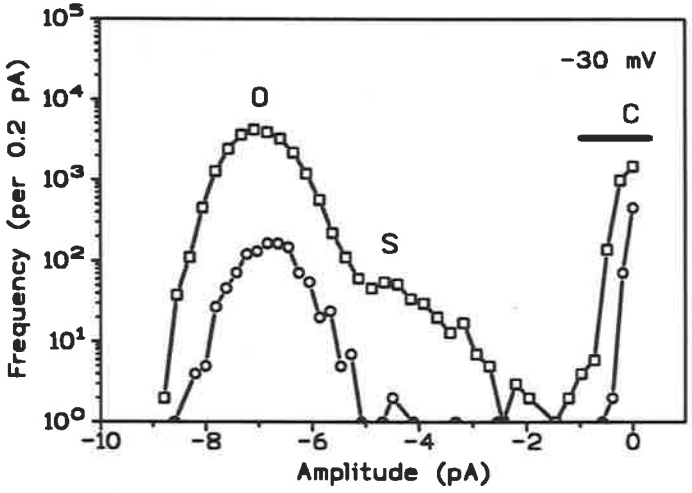
-30 mV
O
C
S
Frequency (per 0.2 pA)
Amplitude (pA)

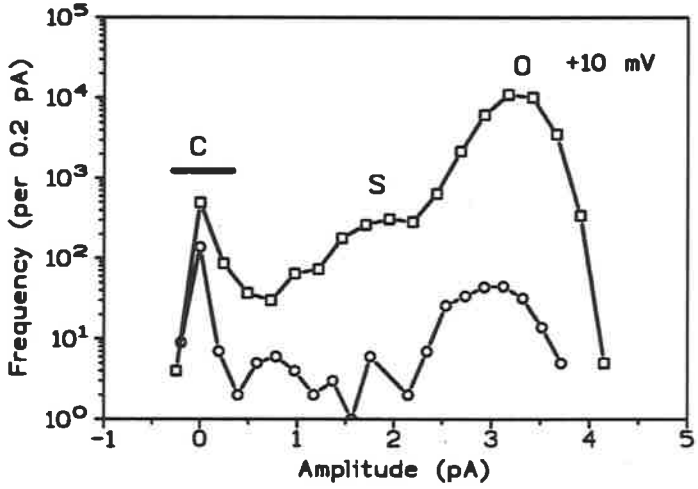
+10 mV
O
C
S
Frequency (per 0.2 pA)
Amplitude (pA)

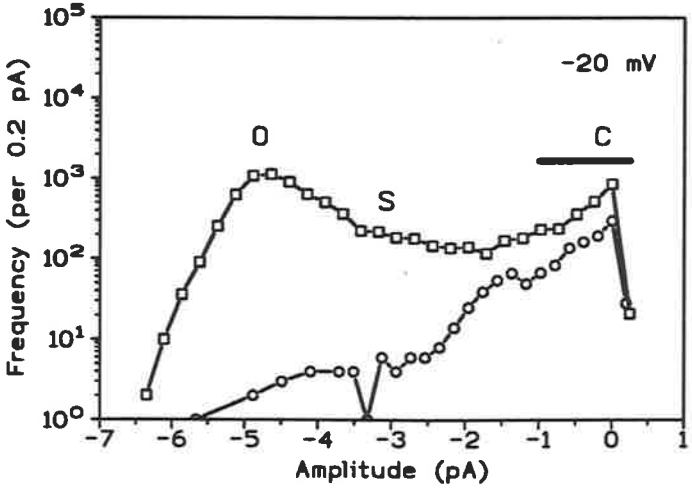
-20 mV
O
C
S
Frequency (per 0.2 pA)
Amplitude (pA)

FIGURE 4.5 Transitions following a substate event
Frequency distribution of events longer than 0.5 ms which follow a substate event (S) are represented by circles. Data was obtained from steady-state recordings made at the potentials indicated. The bar indicates the amplitude discrimination window used to define a substate. Again, the frequency distribution of all events longer than 1 ms is also displayed (squares). At all potentials, transitions to open events (O) were most frequent. Transitions also occurred to other substate levels of greater or lesser amplitude, with the frequency decreasing towards the closed state (C). At all potentials, the transitions to closed states were least frequent.

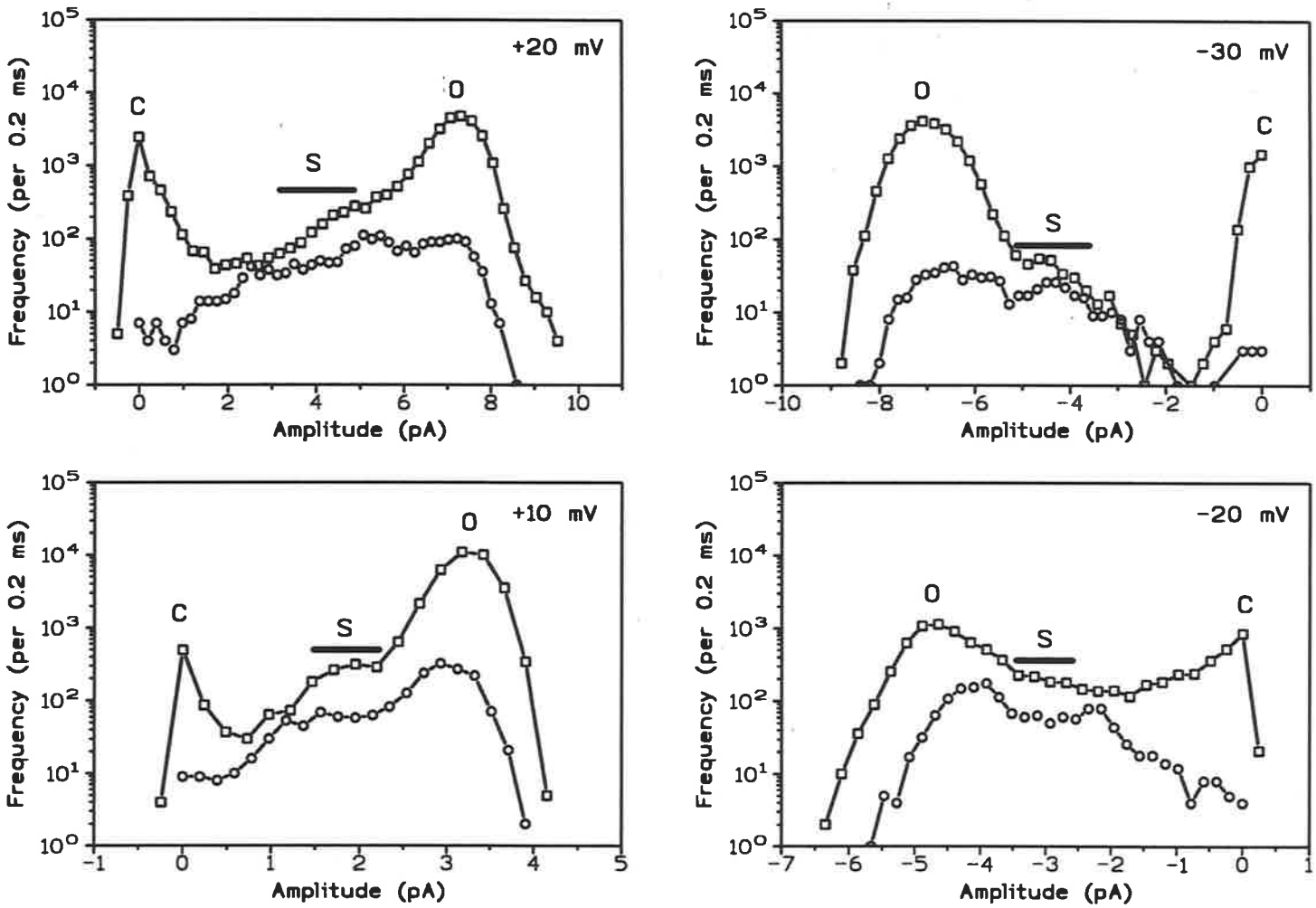
+20 mV
C
O
S
Frequency (per 0.2 ms)
Amplitude (pA)
-30 mV
O
C
S
Frequency (per 0.2 ms)
Amplitude (pA)
+10 mV
C
O
S
Frequency (per 0.2 ms)
Amplitude (pA)
-20 mV
O
C
S
Frequency (per 0.2 ms)
Amplitude (pA)

The event detection criteria were set to collect the distribution of open times that occur between transitions to the closed state. Transitions from the open state to substates occur during these events, however the time spent in the substates is not included in the durations. The reasoning for this is presented in the Discussion. When plotted at a binwidth of 10 ms, the open duration distributions are described by a short time constant of the order of milliseconds and a second, longer time constant of the order tens of milliseconds, which was voltage dependent (Figure 4.6). At +10 mV, the longer time constant was 102.43 ms which is observed to shorten to 72.72 ms at +20 mV. Similarly, at -20 mV the time constant of 82.95 ms shortened to 27.96 ms for data recorded at -30 mV. The short time constants, which ranged from 4.28 to 7.44 ms, were less than the binwidth and so the data were replotted at a smaller binwidth of 0.1 ms (Figure 4.7). This revealed a third time constant between 0.2 and 0.84 ms, and a time constant of a similar order as the short one found when plotted at a binwidth of 10 ms. These results indicate that there are at least three kinetically distinguishable states in the open aggregate.

The event detection criteria for closed times was set to collect the distribution of closed times that occur between transitions to the fully open state. These closed duration distributions, like the open distributions, appear to have three exponential components, although there are inadequate numbers of the longest events for satisfactory statistical analysis. Visual inspection of channel data qualitatively suggests that the longest closed durations might be voltage-dependent, becoming longer at larger potentials. These longer closed times are possibly those included in the tail of long closures in the distributions. Compiling the closed dwell time data at a wider binwidth did not assist in determining the long time constant, because of the low frequency of events. From the few long events in the tail, estimates of the mean duration were obtained by taking the arithmetic mean of the events. These estimates ranged from 722 ms to 70 ms at the four recording potentials. Excluding the longest events, the

remaining data were described by the sum of two exponentials (Figure 4.8). The shorter time constants ranged from 0.39 ms to 1.97 ms and the longer time constants ranged from 2.53 ms to 11.51 ms. No consistent voltage dependence of the closed time distributions is apparent over the range of potentials studied.

c) Autocorrelation functions

To obtain an estimate of the connectivity between the suggested three open states and three closed states, autocorrelation analysis was performed on the series of all open and closed durations. A significant autocorrelation was found for both the open and the closed durations, at each of the recording potentials (Figure 4.9). In each case, the a.c.f. decayed and tended towards zero as the lag increased. The p.a.c.f.'s were also calculated for the open and closed durations (Figure 4.10) and in each case, the p.a.c.f. decayed to within the 95% confidence limits at much shorter lags than for the a.c.f.'s. A number of peaks appeared in the a.c.f. of the closed durations at potentials of +20, +10 and -20 mV (shown in Figure 4.9). These peaks occurred only at short lags and decreased in amplitude with the p.a.c.f. The significant autocorrelation for both the open and closed durations directly implies that the kinetic scheme is branched or cyclic, with a connectivity greater than 1.

The a.c.f.'s were fitted as the sum of geometrically decaying components to obtain an estimate of the number of entry/exit states communicating between the open and closed aggregates. The a.c.f. of the open durations was described by two geometrically decaying components, while the a.c.f. of the closed durations was described by a single component. Table 1 summarises all of the fitted parameters to each of the a.c.f.'s. From these data it is proposed that there are three entry/exit states that connect the open and closed aggregates (see Discussion). Together with the requirement for three open and three closed states, there are only six possible schemes that satisfy these constraints, and these are shown in Figure 4.11

FIGURE 4.6 Frequency distributions of long open times
Log-log plot of the distribution of open times recorded at different steady-state potentials, displayed with a binwidth of 10 ms. The observed data is described by the sum of two exponentials. The continuous line indicates the line of best fit. A voltage dependence is evident, with the second time constant becoming shorter as the magnitude of the potential becomes larger.

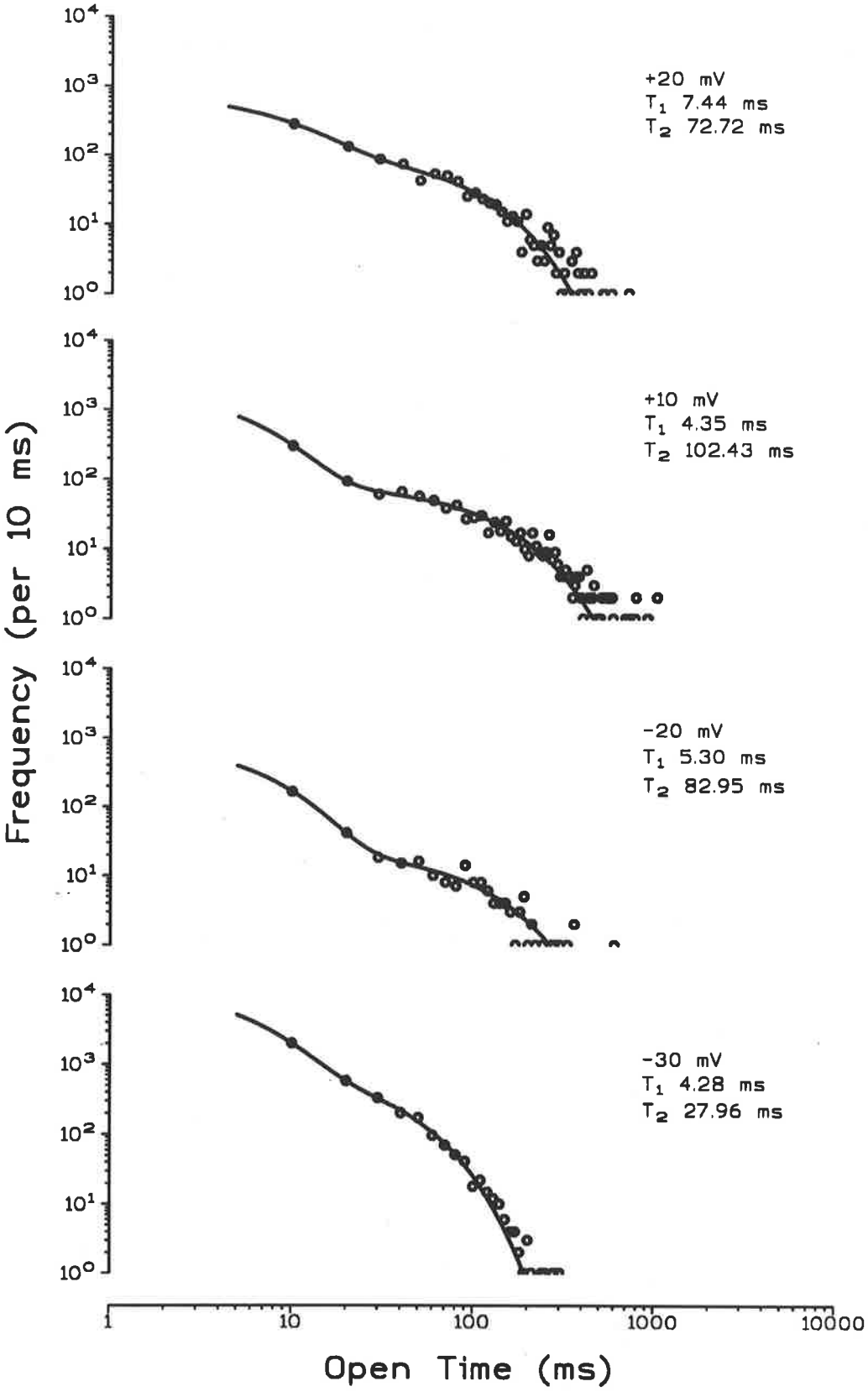
+20 mV
T1 7.44 ms
T2 72.72 ms
+10 mV
T1 4.35 ms
T2 102.43 ms
-20 mV
T1 5.30 ms
T2 82.95 ms
-30 mV
T1 4.28 ms
T2 27.96 ms
Frequency (per 10 ms)
Open Time (ms)
10⁴
10³
10²
10¹
10⁰
1
10
100
1000
10000

FIGURE 4.7 Frequency distributions of short open times
Log-log plot of the distribution of open times recorded at different steady-state potentials, displayed with a binwidth of 0.1 ms. The observed data reveals a shorter time constant between 0.2 and 0.84 ms, which is not seen when the data is displayed with a binwidth of 10 ms. Over the range plotted, the data is described by the sum of two exponentials and the continuous line indicates the line of best fit. Events longer than 40 ms are not included in these plots, nor were they included in the fit. The number of events longer than 40 ms is indicated in each case to the right of the vertical dotted line.

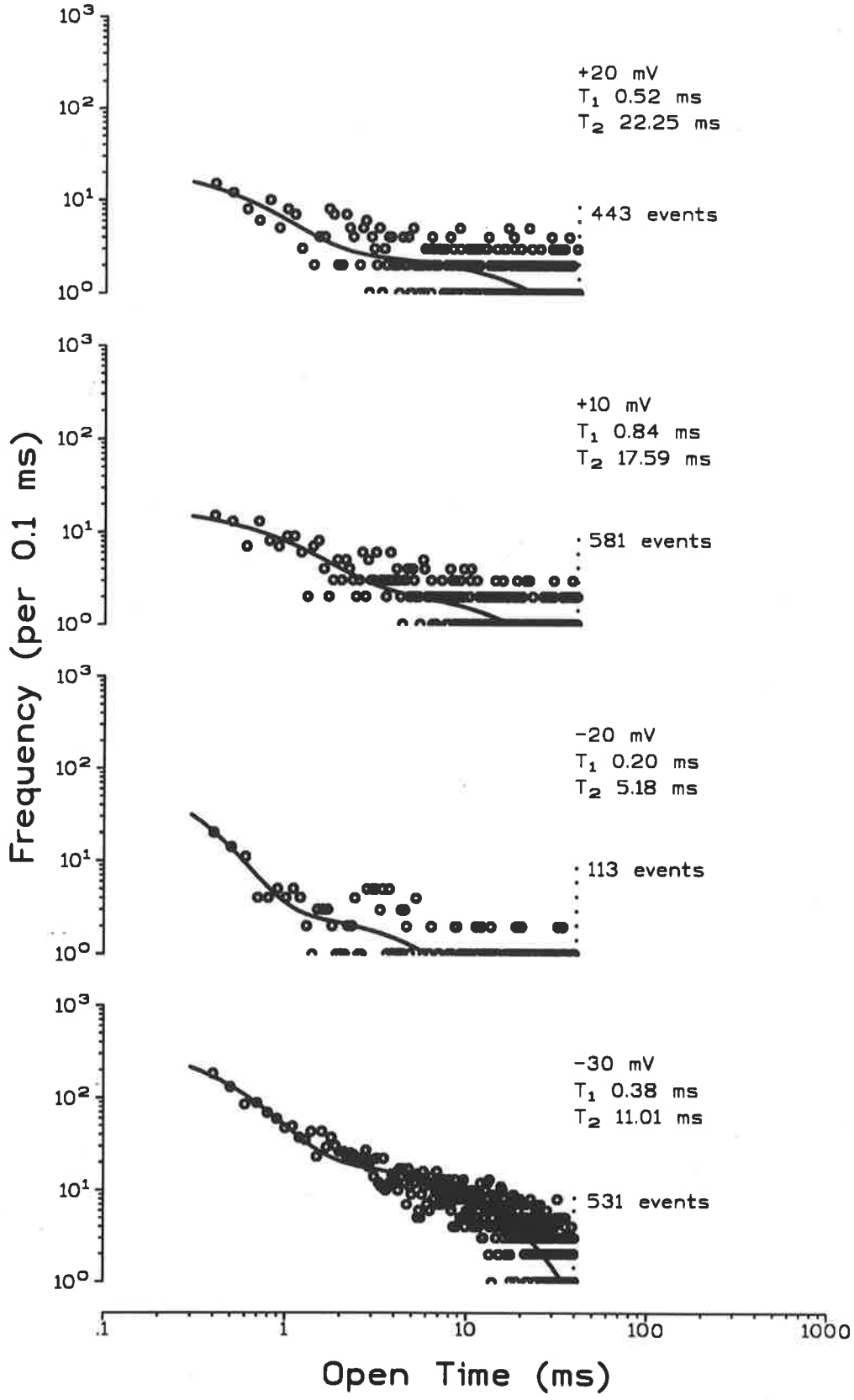
+20 mV
T1 0.52 ms
T2 22.25 ms
443 events
+10 mV
T1 0.84 ms
T2 17.59 ms
581 events
-20 mV
T1 0.20 ms
T2 5.18 ms
113 events
-30 mV
T1 0.38 ms
T2 11.01 ms
531 events
Frequency (per 0.1 ms)
Open Time (ms)
10^3
10^2
10^1
10^0
.1
1
10
100
1000

FIGURE 4.8 Frequency distributions of closed times
Log-log plot of the distribution of closed times recorded at different steady-state potentials. The observed data is described by the sum of two exponentials and the continuous line indicates the line of best fit. A lengthening of the time constants is observed at -30 mV. At each potential, there were several observations at longer times which were not included in the fit, but are displayed here. They are the data to the right of the vertical dotted line in each case and the number of these events is indicated. An estimate for these longer closed times was obtained from the arithmetic mean of the events, which ranged between 70 and 722 ms. There were too few events to obtain a meaningful interpretation of these estimates.

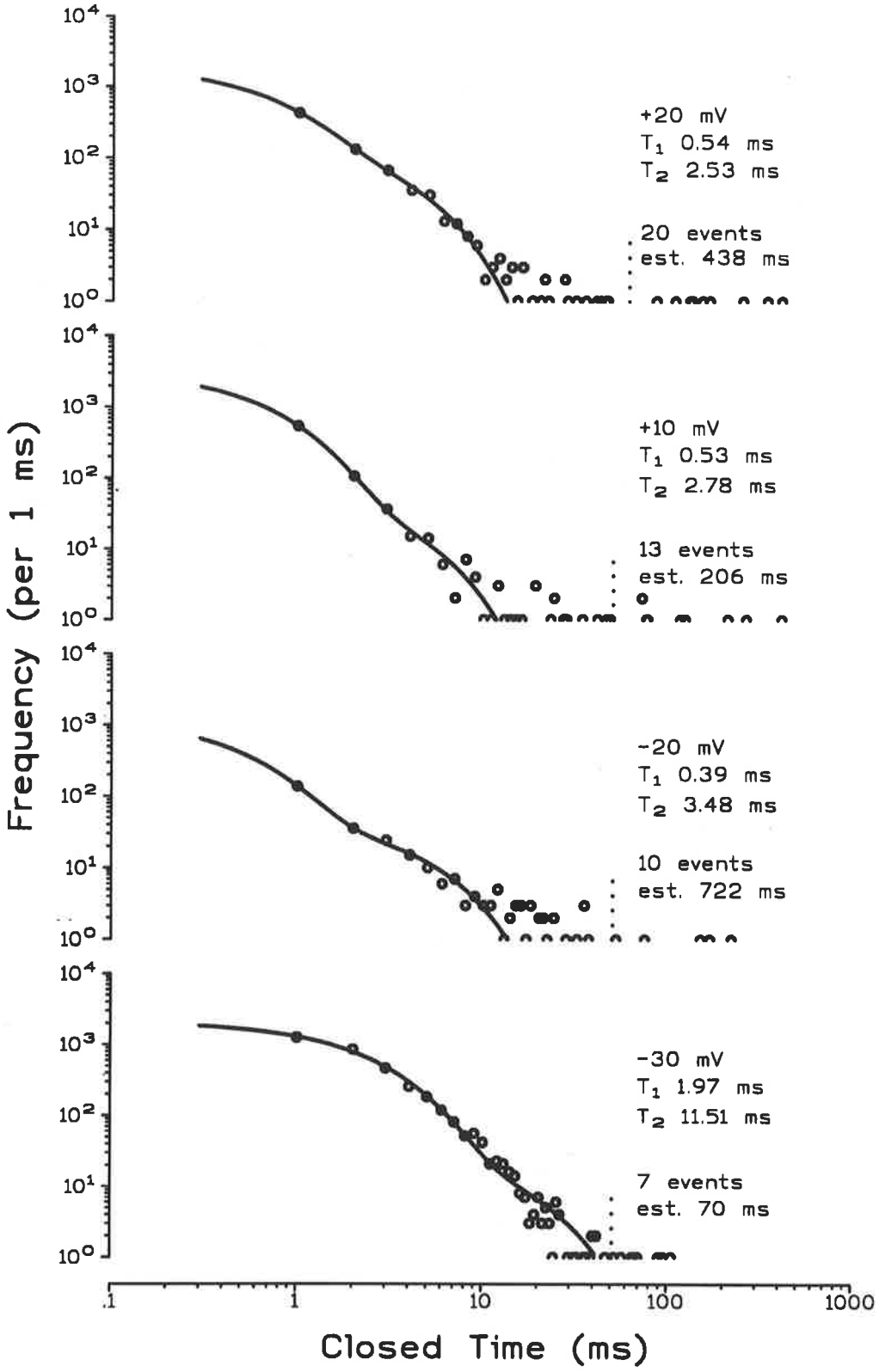
Frequency (per 1 ms)
+20 mV
T1 0.54 ms
T2 2.53 ms
20 events
est. 438 ms
+10 mV
T1 0.53 ms
T2 2.78 ms
13 events
est. 206 ms
-20 mV
T1 0.39 ms
T2 3.48 ms
10 events
est. 722 ms
-30 mV
T1 1.97 ms
T2 11.51 ms
7 events
est. 70 ms
Closed Time (ms)

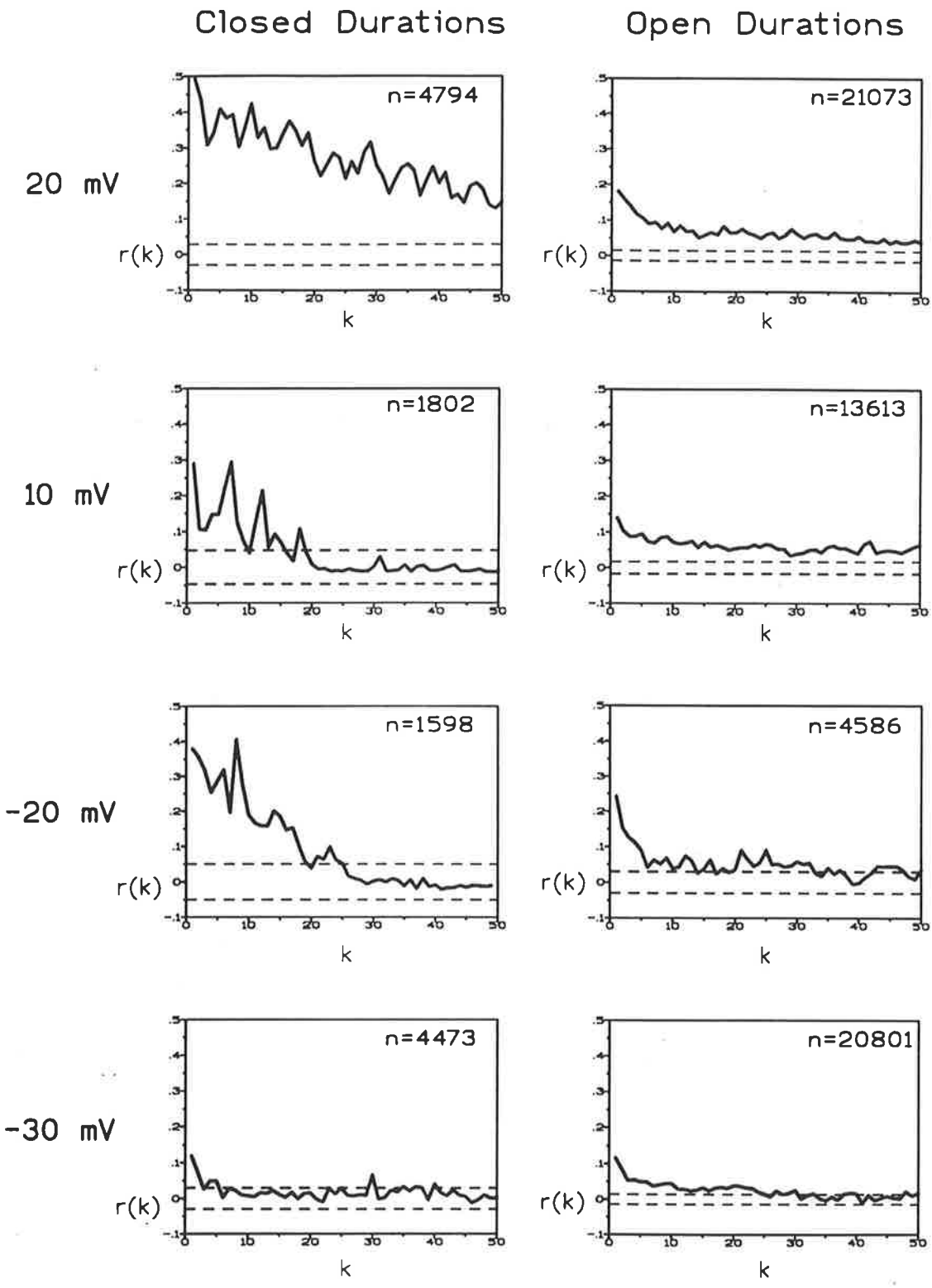

FIGURE 4.9 Autocorrelations of open and closed durations
Estimated autocorrelation functions, r(k), calculated for the series of closed and open durations from steady-state recordings made at the potentials indicated. In each case the dashed lines indicate the 95% confidence limits for the variance expected for white noise alone, estimated from the number of durations in each series (*n*). Autocorrelations which occur outside of these limits are considered significant.

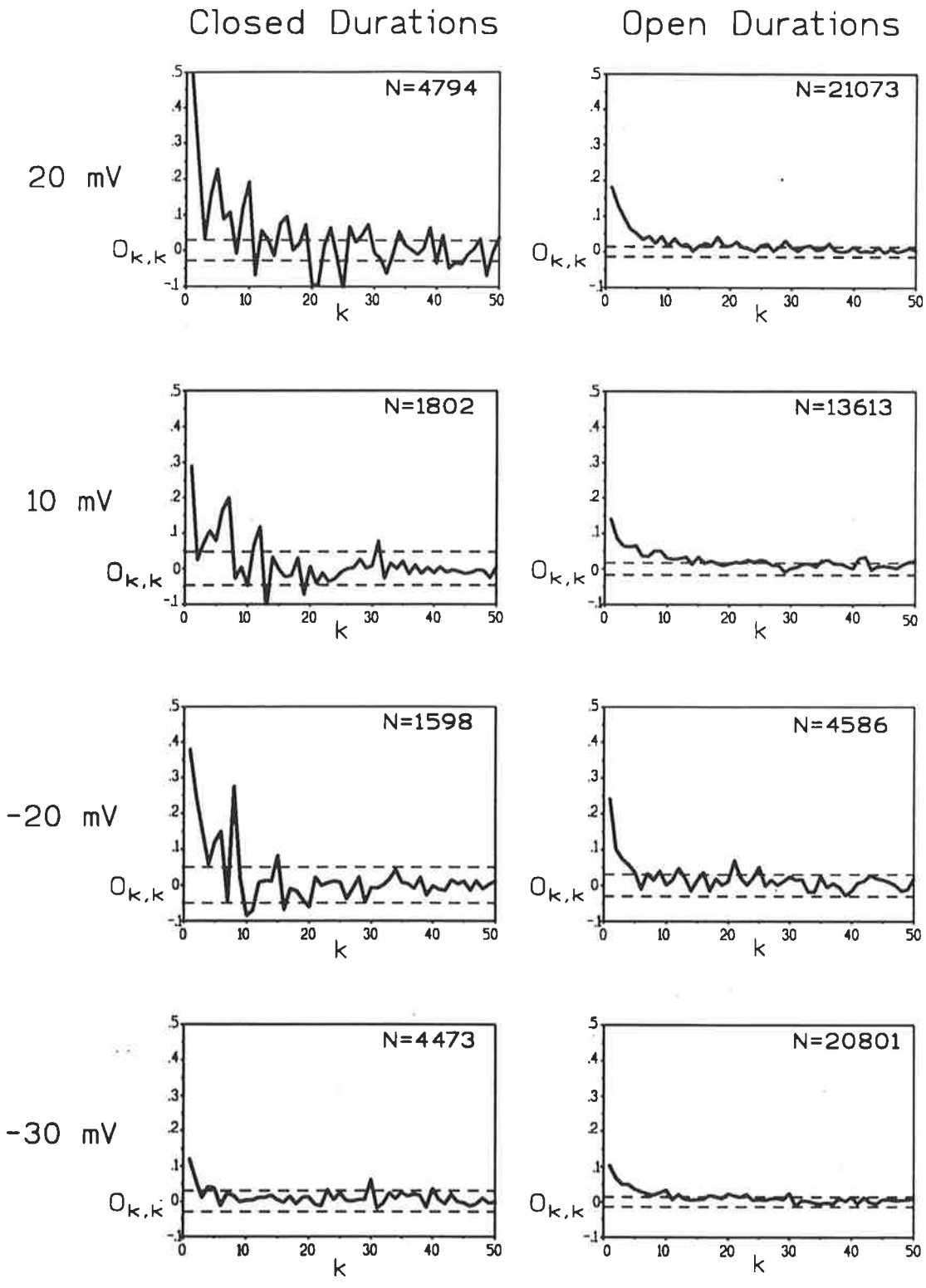

FIGURE 4.10 Partial autocorrelations of open and closed aggregates
Estimated partial autocorrelation functions, $O_{k,k}$, calculated from the autocorrelation functions of the closed and the open durations shown in Figure 4.9. Again, the dashed lines indicate the 95% confidence limits for the variance expected for white noise alone, and *n* is the number of durations in each series. The partial autocorrelation decays to within the 95% confidence limits for a much shorter lag, k, than the autocorrelation function (Figure 4.9). This is indicative of an autoregressive process.

TABLE 4.1
AUTOCORRELATION FUNCTIONS
FOR THE OPEN AND CLOSED AGGREGATES

Vp (mV)	State	*E*-1	*i*	υ_i	±SE	σ_i	±SE
+20	O	2	1	0.1431	0.0097	0.8209	0.0172
			2	0.0602	0.0025	0.9948	0.0005
	C	1	1	0.4280	0.0112	0.9805	0.0009
+10	O	2	1	0.0735	0.0094	0.8378	0.0322
			2	0.0602	0.0032	0.9947	0.0007
	C	1	1	0.2287	0.0450	0.9312	0.0231
-20	O	2	1	0.3040	0.0496	0.5755	0.0645
			2	0.0662	0.0077	0.9824	0.0033
	C	1	1	0.4159	0.0318	0.9327	0.0082
-30	O	2	1	0.1260	0.0275	0.5657	0.0895
			2	0.0454	0.0050	0.9714	0.0036
	C	1	1	0.1690	0.0427	0.6779	0.0814

The a.c.f.'s are described by the sum of *E*-1 geometrically decaying components, where *E* is the number of entry/exit states which communicate between the open (O) and closed (C) aggregates, according to the equation:

$$r(k) = \sum_{i=1}^{E-1} \upsilon_i . \sigma_i^{|k|}, \quad \text{for } k \neq 0$$

where *k* is the lag of the a.c.f. The estimated parameter values ±SE are listed for the various recording potentials.

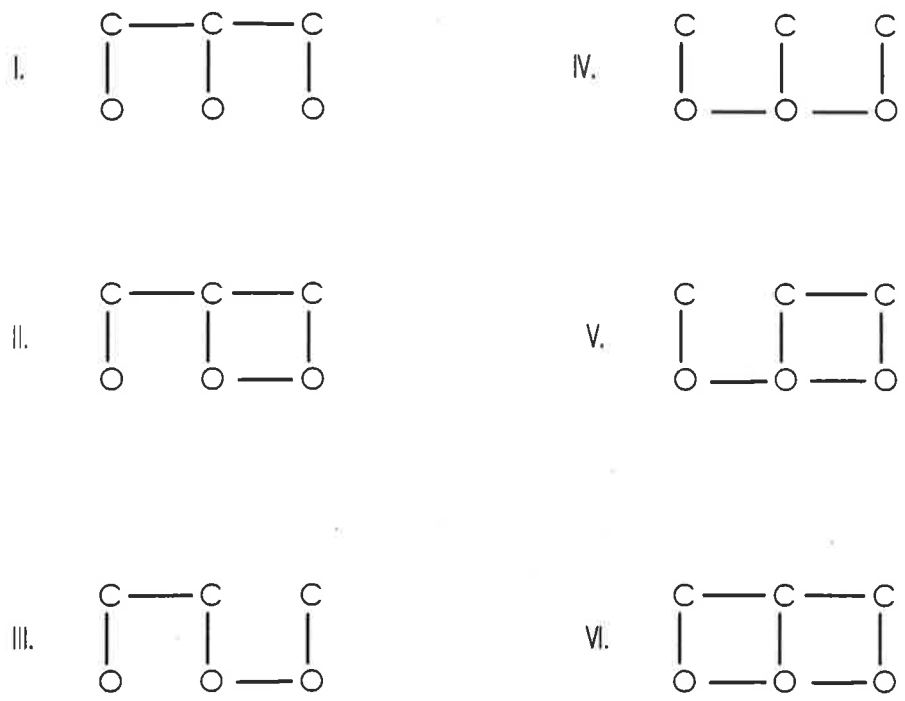

FIGURE 4.11 Possible kinetic schemes.
In each case, there are three open states and three closed states as was determined from the duration frequency distributions. There are also three entry/exit pathways between the open and closed aggregates. With these conditions satisfied, the number of possible kinetic schemes is restricted to the six presented here. The lines connecting the different states represents the reversible transitions that occur between adjacent states.

Non-stationary kinetic analysis

To distinguish between the six possible schemes proposed above, non-stationary kinetic analysis was used. It provided an approach to find out more about the relationship of adjacent kinetic states and the symmetrical behaviour of the channel.

a) Relaxation kinetics

Mean ensemble currents obtained from a voltage-step protocol were expressed as time-dependent open-probability plots, and the $P_O(V)$ curve was routinely determined, as previously described in Chapter 3. An example of the P_O relaxations obtained from mean ensemble currents is shown in Figure 4.12A for positive voltage steps and Figure 4.12B for negative voltage steps. With small voltage steps in the range ±20 mV, the degree of relaxation observed was small and the ensemble currents remained at much the same level over the length of the voltage step. This indicated that a high open probability was maintained in the pseudo-steady state at these small potentials. The almost linear nature of these relaxations meant exponential curves were unable to be fitted to these data meaningfully. At potentials greater than ±20 mV, P_O relaxations reached a new pseudo-steady-state level over the 900 ms period and were well described by single exponential curves. It was observed that the mean time constants of the exponential fits became progressively shorter with an increase in the magnitude of the voltage step applied to the patch (Figure 4.12D). This was true for both positive and negative potentials. In some cases, at the ±50 and ±60 mV potential steps, the relaxations were better described by the sum of two exponential terms, in which case the fast time constants were examined because they were consistently present. The slower time constants showed no consistent change with potential and were regarded as being less reliable (data not shown).

b) Reactivation kinetics

So far, the voltage-step protocols applied to patches has been from a holding potential of 0 mV, where the anion channel is almost always open. By holding at a potential where the channel is mostly closed, the reactivation kinetics of the channel were investigated with voltage steps towards 0 mV.

For each patch, a $P_O(V)$ curve was determined before the reactivation protocol was applied. Isolated patches were then held at potentials of either +30 mV or -30 mV, where there is a low P_O for the channel. On applying voltage steps to +15 and -15 mV, the P_O was observed to increase, and reach a pseudo-steady-state. On returning to the holding potential, the P_O would relax towards the initial low P_O value. An example of this type of recording is shown in Figure 4.13B.

The time course of the change in P_O as the channel reaches a new equilibrium was quite variable between each patch for both steps to potentials of the same sign as the holding potential (that is for both +15 mV from a holding potential of +30 mV and -15 mV from -30 mV) and for those of the opposite sign (that is for both -15 mV from +30 mV and +15 mV from -30 mV). In some cases the time course was quite slow, reaching a steady-state in an exponential-like manner after approximately 100 ms, while in other cases there was an initial rapid increase in the first 10 ms followed by much slower component to reach the final steady-state. Despite these differences in the time course, a similar level of P_O was attained at the end of both the +15 mV and -15 mV steps for an individual ensemble (Figure 4.13A and B). This was true of individual experiments from a holding potential of either +30 mV or -30 mV and is consistent with the symmetrical $P_O(V)$ curve. A comparison of the pseudo-steady state P_O at the end of the 220 ms voltage step (P_O observed) is presented in Table 4.2. In all cases, the open probability level attained at the end of the voltage step was less than that expected from the $P_O(V)$ curve determined by voltage steps from a holding potential of 0 mV (Table 4.2, P_O

FIGURE 4.12 Non-stationary analysis of current relaxations
Multi-channel patches were stepped to a range of positive (**A**) and negative (**B**) potentials for 900 ms, from a holding potential of 0 mV. The mean ensemble currents are expressed here as time-dependent open-probabilities, as previously described in Figure 3.5. **C.** The *Po(V)* curve obtained from the time-dependent open-probabilities shown in **A** and **B**. Each half of the curve was fitted with a Boltzmann equation as described for Figure 3.6. The gating charge values, z, were -7.2±1.3 and 12.2±2.3, while the V_0 values were -10.3±0.7 mV and 15.2±0.4 mV, for negative and positive potentials respectively. **D.** Each time-dependent open-probability relaxation was generally described by a single exponential for potentials of magnitude 20 mV and larger. Shown here are the average time constants obtained from a number of experiments using the same protocol (n=7 to 17). The time constants became shorter as the magnitude of the test potential increased.

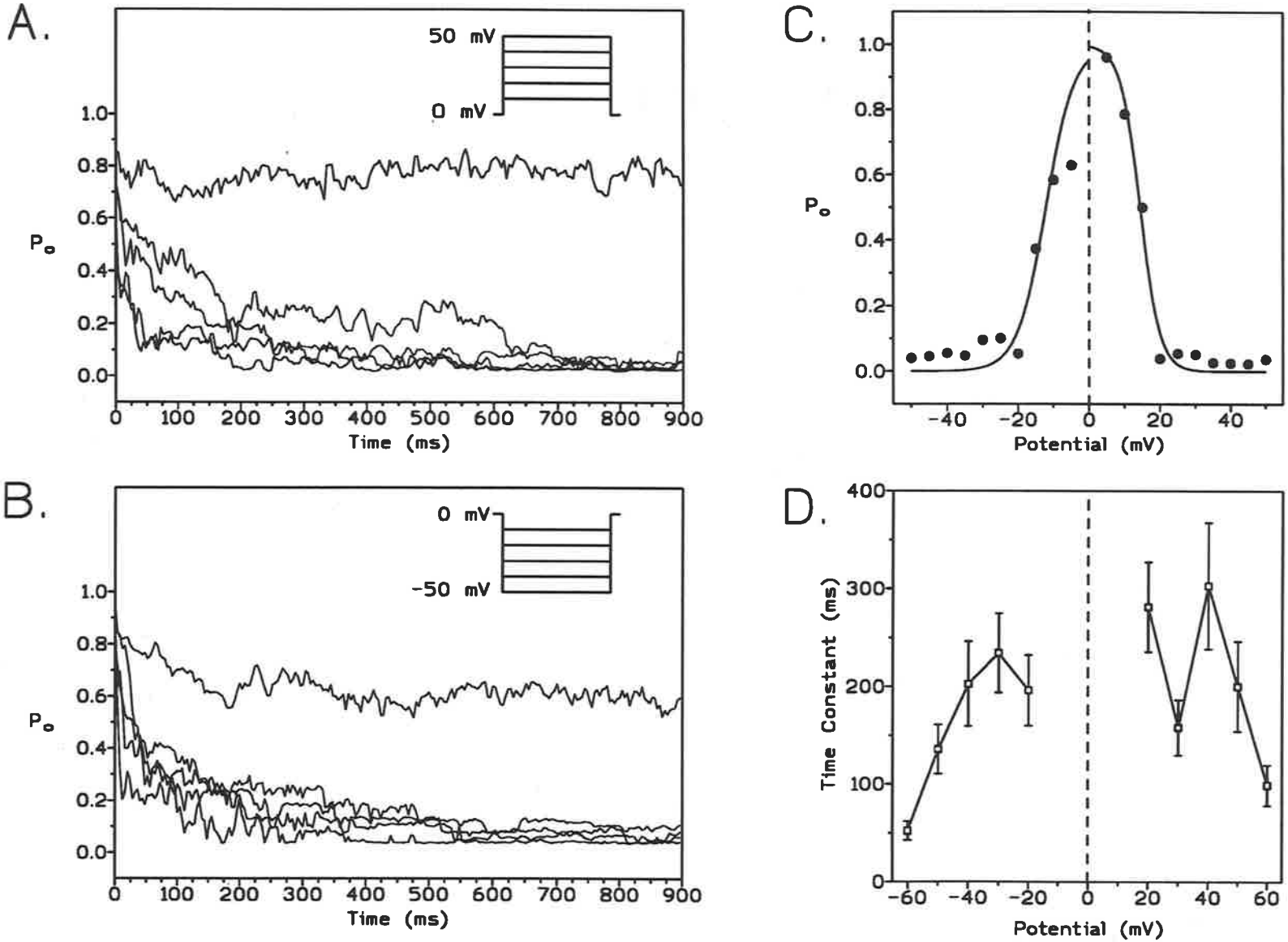
A.
50 mV
0 mV
1.0
0.8
0.6
0.4
0.2
0.0
P_o
0
100
200
300
400
500
600
700
800
900
Time (ms)
B.
0 mV
-50 mV
1.0
0.8
0.6
0.4
0.2
0.0
P_o
0
100
200
300
400
500
600
700
800
900
Time (ms)
C.
1.0
0.8
0.6
0.4
0.2
0.0
P_o
-40
-20
0
20
40
Potential (mV)
D.
400
300
200
100
0
Time Constant (ms)
-60
-40
-20
0
20
40
60
Potential (mV)

FIGURE 4.13 Reactivation from low open-probability condition
Ensemble averaged non-stationary behaviour of multi-channel patches in response to applied potential steps of ±15 mV from a holding potential of -30 mV. **A**. The ensemble averaged currents were expressed as time-dependent open-probabilities. When stepping to -15 mV, the averaged behaviour shifted to a new pseudo-steady-state with a *Po* of 0.45 by the end of the 220 ms step. When stepping to +15 mV, a similar pseudo-steady-state was reached, however the shift was much more rapid. On returning to the holding potential, a peak increase in the *Po* was seen following the +15 mV step but not the -15 mV step. **B**. The *Po(V)* curve (open circles) was obtained for the patch before applying the voltage step protocol. The initial *Po* at the holding potential and the pseudo-steady-state *Po* reached at the end of the 220 ms voltage step are plotted as filled circles. The initial magnitude of the *Po* following the return to the holding potential is shown as an open square for the -15 mV step and a filled square for the +15 mV step.

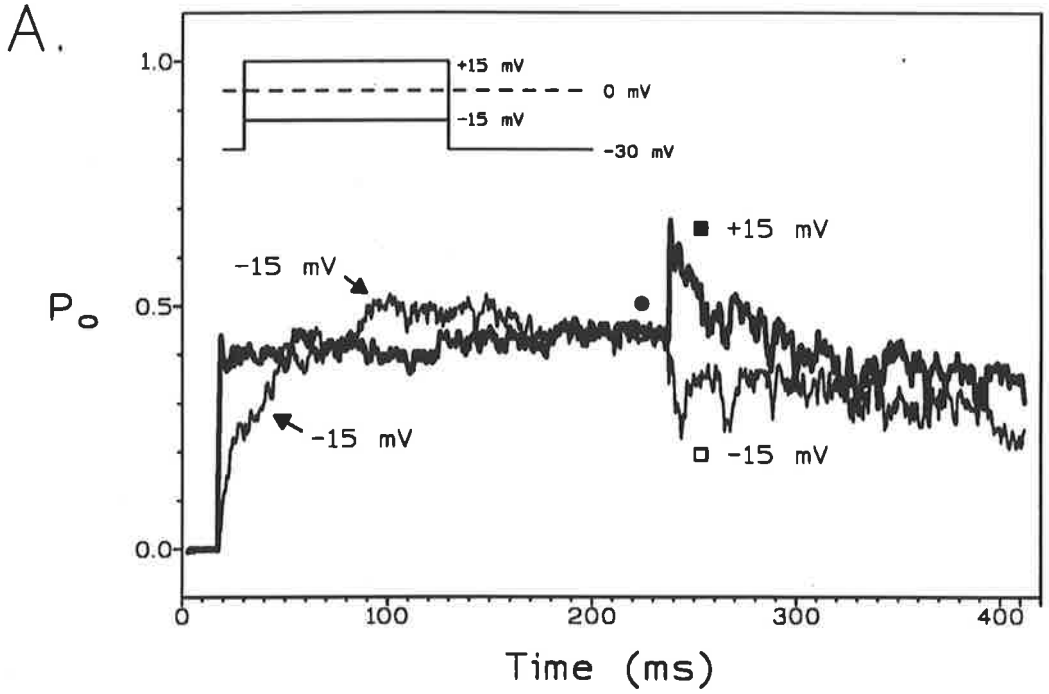
A.
1.0
0.5
0.0
P_o
+15 mV
0 mV
-15 mV
-30 mV
-15 mV
-15 mV
+15 mV
-15 mV
0
100
200
300
400
Time (ms)

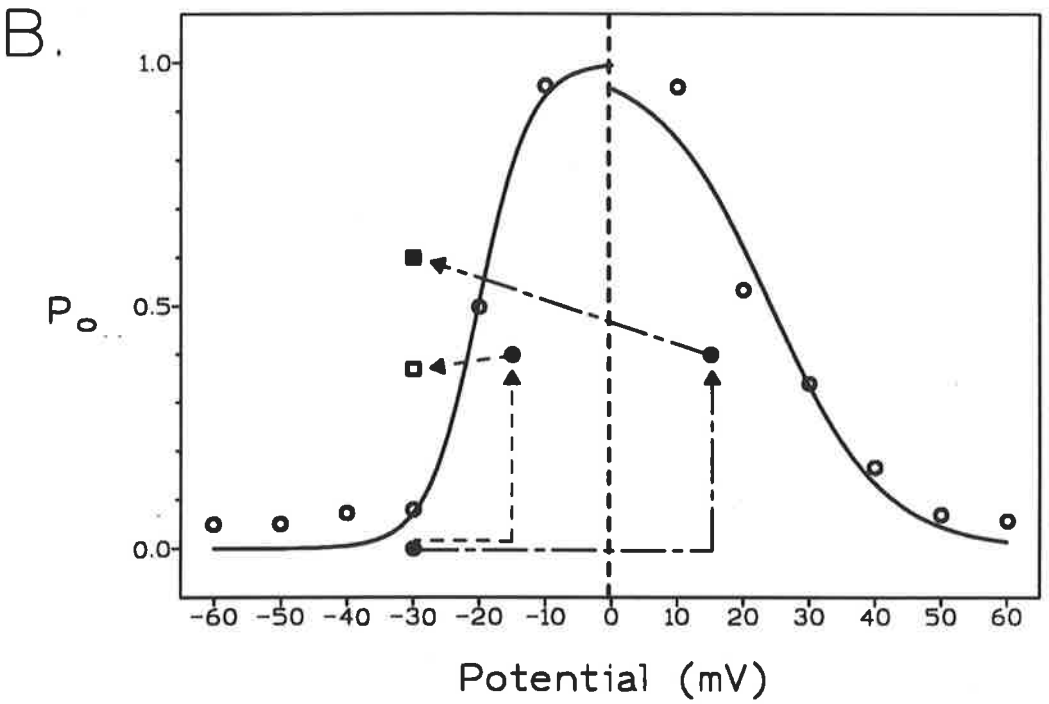
B.
1.0
0.5
0.0
P_o
-60 -50 -40 -30 -20 -10 0 10 20 30 40 50 60
Potential (mV)

TABLE 4.2
PSEUDO-STEADY-STATE OPEN PROBABILITIES

	+15 mV			-15 mV		
Holding Potential	*Po* (obs.)	*Po* (exp.)	Δ*Po*	*Po* (obs.)	*Po* (exp.)	Δ*Po*
+30 mV	0.62 ±0.17	0.76 ±0.06	-0.14 ±0.26	0.38 ±0.19	0.61 ±0.10	-0.23 ±0.12
-30 mV	0.58 ±0.09	0.85 ±0.08	-0.27 ±0.22	0.50 ±0.09	0.60 ±0.09	-0.10 ±0.10

Pseudo-steady-state values of the open probability obtained from current relaxations in response to voltage steps from 0 mV (*Po* expected) are compared to those obtained from voltage steps originating at ±30 mV and stepping towards 0 mV (*Po* observed), the difference being Δ*Po*. Values are mean ± SEM for n=6.

TABLE 4.3
PEAK OPEN PROBABILITY ON RETURNING TO HOLDING POTENTIAL

		+15 mV		-15 mV	
Holding Potential	Po	Peak Po	Δ Po	Peak Po	Δ Po
+30 mV	0.34 ±0.10	0.52 ±0.14	0.18 ±0.09	0.60 ±0.13	0.26 ±0.09
-30 mV	0.22 ±0.08	0.65 ±0.11	0.43 ±0.12	0.38 ±0.06	0.17 ±0.06

Analysis of peak current on return to the holding potential of ±30 mV, following a test potential step to ±15 mV. The non-stationary open probabilities (Peak *Po*) are compared to the pseudo-steady-state open probability (*Po*) at the holding potential, the difference being Δ*Po*. Values are mean ± SEM for n=6.

expected; see example in Figure 4.13B). The difference between the expected $P_O(V)$ values and the observed $P_O(V)$ values, ΔP_O, at the end of both the +15 and -15 mV steps were calculated and then compared. No significant difference was found between the ΔP_O values at +15 mV and -15 mV for either a holding potential of +30 mV ($p>0.05$, two tailed t-test) or a holding potential of -30 mV ($p>0.05$, two tailed t-test).

On returning from the test potential to the holding potential, the relaxations exhibited an initial peak increase in the channel activity, for those steps which involved a change in the sign of the applied electric field (see example in Figure 4.13A, and group data summarised in Table 4.3). In comparison, those cases where no change in the sign of the electric field occurred, the P_O was not significantly greater than that attained at the end of the test voltage step. This was quantified as the ΔP_O at the onset of the relaxation, above the P_O expected at the holding potential. In both cases, they relaxed in a similar manner toward the pseudo-steady state P_O level expected at the holding potential. Thus, for steps returning from -15 mV to +30 mV the ΔP_O was 0.26 ± 0.09 above the pseudo-steady state level expected at the holding potential, and this was significantly greater than the ΔP_O of 0.18 ± 0.09 observed for steps from +15 mV to +30 mV ($p<0.05$, two tailed t-test). Similarly, for steps returning from +15 mV to -30 mV, the ΔP_O was 0.43 ± 0.12 and is significantly greater than the ΔP_O of 0.17 ± 0.06 for steps returning from -15 mV to -30 mV ($p<0.05$, two tailed t-test).

The peak increase in P_O on returning to -30 mV from +15 mV or to +30 mV from -15 mV, suggests a voltage-dependent transition from closed state to an open state. The relaxation which follows is the shift in equilibrium towards a new closed state at the holding potential. Interpretation of this data suggests that the open states form a link between the closed states that have voltage dependent occupancies.

To test specifically for independent closed states, voltage steps were made from a holding potential of -50 mV (where channels have a open probability of 0.2 or less) to +50 mV and then returning to -50 mV. Figure 4.14 shows an example of the mean ensemble current expressed in terms of the channel P_O. Upon application of this step change in potential, the P_O increased rapidly, such that nearly all channels were opened initially reaching a peak of P_O of approximately 0.8. The increase was transient and the ensemble current was observed to relax during the maintained test potential. The relaxation reaches a pseudo-steady-state with a P_O of 0.3, before returning to the holding potential of -50 mV. Here again, almost all the channels are initially opened upon returning to -50 mV, as indicated by a peak P_O of 0.9. This process must be very rapid as there is no distinguishable delay in the onset of the opening of channels. Over time, the P_O relaxes until it reaches a new pseudo-steady-state at the holding potential. The rapid increase and subsequent relaxation in P_O upon applying the test potential of +50 mV from the holding potential of -50 mV is qualitatively similar to a relaxation from a holding potential of 0 mV, for the same test potential.

By itself, this might suggest that the closed state occupied at negative potentials is different from that occupied at positive potentials and that they gate independently and in parallel; opening from one of these states at positive potentials and from the other at negative potentials. Certainly the first part of this statement holds, but the results, where potentials are returning from +15 mV to -30 mV (or -15 mV to +30 mV), have only a small transient increase in P_O before relaxing, which is less than the peak of P_O=0.9 expected from independent gates. Instead, it suggests that either (i) the closed states are linked and that the proportion of channels that transit through closed states as against the proportion that transit through open states before reaching the new closed state is voltage dependent, or (ii) the closed states are linked by the open states only, and that the transient increase in P_O is determined by both the voltage dependent rates of entering the open states and entering the new closed state.

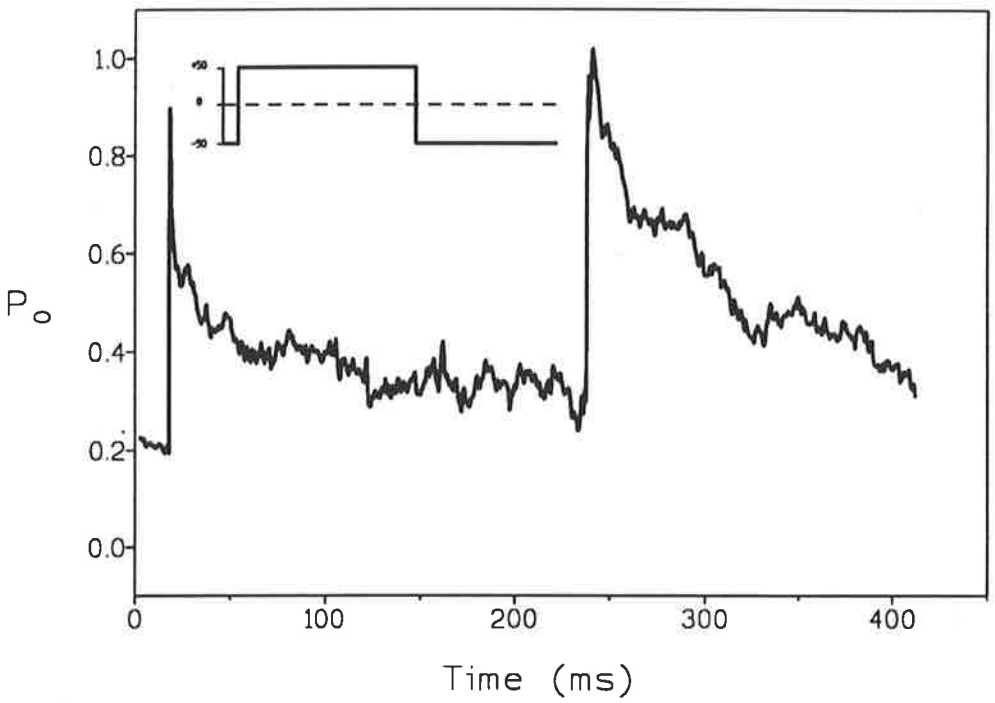

FIGURE 4.14 Rapid opening with a change in the sign of the applied potential.
Ensemble current relaxations expressed as a time-dependent open-probability after stepping from a holding potential of -50 mV to a test potential of +50 mV for 220 ms and then returning to the holding potential. At the onset of the test potential there is a rapid and large increase in the *Po* which relaxes over the period of the test step in a manner similar to that observed for steps to +50 mV from 0 mV. On returning to -50 mV, a rapid increase in the *Po* is again observed which also relaxes. This is an indication that the closed state occupied at negative potentials is not necessarily the same as that occupied at positive potentials.

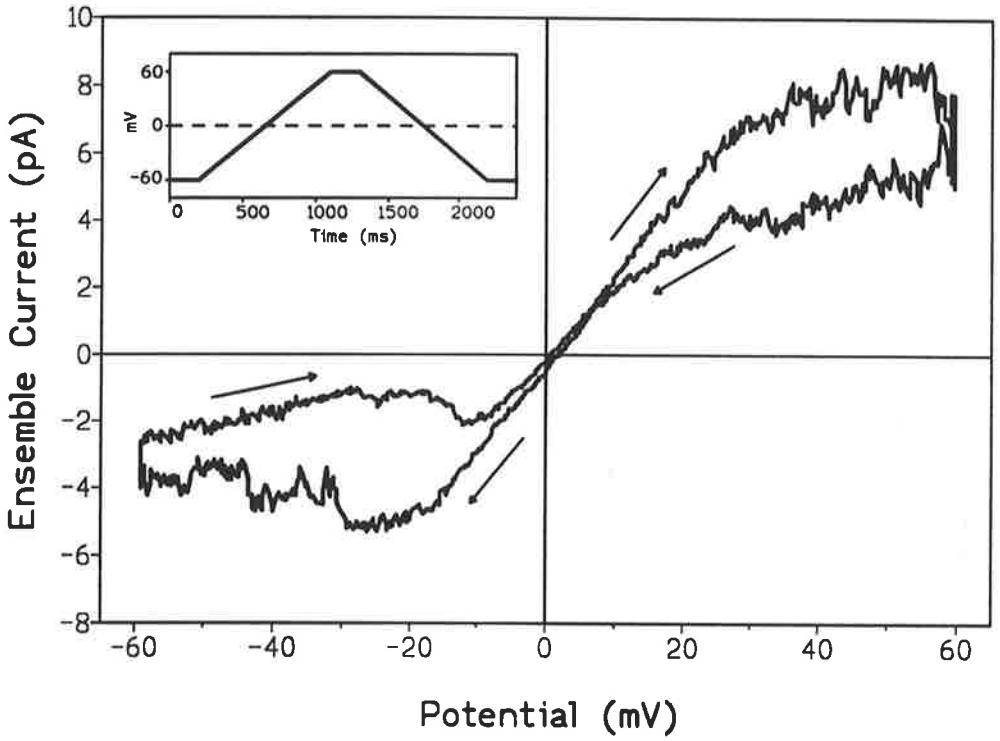

FIGURE 4.15 Ensemble current from applied ramp
A ramping protocol from a holding potential of -60 mV through to +60 mV in 900 ms, pausing for 200 ms and then returning to -60 mV was applied to multi-channel patches. The arrows indicate the direction of the applied ramp. The ensemble current is the average of 18 successive trials. Two channels were present in this example and the linear portions of the ensemble current near zero correspond to a slope conductance of 560 pS, equivalent to two channels of unit conductance 280 pS.

c) Ramps

The ensemble average current obtained from a ramp experiment recorded in an isolated patch is presented in Figure 4.15. When the potential was being ramped from the holding potential of -60 mV towards zero, the conductance (the slope of the mean current-voltage trace) did not increase until about -20 mV, and this is described here as the point where the channels began to "turn-on". Over the range of -10 to +20 mV, the slope conductance was 560 pS, indicative of two anion channels present in the patch, each with a conductance of 280 pS. Continuing the ramp from zero towards +60 mV, channel "turn-off" was not until about +20 mV where the conductance (slope) began to decrease. The amplitude of the current at potentials beyond this "turn-off" region was larger than expected from the voltage dependent $P_O(V)$ curve, estimated from the pseudo-steady-state. This is likely to be due to the ramp rate of 0.13 mV/ms being faster than the movement of the channel equilibrium towards the closed states. As the potential paused at +60 mV, the current continued to relax over this period. On the return ramp, the channel began to "turn-on" at about +20 mV and was fully open at +10 mV. On reaching -15 mV, the conductance declined, indicating the point at which the channels started to "turn-off". At the rate this ramp was applied, the rate of the "turn off" kinetics appeared to be much slower, with a delay in the reduction of the conductance, compared to the rate of "turn on" kinetics. In the example shown, the current did not relax to the same degree during the ramp at positive potentials compared to the current at negative potentials. As discussed in Chapter 3, some channels showed no such asymmetrical behaviour and others were asymmetric in the opposite direction, so that overall, there is insufficient evidence to suggest that this is a real asymmetry in the behaviour of the channel.

A possible model

Of the six possible schemes proposed in Figure 4.11, three of these, schemes I, IV and VI, are likely candidates to describe the behaviour of the sarcoball anion

channel. All three are symmetrical, which is a characteristic that is thought to be important in producing the symmetrical voltage-dependence of the channel. Only scheme VI has each of the open states linked and each of the closed states linked, as is suggested from the non-stationary analysis. Schemes I and IV, however, were not discounted entirely and they were also investigated for their ability to predict a bell-shaped $P_O(V)$ curve. The shape of the $P_O(V)$ curve was determined by calculating the P_O for potentials between -60 mV and +60 mV. This was done for several different arrangements of rate constants within each of the three kinetic schemes. The kinetic schemes are shown in Figure 4.16 to illustrate the convention used to label each of the rate constants and states.

Transitions between the open and closed states are by either voltage-independent rate constants or voltage-dependent rate constants. The voltage dependent rate constants are described by the following equation:

$$\alpha = \alpha_0 \exp(z\, VF/RT) \qquad (4.10)$$

where, in this case, α is a voltage-dependent rate constant, V is the membrane potential, the coefficient α_0 is the value of the rate constant when V is 0 mV, z is the gating charge, F is Faraday's constant, R is the Gas constant and T is temperature in degrees Kelvin. The gating charge, z, will determine the steepness of the voltage-dependence and the coefficient α_0 will influence the equilibrium P_O at 0 mV. The rate constants used in each case were first-guesses obtained by visually fitting predicted p.d.f.'s (generated by the **Q** matrix method of Colquhoun and Hawkes (1981)) to the open and closed duration frequency distributions.

From these rate constants, the equilibrium probabilities of each state were calculated to generate the predicted $P_O(V)$ curve. For example, for scheme VI the equilibrium probabilities, $p_n(\infty)$, can be evaluated, using the conventions shown in Figure 4.16, from the following set of equations.

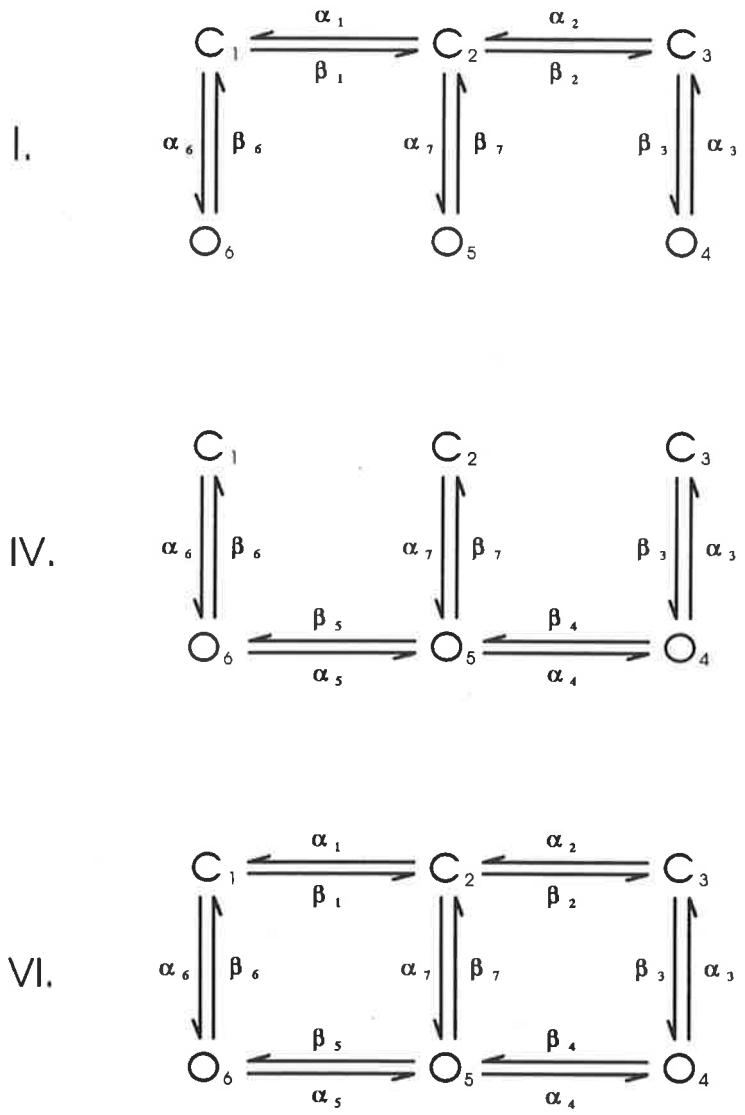

FIGURE 4.16 Three possible kinetic schemes
These are the three kinetic schemes, out of the possible six initially presented in Figure 4.11, which are symmetrical and might describe the behaviour of the sarcoball anion channel. For each of schemes I, IV and VI, the labelling convention of the rate constants between each of the states is shown. Each of these rates could possibly be either voltage-dependent or voltage-independent.

$$\begin{aligned} p_1(\infty) \cdot \beta_1 &= p_2(\infty) \cdot \alpha_1 & \qquad p_4(\infty) \cdot \beta_4 &= p_5(\infty) \cdot \alpha_4 \\ p_2(\infty) \cdot \beta_2 &= p_3(\infty) \cdot \alpha_2 & \qquad p_5(\infty) \cdot \beta_5 &= p_6(\infty) \cdot \alpha_5 \\ p_3(\infty) \cdot \beta_3 &= p_4(\infty) \cdot \alpha_3 & \qquad p_6(\infty) \cdot \beta_6 &= p_1(\infty) \cdot \alpha_6 \end{aligned} \tag{4.11}$$

where

$$p_1(\infty) + p_2(\infty) + p_3(\infty) + p_4(\infty) + p_5(\infty) + p_6(\infty) = 1 \tag{4.12}$$

The open-probability of the channel is therefore the sum of the equilibrium probabilities for each of the open states:

$$P_O = p_4(\infty) + p_5(\infty) + p_6(\infty) \tag{4.13}$$

Further details as to how the equilibrium probabilities were calculated and how the $P_O(V)$ curves were produced is presented in the Appendix.

The task was to determine where the voltage-dependent rate constants needed to be placed in order to predict a bell-shaped $P_O(V)$ curve. If the voltage-dependent rate constants were to be placed only between the open states (O_4 to O_5, O_5 to O_6) or between the closed states (C_1 to C_2, C_2 to C_3), voltage-dependent gating between the open and closed aggregates would not be possible. Therefore, the first choice was to place voltage-dependent rate constants between the open and closed states ie. C_1 to O_6, C_2 to O_5, C_3 to O_4. All remaining rate constants were made voltage-independent.

Since scheme VI is a cyclic kinetic scheme, there is an additional restriction to the nature of the rate constants, which is the necessity to maintain the condition of microreversibility (Colquhoun & Hawkes, 1983). This means that the product of the rate constants in one direction around a closed loop within the kinetic scheme (say, clockwise) must be the same as the product of the rate constants in the other direction around the same loop (anti-clockwise). For example, it is not possible to have an increasing voltage-dependent rate constant going in one direction without another increasing rate constant going in the opposite direction, somewhere in the loop. To achieve this in scheme VI, either (i) $\alpha_3 = \beta_3$, $\alpha_6 = \beta_6$ and $\alpha_7 = \beta_7$, or (ii) $\alpha_6 = \beta_3 = \beta_7$ and $\alpha_3 = \alpha_7 = \beta_6$.

For each of schemes I, IV and VI, when the rate constants between the open and closed states were voltage-dependent, the $P_O(V)$ curve predicted was sigmoidal in shape. As an example, the rate constants and their arrangement is shown for scheme VI in Figure 4.17. The results for all three schemes were qualitatively similar to those shown in Figure 4.18, which were generated from scheme VI.

To obtain a bell-shaped $P_O(V)$ curve, the placement of the voltage-dependent rate constants needed to be changed. For scheme I the only alternative placement of the voltage-dependent rates is between C_1 to C_2 and C_2 to C_3, though there must still be some voltage-dependent rates between the open and closed states. Therefore, voltage-dependent rates were retained between C_1 to O_6 and C_3 to O_4. Using these placements and the rate constants summarised in Figure 4.19, a bell-shaped $P_O(V)$ curve was predicted.

A similar situation applies to scheme IV. When voltage-dependent rate constants were placed between O_4 to O_5 and O_5 to O_6, however, an inverted bell-shaped $P_O(V)$ curve being maximally open at large potentials either side of 0 mV and closed at 0 mV was predicted. A much simpler arrangement, where the voltage-dependent rate constants were placed only between C_1 to O_6 and C_3 to O_4, as summarised in Figure 4.20, was able to predict the required bell-shaped $P_O(V)$ curve.

Where the voltage-dependent rates were placed in scheme VI was influenced by the results from schemes I and IV, and the restrictions of maintaining microreversibility. The arrangement of the voltage-dependent rate constants as in scheme IV violates the condition of microreversibility in scheme VI, and so this option was discarded. An arrangement like that for scheme I is in keeping with the restriction of microreversibility, and using the rate constants summarised in Figure 4.21, a bell-shaped $P_O(V)$ curve was predicted. The bell-shaped $P_O(V)$ curves predicted by schemes I, IV and VI were qualitatively similar and behaved

VI.

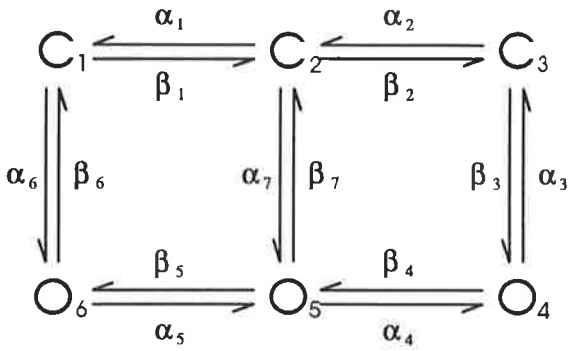

Voltage-independent rate constants

Group 1

$\alpha_4 = \alpha_5 = \beta_1 = \beta_2 = 0.3$

Group 2

$\alpha_1 = \alpha_2 = \beta_4 = \beta_5 = 3.0$

Voltage-dependent rate constants

Group 1

$\alpha_6 = \alpha_7 = \beta_3 = 0.5 \exp (1.8\ VF/RT)$

Group 2

$\alpha_3 = \beta_6 = \beta_7 = 0.3 \exp (-0.8\ VF/RT)$

FIGURE 4.17 Configuration of scheme VI which predicts a sigmoidal curve
Using the rate constants shown here, a sigmoidal *Po(V)* curve was predicted by scheme VI and microreversibility was maintained. In this case, voltage-dependent rate constants were required between the open and closed states (C_1 and O_6, C_2 and O_5, C_3 and O_4).

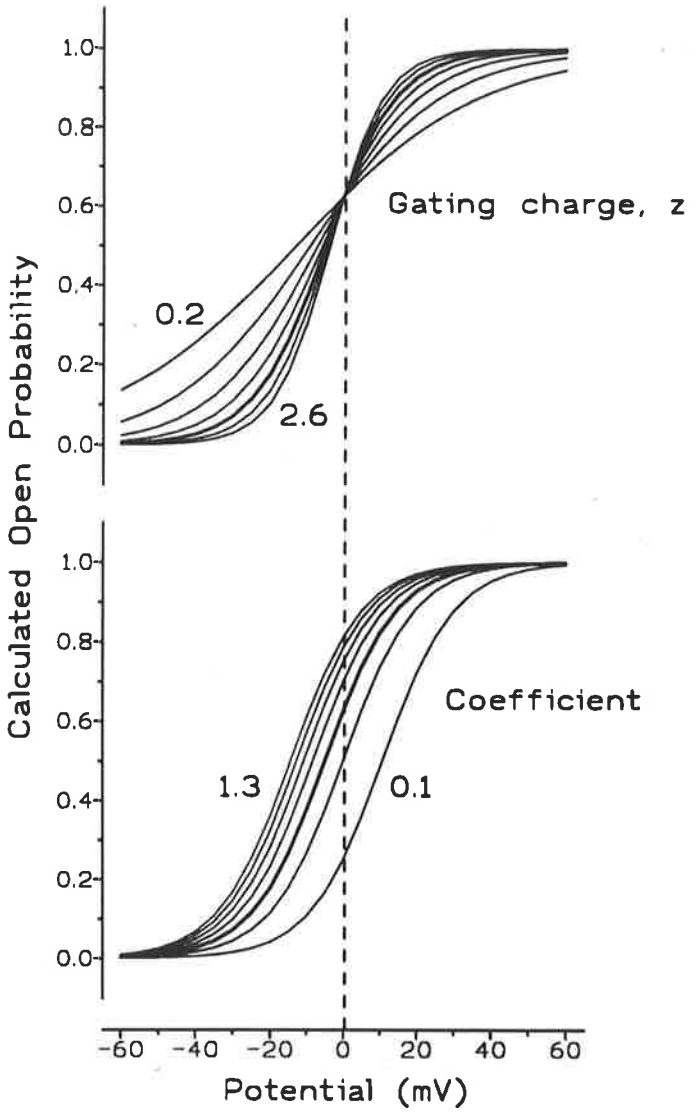

FIGURE 4.18 Predicted sigmoidal *Po(V)* curves
With the voltage-dependent rate constants placed between the open and closed states, a sigmoidal *Po(V)* curve is predicted. By varying the value of the gating charge, z, in the voltage-dependent rates, a change in the steepness of the *Po(V)* curve results. Shown in the top panel is the effect of changing the gating charge of the Group 1 voltage-dependent rates listed in Figure 4.17, from a value of 0.2 to 2.6 in steps of 0.4. The equilibrium *Po* value at 0 mV, however, remains constant. Only by varying the coefficient value is the *Po* value at 0 mV altered, producing parallel shifts in the *Po(V)* curve. The bottom panel shows the effect of changing the coefficient value of the same Group 1 voltage-dependent rates, from a value of 0.1 to 1.3 in steps of 0.2. Similar effects are also found for the Group 2 voltage-dependent rates. Changes in the independent rates had no effect upon the *Po(V)* curve with either schemes I, IV or VI.

I.

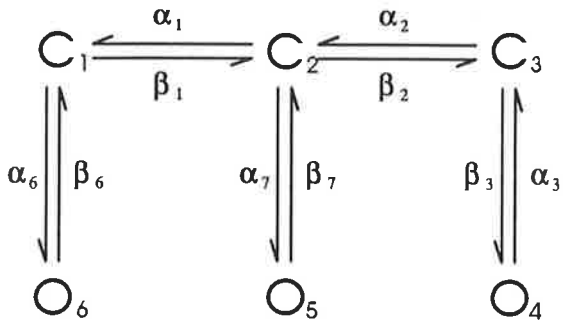

Voltage-independent rate constants

Group 1

$\alpha_7 = 7.0$

Group 2

$\beta_7 = 0.1$

Voltage-dependent rate constants

Group 1

$\alpha_2 = \beta_3 = 0.05 \exp (-3.9\ VF/RT)$

$\alpha_6 = \beta_1 = 0.05 \exp (3.9\ VF/RT)$

Group 2

$\alpha_1 = \beta_6 = 0.3 \exp (-0.6\ VF/RT)$

$\alpha_3 = \beta_2 = 0.3 \exp (0.6\ VF/RT)$

FIGURE 4.19 Configuration of scheme I which predicts a bell-shaped curve Using the rate constants shown here, a bell-shaped *Po(V)* curve was predicted by scheme I. Voltage-dependent rate constants were required between the closed states (C_1 and C_2, C_2 and C_3), as well as between the open and closed states (C_3 and O_4, C_1 and O_6).

IV.

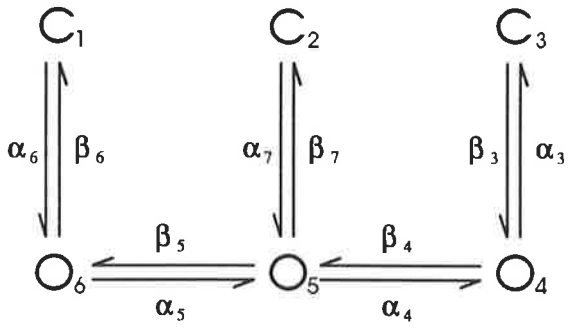

Voltage-independent rate constants

Group 1

$\alpha_7 = \alpha_4 = \beta_5 = 0.05$

Group 2

$\beta_7 = \beta_4 = \alpha_5 = 20.0$

Voltage-dependent rate constants

Group 1

$\alpha_6 = 0.05 \exp (3.9\ VF/RT)$

$\beta_3 = 0.05 \exp (-3.9\ VF/RT)$

Group 2

$\alpha_3 = 0.3 \exp (0.6\ VF/RT)$

$\beta_6 = 0.3 \exp (-0.6\ VF/RT)$

FIGURE 4.20 Configuration of scheme IV which predicts a bell-shaped curve
Using the rate constants shown here, a bell-shaped *Po(V)* curve was predicted by scheme IV. In this case voltage-dependent rate constants were only required between C_3 and O_4, and between C_1 and O_6.

VI.

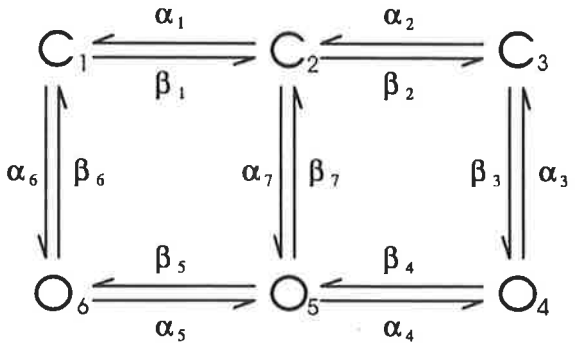

Voltage-independent rate constants

Group 1

$\alpha_4 = \beta_5 = \beta_7 = 0.3$

Group 2

$\beta_4 = \alpha_5 = \alpha_7 = 3.0$

Voltage-dependent rate constants

Group 1

$\alpha_3 = \beta_2 = 0.05 \exp (-3.8\ VF/RT)$

$\alpha_1 = \beta_6 = 0.05 \exp (3.8\ VF/RT)$

Group 2

$\alpha_2 = \beta_3 = 0.3 \exp (0.6\ VF/RT)$

$\alpha_6 = \beta_1 = 0.3 \exp (-0.6\ VF/RT)$

FIGURE 4.21 Configuration of scheme VI which predicts a bell-shaped curve Using the rate constants shown here, a bell-shaped *Po(V)* curve was predicted by scheme VI and microreversibility was maintained. In this case, voltage-dependent rate constants were required between the closed states (C_1 and C_2, C_2 and C_3), as well as between the open and closed states (C_1 and O_6, C_3 and O_4,).

FIGURE 4.22 Predicted bell-shaped *Po(V)* curves
A bell-shaped *Po(V)* curve is predicted by schemes I, IV and VI with the placement of voltage-dependent rate constants as shown in Figures 4.19, 4.20 and 4.21, respectively. The predictions shown here are for scheme VI. The steepness of the *Po(V)* curve is altered by changing the either of the gating charge values, while the *Po* value at 0 mV remains unchanged. The top panel shows the effect of increasing the z value of the Group 1 voltage-dependent rates from 3.8 to 7.0 in steps of 0.8, producing a steeper and narrower *Po(V)* curve. Decreasing the z value to 2.8 and 1.8 produces a broader *Po(V)* curve. Similar effects are seen for the z value of the Group 2 voltage-dependent rates. The peak *Po* value at 0 mV is influenced by the coefficient values without altering the steepness of the *Po(V)* curve, though as a consequence, the *Po(V)* curve also becomes narrower. This is illustrated in the middle panel with the coefficient for the Group 1 voltage-dependent rates increasing from a value of 0.05 to 1.65 in steps of 0.4, and decreasing to 0.03 and 0.01. The bottom panel shows the effects of changing the voltage-independent rate constants. As the Group 1 voltage-independent rate is increased from 0.3 to 2.3 in steps of 0.5, the peak is reduced and the *Po(V)* curve becomes narrower, but the steepness is constant. Decreasing the same voltage-independent rate to 0.2 and 0.1 increases the peak *Po* and the width of the curve.

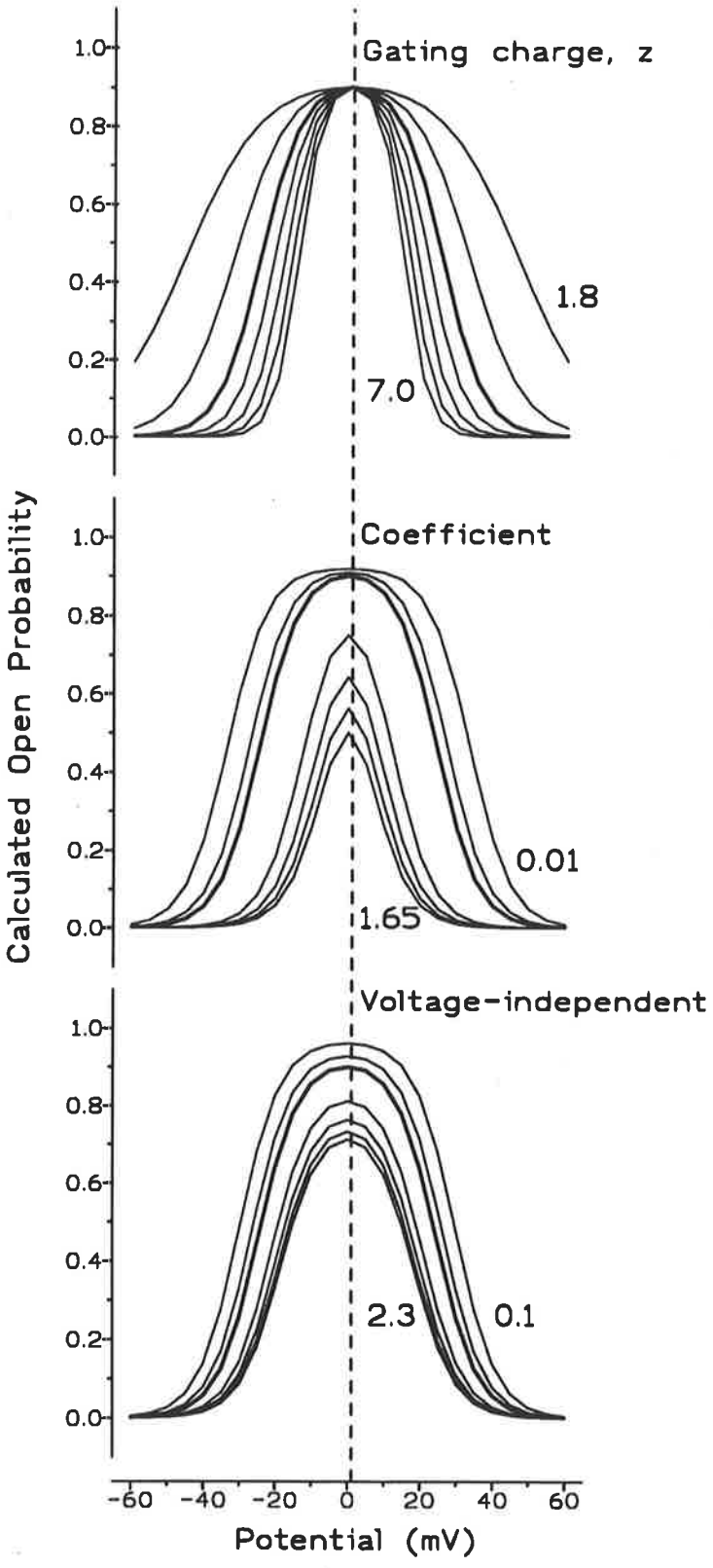
Gating charge, z
1.8
7.0
Coefficient
0.01
1.65
Voltage-independent
2.3
0.1
Calculated Open Probability
1.0
0.8
0.6
0.4
0.2
0.0
-60
-40
-20
0
20
40
60
Potential (mV)

in the same manner as the results shown in Figure 4.22, which were generated from scheme VI.

4.5 Discussion

The kinetic behaviour of the anion channel found in the sarcoball preparation has been investigated here using a combination of steady-state and non-stationary kinetic analysis techniques. The tendency to find multiple channels in the patches made it difficult to obtain large amounts of steady state data for single channels. The steep voltage dependence of the open probability of the channel also meant that meaningful steady-state recordings of the channel could only be made over a limited range of potentials where there were sufficient numbers of transitions within reasonable recording times (considering that patches have a limited lifetime from which recordings can be made). Channel behaviour is also complicated by the presence of numerous subconductance states. Nevertheless, the voltage-dependent nature of the channel meant that non-stationary analysis could be appropriately used to investigate the behaviour of the channel. So while steady state information could not be investigated fully, non-stationary analysis provided additional information on the kinetic behaviour of the channel.

Markov models of channel kinetics provide a well established framework within which to describe the behaviour of ion channels (Colquhoun & Hawkes, 1981, 1982). They provided tools of analysis for determining a lower bound for the number of kinetic states and in some cases the ability to estimate certain rate constants. Kinetic analysis only detects those states that affect the gating of the channel which are within the window of time resolution allowed by the analysis. Additional states may remain undetected if the time constant is sufficiently close to that of another component such that the two cannot be resolved. As a consequence, the models are minimalist and do not include the possibility of one or more conformational states responsible for each kinetic state detected.

Steady state kinetics

To assist in the analysis of the complex kinetics exhibited by the anion channel, the behaviour was approximated as transitions occurring directly between the open and closed aggregates, with sojourns to the 60% substate occurring only from the open aggregate. This approximation was reached after inspection of the transition histories. While other more complex transitions do occur, especially between substates, they are less frequent than those described by the approximated scheme. By accepting this approximated scheme, the analysis of the frequency distributions of open and closed durations is simplified. The exclusion of transitions between the open and closed aggregates via the substates, means it is possible to describe the transitions from the closed aggregate to the open aggregate by a single set of rate constants.

With the open aggregate, transitions are possible to both the substates and the closed aggregate. Successive transitions between the open aggregate and the substates are treated like a burst, which is terminated by a transition to the closed aggregate. The entire duration of the burst, including dwell times in both the open aggregate and the substates, will have a frequency distribution dependent upon the set of rate constants that lead away from the open aggregate to the closed aggregate and the substates, as well as the set of rate constants that lead from the substates back to the open aggregate, whereas the frequency distribution of the individual durations spent in the open aggregate will be determined by both the set of rate constants which lead to the closed aggregate and those which lead to the substates. By summing only the open durations within a burst which is terminated by a transition to the closed aggregate, the distribution of these summed durations are, on average, determined only by the set of rate constants leading from the open aggregate to the closed aggregate (see treatment in Colquhoun & Hawkes, 1983 and more general principles in Colquhoun & Hawkes, 1982). Therefore, for the analysis of the sarcoball anion channel, open durations were defined as beginning with a transition from the closed aggregate

and terminated upon returning to the closed aggregate, and the duration of sojourns in the substates during this event were not included in the summed open duration.

a) Duration frequency distributions

Both the open- and closed-time distributions were well described by the sum of exponential components, which appear as "bumps" on a log-log plot of the dwell time data. This characteristic is sufficient to reject the application of any fractal model to the gating of this channel (McManus et al., 1989). In terms of a Markov model, the number of exponential components describing the duration frequency distributions are interpreted as identifying the minimum number of kinetic states in the underlying scheme. This type of analysis suggested the presence of at least three kinetic states in both the closed aggregate and the open aggregate of the sarcoball anion channel recorded here. Previous analysis by Hals et al. (1989) indicated the presence of at least three closed states and two open states, however there are slight differences in the voltage dependence compared to the anion channel recorded here. In the present case, the long open time was found to shorten with increasing voltage steps in either direction from 0 mV, while Hals et al. (1989) found the open time to lengthen slightly. Little voltage dependence is exhibited by the other open time constants. By far the greatest effect upon P_O of the channel, is the appearance of the third long closed state at large positive and large negative potentials, which is also seen by Hals et al. (1989).

A voltage-dependent anion channel has also been recorded from cardiac SR vesicles incorporated into bilayers (Rousseau, 1989). This channel exhibits a similar bell-shaped $P_O(V)$ curve, but is of a much smaller conductance (38 pS in symmetrical 60 mM Cl^-) than that observed here. The kinetics of the cardiac SR anion channel exhibit only a single open state and at least three closed states, as determined from the dwell time distributions. The open times became shorter and the closed times became longer with an increase in the magnitude of the

applied potential, which is similar to the behaviour seen here. Why only a single open state was detected can merely be speculated upon, but might have been due to the bandwidth of the recording (filtered at 300 Hz), to the nature of the threshold analysis of the open durations, or, indeed, to truly different kinetics of this channel compared to that recorded here.

b) Autocorrelations

Examination of the a.c.f. of the series of all open and closed durations provides, in theory, a simple and general strategy for the extraction of information on the number of pathways leading between the open and closed aggregates (Fredkin et al., 1985; Colquhoun & Hawkes, 1987). Prior to the work of Ball and Sansom (1988), a.c.f.'s were used only as a qualitative tool to assist in kinetic scheme discrimination (Jackson et al., 1983; Colquhoun & Sakmann, 1985; Labarca et al., 1985; Colquhoun & Hawkes, 1987). Since then, a.c.f.'s have been successfully applied to the analysis of the glutamate receptor in determining the number of entry/exit pathways between aggregates of the underlying kinetic (Kerry et al., 1988).

The presence of significant short term autocorrelation for both open and closed dwell times is interpreted as indicating a connectivity of at least two for the kinetic scheme. Fitting of the a.c.f.'s with the sum of geometrical components indicates that there are at least three entry/exit states in the open aggregate and two in the closed aggregate. In a kinetic scheme of three open states and three closed states it is not possible to have three entry/exit pathways from the open aggregate and only two from the closed aggregate. Since the estimates of the number of entry/exit pathways are lower bounds, it is proposed that there are three entry/exit pathways linking the open and closed aggregates. A consequence of this is that the kinetic scheme must be branched or cyclic; a simple linear scheme is not sufficient. These results place important constraints upon the

development of possible models to describe the channel gating mechanism and the six possible schemes are presented in Figure 4.11.

It is possible that the peaks observed in the a.c.f.'s at +20, +10 and -20 mV indicate periodic behaviour in the closed dwell time series, however the significance of this with regard to a kinetic scheme is not understood. It would seem that any periodic behaviour is not in keeping with the Markov assumption of independence of events.

Markov models are autoregressive processes and are time reversible (Box & Jenkins, 1976). An autoregressive process is a stochastic process which describes a random series of events, where each element of the series has a regressive dependence upon the preceding elements. A time reversible process means that analysis of the channel record from the beginning to the end gives the same results as analysis of the record in the reverse order. The form of the a.c.f.'s being positive, decreasing and convex, indicates that the underlying process is time-reversible (Box & Jenkins, 1976). Further, the p.a.c.f. for the same data indicates that the underlying process is autoregressive, as the p.a.c.f.'s are seen to tend toward zero for much shorter lags than observed for the a.c.f.'s (Box & Jenkins, 1976). Therefore, the use of a Markov process to model the behaviour of the sarcoball anion channel seems to be most appropriate.

Non-stationary kinetics

The interpretation of the non-stationary kinetics provides a qualitative description of the relative relationship between the different identifiable kinetic states within the kinetic scheme.

a) Relaxations

The voltage-dependent decline of the time constants describing the ensemble current relaxations has also been reported by Zahradnik et al. (1990) for the

sarcoball anion channel. They found that for voltage steps as small as ±10 mV, from a holding potential of 0 mV, the relaxations were described by double exponentials. The first time constant decreased from 100 ms to 10 ms and the second time constant decreased from 10 ms to 1 ms as the magnitude of the voltage step was increased from 10 mV to 80 mV. Much longer time constants were found here and this is may be why relaxations were mainly single exponentials. The second exponential seen in some cases at larger potentials might be too long to be detected within the 900 ms step at smaller potentials.

How these relaxations should be interpreted in relation to the kinetic behaviour of the anion channel is uncertain. Current relaxations have been investigated theoretically by Colquhoun and Hawkes (1977) who found the number of exponential components describing the relaxation is expected to be one less than the total number of states in the kinetic scheme. In the present study, ensemble current relaxations recorded from the anion channel could generally be described by a single exponential and, at most, by a double exponential. While this suggests first order kinetics with two states, it is neither consistent with the presence of three open and closed states determined from dwell time analysis, nor the presence of significant autocorrelation from the dwell time series. From the steady-state analysis of the anion channel, it might be expected that the relaxations should be described by the sum of five exponentials (one less than the total number of kinetic states). In practice, the identification of all the exponential components will be limited by the temporal resolution of the recording and analysis, and those which are too fast or too slow will not be detected.

Alternatively, the relaxations might be useful in describing the distribution of channel openings between long channel closures. This has been the approach of Schwarze and Kolb (1984) who described the kinetics of a large conductance anion channel from mouse macrophages, which also has a bell-shaped $P_O(V)$ curve similar to that of the sarcoball anion channel. The relaxations were able to be

described as the sum of two exponentials, though they considered the second, longer time-constant to be unreliable, and used only the faster time-constant in developing the approximate kinetics of the channel. Using a derivation of the Hodgkin-Huxley model, the channel behaviour was approximated as two voltage dependent gates, one operating at positive potentials and the other at negative potentials, each with an open and a closed state. With this model, they show that the time constant of the current relaxation is equivalent to the mean burst duration. The similarities between this large conductance anion channel from macrophages (Schwarze & Kolb, 1984) and the anion channel studied here are enough to entertain ideas of similar gating kinetics. If this is the case, then the voltage dependence of the current relaxations is due to the burst durations becoming shorter with larger voltage steps from 0 mV. The rationale for this is based upon the patch being held at a potential where the channel is open almost all of the time. By stepping to a new potential where the open probability is reduced, presumably by reducing the mean burst time, the relaxation of the ensemble current to the new steady state will be describe by an exponential decay. The time constant of this curve is an estimate of the mean burst time at this new potential. The presence, however, of complex kinetic behaviour, with substates, prevented an adequate definition of what is a burst for analysis of the events lists here. So a comparison was not able to be made between the current relaxation time constants and the mean burst durations.

The information gained from these relaxations is limited, but suggests that the pathway leading from the open aggregate to the closed aggregate is dominated by one rate constant. The symmetrical nature of the relaxations, and the $P_O(V)$ curve derived from them, strongly suggests that there is a separate closed state occupied at positive potentials to that occupied at negative potentials.

b) Separate closed states

The presence of separate closed states was tested for by applying steps from a negative voltage (-50 mV) where the channel is closed (P_O <0.2), to a positive potential (+50 mV) where it is also closed (P_O <0.2). If the same closed state was occupied in each case, it is expected that the majority of channels would continue to reside in the closed state upon changing the potential. Quite the opposite was found, with almost all the channels entering an open state extremely rapidly. The ensemble P_O then relaxed as the channels entered into the closed states at the new potential. The peak P_O attained at the onset of this voltage step, was less than unity which indicates not all of the channels were simultaneously opened. This can be interpreted in two ways; either (i) the rate of leaving the open aggregate is faster than that of entering the open aggregate from the closed state, or (ii) the closed states are linked and a proportion of channels shift within the closed aggregate to the new equilibrium.

c) Linked open states

Non-stationary results also indicate the open states are linked, with the possibility that there are two different open states; one which is preferentially occupied at positive potentials, the other at negative potentials. This is inferred from the reactivation kinetics, where a similar pseudo-steady-state P_O is attained at the end of voltage steps which are of the same magnitude but of opposite sign. The change in the electric field is in the same direction for both steps. For example, from a holding potential of -30 mV, there is a positive increase in the electric field stepping to -15 mV and then a much larger increase with a step to +15 mV. This will shift the equilibrium of the kinetic scheme in the same direction for each step, and a much larger shift is predicted for the +15 mV step. The observable outcome, however, is a similar P_O. To account for this shift in the equilibrium and the symmetry of the P_O behaviour of the channel, it is proposed that the open

states are linked within the open aggregate. Of the linked states, one is preferentially occupied at negative potentials and another at positive potentials.

A possible model

From the results of this study, three possible kinetic schemes are able to be proposed to account for the bell-shaped voltage-dependence of the channel open-probability. Where the voltage-dependent rate constants were placed was influenced by the concept of the kinetic behaviour of the channel developed from the non-stationary analysis, and the ability of the kinetic scheme to predict a bell-shaped $P_O(V)$ curve. An equilibrium favouring the occupancy of C_1 at negative potentials was arbitrarily assigned, so that C_3 would be favoured at positive potentials. With schemes I and VI, the voltage-dependent rates between the closed states cause this shift in the equilibrium between C_1 and C_3. Rapid access to the open states is provided by two voltage-dependent gates; one from C_1 to O_6 for steps from negative potentials to positive potentials and one from C_3 to O_4 for steps from positive to negative potentials. Voltage dependent transitions to closed states occur from O_6 to C_1 at negative potentials and from O_4 to C_3 at positive potentials to account for the current relaxations. These processes are thought to be essential for describing the voltage-dependent behaviour of the channel and are a part of schemes I, IV and VI.

At present, it is not possible to distinguish which of the three schemes provides the better description of the anion channel kinetics, though scheme VI is favoured as both the open states and the closed states are all linked. Better estimates of the rate constants would be required to assist in determining which scheme best describes the kinetic behaviour. With these estimated rate constants, comparisons could be made between the predicted open and closed p.d.f.'s and the frequency distributions obtained from channel recordings. Even more telling would be the ability of the kinetic scheme to predict the non-stationary behaviour of the channel, like that recorded here. This could be achieved by using the rate

constants to simulate the stochastic behaviour of the channel and generate ensemble currents in response to simulated voltage steps.

The model, whether best described by scheme I, IV or VI, is a first approximation, as the subconductance states seen throughout the single channel records are not included in the model. Since the frequency of transitions between the fully open state and the closed state is generally greater than for transitions from the substates to the closed states, this is thought to be a reasonable approximation. It is recognised that the contribution of the subconductance states is likely to be quite important in establishing the pseudo-steady-state P_O of the channel. Inclusion of substates in this model, however, would be premature because of the number of substates and difficulties in resolving the individual substates.

The contribution of substates to the behaviour of another SR anion channel has been recently modelled using parallel conductances. This large conductance anion channel, from SR vesicles incorporated into bilayers, has a rectifying voltage-dependence, with a higher P_O at negative potentials (*cis* side with respect to *trans*) (Kourie et al., 1992). To account for the ten equally spaced, long-lived conductance levels, nine parallel identical gating processes (or units) are proposed (Laver et al., 1993). While this is might also be able to describe the multiple subconductance states of the sarcoball anion channel, it would not be sufficient to describe the bell-shaped $P_O(V)$ curve.

Conclusions

The sarcoball anion channel recorded here can be described by a branched or cyclic kinetic scheme with at least three open and three closed states. The bell-shaped $P_O(V)$ curve, which is an important characteristic of the sarcoball anion channel, is able to be predicted by three different kinetic schemes which were derived from the analysis of the channel behaviour. Of these three schemes, it is thought that scheme VI is most likely to best describe the channel kinetics.

PART II.
STRUCTURE AND COMPOSITION OF SARCOBALLS

5. GLIMPSES OF SARCOBALL STRUCTURE

5.1 Aims and Introduction

When the sarcoball preparation was first described, a solitary electron micrograph accompanied the report, depicting sarcoballs as being bound by a single bilayer and containing flocculent material (Stein & Palade, 1988). This structure seemed inconsistent with the observations which had been made during the initial stages of the present study. As described in Chapter 3, the sarcoball surface and shape was much more pliable than might be expected from a single bilayer envelope with a fluid filled interior and unlike sarcolemmal vesicles, the structure does not collapse when it is punctured by a microelectrode.

The issue of structure was again raised when conducting antibody labelling studies at the electron microscope level to determine the origin of the membranes present in sarcoballs (presented in Chapter 6). The structure of the sarcoballs processed for immuno-electron microscopy was different from that previously published and warranted further description.

The aim was therefore to investigate sarcoballs using several fixation and dehydration techniques to gain an elementary insight to the structure and determine what elements were artefacts of processing. The effects of processing were assessed by comparison with conventionally fixed fibres. Both the internal membrane structures of the skinned fibres and the structures of the extruded membrane vesicles forming sarcoballs at the fibre surface were observed.

Studies with Xenopus laevis muscle

Parts of this study using muscle fibres from *Xenopus laevis* were done in collaboration with Dr A.F. Dulhunty and C. Stanhope, Muscle Research Group, Division of Neuroscience, John Curtin School of Medical Research, Australian National University, Canberra. I prepared and processed the sarcoballs at the John Curtin School of Medical Research. This material was sectioned and mounted by C. Stanhope, and the electron microscopy was performed by Dr A.F. Dulhunty. Aspects of this study have been published in Lewis et al., (1992).

Studies with Bufo marinus muscle

Those parts of this study using muscle fibres from *Bufo marinus* were done at the Center for Electronmicroscopy and Microstructural Analysis, The University of Adelaide. Assistance was provided by Dr M. Henderson and D. Smith, who sectioned the material for me, and I carried out all other aspects of the study.

5.2 Methods

Conventional processing

Sarcoballs prepared, as described in Chapter 2, from the semitendinosus muscle of the clawed toad, *Xenopus laevis*, were fixed in the Ringer's solution containing 2% glutaraldehyde for 2 hours at room temperature, washed in the Ringer's solution and post-fixed with 2% OsO_4 in 100 mM cacodylate buffer for 1 hour. A gradual procedure was used to dehydrate the fibres in methanol (70%, 80%, 90% and 100%) for 1 hour in each dilution at room temperature. The fibres were infiltrated overnight with Spurr's resin (Spurr, 1969) diluted in ethanol (1:1, v:v) and then embedded in 100% Spurr's resin cured at 70°C for 8 hours. Grey to silver sections were cut with a diamond knife on an ultramicrotome (LKB Instruments, Inc.,) and mounted on copper grids. Sections were stained with 5% uranyl acetate and Reynold's lead citrate before being examined on a Hitachi H 7000 or a Joel 100s transmission electron microscope at 80 kV.

Modified processing

This modified protocol is similar to that used for immuno-electron microscopy in Chapter 6. Skinned fibres with sarcoballs from the semitendinosus muscle of the cane toad *Bufo marinus*, or the clawed toad, *Xenopus laevis*, were fixed in Ringer's solution with 2% formaldehydes (prepared fresh from paraformaldehyde) and 0.1% glutaraldehyde for 2 hours at room temperature. After washing the fibres in Ringer's solution, dehydration was a single step procedure in 90% methanol for 1 hour at room temperature. The fibres were infiltrated with LR White acrylic resin (London Resin Company) overnight at 4°C, rinsed in fresh resin and then embedded in LR White resin cured at 60°C for at least 12 hours. Grey to silver sections were cut as before and mounted on collodion-coated copper grids or nickel grids. Sections were stained and examined as for conventionally processed material.

5.3 Results

The appearance of sarcoballs

A wide variety of sarcoballs were observed under the electron microscope, the majority of which were similar to those routinely observed under the light microscope during patch clamp experiments. A selection of sarcoballs seen on conventionally fixed fibres are shown in Figure 5.1. Some sarcoballs appeared flattened and extended along the length of the fibre for 50 to 100 μm, as shown in Figure 5.1A. By inspecting several thick and thin serial sections of the same skinned fibre, the flattened structure shown in Figure 5.1A was also found to extend along the fibre in a direction perpendicular to the plane of the section. Other sarcoballs with a similar flattened appearance were found to be elongated at an angle between 45° and 90° to the plane of serial sections. This type of flattened sarcoball comprised approximately 10% of the sarcoball population. The majority of sarcoballs observed under the electron microscope exhibited a hemispherical cross-section (Figure 5.1C and D), ranging in diameter from 1 μm

to 150 µm. In the patch clamp experiments described in previous chapters, it was the larger sarcoballs of 50 to 100 µm diameter (for example in Figure 1D) that were normally chosen under the light microscope for recording channel activity.

Structures were also seen which were composed of two or more sarcoballs joined together (Figure 5.1B and Figure 5.2). A variety of these compound structures were seen, ranging from the smaller sarcoballs stacked on top of each other, extending 10 to 15 µm from the fibre surface (Figure 5.1B and Figure 5.2A and B), to quite large neighbouring sarcoballs joined together (Figure 5.2C). In the examples shown in Figure 5.2, a boundary is able to be seen where two sarcoball or bleb surfaces are closely opposed to form a double membrane. During the routine preparation of sarcoballs for patch clamp experiments, neighbouring sarcoballs were often observed under the light microscope to merge during the process of sarcoball formation and for a short time after the fibre had completed the contracture. Presumably, the compound structures seen here under the electron microscope were a result of neighbouring sarcoballs merging.

Internal structure of sarcoballs

The internal structure of the sarcoballs was found to be quite sensitive to the method of processing utilised for electron microscopy. Sarcoballs on conventionally fixed fibres were defined by a continuous membrane enclosing mainly flocculent material which is presumed to be cell debris (Figure 5.1 and 5.2). At the base of the sarcoball, the region in contact with the fibre surface contained mainly rounded vesicles with diameters ranging from 400 to 500 nm. Swollen mitochondria of diameter 600 to 800 nm were also packed into this region and were identified by the electron dense mitochondrial matrix and the laminae of internal membranes. This base region of vesicles extended only 2 to 3 µm from the fibre surface and at distances greater than this the vesicle structure was disrupted. In some instances, large irregularly shaped vesicles extended from this base region further into the sarcoball interior (Figure 5.1C and 5.2C). Those

Figure 5.1 Sarcoballs on the surface of skinned fibres.
A selection of four sarcoballs (S), representative of the variety of shapes and sizes observed on the surface of conventionally processed skinned muscle fibres from *Xenopus laevis*. **A**. Approximately 10% of the sarcoballs observed had a flattened appearance like that shown here. **B**. Some sarcoballs appeared to be compound structures, comprised of smaller membrane blebs (B) which protruded from the fibre surface. **C** and **D**. Hemispherical sarcoballs were the majority of structures seen. Mitochondria (M) were often seen in the region of vesicles (V) covering the skinned fibre surface and at the base of the sarcoball structures. The short arrows in **A** and **D** indicate regions of the fibre surface covered by a monolayer of small vesicles. Calibration bar: A, 8 µm; B, 3.3 µm; C, 2 µm; and D, 6.6 µm.
Courtesy of Dr A. F. Dulhunty.

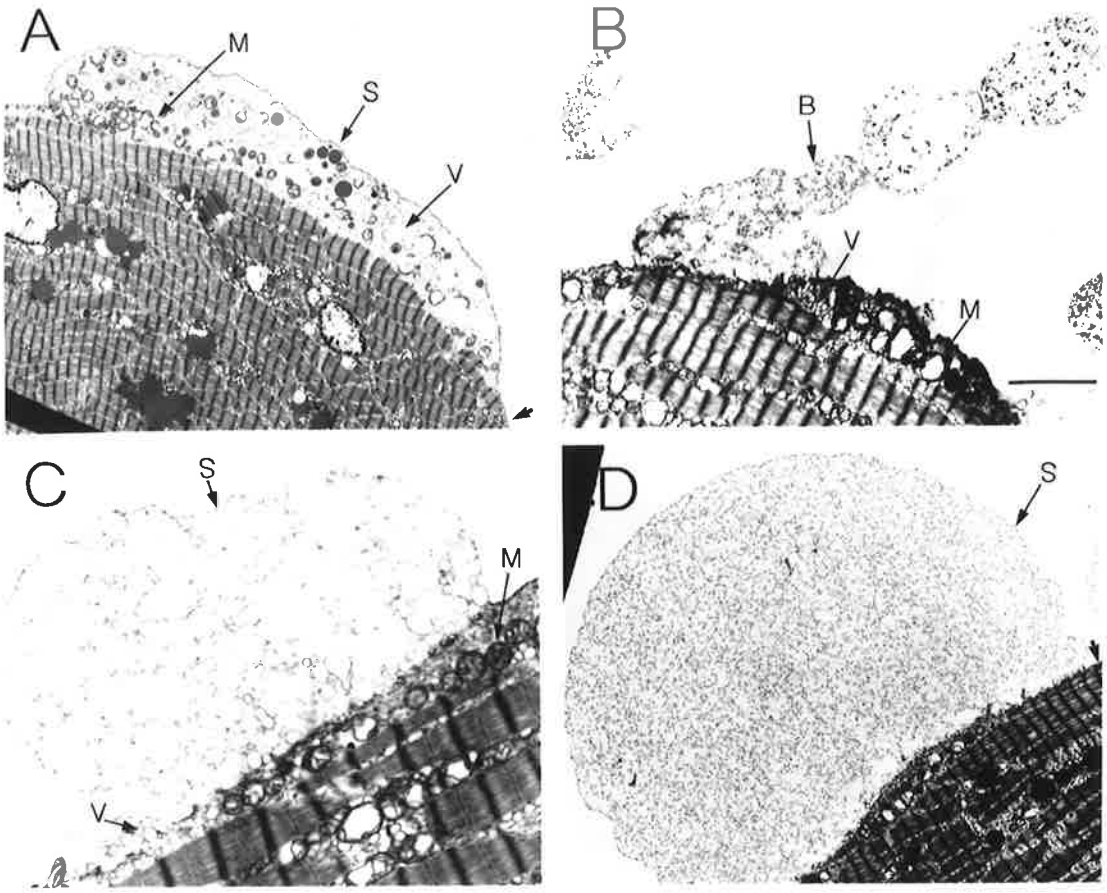
A
M
S
V
B
B
V
M
C
S
M
V
D
S

Figure 5.2 Possible enlargement of sarcoballs by fusion.
In some cases, sarcoballs on the surface of conventionally processed skinned fibres were found to be closely associated. As shown in the examples here from *Xenopus laevis*, this varied from compound structures of smaller blebs extending 10 to 15 µm from the fibre surface (**A.**) to neighbouring hemispherical sarcoballs (**C.**). The arrows indicate where membranes of apposed structures meet and might fuse to form a larger structure. Calibration bar: A and B, 3.3 µm; and C, 2.7 µm.
Courtesy of Dr A. F. Dulhunty.

Figure 5.3 A possible foam-like structure.
The surface and interior of sarcoballs processed with the modified protocol were different from that of conventionally processed fibres. The sarcoballs shown here are from *Xenopus laevis*. **A.** This shows the surface of a sarcoball with some myofilaments (F) which had been pulled away from the surface during skinning. The surface was not a single, continuous membrane which bounds the sarcoball but was comprised of aggregated vesicles. The interior of the sarcoball was a close aggregation of membrane vesicles, some of which were identified as mitochondria (M). **B.** Some vesicles within the sarcoball interior were tubular in form (T) and may have originated from the T-tubules from within the skinned fibre (as shown in **D.**) where they are flanked by terminal cisternae (TC). **C.** An overview of another sarcoball at a lower magnification, showing the vesicle structure of the interior and at the surface of the sarcoball. Calibration bar: A, 0.4 µm; B, 0.54 µm; C, 1.6 µm; and D, 0.46 µm. Courtesy of Dr A. F. Dulhunty.

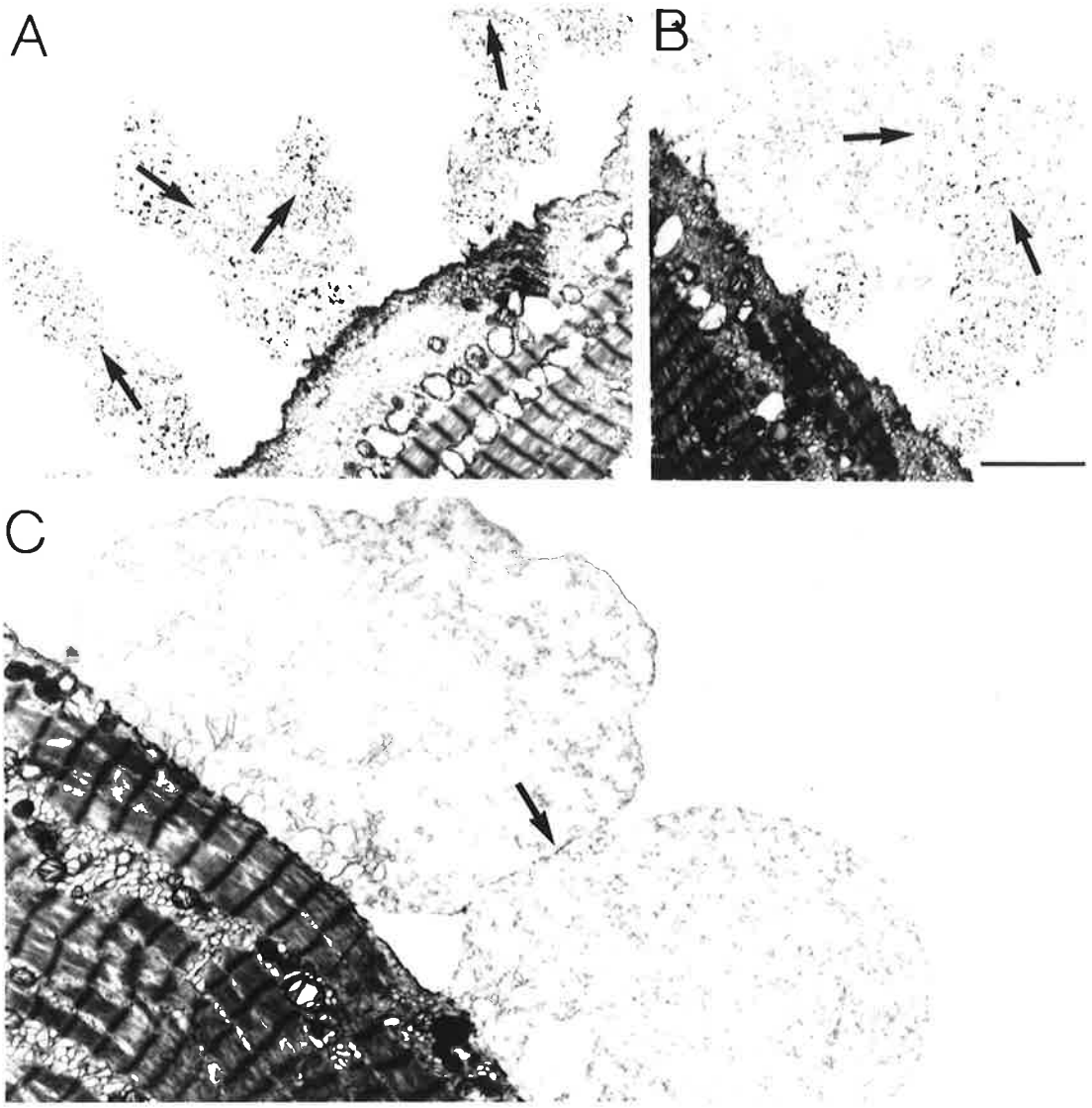
A
B
C

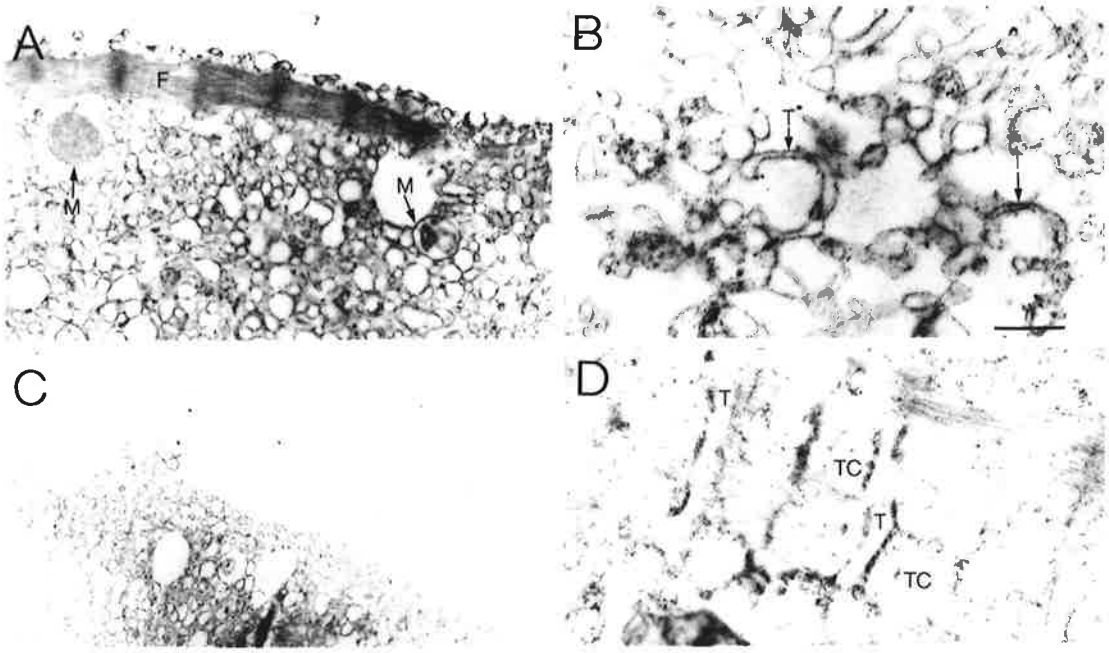
A
F
M
M
B
T
C
D
T
TC
T
TC

sarcoballs with a flattened appearance, extending no further than 5 μm from the fibre surface, showed no signs of disruption within the sarcoball interior. The vesicle structure, including mitochondria, which is found only in the base region of the larger hemispherical sarcoballs, was found throughout the flattened sarcoballs (Figure 5.1A).

The disruption of structure within the interior of the large hemispherical sarcoballs could be due to the processing of the skinned fibre. Variations in the fixation step, with alterations in the proportion of formaldehydes and glutaraldehydes were attempted, but these did not have noticeable effects. Alternative dehydration processes were also attempted, on muscle fibres from *Bufo marinus*, including making the dehydration step more rapid and using cold acetone to prevent lipid extraction in some cases. Often significant shrinkage of sarcoballs was observed and the results were inconclusive. Sections of sarcoballs with the greatest amount of interior detail were obtained when the fibres were processed with the modified protocol, as for immuno-electron microscopy.

Skinned fibres processed with the modified protocol exhibited sarcoballs with an interior composed entirely of membrane vesicle structures. The rounded vesicles are tightly packed together in the sarcoball structure (Figure 5.3A, B and C) and ranged in size from 100 nm to 1 μm in diameter. The surface of these sarcoballs was composed of closely abutting vesicles, as shown in Figures 5.3A and C, and was not delimited by a continuous membrane as in the conventionally fixed fibres. Most of the vesicles had lost any characteristic geometry which might identify the origin of the membranes. There were no structures which could be identified as intact triads or T-tubules in the outer regions of the sarcoball. Some membranes close to the surface of the muscle fibre, however, did have characteristic structures. For example, tubular membranes were seen (Figure 5.3B) and presumed to be from T-tubules within the fibre (Figure 5.3D). Large vesicles containing membrane laminae with an electron dense matrix were

swollen mitochondria (Figure 5.3A). As these fibres were not post-fixed in OsO_4, the membrane definition is less distinctive than conventionally fixed fibres. It would seem, however, that the vesicles within the sarcoball structure do not share adjacent membranes and therefore have not fused together. Instead, the structure appears to be an aggregation of vesicles.

The surface of skinned fibres

In the regions of the skinned fibres between sarcoballs, the myofilaments were covered by layers of vesicles. In conventionally fixed fibres, vesicles at the surface were covered with a membrane-like structure which was observed to be continuous with that surrounding the sarcoballs (Figure 5.4A-C). In some places, this membrane protruded from the fibre surface to form small blebs (Figure 5.4A and B). These features were less prevalent in skinned fibres processed with the modified protocol.

The thicker regions of vesicles were often associated with interfilament spaces approaching the surface of the skinned fibre and had a similar appearance to the base region of sarcoballs. Within the thicker layers of vesicles, some membrane organelles were found, which were not normally seen where a monolayer of vesicles covered the fibre surface.

A variety of mitochondrial structures were observed amongst the surface vesicles (Figure 5.5). While some mitochondria remained intact (Figure 5.5A), the majority appeared swollen and in some cases contained large internal vacuoles (Figure 5.5A-D). Others had become a loose arrangement of membrane laminae, no longer contained by an outer membrane, which suggested that they were disintegrating (Figure 5.5A and B). If, during expansion, the surface area of sarcoballs increases by including vesicles from the interior into the surface layers, then mitochondrial membrane might also be included at the surface of sarcoballs.

Figure 5.4 Presence of a membrane-like covering in conventionally fixed fibres.
The surface of skinned muscle fibres and sarcoballs which were seen in conventionally fixed fibres from *Xenopus laevis*. The vesicles which covered the fibre surface varied from a monolayer to several layers, extending 0.5 to 1.5 µm from the surface. **A.** Mitochondria (M) were often seen amongst the vesicles (V) and a membrane covered the surface of the vesicles (SM). The long thick arrow indicates a triadic structure, possibly from an interfilament space reaching the fibre surface. Blebs (B) of the membrane covering (SM) were observed to protrude from the skinned fibre surface with diameters of 0.5 to 1 µm (**A** and **B**). **C.** The membrane covering (SM) was continuous with that which bounded the sarcoball structures. **D.** Tubular vesicles (TV; also seen in **C**), which might be from T-tubules, were often seen in regions where several layers of vesicles covered the fibre. Calibration bar: A and B, 0.66 µm; C, 2 µm; and D, 0.8 µm. Courtesy of Dr A. F. Dulhunty.

Figure 5.5 Mitochondrial membranes.
Examples of mitochondria that are intimately associated with sarcoballs from conventionally processed *Xenopus laevis* fibres.. **A.** Some mitochondria remained intact (M), though most were swollen and contained large vacuoles (MV). Some mitochondria appeared to be disintegrating (DM). **B.** This region of tightly packed mitochondrial structures is from a base region between the surface of a skinned fibre and a sarcoball. The vacuolated (MV) and disintegrating mitochondria (DM) shown here suggest the possibility of mitochondrial membrane contributing to the sarcoball structure. **C.** The membranes from vacuolated mitochondria loose their identifying features. **D.** This vacuolated mitochondrion is near the surface of a sarcoball, close to the corner with the skinned fibre surface. It suggests the possible incorporation of mitochondria into the sarcoball surface. Calibration bar: A, 1.0 µm; B, 0.8 µm; C, 0.85 µm; and D, 0.5 µm.
Courtesy of Dr A. F. Dulhunty.

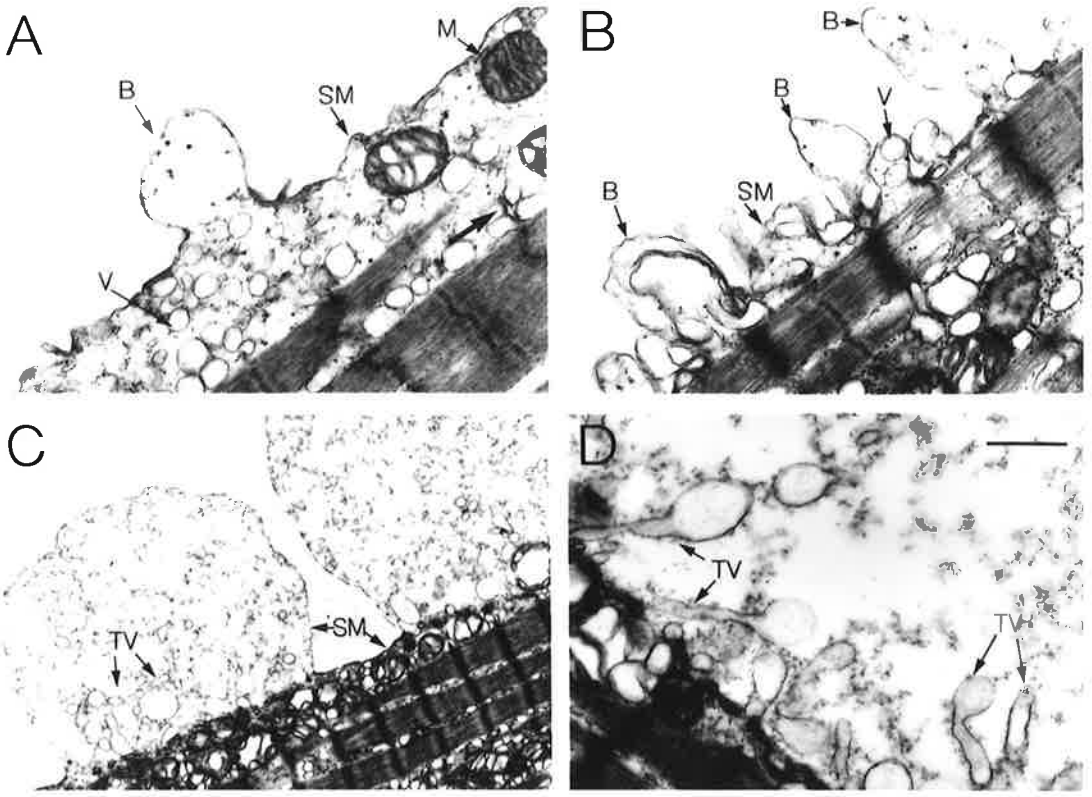
A
M
B
SM
V
B
B
V
B
SM
C
TV
SM
D
TV
TV

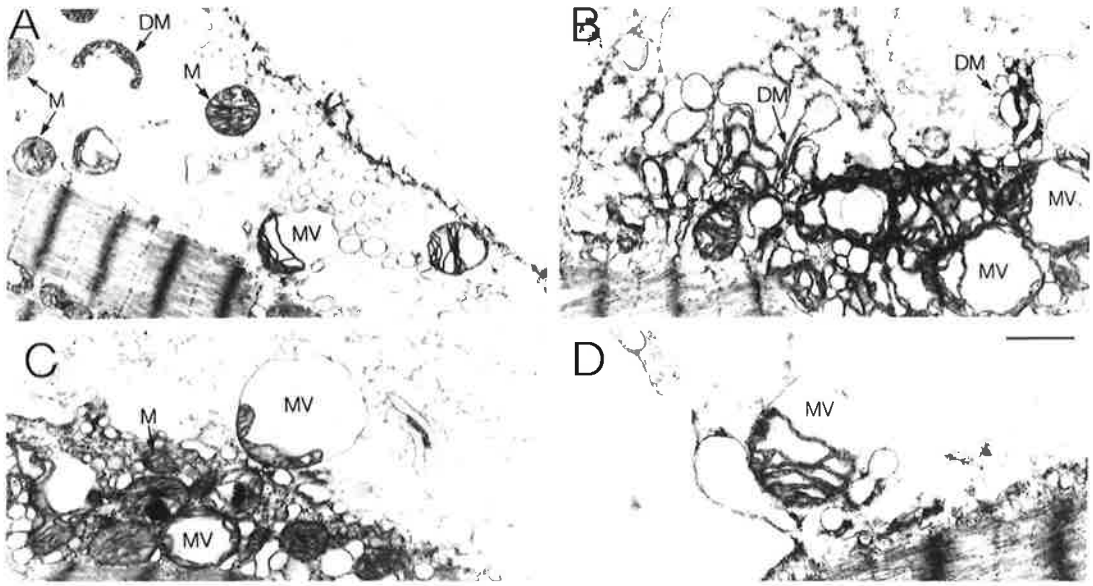
A
DM
M
M
MV
B
DM
DM
MV
MV
C
M
MV
MV
D
MV

Figure 5.6 Interior of skinned fibres.
A. A relaxed, intact skeletal muscle fibre from *Bufo marinus* which has been conventionally processed, showing regular A and I bands. The sarcomere length between successive Z-lines was 2.5 µm. **B**. Conventionally processed, mechanically skinned muscle fibre from *Bufo marinus*, allowed to contract unrestrained. In this case the sarcomere length was 1.8 µm. **C**. Mechanically skinned muscle fibre from *Bufo marinus*, processed with the modified protocol. While the terminal cisternae (TC) and T-tubules (T) remained in register with the Z-line, they were considerably swollen in comparison to normal membranes. **D and E**. The vesiculated internal membrane systems (V) deep within mechanically skinned muscle fibres from *Xenopus laevis* following conventional processing. The short arrows point to triad junctions of terminal cisternae (TC) and T-tubules (T), with electron dense foot structures spanning the junctional gap. Calibration bar: A and B, 0.52 µm; C, 0.20 µm; D, 0.54 µm; and E, 1.0 µm.
D and E courtesy of Dr A. F. Dulhunty.

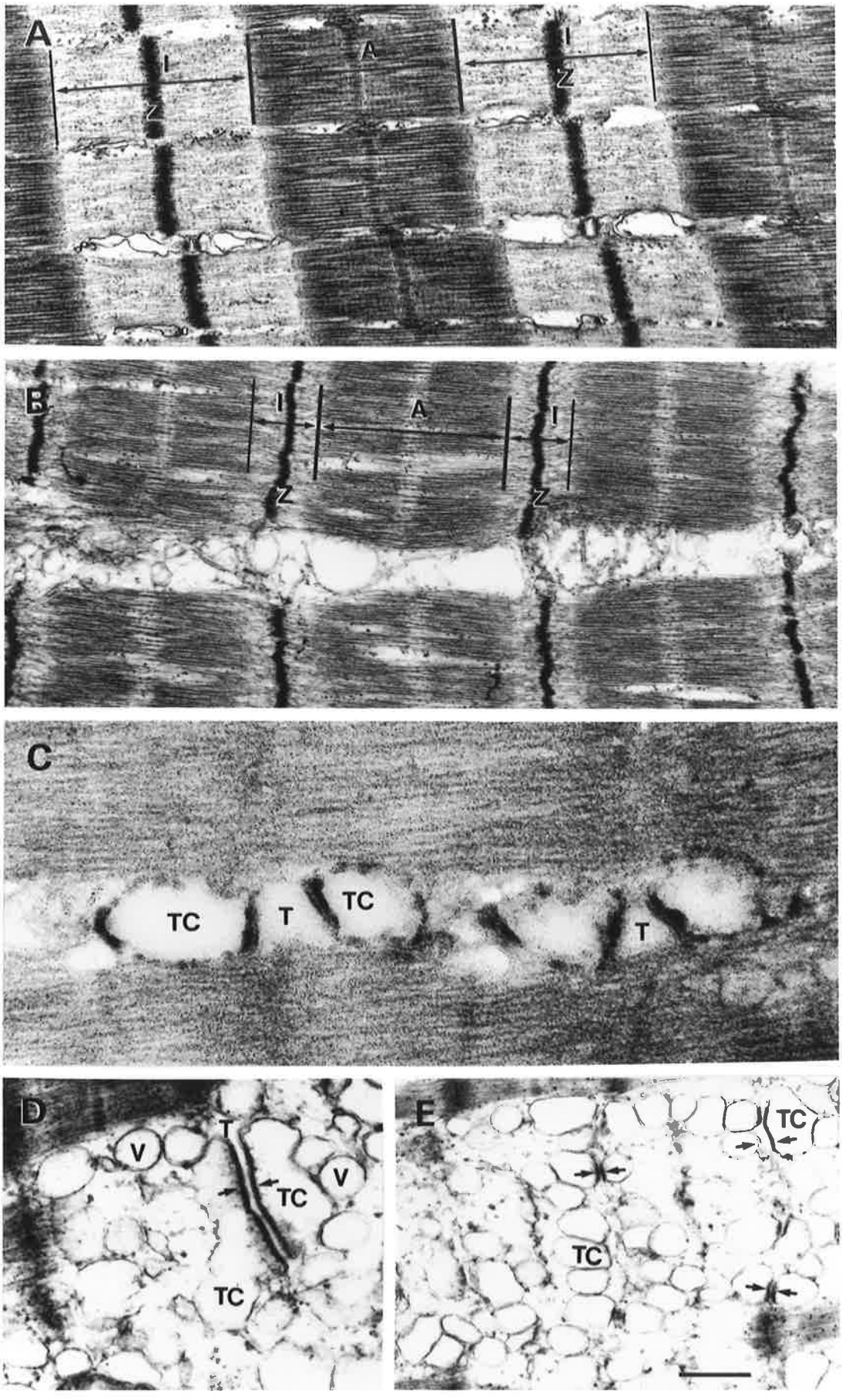
A
I
A
I
Z
Z
B
I
A
I
Z
Z
C
TC
T
TC
T
D
V
T
V
TC
TC
E
TC
TC

The interior of skinned fibres

When observed under the electron microscope, a striking feature of these skinned fibres was the very short sarcomere lengths of between 1.0 and 1.8 μm, compared to relaxed, intact amphibian skeletal muscles which had a sarcomere length of about 3.0 μm (Figure 5.6). The short sarcomere lengths in the skinned fibres reflected the extent of the unrestrained contracture which occurred during the sarcoball formation process.

The internal membrane systems of the skinned fibres were found to be disrupted. The normal geometry of amphibian muscle is for T-tubules to be in register with the Z-line, flanked by terminal cisternae which are linked by longitudinal SR in the A band (Figure 5.6A). In skinned muscle fibres, the triads remained in register with the Z-line (Figure 5.6C) and electron dense junctional feet were also observed (Figure 5.6D and E). The T-tubules and the terminal cisternae, however, were swollen and the longitudinal SR was vesiculated (Figure 5.6B and C). The normal dimensions for the T-tubule short axis is in the range of 10 to 30 nm, while terminal cisternae are normally found to extend 80 to 100 nm into the I band (Dulhunty, 1984). An example of a conventionally fixed skinned fibre is shown in Figure 5.6B, where the T-tubule diameters were 100 to 200 nm along the short axis and the terminal cisternae extended 200 to 300 nm into the I band. In comparison, skinned fibres processed with the modified protocol exhibited a similar length of 100 to 200 nm for the short axis of the T-tubules, though the terminal cisternae were much more swollen, extending 350 to 550 nm into the I band. Generally, it was found that the T-tubules and terminal cisternae of skinned fibres which were processed with the modified protocol were swollen more than skinned fibres conventionally fixed. Swelling of T-tubules and terminal cisternae has been observed previously in relaxed, intact, amphibian skeletal muscle fibres processed for immunoelectron microscopy (Dulhunty et al. 1987).

Longitudinal SR was found to be vesiculated in all skinned fibres, irrespective of the differences in processing for electron microscopy. The A band region in skinned fibres was occupied with rounded vesicles which were typically 300 to 400 nm in diameter (Figure 5.6D). These vesicles are somewhat smaller in comparison to the 400 to 500 nm diameter vesicles seen at the surface of the muscle fibre. The disruption in the normal geometry of longitudinal SR has also been observed in mechanically skinned fibres fixed at resting length (Ford & Surdyk, 1978).

5.4 Discussion

Clear differences exist between the structure of sarcoballs on fibres processed conventionally compared to those processed with the modified protocol. A membrane bound structure with a disrupted interior was seen in conventionally processed fibres, which is similar to the sarcoball shown in Stein and Palade (1988). In contrast, sarcoballs on fibres processed with the modified protocol are comprised of an aggregation of vesicles throughout the structure. What is responsible for the differences in the sarcoball structures has not been able to be definitively identified. Many factors may be important, but it seems unlikely that it is simply due to differences in the proportion of glutaraldehyde and formaldehydes used during fixation. The more important factor apparent from the present study seems to be the dehydration process.

The differences may be due to the dehydration process

The actions of dehydration agents upon the structure may occur in two ways. Firstly, the ability of the dehydration agent to dissolve lipids can cause the extraction of lipids from membranes. The degree to which this occurs is dependent upon the temperature, the partition co-efficient of the dehydration agent and the length of time spent in the dehydration agent. Even post-fixation with OsO_4 does not necessarily prevent extraction of lipids as OsO_4 only fixes

phospholipids with enoic fatty acid bonds (Hayat, 1989). Thus saturated phospholipids remain unfixed. A total of 4 hours dehydration in methanol during conventional processing gives ample opportunity for extraction of lipids to occur in comparison to the one hour dehydration during processing with the modified protocol. Attempts were made to reduce any extraction of lipids that may be occurring by using cold acetone, which had been proven to be useful in preserving lipids in rat lung lamella bodies (Hallman et al., 1976). With the sarcoball preparation however, the use of cold acetone was severely hampered by the shrinkage which accompanied the dehydration. It should also be noted that during infiltration with the resin, extraction of lipids has also been known to occur (Hayat, 1989).

The second possible action upon the sarcoball structure by the dehydration agent could be to cause the rupture of membrane vesicles. Vesicles can be induced to aggregate upon addition of Ca^{2+} which reduces the hydration forces between neighbouring vesicles and the ensuing fusion step is rapid, resulting in rupture and collapse of the vesicles, with few exceptions (Rand et al., 1985). Analogous effects have been described by Pattle (1950) for both ethanol and methanol upon foams of saponin and egg albumen. The effects of ethanol and methanol upon these foams was brief, causing the outer layers of a foam to collapse rapidly, while the rest of the foam remained intact. It is possible that the dehydration agents used in the processing are able to cause the rupture and collapse of vesicles. If this is the case, then the continuous membrane surrounding the sarcoballs and surface vesicles in conventionally processed fibres may be due to rupture of outer layers of vesicles which collapse upon the vesicles beneath them.

It is most likely that the continuous membrane seen in conventionally processed fibres is an artefact, even if not produced by the procedure described above. The fact that skinned fibres prepared for contractile studies can release and take up Ca^{2+}, and external Ca^{2+} is able to penetrate and activate the myofibrils, indicates

there is not a continuous ion-selective membrane surrounding the skinned fibre. If a membrane is present, it must be very leaky.

Possible foam-like structure

The aggregation of vesicles observed is reminiscent of a foam-like structure. It is recognised that any fixation and processing of the skinned fibres with sarcoballs will interfere with the membrane structure in some way but to what degree cannot be predicted. Ideally, this could be minimised by application of techniques which rapidly freeze the tissue, followed by cryosectioning for direct inspection, or freeze substitution before normal sectioning for inspection. In the absence of these techniques, however, it is assumed that the greater structural detail found inside sarcoballs processed with the modified protocol is a reasonable reflection of the true structure.

This foam-like structure also assists in explaining other observations encountered when working with sarcoballs under the light microscope. When sarcoballs are punctured by an electrode they do not collapse, unlike sarcolemmal vesicles (Bretag, Feutrill and Fink, unpublished observations). Sarcolemmal vesicles are fluid filled vesicles containing ribosomes and glycogen granules, bounded by a single membrane bilayer (Burton et al., 1988). A foam structure for sarcoballs would not be expected to collapse, since only some of the vesicles would have been punctured, with the other vesicles maintaining the structure. When sarcoballs are approached by patch pipettes with a high positive pressure, they can be deformed by flattening or spreading them over the fibre surface. In some cases the sarcoballs eventually return to the hemispherical shape they were before. This behaviour would be possible with an aggregation of vesicles in a foam structure, but a single-bilayer, fluid-filled structure would be expected to only dimple in response to the applied pressure and return immediately to its previous shape once the pressure was removed.

A foam structure might also provide an explanation for the common occurrence of tethers forming when patching onto the sarcoball surface, as described in Chapter 3. When removing the patch electrode from the sarcoball surface, a string of vesicles might pull away from the aggregated vesicle structure, forming a tether. There is also the possibility that a single vesicle might be removed from the structure at the tip of the pipette, which is in accord with the behaviour described in Chapter 3 that suggests vesicles were sometimes present.

Disruption of the internal membranes

The internal membranes of the muscle fibre are disrupted within the interior of skinned fibres which have been allowed to contract unrestrained to form sarcoballs. Clearly there are two interventions which could contribute to this disruption; the skinning process and the unrestrained contracture. The effects of the skinning process upon the internal membranes has been investigated in both amphibian (Ford & Surdyk, 1978) and mammalian (Eastwood et al., 1979) skeletal muscle fibres which were maintained in the relaxed state. Swelling of both the SR membrane compartment and mitochondria was seen in each case. The longitudinal SR was extensively vesiculated and disrupted in the mechanically skinned amphibian muscle fibres (Ford & Surdyk, 1978), while the chemically skinned mammalian fibres were swollen only in the terminal cisternae (Eastwood et al., 1979). Only after storage at -20°C for one week did more extensive disruption occur in chemically skinned fibres (Sorenson et al., 1980). The results of these previous studies suggest that the disruption of the internal membranes observed here is likely to be due to the mechanical skinning process, though a further contribution to the disruption from the unrestrained contracture cannot be discounted.

Contribution of mitochondrial and T-tubule membranes to sarcoballs

In the base region of sarcoballs, close to the fibre surface, both mitochondria and tubular vesicles were observed. In many cases the mitochondria were apparently disintegrating and the tubular vesicles, thought to be T-tubules, were not associated with triad structures. These types of organelles were not seen further out in the sarcoball structure, which might mean they are physically restricted to the region near the fibre surface. If this is the case, then neither mitochondrial or T-tubule membrane would be expected to contribute to the surface of the sarcoball. Alternatively, as the mitochondria and T-tubules disintegrate, they may lose any identifying feature and might not be restricted to the fibre surface. These membranes could assimilate into the foam structure during the formation of sarcoballs and be anonymous to visual inspection.

Possible mechanism of formation

The hypothesis proposed here assumes that when the fibres are mechanically skinned, the internal membranes become vesiculated. These vesicles of internal membrane are then squeezed out of the interfilament spaces and stream to the surface of the fibre under the force of the unrestrained contracture. At the surface, they form stable aggregated foam structures, which are the sarcoballs observed.

Observations suggested that smaller diameter vesicles occurred within the fibre, compared with those seen at the fibre surface. Assuming that they are of the same population, it is thought that the increase in vesicle diameter from the interior of the fibre to the surface is an indication of a pressure gradient, decreasing from the interior towards the surface. An applied pressure is able to alter the diameter of a vesicle. This is derived from a special case of the Laplace-Young equation for spherical vesicles

$$P = 4\gamma / r \qquad (5.1)$$

where P is the pressure difference across an interface of principle radius of curvature r (assuming the vesicles are perfectly spherical), and γ is the bifacial tension, since there are two aqueous-lipid interfaces. The bifacial tension is not simply twice the surface tension of a monolayer aqueous-lipid interface, since the leaflets of the lipid bilayer are closely associated due to steric, Van der Waals and ionic forces between the two lipid layers.

If vesicles are extruded from the interfilament spaces, emerging at the fibre surface where the applied pressure is less, any increase in vesicle diameter will be influenced by the bifacial tension of the membrane. Measurements of bifacial tension for native SR membrane do not appear to be present in the literature. Although the SR membrane is known to be composed of phosphatidylcholine, phosphatidylethanolamine, phosphatidylserine and phosphatidylinositol (Owens et al., 1972), artificial membranes composed of these lipids do not appear to have had measurements made of the bifacial tension. Even if estimates of the SR bifacial tension were available from artificial lipid membrane mixtures, it may not accurately reflect the *in vivo* SR membrane because of the large amounts of Ca^{2+}/Mg^{2+}-ATPase protein present. In model membranes, addition of gramicidin (at <50 mol%) significantly reduces the elasticity of the membrane (Tournois et al., 1989). The elasticity describes the capacity of the membrane to absorb small changes in surface area with a compensatory change in bifacial tension. It is likely that the presence of Ca^{2+}/Mg^{2+}-ATPase protein in the SR membrane will influence the elasticity.

Once the extruded vesicles reach the surface of the fibre, it is my view that there is not extensive fusion of vesicles within the sarcoball structure, but that the sarcoball is comprised mainly of a stable aggregation of vesicles. This is suggested from observing vesicles in sarcoballs processed with the modified protocol where there does not appear to be sharing of common bilayers between adjacent vesicles. If this is the case, then for a stable aggregation to occur the

hydration, ionic and Van Der Waals forces between adjacent membranes need to be overcome to some degree. The stable aggregation may be achieved by capillary attractive forces which are known to contribute to the formation of foams (Bikerman, 1973).

There may be some fusion of vesicles to produce the larger 1 μm vesicles observed within the sarcoball structure. Since the active phase of vesicle extrusion in the formation of sarcoballs is completed well before the fibre is processed, non-bilayer structures indicative of the fusion process occurring (Siegel et al., 1989) may not be seen. A reduction in free surface energy would provide the thermodynamic driving force for fusion to occur, although an initial perturbation is required. In isolated vesicle systems, spontaneous fusion of small liposomes (<50 nm diameter) occurs because of the inbuilt tension with such small diameters, which drives the fusion with a reduction in free surface energy (Schullery et al., 1980). Larger liposomes need to be aggregated first before fusion can occur (Wilschut & Hoekstra, 1984) which requires a reduction in the hydration energy between adjacent bilayers (Rand et al., 1985). If the hydration energy is sufficiently overcome, then intermediate non-bilayer structures are formed to accomplish fusion. In isolated systems, this is achieved by addition of millimolar concentrations of Ca^{2+} or polycations to reduce the hydration energy between vesicles comprised of acidic phospholipids (Papahadjopoulos et al., 1990). Fusion of cells can be induced by dehydration of phospholipid head groups to allow aggregation followed by rehydration to initiate the fusion process (Ahkong et al., 1975). In contrast, the process of vesicle fusion to planar bilayers in the presence of an osmotic gradient and Ca^{2+} (Miller & Racker, 1976), although a well established technique, is thought to occur in a quite different manner to the fusion of spherical vesicles (Rand et al., 1985), and therefore may not be relevant to sarcoball formation.

Conclusions

The results of this study suggest that sarcoballs are composed of an aggregation of vesicles in a foam-like structure. It is proposed that the SR and T-tubules are vesiculated when the muscle fibres are mechanically skinned. It is also likely that mitochondria disintegrate and produce vesicles, which could contribute to the sarcoball structure. The vesicles are thought to be extruded to the surface from the interfilament spaces by the force of the unrestrained contracture. At the surface, the vesicles aggregate to form sarcoball structures.

6. ANTIBODY LABELLING OF MEMBRANES

6.1 Aims and Introduction

The ion channel activity which has been recorded from the sarcoball preparation has shown, in addition to the high conductance anion channel (Hals et al., 1989; Lewis & Bretag, 1991), a K^+ channel (Stein et al., 1989) and a Ca^{2+} channel (Stein & Palade, 1988; Wang & Best, 1992). Both the K^+ and Ca^{2+} channel recorded from the sarcoball have similar characteristics to their counterparts recorded from SR vesicles incorporated into bilayers. On the basis of this similarity, the sarcoball preparation has been considered to be a preparation of mainly SR membrane. Consequently, the high conductance anion channel recorded in sarcoballs has also been considered to be from the SR membrane.

Identifying the origin of the anion channel by this association with the K^+ and Ca^{2+} channels in the same preparation is insufficient. Unlike the K^+ and Ca^{2+} channels, the anion channels recorded from SR vesicles in bilayers (Miller, 1978; Tanifuji et al., 1987; Rousseau et al., 1988) have some different properties from those in sarcoballs, for example, they don't exhibit the same steep voltage dependence (Hals et al., 1989; Lewis & Bretag, 1991). There is an indication from my structural studies (Chapter 5) that mitochondrial membrane may be incorporated in the sarcoball structure. The voltage dependent anion selective channel (VDAC) from outer mitochondrial membrane has a similar steep voltage dependence, though there are also some properties which are clearly different.

Therefore, the aim of this study was to ascertain what internal membranes might be contributing to the membrane in sarcoballs by using immunolabelling at the electron microscope level. The presence of SR membrane was investigated using specific antibodies to the Ca^{2+}/Mg^{2+}-ATPase and the ryanodine receptor, which are distinctive marker proteins of SR membrane. An antibody to the VDAC was used as I considered that it would be a marker for the presence of mitochondrial outer membrane, and particularly for mitochondrial VDAC.

Studies with Xenopus laevis muscle

The immunolabelling with the D12 antibody to Ca^{2+}/Mg^{2+}-ATPase and 5C3 antibody to the ryanodine receptor was done in collaboration with Dr A.F. Dulhunty, Dr P. Junankar and C. Stanhope, Muscle Research Group, Division of Neuroscience, John Curtin School of Medical Research, Australian National University, Canberra. I prepared and processed the sarcoballs at the John Curtin School of Medical Research. This material was sectioned and mounted by C. Stanhope. Post-embedding labelling with the D12 and 5C3 antibodies was performed by C. Stanhope while training me in this technique. Electron microscopy of this material was performed by Dr A.F. Dulhunty. Aspects of this study have been published in Lewis et al., (1992).

Studies with Bufo marinus muscle

Immunolabelling studies with the antibody to mitochondrial VDAC, using muscle fibres from *Bufo marinus*, were done at the Center for Electronmicroscopy and Microstructural Analysis, The University of Adelaide. Assistance was provided by Dr M. Henderson and D. Smith, who sectioned the material for me, and I carried out all other aspects of this study.

6.2 Methods

Immunolabelling of sarcoballs for SR membrane

Sarcoballs were prepared, as described in Chapter 2, from semitendinosus muscle of the clawed toad, *Xenopus laevis*. The skinned muscle fibres with sarcoballs were fixed in Ringer's solution containing 2% formaldehydes (prepared fresh from paraformaldehyde) and 0.1% glutaraldehyde for 2 hours at room temperature, washed in Ringer's solution and then dehydrated in 90% methanol for 1 hour at room temperature. Some shrinkage of sarcoballs was seen during the fixation and dehydration procedures. The fibres were infiltrated with LR White acrylic resin (London Resin Company) overnight at 4°C and then rinsed in fresh resin at room temperature. They were embedded in LR White resin in small gelatin capsules and cured at 60°C for at least 12 hours.

Grey to silver sections were cut with a diamond knife on an ultramicrotome and mounted on collodion coated, copper grids. Grids were blocked for 15 hours with 5% skimmed milk powder (Diploma) in water and rinsed in 0.5% bovine serum albumin in phosphate buffered saline (PBS) containing (in mM): 7.0 Na_2HPO_4, 2.6 NaH_2PO_4, 137 NaCl, pH 7.0. The primary antibodies used for labelling were a) the purified D12 Ca^{2+}/Mg^{2+}-ATPase antibody as prepared by Dulhunty et al. (1987) diluted with PBS to a final protein concentration of 1.7 $\mu g\ ml^{-1}$; or b) the ryanodine receptor antibody, 5C3, as prepared by Dulhunty et al. (1992), diluted 1:10 with PBS. Sections were exposed for 1 hour to the primary antibody, washed in PBS, exposed to the second antibody (5 nm gold-conjugated goat anti-mouse antibody; Janssen Pharmaceuticals) for 1 hour, washed in distilled water and lightly stained with 5% aqueous uranyl acetate. Type I controls, where serial sections were labelled according to the above protocol, except for omitting the primary antibody labelling step, were performed to check for non-specific labelling by the gold-conjugated antibody alone. All sections were examined on a Hitachi H 7000 electron microscope.

The specificity of each of the antibodies used here has been well established. Independent studies have shown that the D12 monoclonal antibody is specific for the ATP binding region of skeletal muscle Ca^{2+}/Mg^{2+}-ATPase (Molnar et al., 1992). The specificity of the 5C3 antibody for labelling the ryanodine receptor was shown by immunostaining of Western blots obtained from electrophoresis gels of junctional face membrane proteins (Dulhunty et al., 1992).

Immunolabelling of sarcoballs for VDAC

Sarcoballs produced by mechanically skinning single muscle fibres from the semitendinosus muscle of the cane toad, *Bufo marinus*, in 200 mM CsF, were fixed with 2% formaldehydes (prepared fresh form paraformaldehyde) and 0.25% glutaraldehyde in the following solution (in mM): 117 KCl, 4.7 NaCl, 1.2 $CaCl_2$, 5.0 TES, pH 7.4 adjusted with KOH. Fixation was for 1 hour at 4°C. Fibres were then washed in the same solution before being dehydrated in methanol with 20% (w:v) polyvinylpyrrolidone (PVP, MW 25 000; BDH Chemicals) at 4°C, at the following dilutions: 15 minutes each at 50% and 70% methanol and 25 minutes at 90% methanol. The fibres were infiltrated with LR White acrylic resin (hard mixture; Bio-Rad Laboratories) overnight at 4°C and then rinsed in fresh resin at room temperature. The fibres were then embedded in LR White resin in small gelatin capsules. These were filled and degassed under vacuum for 30 minutes before being capped and polymerised at 60°C for at least 48 hours.

The fibres were sectioned as before and mounted on nickel grids. The mounted sections were first pretreated with glycine (20 mM) in PBS. Pretreatment with glycine chemically reacts with residual fixative and other reactive groups in the resin to render them neutral and prevent anomalous reactions with the antibodies (Roth et al., 1989). Sections were blocked with 1% fish gelatin (teleostean gelatin; Sigma Chemical Co.) in PBS for 15 minutes and then exposed for 2 hours to the primary antibody raised against bovine heart mitochondrial porin (VDAC) (De Pinto et al., 1989) diluted 1:200 in PBS. Sections were then washed with 1% fish

gelatin in PBS and exposed to the second antibody (5 nm colloidal gold conjugated to goat-anti-rabbit antibody; Sigma Chemical Co.) diluted 1:60 in PBS, for 1 hour. The second antibody was spun down at 10 000 g for 15 minutes in a bench centrifuge to pellet any aggregated antibody before treating the sections. Washes with 1% fish gelatin in PBS and then distilled water were applied to sections before being stained with 5% aqueous uranyl acetate and Reynold's lead citrate. Two types of controls were performed on serial sections of the same skinned fibres: Type I, omitting the VDAC antibody labelling step to check for non-specific labelling of the secondary antibody; and Type II, replacing the VDAC antibody with normal rabbit serum at the same dilution in PBS, to check for non-specific binding of the primary antibody.

All grids were lightly coated with carbon to stabilise the resin sections under the electron beam. Sections were examined on a Phillips 300EM transmission electron microscope at 80 kV.

The antibody to bovine mitochondrial VDAC was a gift from Dr V. De Pinto, University of Bari, Italy. The specificity of the antibody to identify mitochondrial VDAC has been established with immunoblotting of mitochondrial proteins after SDS gel electrophoresis (antibody diluted 1:1000; De Pinto et al., 1989).

Interpretation of results

The observations have been interpreted with an understanding of the limitations inherent in post-embedding immunolabelling. Labelling can only occur at those antigenic sites exposed at the surface of the thin sections. Thus, labelling is less than that expected from the amount of membrane present in the thin sections, although the density of labelling is proportional to the density of antigenic sites (Dulhunty et al., 1987). Label can also be remote from the antigenic site for a number of different reasons. The physical dimensions of the two antibodies and the conjugated 5 nm gold particle means that label can be displaced up to 30 nm

from the antigenic site. The shearing action of the sectioning knife can displace membranes slightly away from the normal orientation at the surface, resulting in remote label. Label can also occur at antigenic sites separated from the membrane or portions of membrane by sectioning in the same plane as the membrane. This gives the appearance of the labelling not being associated with any membrane at all.

6.3 Results

SR antibodies label sarcoballs

a) Ca^{2+}/Mg^{2+}-ATPase

Both the interior of the skinned fibres and the sarcoball structures were inspected for specific labelling with the Ca^{2+}/Mg^{2+}-ATPase antibody. Sites where the Ca^{2+}/Mg^{2+}-ATPase is localised are approximately marked by the electron dense 5 nm gold particle conjugated to the second antibody. Type I control sections showed no labelling at all. All sections exposed to both the primary and secondary antibodies were inspected for non-specific labelling in the extra-cellular regions of the section, which would indicate unsuccessful blocking or contamination of the section surface. Those few sections with non-specific labelling in the extra-cellular regions were rejected and only uncontaminated sections were examined further.

Membranes at the surface of sarcoball structures, which are therefore accessible for patch clamping, were clearly decorated with the electron dense gold (Figure 6.1A-6.1C). This indicates the presence of the Ca^{2+}/Mg^{2+}-ATPase in these membranes. Labelling was also observed on the membrane structures within the interior of sarcoballs. Within the myofibrillar regions of the skinned fibres, specific labelling was observed only on the vesiculated SR membrane. No labelling was observed on mitochondrial membranes (Figure 6.1D) or on the myofibrillar filaments (Figure 6.1E).

Figure 6.1 Labelling of membranes with Ca^{2+}/Mg^{2+}-ATPase antibody. Skinned fibres from *Xenopus laevis*, with sarcoballs, were labelled with a monoclonal antibody to the Ca^{2+}/Mg^{2+}-ATPase. The arrows indicate small electron dense spots which are the 5 nm gold particles conjugated to the second antibody, marking the approximate sites of the Ca^{2+}/Mg^{2+}-ATPase. **A**. Shown here is a serial section of the same sarcoball shown in Figure 5.3A, where the vesicles and myofibrils (F) are at the top of a sarcoball structure. Labelling can be seen at the surface of sarcoball structure. **B** and **C**. Further examples of labelling at the surface of sarcoballs, which are 30 to 40 μm from the skinned fibre surface. **D**. Vesiculated longitudinal SR within the skinned fibre was also labelled but not mitochondrial membranes (M). **E**. Labelling within the myofilament lattice was confined to the SR. Calibration bar: A,B,C and E, 0.13 μm; and D, 0.2 μm. Courtesy of Dr A. F. Dulhunty.

Figure 6.2 Labelling of membranes with ryanodine receptor antibody. Sections of skinned fibres, from *Xenopus laevis*, with sarcoballs were labelled with a monoclonal antibody to the ryanodine receptor. The arrows indicate the gold label which identifies the presence of the ryanodine receptor. **A**. This is a serial section of the same sarcoball surface shown in Figure 6.1A. The arrow points to the area of the sarcoball surface magnified in **B.** which shows clear labelling with the ryanodine receptor antibody. **C**. This is taken from further along the same sarcoball surface shown in **B.**, showing additional labelling. **D**. Membranes within the interior structure of sarcoballs were also labelled with gold particles. Calibration bar: A, 0.58 μm; B,C and D, 0.1 μm. Courtesy of Dr A. F. Dulhunty.

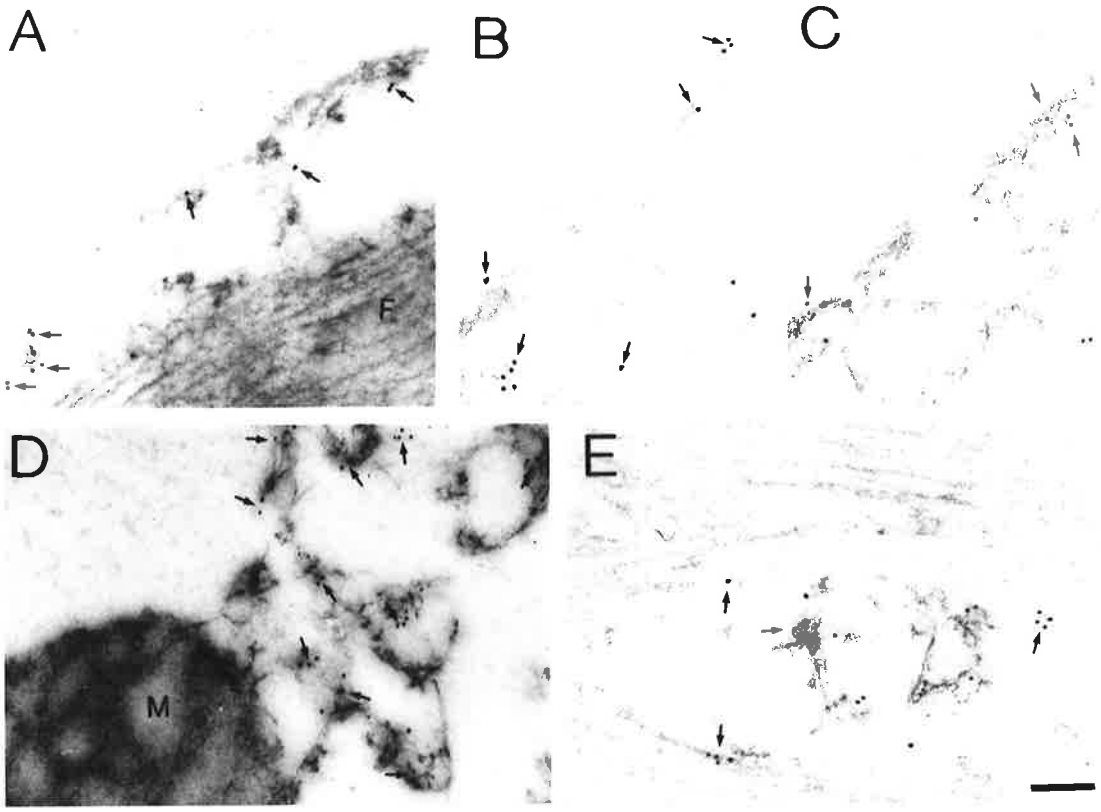
A
B
C
F
D
M
E

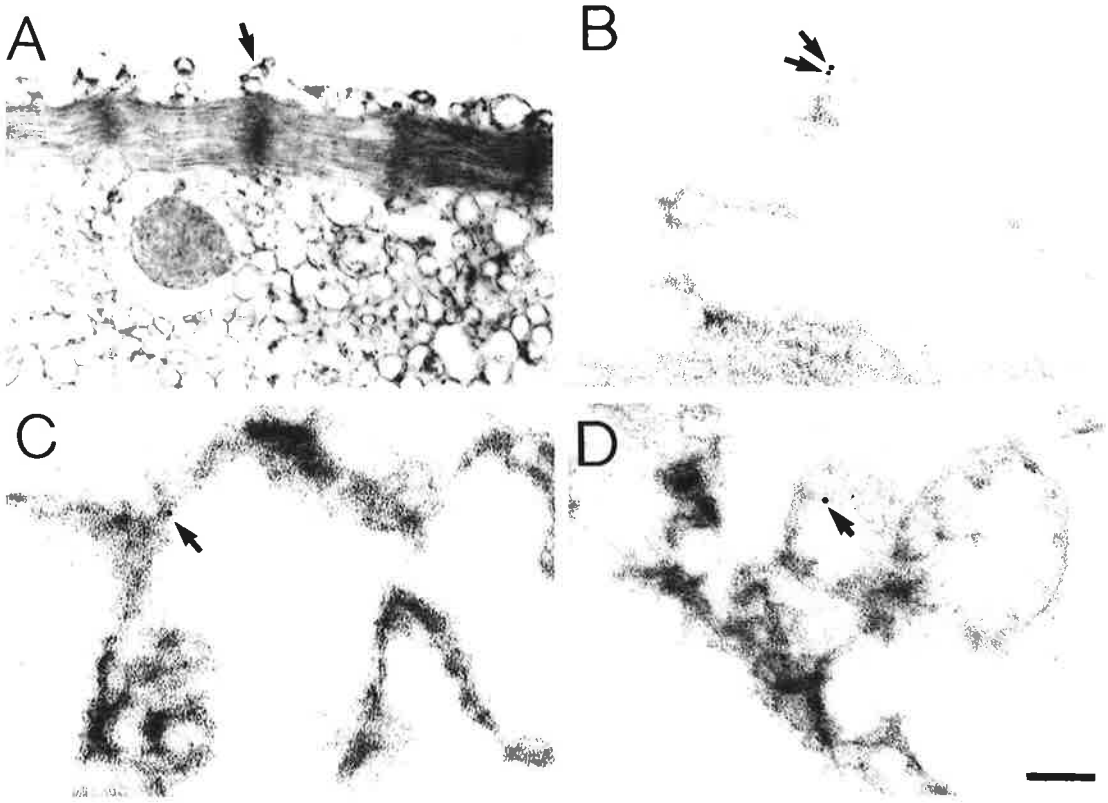
A
B
C
D

b) Ryanodine receptor

Gold particles were observed to decorate membranes at the surface of both sarcoball structures and small blebs, in sections of skinned fibres labelled with the ryanodine receptor antibody (Figure 6.2). These results indicate the presence of the Ca^{2+} release channel and junctional SR membrane in the sarcoball preparation.

A low density of labelling was expected with the 5C3 ryanodine receptor antibody, as it has been shown to bind to fewer than 1% of potential ryanodine receptor sites (Dulhunty et al., 1992). The low levels of labelling observed on the skinned fibres are unlikely to be due to non-specific labelling. Type I control sections were found to have no evidence of labelling. As with the D12-labelling, sections labelled with the 5C3 antibody which showed non-specific binding in the extracellular regions were rejected. All of the specific gold labelling seen in sections was associated with either sarcoball membranes or membranes which could be identified as SR terminal cisternae within myofibrillar regions of skinned fibres. No labelling was seen on the myofilament lattice or within the empty interior of vesiculated membrane structures.

Labelling with a VDAC antibody

Sections labelled with the VDAC antibody were examined for specific labelling on mitochondrial membrane, SR membrane, T-tubules and sarcoball structures. Type I controls on serial sections from the same skinned fibres showed no labelling. In type II controls, rare occurrences of background labelling were found on the nucleus of the muscle fibre, but no labelling was found on any of the other structures examined. As above, all sections were examined for non-specific labelling in the extracellular regions and contaminated sections were rejected.

a) Mitochondria

Specific labelling was clearly observed on the outer membrane of mitochondria within mechanically skinned skeletal muscle fibres. This is to be expected, since this is the known location of the VDAC. Figure 6.3 shows examples of the labelling observed, which was distributed around the outer membrane of mitochondria in a similar manner to that shown by Weiler et al. (1985) with a specific antibody to mitochondrial VDAC on isolated mitochondria. It is also similar to labelling on isolated mitochondria with antibodies to hexokinase I, which is known to be associated with the VDAC in mitochondria at contact sites between the inner and outer membranes (Weiler et al., 1985; Kottke et al., 1988).

b) Sarcoplasmic reticulum and T-tubules

Surprisingly, regions of SR within mechanically skinned muscle fibres were also decorated with electron dense gold-label (Figure 6.4.), however, the amount of label found on SR membrane was not nearly as much as that found on mitochondria. Although the density of this labelling is low, it cannot be dismissed as non-specific since no labelling of SR membranes was observed in either type I or type II control sections.

In those few cases where intact triad structures could be identified, labelling was seen only on terminal SR and not on T-tubules (Figure 6.4A and B). Most labelling on the SR was seen on the vesiculated membranes within the myofibrillar region of the skinned fibres (Figure 6.4C and D). It could not be determined if there was any localisation of the antibody labelling to particular regions of the SR. These results indicate the presence of a protein in SR with an antigenic site which is recognised by the VDAC antibody.

c) Sarcoball structures

Membranes at the surface and within the interior structure of sarcoballs were decorated with gold label in sections of skinned muscle fibres exposed to the

Figure 6.3 Outer mitochondrial membrane labelled with VDAC antibody. The presence of mitochondrial VDAC was identified in skinned fibres by labelling with a specific VDAC antibody. The fibres shown here are from *Bufo marinus*. The arrows indicate the location of VDAC marked by the gold label. Labelling is shown here on the outer mitochondria membrane, which is the established location of VDAC. Calibration bar: A, 0.53 µm; B, 0.48 µm; C and D, 0.40 µm.

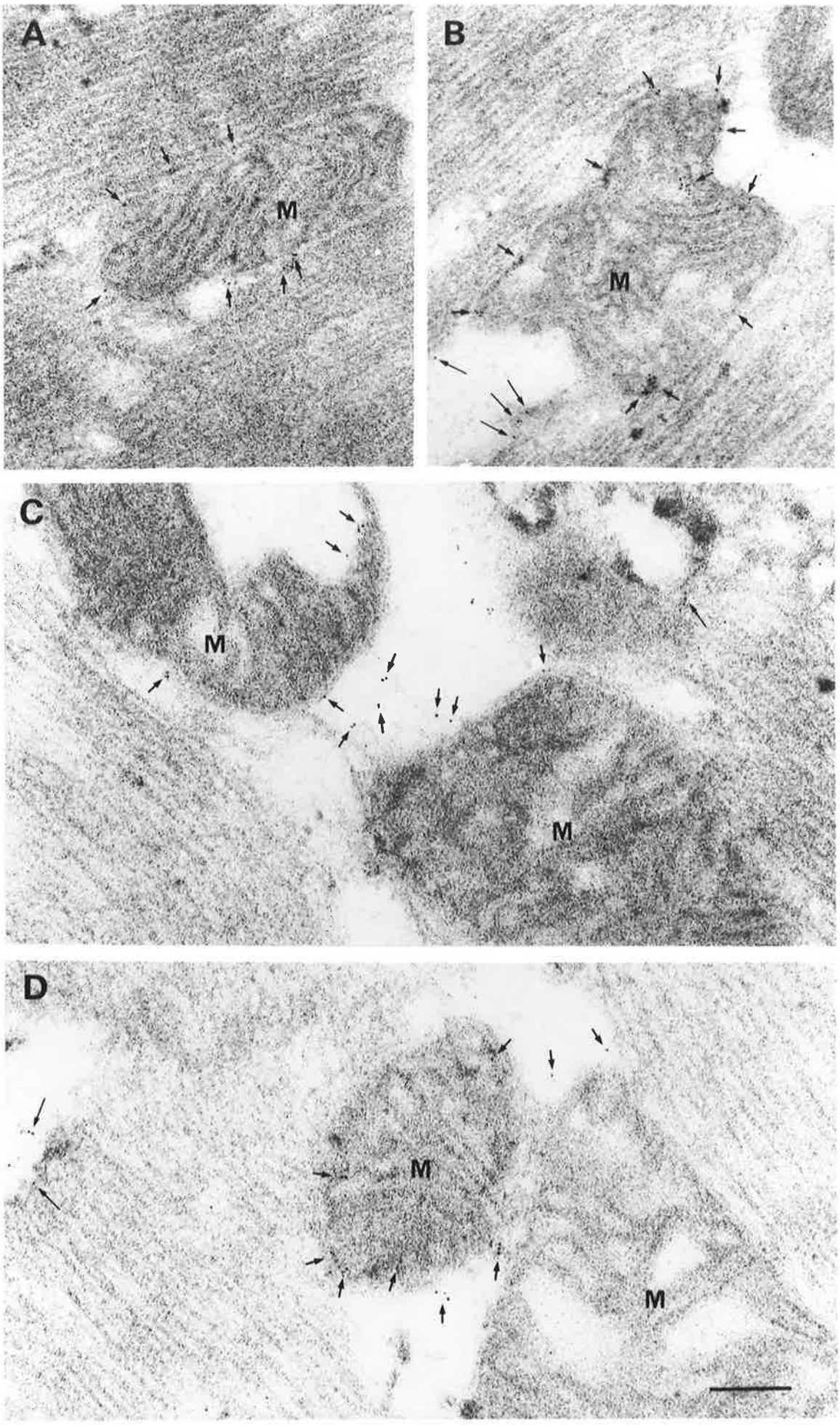
A
M
B
M
C
M
M
D
M
M

Figure 6.4 VDAC antibody labels SR membrane.
As in Figure 6.3, the arrows indicate the location of VDAC antibody, marked by the gold label. The VDAC antibody is shown here to label SR membranes within the myofibrillar region of the skinned fibres from *Bufo marinus*. **A.** One of the few examples of labelling in a region which could be identified as junctional SR, in alignment with the Z-line of the myofilaments. **B.** An enlargement of the labelling region shown in A. **C and D.** Labelling on vesiculated SR. Calibration bar: A, B and C, 0.46 μm; and D, 0.10 μm.

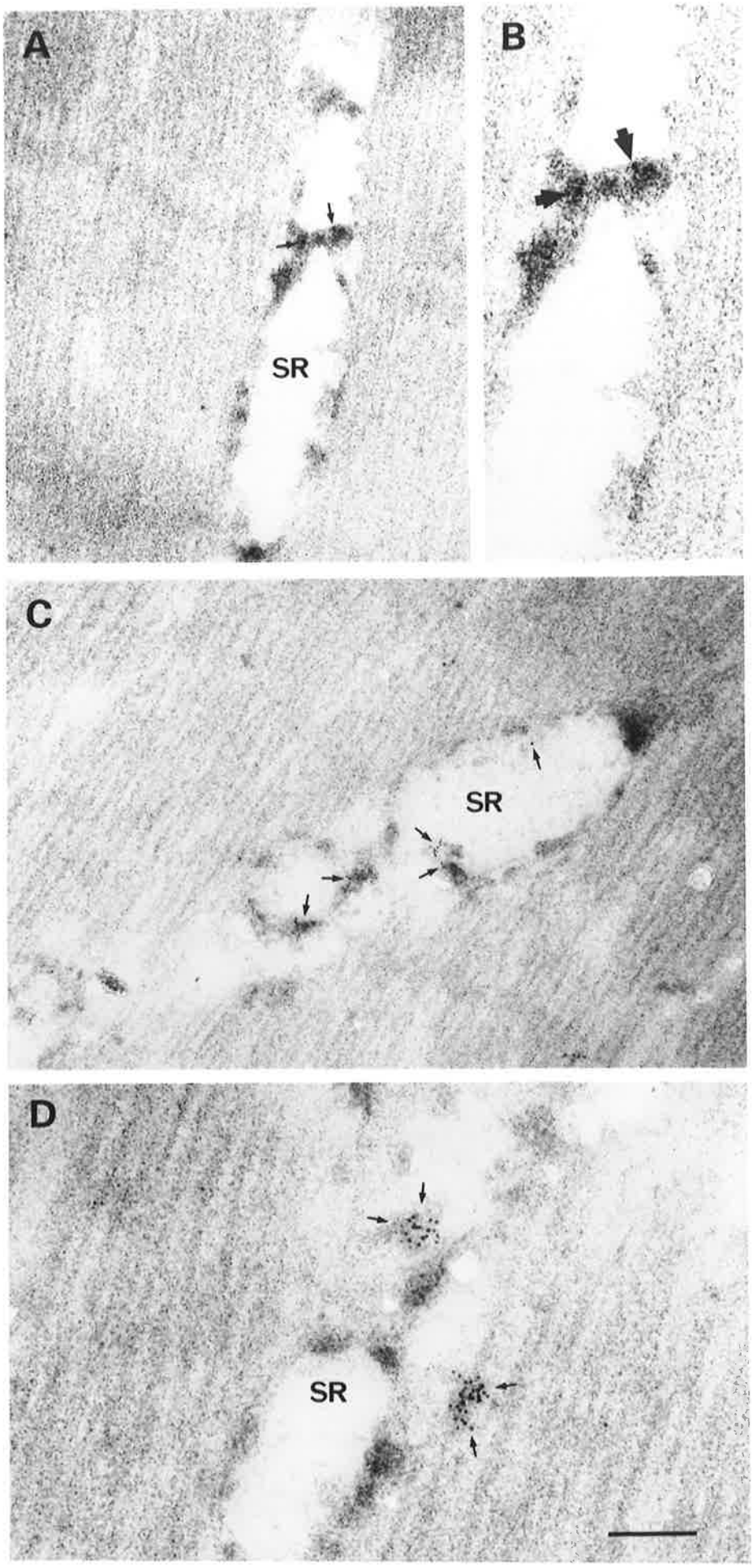
A
SR
B
C
SR
D
SR

Figure 6.5 Sarcoball membranes labelled with VDAC antibody.
Again, as in Figure 6.3, the arrows indicate the location of VDAC antibody, marked by the gold label. Labelling with the VDAC antibody is shown here on the surface membranes of sarcoballs from *Bufo marinus*. Each of the sarcoballs shown extended 80 to 100 μm out from the myofibrillar surface. These are regions which would be accessible for patch clamping. Labelling was also found on membranes which form the interior structure of the sarcoball. Calibration bar: 0.10 μm for all.

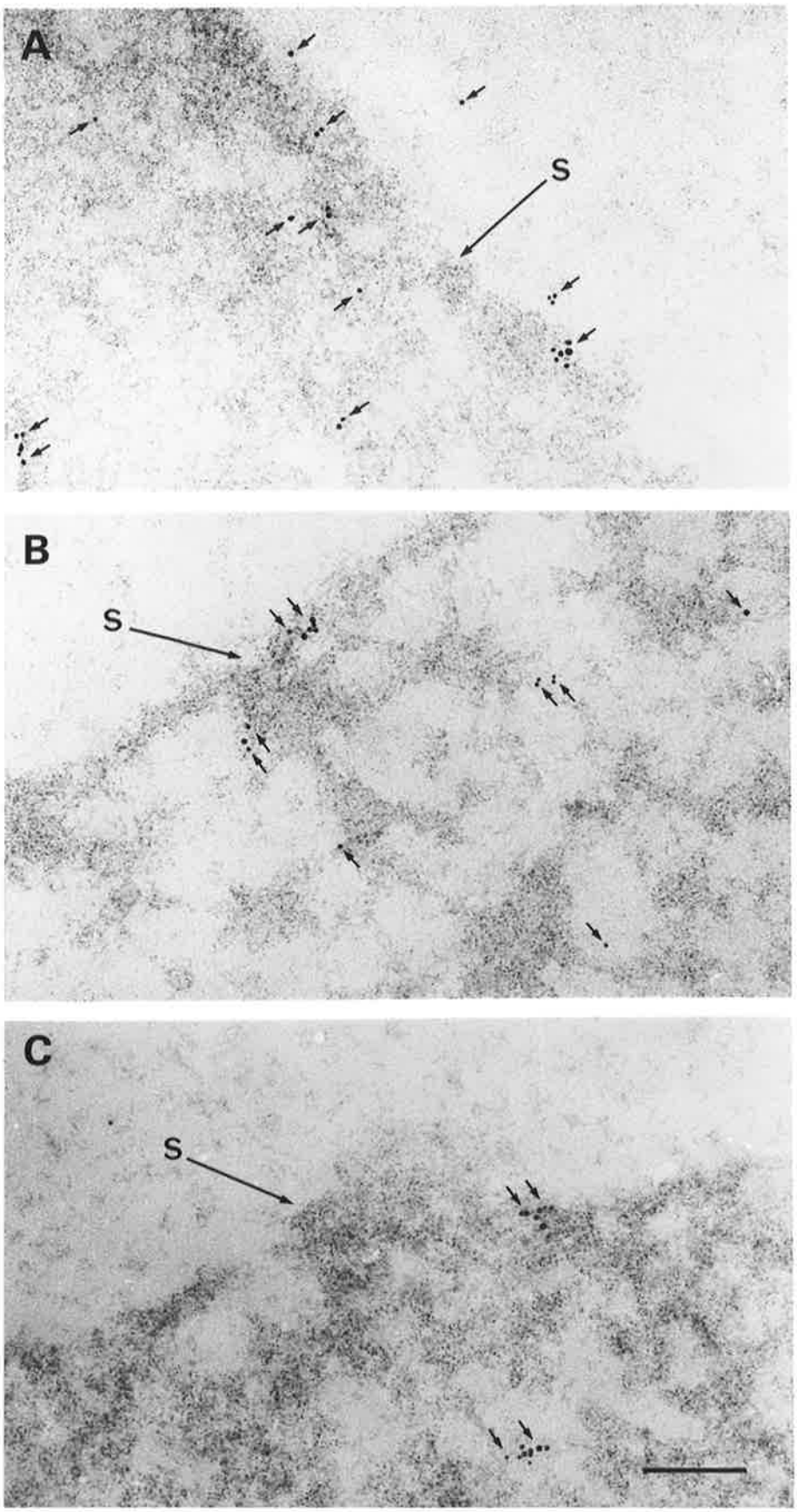
A
S
B
S
C
S

VDAC antibody (Figure 6.5.). There did not appear to be any bias in the distribution of the labelling on the sarcoball and not all membranes associated with sarcoballs were labelled. The presence of label at the surface of the sarcoball is significant as this is the surface accessible for patch clamp recordings.

6.4 Discussion

Sarcoballs contain SR membrane.

Immuno-gold labelling with the Ca^{2+}/Mg^{2+}-ATPase and ryanodine receptor antibodies conclusively demonstrates that sarcoballs contain SR membrane. The extensive labelling with the Ca^{2+}/Mg^{2+}-ATPase antibody over much of the sarcoball surface and interior suggests a large contribution from SR membrane to sarcoball composition. The labelling of ryanodine receptor indicates the presence of some junctional face membrane in the sarcoball too, which is consistent with the recordings of the Ca^{2+} release channel from this preparation (Stein & Palade, 1988; Kwok & Best, 1990; Wang & Best, 1992). Prior to the results presented here, it had been assumed that the sarcoball structure contained SR membrane on the basis of Ca^{2+} and K^{+} channel recordings similar to those obtained from SR vesicles in bilayers.

Not all membranes within the sarcoball interior or at the surface were labelled with the Ca2+/Mg2+-ATPase and ryanodine receptor markers. This can indicate either that these membranes did not have antigenic sites available for binding or that the membranes were not of SR origin. Evidence from Chapter 6 suggests that mitochondria and T-tubules may contribute membrane to the sarcoball structure. From stereological measurements on amphibian skeletal muscle, SR (including terminal cisternae) membranes comprise 73% of all internal membranes, mitochondria 19% and T-tubules comprise 7.9% (Mobley & Eisenberg, 1975). If the relative contribution of internal membranes to the sarcoball structure is dependent upon the relative proportion within muscle

fibres, then sarcoballs would be comprised overwhelmingly of SR membrane, but with a significant contribution from mitochondria.

Mitochondrial membrane and VDAC

The VDAC antibody was chosen to determine whether mitochondrial membrane was present in sarcoballs. It was also expected to resolve the possibility that VDAC is at the sarcoball surface where it may be recorded using patch-clamp techniques. This possibility was raised when patch-clamp recordings with many channels present were observed to have a reduced voltage dependence, similar to the VDAC from outer mitochondrial membrane. While the surface membranes of sarcoballs were labelled with the VDAC antibody, both the mitochondrial and SR membranes within the interior of the skinned fibre were also labelled. It is not possible from these results to distinguish the origin of the labelled membrane in the sarcoballs, though it is likely that both mitochondrial and SR membranes contribute.

An antibody to a marker protein of the mitochondrial inner membrane would be useful in determining to what extent mitochondrial membranes do contribute to sarcoballs. If inner mitochondrial membranes were identified in sarcoballs it would also confirm speculations that mitochondria disintegrate before contributing lipid membranes to the structure.

The labelling observed on the SR with the VDAC antibody poses the interesting possibility that there is a protein present in the SR membrane which is similar to the mitochondrial VDAC. At least there is a protein which has an antigenic site similar to that of the VDAC. Further evidence of a VDAC-like protein in SR has been provided by western blot analysis, where the VDAC antibody recognises a protein of the same molecular weight from fractionated SR vesicles as mitochondrial membranes (Junankar et al., 1993). It could be speculated that perhaps the anion channel recorded from sarcoballs could also be the protein in

SR recognised by the VDAC antibody. Since the VDAC and the sarcoball anion channel do share some similar biophysical properties, it may be not unreasonable therefore to propose they also share some similar structural properties. The application of the VDAC antibody to the bath solution of excised patches of sarcoball membrane had no detectable effects upon the channel behaviour (Chapter 3), though this does not necessarily exclude the channel as the protein recognised by the antibody. There could be a number of reasons for this, including the antibody binding to a region of the channel protein which has no effect upon the channel behaviour. VDAC-like proteins have been found in a range of different tissues (Thinnes, 1992) and have been identified by protein sequence analysis. So far, there has been little investigation as to the ion channel properties of these proteins (see Chapter 7).

Expected contribution of each internal membrane

Not all of the SR, or all of the other internal membranes are extruded to the surface of the skinned fibres during the unrestrained contracture, as these membranes can still be observed in the myofibrillar spaces. Thus, the portion which remains may represent a fraction of the membranes which are perhaps anchored in some way and so are not as mobile. The contribution of the internal membranes may also be dependent upon their initial position, such that those which are close to the surface of the skinned fibre will contribute more than membranes which are deep within the bundles of myofilaments.

The suggestion that not all membranes contribute equally is also supported by observations made by Stein and Palade (1988), who found that the distribution of SR Ca^{2+} release channels was estimated to be an order of magnitude too dilute if it is assumed that there is an even distribution of all membrane components in sarcoballs. Thus, it is possible that regions of internal membranes, and particularly junctional (or terminal cisternae) SR with associated Ca^{2+} release channels, remain anchored in the fibre structure, unable to contribute to the

sarcoball. The results of the present study show that terminal cisternae membranes, indicated by the ryanodine receptor, are a part of sarcoballs and so are not precluded entirely from inclusion by any structural restrictions.

Conclusions

This study conclusively demonstrates the presence of SR membranes, including terminal cisternae membrane, in the sarcoball structure and more significantly, at the sarcoball surface. Immunolabelling with the VDAC antibody indicates that the SR membrane contains a VDAC-like protein.

PART III.
GENERAL DISCUSSION

7. A FAMILY OF HIGH CONDUCTANCE ANION CHANNELS

7.1 Recapitulation

A high conductance anion channel was recorded here from a preparation of internal membranes extruded to the surface of skinned skeletal muscle fibres from *Bufo marinus*. Although a modified method and different species was used, this is considered to be homologous to the anion channel previously recorded from skeletal muscle fibres of *Rana catesbeiana* (Hals et al., 1989). This channel was selective for anions over cations and the conductance saturated with increasing anion concentration. Multiple substates were a characteristic of the complex gating behaviour of the channel.

Of particular interest was the bell-shaped voltage-dependence, where the channel was maximally open at potentials near 0 mV and closed at potentials >±30 mV. The number of kinetic states underlying the behaviour was inferred from the steady-state analysis. A description of the dynamic behaviour was obtained from the non-stationary analysis and inferences were made about the arrangement of the kinetic states. From this analysis, three possible kinetic schemes were found, each of which predicted a bell-shaped voltage dependence. Each of the schemes consisting of 3 open and 3 closed states, which were linked by 3 entry/exit pathways between the open and closed aggregates.

A description of the structure and composition of sarcoballs obtained from electron microscopy studies has been presented here. Sarcoballs were shown to be an aggregation of vesicles, similar to a foam structure. It is proposed that sarcoballs form by the extrusion of vesiculated internal membranes to the surface during the unrestrained contracture. By using specific monoclonal antibodies to SR marker proteins, it was shown conclusively that SR membrane was present in the sarcoball preparation. It was also shown that mitochondrial membrane was likely to be present. It had always been a concern that the anion channel had some characteristics similar to the VDAC channel from the mitochondrial outer membrane and by using a specific antibody to the VDAC protein, it was hoped that the presence or absence of the VDAC in the sarcoball membrane could be determined. As it turned out, a definitive answer could not be provided because of the unexpected cross-reactivity of the VDAC antibody with an SR protein. The labelling which occurs in the sarcoball membrane cannot be attributed solely to the VDAC from mitochondrial membrane, as it may also indicate labelling of the VDAC-like protein from SR membranes.

Is the sarcoball anion channel the mitochondrial VDAC?

It is still unclear as to whether the sarcoball anion channel is from SR membrane, or is the mitochondrial VDAC exhibiting different behaviour because of the preparation. As proposed by Hals et al. (1989), the differences in the biophysical behaviour suggests that the sarcoball anion channel is not the mitochondrial VDAC. The divergent behaviour of these two channels is: (i) the sarcoball anion channel has a saturating conductance with increasing anion concentration, whereas the VDAC has an increasing linear relationship; (ii) the sarcoball anion channel has a high selectivity for anions over cations, while the VDAC is only weakly selective for anions when it is in the open state, and becomes selective for cations when in the closed state; (iii) the closed state of the sarcoball anion channel is a non-conducting state, whereas the VDAC still has a significant conductance,

though smaller than that of the open state. These characteristics are consistent between isolated VDAC incorporated into artificial bilayers and recordings made from whole mitochondrial membranes reconstituted into liposomes (Wunder & Colombini, 1991). In comparison, the anion channels recorded from SR vesicles reconstituted into bilayers (Tanifuji et al., 1987; Rousseau et al., 1988) or into liposomes (Hals et al., 1989) are relatively voltage-independent in comparison to the steep voltage dependence of the anion channel recorded from sarcoballs.

The immunolabelling of sarcoball membranes with VDAC antibody might indicate the presence of mitochondrial VDAC in this preparation, although an anion channel with behaviour matching that of VDAC in planar bilayers has not been reported in sarcoballs. Alternatively, the labelling might indicate the presence of the VDAC-like protein identified in SR membranes. It is possible that the large conductance, voltage-dependent, anion channel recorded here is the VDAC-like protein from SR membranes. As the identity of the VDAC-like protein in SR is unknown, this is yet to be resolved.

7.2 Large conductance anion channels in other cells

The characteristics of the anion channel recorded from sarcoballs are not peculiar to just this preparation. There are a range of other cell types with anion channels that are similar to the sarcoball anion channel. The common properties of these channels are: (i) a large conductance which is generally >300 pS, (ii) a steep voltage-dependence, where the channel is maximally open at potentials near 0 mV and closes at potentials >±30 mV, (iii) complex gating behaviour with multiple subconductance states, (iv) generally a weak selectivity for anions over cations, and (v) generally only seen in excised patches where large shifts in membrane potential are often required initially to induce channel activity, after which the channel displays the normal bell-shaped voltage-dependence. A selection of the different cell types which have anion channels that share these properties is shown in Table 7.1. Although there are variations, the degree of similarity across

such a diverse range of cells, suggests that these channels all belong to the same family. The SR anion channel recorded in sarcoballs is also likely to be a member of this family. While the SR channel displays a better selectivity for anions over cations than most other large conductance channels, it is comparable to the anion channels in alveolar type II cells (Schneider et al., 1985) and human T-lymphocytes (Schlichter et al., 1990).

Voltage dependent behaviour

The bell-shaped voltage-dependence is a prominent feature of all these anion channels. Typically, recordings from patches containing several anion channels show a staircase-like closure as the channel behaviour relaxes in response to applied voltage steps. In most cases this behaviour is symmetrical, though rat myotube anion channels inactivate much more slowly at negative potentials (Blatz & Magleby, 1983) and those from alveolar type II cells inactivate more slowly at positive potentials (Schneider et al., 1985). Where there is a resting membrane potential (-50 mV approx. for macrophages; Schwarze & Kolb, 1984), this voltage-dependence means that the channel is normally closed at resting potential; while for the SR anion channel where the membrane potential is close to 0 mV, the channel is normally open.

Modulation of anion channels

Voltage dependence is often the only modulatory process reported for these anion channels. There have been no reports of large conductance anion channels of this type being modulated by changes in intra- or extracellular free Ca^{2+} concentrations. Though, there has been one recent report of an anion channel of smaller conductance (75 pS in symmetrical 250 mM Cl^-) from SR vesicles in bilayers which is activated by increases in free Ca^{2+} concentrations on the *cis* side (Kourie et al., 1993). It would seem logical that an SR anion channel might be modulated by free Ca^{2+} concentrations if the channel is a counter-ion pathway for

Table 7.1 A family of large-conductance, voltage-dependent anion channels. Shown here is a selection of large conductance anion channels from a variety of different cell types. All channels listed exhibited a bell-shaped voltage-dependence of channel open probability. The selectivity for Cl^- over Na^+ is given as the permeability ratio determined in each study from the shift in reversal potentials. Where values are missing indicates the selectivity was not determined in the study.

Location	Activation	Conductance	Selectivity	Remarks	Reference
Epithelial cells					
bovine kidney cortex epithelial cells	induced (>±30 mV) only in excised patches	300 pS (150 mM Cl^-)	P_{Cl}/P_{Na} = 5 to 13	activity independent of changes in free Ca^{2+} concentration	Velasco et al., (1989)
alveolar type II cells (apical membrane)	spontaneous in excised patches	382 pS (145 mM Cl^-)	P_{Cl}/P_{Na} = 67	multiple subconductance states; propose 6 co-channels; recorded from outside-out patches	Schneider et al., (1985) Krouse et al., (1986)
Endothelial cells					
pig aortic endothelium	delayed appearance in excised patches	385 pS (140 mM Cl^-)	P_{Cl}/P_{Na} = 4 to 5	activity can be induced by A23187 ionophore or by polymyxin B applied to cell-attached patches	Groschner and Kukovetz (1992)
bovine aortic endothelial cells	spontaneous in excised patches	382 pS (140 mM Cl^-)		activity independent of ATP and changes in free Ca^{2+} concentration; numerous substates; at least 4 identified	Olesen and Bundgaard (1992)
Muscle cells					
rabbit colonic smooth muscle	induced by large polarisations (>±30 mV) only in excised patches	309 pS (130 mM Cl^-)	P_{Cl}/P_{Na} = 6	activated by NK1 on outside-out patches and GTPγS on inside out patches; multiple substates	Sun et al., (1992)
rat myotubes	spontaneous in excised patches	430 pS (143 mM Cl^-)		inactivation slower at negative potentials; only found in 5-10% of patches	Blatz and Magleby (1983)

Table 7.1 continued.

Location	Activation	Conductance	Selectivity	Remarks	Reference
Leukocytes					
mouse B-lymphocytes	induced (>±30 mV) in both excised patches and cell attached	400 pS (165 mM Cl^-)	$P_{Cl}/P_{Na} = 10$	bell-shaped voltage dependence in cell attached recordings and shifted to the right in excised patches; multiple subconductance states	Bosma (1989)
human T-lymphocytes	95 % spontaneous; quiescent patches can be induced	305 pS (140 mM Cl^-)	$P_{Cl}/P_{Na} = 30$	conductance saturates with increasing Cl^- concentration; two subconductance states	Schlichter et al., (1990)
mouse macrophages	delayed appearance in excised patches	342 pS (144 mM Cl^-)	$P_{Cl}/P_{Na} = 4$ to 6	subconductance states; activity can be induced by A23187 ionophore applied to cell-attached patches	Schwarze and Kolb (1984) Kolb and Ubl (1987)
Neural cells					
rat astrocytes	spontaneous in excised patches	200 pS (165 mM Cl^-)		multiple subconductance states	Jalonen et.al., (1989)
rat Schwann cells	delayed appearance only in excised patches	450 pS (150 mM Cl^-)	$P_{Cl}/P_{Na} = 5$ to 6	multiple subconductance states	Gray et al., (1984)
rat hippocampus pyramidal cells	spontaneous in excised patches	577 pS (140 mM Cl^-)		activity independent of changes in free Ca^{2+} concentration	Gage et al., (1986)

Ca^{2+} release. The large conductance anion channel from sarcoballs, however, is insensitive to changes in free Ca^{2+} concentrations.

In contrast, channel activity in the cell-attached mode has, in some cases, been induced upon the addition of the Ca^{2+} ionophore A23187 to the bath (Schwarze & Kolb, 1984; Groschner & Kukovetz, 1992). The long lag time between the addition of A23187 and the appearance of activity suggests that there are intermediate steps in the regulation of the channel activity. This is further indicated in the case of pig aortic endothelial cells, where the action of A23187 can be mimicked by the protein kinase C inhibitor, polymyxin B, suggesting the involvement of phosphorylation-dephosphorylation in the channel regulation (Groschner & Kukovetz, 1992). This may also be the case with rabbit colonic smooth muscle, where the anion channel is activated by neurokinin 1 (NK1) from the extracellular surface and GTPγS from the intracellular surface (Sun et al., 1992).

Apart from these specific examples, there is also indirect evidence of a more general regulation of large conductance anion channels. In most cases, channel activity only appears in excised patches and then only after a short delay (Gray et al., 1984; Schwarze & Kolb, 1984) or upon a large depolarising potential applied to the patch (Bosma, 1989; Velasco et al., 1989; Sun et al., 1992). The lack of channel activity in cell-attached mode suggests that perhaps the channel is tightly regulated in intact cells, and this regulation is lost upon excising the patch. One way this might occur is by regulation associated with the cyto-skeleton.

Filamentous actin (F-actin) is one of the cyto-skeletal elements and it has been implicated in the regulation of several ion channels. In snail ganglionic neurons, "run-down" of the Ca^{2+} channel activity occurs with an increase in intracellular free Ca^{2+} concentration and a decrease in intracellular ATP (Johnson & Byerly, 1993). In large excised patches of neuronal cell membrane, the Ca^{2+} channel run-down could be prevented by using the mushroom toxin phalloidin, which

stabilises F-actin polymers. By applying cytochalasin B to disrupt the F-actin network, the Ca^{2+} channel activity from these neurons was rapidly reduced even in the presence of ATP. These results suggest that F-actin plays a role in regulating the behaviour of the Ca^{2+} channel. In a similar manner, the NMDA receptor channel from hippocampal neurons also shows run-down behaviour which is regulated by the state of the F-actin cyto-skeletal elements (Rosenmund & Westbrook, 1993). Further, the regulation of the NMDA channel involves a secondary protein which confers Ca^{2+} sensitivity in whole-cell recordings, but in excised inside-out patches where the protein is lost or the F-actin is disrupted, the channel is Ca^{2+} insensitive. A Cl^- channel from renal proximal tubule cells also appears to be regulated by F-actin (Suzuki et al., 1993). The Cl^- channel activity in excised patches and whole-cell Cl^- currents were rapidly reduced upon the application of cytochalasin D, and addition of F-actin polymer restored the channel activity. It is conceivable that the large conductance anion channels are normally closed under the regulation of F-actin and with excised patches, channel behaviour appears as the actin filaments are altered in some manner. This might be equally applicable to the sarcoball anion channel, with the cyto-skeletal elements of the SR being left behind when the membrane is extruded to the fibre surface.

Alternatively, the anion channels might be regulated by a cytoplasmic protein or by phosphorylation, both of which do not need to be independent of the cyto-skeleton. In this regard, the regulation of a large conductance anion channel from pig aortic endothelium by phosphorylation (Groschner & Kukovetz, 1992) has already been mentioned. A small anion channel (116 pS, 500 mM Cl^- *cis*, 50 mM Cl^- *trans*) from cardiac SR membrane also appears to be regulated by phosphorylation (Kawano et al., 1992). This channel is activated by the catalytic subunit of protein kinase A in the presence of MgATP and activation is prevented in the presence of the protein kinase inhibitor. The regulation of the VDAC from

mitochondrial outer membrane by a soluble protein has previously been discussed in Chapter 3.

There is also the question of how, in some cases, the large conductance anion channel activity can be induced in excised patches by large depolarisations, and whether this is related to the normal regulation of the channel. In only one case has depolarisation been successful in activating channels in cell-attached patches (Bosma, 1989). Perhaps the depolarisation causes a conformational change in the channel protein that releases any bound regulatory factor which is able to diffuse free in excised patches, but is held in place, perhaps by the cyto-skeleton, when the membrane is still attached to the cell.

These anion channels are not just an artefact of cultured cells

It has been suggested that the large conductance anion channels are a feature only of cultured cells (Schneider et al., 1985; Gage et al., 1986). Certainly, a number of the anion channels reported are from cultured cell lines, but there are a number of acutely isolated cells such as the mouse macrophages (Schwarze & Kolb, 1984) that also show these channels. There is also a report where the large conductance anion channel is able to be recorded from the freshly isolated cells, but not after two days cell culture (Kolb & Ubl, 1987). In pig aortic endothelial cells, the same large conductance anion channel can be recorded from primary cultured, sub-cultured and freshly isolated cells (Groschner & Kukovetz, 1992). It is concluded that these anion channels are a normal part of these cells and not a response induced by the culturing of the cells.

7.3 Extra-mitochondrial VDAC

The finding of large conductance anion channels in a diverse range of cells has an interesting parallel with the finding of VDAC in a similar range of cells. VDAC had been characterised as an ion channel exclusively from the mitochondrial outer membrane, but like the immunolabelling studies in Chapter 6 where a VDAC-like

protein was found in SR membrane, VDAC-like proteins have now been localised in the plasmalemma of a number of different cells (Thinnes, 1992). A 31 kDa VDAC-like protein was first isolated from the plasmalemma of human B lymphocytes ("Porin 31HL", Thinnes et al., 1989) and subsequent sequencing of the protein indicates 24% to 29% identity to the mitochondrial VDAC of *Neurospora crassa* and *Saccharomyces cerevisiae* (Kayser et al., 1989). Reconstitution of the "Porin 31HL" in bilayers showed it to exhibit behaviour very similar to the mitochondrial VDAC (Benz et al., 1992). The protein has also been specifically localised to the plasmalemma of B lymphocytes using immunogold labelling at the electron microscope level (Cole et al., 1992).

From the published sequence of the human B lymphocyte "Porin 31HL", probes were produced to screen a human pituitary cDNA library, which identified a single clone with a protein sequence perfectly matching that from B lymphocytes (Blachly-Dyson & Forte, 1991). Subsequently, a second clone with a similar sequence was also found (Blachly-Dyson et al., 1993). These human VDAC-homologues were expressed in yeast lacking endogenous VDAC, and the human VDAC was isolated to be incorporated into planar bilayers. Both VDAC-homologues show very similar channel characteristics to those previously described for mitochondrial VDAC (Blachly-Dyson et al., 1993). A porin has also been purified from a crude plasma membrane preparation from human skeletal muscle, again showing an identical protein sequence to that of B lymphocytes (Jürgens et al., 1991). Immunoenzyme labelling using antibodies directed against the N-terminus of the "Porin 31HL", localised the presence of the VDAC-like protein to the sarcolemma and mitochondria in cryosections of human skeletal muscle (Babel et al., 1991).

Indirect evidence also exists which indicates the presence of VDAC-like proteins in other tissues. Preliminary immunofluoresence has indicated the presence of VDAC at the apical membrane of bovine tracheal epithelial cells and in rat

peripheral myelin (Thinnes, 1992). Jürgens et al. (1991) make mention of immunological and biochemical data that indicates VDAC is expressed in the SR of mammalian skeletal muscle. The nuclear envelope also appears to have VDAC present (König et al., 1991). Patch clamp recordings from the nuclear envelope of isolated rat liver nuclei exhibit a large conductance (150 pS in symmetrical 140 mM KCl) anion selective channel, however, unlike the VDAC, the voltage dependence indicated an increase in activity as the cytoplasmic side of the membrane was made more positive (Tabares et al., 1991).

VDAC co-purifies with receptor proteins

Most intriguing is the identification of a 36 kDa polypeptide which co-purifies with the benzodiazepine (BZD) receptor protein ($GABA_A$) from mammalian cerebral cortex (Bureau et al., 1992). This polypeptide has a 24% sequence identity with the mitochondrial VDAC protein from *Saccharomyces cerevisiae* and at least 70% sequence identity with the porin from human B lymphocytes. Clearly this VDAC-like polypeptide is tightly associated with the $GABA_A$ receptor, as indicated by co-purification with BZD, and a 60% reduction in the [^{3}H]muscimol binding to the $GABA_A$ protein complex by immunoprecipitation with a specific antibody to the 36 kDa polypeptide.

There is also a range of biochemical and immunological evidence that indicates that the peripheral BZD receptor is the VDAC from mitochondrial outer membrane (reviewed by McEnery, 1992). The solubilised peripheral BZD receptor complex is comprised of three subunits; a 32 kDa protein identified as the VDAC, a 30 kDa protein identified as the adenine nucleotide carrier (ADC) and an 18 kDa protein (McEnery et al., 1992). This association between the VDAC from the mitochondrial outer membrane and the ADC from the inner membrane is thought to be the contact sites between these two membranes which are associated with hexokinase and creatine kinase binding (Weiler et al., 1985; Kottke et al., 1988; Brdiczka, 1990). The role of VDAC in mitochondrial respiration has

been recently demonstrated (Liu Y & Colombini, 1992) and peripheral BZD ligands are also known to inhibit respiration in isolated mitochondria (Hirsch et al., 1989; Moreno-Sanchez et al., 1991).

Evidence from the association of VDAC with the $GABA_A$ protein complex in mammalian cerebral cortex, and with cytosolic hexokinase and the ADC at contact sites in mitochondria, suggests that this channel may not normally occur or operate in isolation. At present there is no explanation for the presence of a voltage gated channel so closely associated with a receptor operated channel. The VDAC family may prove to be a ubiquitous anion channel which performs a specific role according to the complexes which it forms with receptor or regulator proteins. A similar association between Cl^- channels and a conserved 64 kDa integral membrane protein has been demonstrated to occur in both the intracellular and plasma membranes of kidney cortex epithelial cells (Redhead et al., 1992). It is possible that this might also be the case for the family of large conductance anion channels described here.

7.4 Role of the SR anion channel

From SR permeability studies and the incorporation of vesicles into bilayers, it was thought that the SR anion conductance provided a passive pathway for the movement of anions to balance the movement of Ca^{2+} during release or uptake (Miller, 1978; Meissner, 1983). When the anion channel was recorded in sarcoballs, the steep voltage-dependence suggested that the channel might have a more active role in the SR (Hals et al., 1989). Any changes in potential across the SR membrane which might occur, would influence the contribution of the anion conductance to the overall state of the SR membrane.

Potentials across the SR membrane

Electron-probe analysis of skeletal muscle at rest indicates no asymmetric distribution of ions between the myoplasm and the SR which might support a

membrane potential (Somlyo et al., 1981). Even when the K^+ selective ionophore valinomycin is present, which would allow K^+ to distribute across the SR in accordance with any electrochemical potential, there was no detectable change in the K^+ distribution (Kitazawa et al., 1984). So, the resting SR membrane potential is estimated to be close to 0 mV. The rapid release of Ca^{2+} from the SR will generate a potential across the SR and with compensating counter-ion movements to balance this flux of Ca^{2+}, it is estimated that the potential would be at most +7 mV (potential of the myoplasmic space with respect to the SR lumen; Oetliker, 1982; Garcia & Miller, 1984). Electron-probe analysis of skeletal muscle fibres after a 1.2 s tetanus, in the presence of valinomycin, reveals an increase in the K^+ content of the terminal cisternae, demonstrating the electrogenic nature of Ca^{2+} release (Kitazawa et al., 1984).

If these estimates are correct, with such a small shift in potential of +7 mV during Ca^{2+} release, the membrane potential is still within the range where the anion channel is mostly open. Hals et al. (1989) propose that the voltage-dependent behaviour of the channel could make a much more significant contribution to the channel function if there is a small resting potential of +8 to +10 mV across the SR membrane. A resting potential of this order is in the steep shoulder region of the $P_o(V)$ curve, and so a small change of +7 mV would result in a significant decrease in the anion channel open probability. This reduction in the contribution of anions to the counter-ion flux might then act to slow the rate of Ca^{2+} release and aid in the electrogenic uptake of Ca^{2+} into the SR by the Ca^{2+}/Mg^{2+}-ATPase (Hals et al., 1989).

Is the in vivo conductance what is seen in vitro?

As yet, there has been no functional demonstration that anions play a physiological function in the Ca^{2+} release or uptake mechanisms. The evidence from electron-probe analysis indicates that while K^+ and Mg^{2+} balance part of the release of Ca^{2+}, there is no detectable contribution from Cl^- (Somlyo et al., 1981).

Even if the anions were bicarbonate or phosphate, which are not detected by the electron-probe, the lack of Cl^- movement is inconsistent considering the anion channel shows weak selectivity between monovalent anions and a preference for monovalents over divalent anions (Hals et al., 1989). Alternatively, there might be little or no movement of any of these anions, though this would be inconsistent with the large permeability of the SR in isolated systems (Kometani & Kasai, 1978). This may mean that the anion permeability *in vivo* is actually less than that seen in isolated systems. This has been found to be the case for the K^+ permeability, which was much less when measured with radio labelled tracer in skinned muscle fibres compared to isolated SR vesicles (Best & Abramcheck, 1985).

There is a real possibility that the SR anion permeability is less than that estimated from behaviour in isolated systems. This might be due to a regulatory mechanism, which is lost when SR membranes are isolated and even when excised patches are formed from sarcoballs. In addition, the bell-shaped voltage-dependence of the anion channel might also be different *in vivo*. Differences in the voltage dependent behaviour exist between anion channels recorded from SR vesicles incorporated into bilayers, from liposomes and from sarcoballs. Asymmetrical distributions of permeant anions across the membrane are also known to shift the bell-shaped open-probability curve along the voltage axis (Hals & Palade, 1990). Although there does not appear to be an asymmetrical anion distribution across the SR membrane which might cause such a shift, a regulatory action could possibly have a similar influence upon the voltage-dependence.

7.5 Future directions

The understanding of the sarcoball anion channel is confounded by the lack of a highly specific binding agent or ligand. Without such an agent, it is difficult to be absolutely certain of the localisation of the anion channel. It would also assist in the isolation of the channel protein for sequencing and other biochemical

studies. Localisation will need to be more definitely established in the SR if the channel is to continue being thought of as a counter-ion pathway. A specific ligand which modified channel activity would also allow a functional assessment of the role this channel performs.

In the absence of such a ligand, aspects of the channel regulation can be pursued in isolated patches from sarcoballs or in bilayers. The role of cyto-skeletal elements and cytoplasmic soluble factors have been discussed above in relation to other large conductance anion channels. In particular, the regulation of activity by phosphorylation-dephosphorylation observed with the cardiac SR anion channel (Kawano et al., 1992) might also occur with the skeletal muscle SR anion channel. It is important to explore these ideas of regulating large conductance anion channels, because the sarcoball anion channel might behave quite differently in the intact SR membrane compared to isolated systems. It might also provide an explanation for the differences in behaviour between sarcoball anion channels and those from SR vesicles in bilayers or liposomes.

The identity of the protein recognised by the VDAC antibody and any channel forming properties which it might have also needs to be established. Without this information, the doubt remains about the nature of the sarcoball anion channel. One way this could be approached is by immobilising the VDAC antibody on a separation column and using it to affinity purify the protein from the SR which is recognised by the antibody. If sufficient protein is able to be recovered, it could be reconstituted into planar bilayers and its channel forming properties assessed. Further characterisation of the channel might be possible using a molecular biological approach similar to the used for mitochondrial VDAC (Colombini, 1984; Blachley-Dyson et al., 1989).

The presence of multiple subconductance states is a characteristic shared by many large conductance anion channels. Strategies need to be developed to address adequately the contribution of these substates to the kinetic behaviour of the

channel. The approach of Laver et al. (1993) to model the behaviour as a number of parallel processes depends upon sufficiently long-lived substates for characterisation. This may be appropriate for the sarcoball anion channel, but at this stage it is not clear how the voltage-dependent behaviour would be incorporated in such a model.

The ultimate aim of the investigation of the SR anion channel is to be able to describe the contribution of the channel to the normal processes of Ca^{2+} release and uptake by the SR membrane. In considering the contribution of the anion channel, the characteristics of the other components in the SR membrane need also be considered. At this stage there is insufficient information to be certain of the role of the anion channel, but with further investigation it is hoped that a model of the SR membrane , with each of the contributing conductances, might be able to be proposed.

APPENDIX

Modelling the voltage-dependent behaviour of the sarcoball anion channel

The voltage-dependent behaviour of the sarcoball anion channel was modelled using several different kinetic schemes. The equilibrium probabilities of each of the states were evaluated from the rate constants, which were first guesses. The exact value of the rate constants is not critical to determine the shape of the *Po(V)* curve predicted by the kinetic schemes.

At equilibrium, there is no net movement between the kinetic states. Therefore, using scheme VI as an example (Figure 4.21), the equilibrium probabilities, as previously shown at Equations 4.11, are:

$$\begin{aligned} p_1(\infty) \cdot \beta_1 &= p_2(\infty) \cdot \alpha_1 & \qquad p_4(\infty) \cdot \beta_4 &= p_5(\infty) \cdot \alpha_4 \\ p_2(\infty) \cdot \beta_2 &= p_3(\infty) \cdot \alpha_2 & \qquad p_5(\infty) \cdot \beta_5 &= p_6(\infty) \cdot \alpha_5 \\ p_3(\infty) \cdot \beta_3 &= p_4(\infty) \cdot \alpha_3 & \qquad p_6(\infty) \cdot \beta_6 &= p_1(\infty) \cdot \alpha_6 \end{aligned} \tag{A.1}$$

The sum of the equilibrium probabilities for each state is unity, so:

$$p_1(\infty) + p_2(\infty) + p_3(\infty) + p_4(\infty) + p_5(\infty) + p_6(\infty) = 1 \tag{A.2}$$

Now, by rearrangement, $p_2(\infty)$ (from Equations A.1) can be expressed in terms of $p_1(\infty)$ in the following manner:

$$p_2(\infty) = p_1(\infty) \, (\beta_1 \, / \, \alpha_1) \tag{A.3}$$

This expression for $p_2(\infty)$ can subsequently be used to express $p_3(\infty)$ (from Equations A.1) in terms of $p_1(\infty)$ also:

$$p_3(\infty) = p_1(\infty) \, (\beta_1 \, \beta_2) \, / \, (\alpha_1 \, \alpha_2) \tag{A.4}$$

Following in the same manner, $p_4(\infty)$, $p_5(\infty)$ and $p_6(\infty)$ can also be expressed in terms of $p_1(\infty)$. With each of the state equilibrium probabilities expressed now in terms of $p_1(\infty)$, substitution back into Equation A.2 gives:

$$p_1(\infty) + p_1(\infty)\frac{\beta_1}{\alpha_1} + p_1(\infty)\frac{\beta_1\beta_2}{\alpha_1\alpha_2} + p_1(\infty)\frac{\beta_1\beta_2\beta_3}{\alpha_1\alpha_2\alpha_3} + p_1(\infty)\frac{\beta_1\beta_2\beta_3\beta_4}{\alpha_1\alpha_2\alpha_3\alpha_4} + p_1(\infty)\frac{\beta_1\beta_2\beta_3\beta_4\beta_5}{\alpha_1\alpha_2\alpha_3\alpha_4\alpha_5} = 1 \tag{A.5}$$

and by rearrangement,

$$p_1(\infty) = \frac{1}{1+\frac{\beta_1}{\alpha_1}+\frac{\beta_1\beta_2}{\alpha_1\alpha_2}+\frac{\beta_1\beta_2\beta_3}{\alpha_1\alpha_2\alpha_3}+\frac{\beta_1\beta_2\beta_3\beta_4}{\alpha_1\alpha_2\alpha_3\alpha_4}+\frac{\beta_1\beta_2\beta_3\beta_4\beta_5}{\alpha_1\alpha_2\alpha_3\alpha_4\alpha_5}} \qquad (A.6)$$

Thus, $p_1(\infty)$ can be evaluated from the rate constants. Once $p_1(\infty)$ is known, all of the other state equilibrium probabilities can also be evaluated, as they were expressed in terms of $p_1(\infty)$ (eg. Equation A.3 and A.4). The open-probability of the channel is then the sum of the equilibrium probabilities for each of the open states:

$$P_O = p_4(\infty) + p_5(\infty) + p_6(\infty) \qquad (A.7)$$

A structured Quick Basic (Microsoft Inc.) program was written to calculate the open probability for a range of potentials. The listing of the programs follows.

```
'*************************************************************************************************************
'                    OPEN PROBABILITY
'This program models the equilibrium probabilities of a six state kinetic scheme, comprised of
'three open states and three closed states, all of which are linked to form a cyclic scheme. This is
'equivalent to Scheme VI described in Chapter 4. This scheme can be represented in the following
'manner:
'
'          C1 --- C2 --- C3
'           |      |      |
'           |      |      |
'          O6 --- O5 --- O4
'
'The states are linked by either voltage-dependent or voltage-independent rate constants, which
'are the variable arrays Alpha! and Beta! The rate constants used are first guesses. The
'equilibrium probabilities are calculated from these rate constants. The sum of the equilibrium
'probabilities for states O6, O5 and O4 gives the open probability. The open probability was
'determined for a range of voltages between -60 mV and +60 mV.
'Trevor M Lewis, Department of Physiology, The University of Adelaide, May 1993.
'*************************************************************************************************************
'===========================================
'      Declare subroutines
'===========================================
DECLARE SUB PopenDisplay ()
DECLARE SUB CalculatePopen (ConductingStates#)
DECLARE SUB Microreversibility ()
'===========================================
'    Declare shared variable arrays
'===========================================
DIM SHARED EquilProb#(1 TO 6)
DIM SHARED Alpha!(1 TO 7)
DIM SHARED Beta!(1 TO 7)

CLS 0
SCREEN 3      'Hercules Graphics display mode
'OPEN "c:\kinetic\programs\bell2.dat" FOR OUTPUT AS #1     'optional output of data
CALL PopenDisplay      'Set up viewport to display open probability curve
```

```
OldMV! = -60: OldPopen# = 0    'Set starting values

'==================================
'   Rate-constant parameters
'==================================
Z1 = 3.8 : Z2 = .6
Coeff1 = .05 : Coeff2 = .3
IndepOne = .3 : IndepTwo = 3

'====================================
'   Voltage-independent rates
'====================================
Alpha!(4) = IndepOne    'From O5 to O4
Beta!(5) = IndepOne     'From O5 to O6

Alpha!(5) = IndepTwo    'From O6 to O5
Beta!(4) = IndepTwo     'From O4 to O5

Alpha!(7) = IndepTwo    'From C2 to O5
Beta!(7) = IndepOne     'From O5 to C2

FOR MV! = -60 TO 60 STEP 5   'Membrane potential in millivolts
    '================================================
    '      Voltage-dependent rate constants
    '================================================
    'The constant 25.4 is the value of (R.T)/F, where
    'R is the gas constant, T is temperature in degrees
    'Kelvin (295.16 in this case, equivalent to 22 degrees
    'centigrade), and F is Faraday's constant.

    Alpha!(3) = Coeff1 * EXP(-Z1 * MV! / 25.4)  'From C3 to C2
    Beta!(2) = Coeff1 * EXP(-Z1 * MV! / 25.4)   'From C3 to O4

    Alpha!(2) = Coeff2 * EXP(Z2 * MV! / 25.4)   'From O4 to C3
    Beta!(3) = Coeff2 * EXP(Z2 * MV! / 25.4)    'From C2 to C3

    Alpha!(1) = Coeff1 * EXP(Z1 * MV! / 25.4)   'From C1 to O6
    Beta!(6) = Coeff1 * EXP(Z1 * MV! / 25.4)    'From C1 to C2

    Alpha!(6) = Coeff2 * EXP(-Z2 * MV! / 25.4)  'From C2 to C1
    Beta!(1) = Coeff2 * EXP(-Z2 * MV! / 25.4)   'From O6 to C1

    CALL CalculatePopen(Popen#)
    CALL Microreversibility     'Diagnostic subroutine to check for microreversibility

    '============================================================
    '        Plot the open probability curve
    '============================================================
    VIEW (432, 112)-(584, 231), , 1: WINDOW (-60, -.1)-(60, 1)
    LINE (OldMV!, OldPopen#)-(MV!, Popen#)
    'PRINT #1, USING "##.####"; MV!; TAB(1); Popen#
    OldPopen# = Popen#
    OldMV! = MV!
NEXT MV!
CLOSE #1
END

SUB CalculatePopen (ConductingStates#)
```

```
'*****************************************************************************************************
'This subroutine calculates the equilibrium probabilities for each state, and subsequently the open
'probability from the sum of the equilibrium probabilities of the conducting states.  The variable
'Sum# is equivalent to the denominator in Equation A.6
'*****************************************************************************************************
    AlphaProduct# = 1: BetaProduct# = 1: Element% = 1: Sum# = 0
    FOR Element% = 1 TO 5    'Since there are 6 states
        AlphaProduct# = AlphaProduct# * Alpha!(Element%)
        BetaProduct# = BetaProduct# * Beta!(Element%)
        Sum# = (BetaProduct# / AlphaProduct#) + Sum#
    NEXT Element%

    EquilProb#(1) = 1 / (1 + Sum#)
    EquilProb#(2) = EquilProb#(1) * Beta!(1) / Alpha!(1)
    EquilProb#(3) = EquilProb#(2) * Beta!(2) / Alpha!(2)
    EquilProb#(4) = EquilProb#(3) * Beta!(3) / Alpha!(3)
    EquilProb#(5) = EquilProb#(4) * Beta!(4) / Alpha!(4)
    EquilProb#(6) = EquilProb#(5) * Beta!(5) / Alpha!(5)

    '** Diagnostic checks
    '** EquilProb#(1) = EquilProb#(6) * Beta!(6) / Alpha!(6)
    '** EquilProb#(2) = EquilProb#(5) * Beta!(7) / Alpha!(7)

    ConductingStates# = EquilProb#(4) + EquilProb#(5) + EquilProb#(6)

END SUB

SUB Microreversibility
'*****************************************************************************************************
'This is a diagnostic subroutine to check for the condition of microreversibility.  The product of
'the rate constants around closed loops within the kinetic scheme in clockwise and anticlockwise
'direction are calculated and printed on to the screen.  The product in the clockwise direction
'must be equal to the product in the anticlockwise direction if microreversibility is to be
'maintained.
'*****************************************************************************************************
    VIEW PRINT 5 TO 17

    PRINT "Clockwise Product";
    PRINT Beta!(1) * Beta!(2) * Beta!(3) * Beta!(4) * Beta!(5) * Beta!(6)
    PRINT "Anticlockwise Product";
    PRINT Alpha!(1) * Alpha!(2) * Alpha!(3) * Alpha!(4) * Alpha!(5) * Alpha!(6)
    PRINT "Left-half, clockwise";
    PRINT Beta!(1) * Alpha!(7) * Beta!(5) * Beta!(6)
    PRINT "Left-half, anticlockwise";
    PRINT Alpha!(1) * Alpha!(6) * Alpha!(5) * Beta!(7)
    PRINT "Right-half, clockwise";
    PRINT Beta!(2) * Beta!(3) * Beta!(4) * Beta!(7)
    PRINT "Right-half, anticlockwise";
    PRINT Alpha!(2) * Alpha!(7) * Alpha!(4) * Alpha!(3)

END SU

SUB PopenDisplay
'*****************************************************************************************************
'This subroutine sets up the viewport and draws the grid lines for the display of the calculated
'open probability curve.
'*****************************************************************************************************
    VIEW (432, 112)-(584, 231), , 1: WINDOW (-60, -.1)-(60, 1)
```

```
    LINE (-60, .5)-(60, .5), , , &H5555
    FOR Grid% = -50 TO 50 STEP 10
        LINE (Grid%, -.1)-(Grid%, 1), , , &H5555
    NEXT Grid%

END SUB
```

REFERENCES

ABRAMCHECK, C. W. & BEST, P. M. (1989). Physiological role and selectivity of the in situ potassium channel of the sarcoplasmic reticulum in skinned frog skeletal muscle fibers. *Journal of General Physiology* **93**, 1-21.

AHKONG, Q. F., FISHER, D., TAMPION, W. & LUCY, J. A. (1975). Mechanisms of cell fusion. *Nature* **253**, 194-195.

ALLEN, G. (1980a). Primary structure of the calcium ion-transporting adenosine triphosphatase of rabbit skeletal sarcoplasmic reticulum. Soluble peptides from the α-chymotryptic digest of the carboxymethylated protein. *Biochemical Journal* **187**, 565-575.

ALLEN, G. (1980b). The primary structure of the calcium-transporting adenosine triphosphatase of rabbit skeletal sarcoplasmic reticulum. Soluble tryptic peptides from the succinylated carboxymethylated protein. *Biochemical Journal* **187**, 545-563.

ALLEN, G., BOTTOMLEY, R. C. & TRINNAMAN, B. J. (1980a). Primary structure of the calcium ion-transporting adenosine triphosphatase from rabbit skeletal sarcoplasmic reticulum. Some peptic, thermolytic, tryptic and staphylococcal-proteinase peptides. *Biochemical Journal* **187**, 577-589.

ALLEN, G., TRINNAMAN, B. J. & GREEN, N. M. (1980b). The primary structure of the calcium ion-transporting adenosine triphosphatase protein of rabbit skeletal sarcoplasmic reticulum. Peptides derived from digestion with cyanogen bromide, and the sequences of three long extramembranous segments. *Biochemical Journal* **187**, 591-616.

ANDERSON, C. R. & STEVENS, C. F. (1973). Voltage clamp analysis of acetylcholine produced end-plate current fluctuations at frog neuromuscular junction. *Journal of Physiology, London* **235**, 655-691.

ASHLEY, C. C., MULLIGAN, I. P. & LEA, T. J. (1991). Ca^{2+} and activation mechanisms in skeletal muscle. *Quarterly Reviews of Biophysics* **24**, 1-73.

BABEL, D., WALTER, G., GÖTZ, H., THINNES, F. P., JÜRGENS, L., KÖNIG, U. & HILSCHMANN, N. (1991). Studies on human porin VI. Production and characterization of eight monoclonal mouse antibodies against the human VDAC "Porin 31HL" and their application for histotopological studies in human skeletal muscle. *Biological Chemistry Hoppe-Seyler* **372**, 1027-1034.

BALL, F. G. & SANSOM, M. S. P. (1988). Single-channel autocorrelation functions: the effects of time interval omission. *Biophysical Journal* **53**, 819-832.

BARRY, P. H. & DIAMOND, J. M. (1970). Junction potentials, eletrode standard potentials, and other problems in interpreting electrical properties of membranes. *Journal of Membrane Biology* **3**, 93-122.

BEGENISICH, T. B. & CAHALAN, M. D. (1980). Sodium channel permeation in squid axons I: Reversal potential experiments. *Journal of Physiology, London* **307**, 217-242.

BELL, J. E. & MILLER, C. (1984). Effects of phospholipid surface charge on ion conduction in the K^+ channel of sarcoplasmic reticulum. *Biophysical Journal* **45**, 279-287.

BENZ, R., MAIER, E., THINNES, F. P., GÖTZ, H. & HILSCHMANN, N. (1992). Studies on human porin VII. The channel properties of the human B-lymphocyte membrane-derived "Porin 31HL" are similar to those of mitochondrial porins. *Biological Chemistry Hoppe-Seyler* **373**, 295-303.

BEST, P. M. & ABRAMCHECK, C. W. (1985). Potassium efflux from single skinned skeletal muscle fibers. *Biophysical Journal* **48**, 907-913.

BIKERMAN, J. J. (1973). *Foams*, 337 pages. New York: Springer-Verlag.

BLACHLY-DYSON, E. & FORTE, M. (1991). Cloning of a human VDAC cDNA. *Biophysical Journal* **59**, 216a.

BLACHLY-DYSON, E., PENG, S. Z., COLOMBINI, M. & FORTE, M. (1989). Probing the structure of the mitochondial channel, VDAC, by site-directed mutagenesis: A progress report. *Journal of Bioenergetics and Biomembranes* **21**, 471-483.

BLACHLY-DYSON, E., ZAMBRONICZ, E. B., YU, W. H., ADAMS, V., McCABE, E. R. B., ADELMAN, J., COLOMBINI, M. & FORTE, M. (1993). Cloning and functional expression in yeast of two human isoforms of the outer mitochondrial membrane channel, the voltage-dependent anion channel. *Journal of Biological Chemistry* **268**, 1835-1841.

BLATZ, A. L. & MAGLEBY, K. L. (1983). Single voltage-dependent chloride-selective channels of large conductance in cultured rat muscle. *Biophysical Journal* **43**, 237-241.

BLATZ, A. L. & MAGLEBY, K. L. (1986). Correcting single channel data for missed events. *Biophysical Journal* **49**, 967-980.

BOSMA, M. M. (1989). Anion channels with multiple conductance levels in a mouse B lymphocyte cell line. *Journal of Physiology, London* **410**, 67-90.

BOX, G. E. P. & JENKINS, G. M. (1976). *Time series analysis. Forcasting and control*, Revised edn., 575 pages. San Francisco: Holden-Day Inc.

BRADLEY, R. J., HOWELL, J. H., ROMINE, W. O., CARL, G. F. & KEMP, G. E. (1976). Characterization of a nicotinic acetylcholine receptor from rabbit skeletal muscle and reconstitution in planar phospholipid bilayers. *Biochemical and Biophysical Research Communications* **68**, 577-584.

BRDICZKA, D. (1990). Interaction of mitochondrial porin with cytosolic proteins. *Experientia* **46**, 161-167.

BRETAG, A. H. (1969). Synthetic interstitial fluid for isolated mammalian tissue. *Life Science* **8**, 319-329.

BRETAG, A. H., DAWE, S. R. & MOSKWA, A. G. (1980). Chemically induced myotonia in amphibia. *Nature* **286**, 625-626.

BULL, R., MARENGO, J. J., SUAREZ-ISLA, B. A., DONOSO, P., SUTKO, J. L. & HIDALGO, C. (1989). Activation of calcium channels in sarcoplasmic reticulum from frog muscle by nanomolar concentrations of ryanodine. *Biophysical Journal* **56**, 749-765.

BUREAU, M. H., KHRESTCHATISKY, M., HEEREN, M. A., ZAMBROWICZ, E. B., KIM, H., GRISAR, T. M., COLOMBINI, M., TOBIN, A. J. & OLSEN, R. W. (1992). Isolation and cloning of a voltage-dependent anion channel-like M_r 36,000 polypeptide from mammalian brain. *Journal of Biological Chemistry* **267**, 8679-8684.

BURTON, F., DÖRSTELMANN, U. & HUTTER, O. F. (1988). Single-channel activity in sarcolemmal vesicles from human and other mammalian muscles. *Muscle and Nerve* **11**, 1029-1038.

BYERS, T. R. & MEISSNER, G. (1986). Unpublished results. Cited in MEISSNER, G. (1986). Permeability of sarcoplasmic reticulum to monovalent ions. In *Sarcoplasmic reticulum in muscle physiology*, vol. 2, Eds. ENTMAN, M. L. & VAN WINKLE, W. B., pp. 21-29. Boca Raton, FL: CRC Press Inc.

CAMPBELL, K. P. & MACLENNAN, D. H. (1980). DIDS inhibition of sarcoplasmic reticulum anion efflux and calcium transport. *Annals of the New York Academy of Science* **358**, 328-331.

CHUNG, S. H. & KENNEDY, R. A. (1991). Forward-backward non-linear filtering technique for extracting small biological signals from noise. *Journal of Neuroscience Methods* **40**, 71-86.

CLARKE, D. M., LOO, T. W., INESI, G. & MACLENNAN, D. H. (1989). Location of high affinity Ca^{2+}-binding sites within the predicted transmembrane domain of the sarcoplasmic reticulum Ca^{2+}-ATPase. *Nature* **339**, 476-478.

COLE, T., AWNI, L. A., NYAKATURA, E., GÖTZ, H., WALTER, G., THINNES, F. P. & HILSCHMANN, N. (1992). Studies on human porin VIII. Expression of "Porin 31HL" channels in the plasmalemma of the acute-lymphoblastic-leukemia cell line KM3 as revealed by light- and electron-microscopy. *Biological Chemistry Hoppe-Seyler* **373**, 891-896.

COLOMBINI, M. (1986). Voltage gating in VDAC: Toward a molecular mechanism. In *Ion channel reconstitution*, Ed. MILLER, C., pp. 533-552. New York: Plenum.

COLQUHOUN, D. (1987). Practical analysis of single channel records. In *Microelectrode techniques. The Plymouth workshop handbook*, Eds. STANDEN, N. B., GRAY, P. T. A. & WHITAKER, M. J., pp. 83-104. Cambridge: The Company of Biologists Limited.

COLQUHOUN, D. & HAWKES, A. G. (1977). Relaxation and fluctuations of membrane currents that flow through drug-operated channels. *Proceedings of the Royal Society, London* **B 199**, 231-262.

COLQUHOUN, D. & HAWKES, A. G. (1981). On the stochastic properties of single ion channels. *Proceedings of the Royal Society, London* **B 211**, 205-235.

COLQUHOUN, D. & HAWKES, A. G. (1982). On the stochastic properties of bursts of single ion channel openings and of clusters of bursts. *Philosophical Transactions of the Royal Society of London* **B 300**, 1-59.

COLQUHOUN, D. & HAWKES, A. G. (1983). The principles of the stochastic interpretation of ion-channel mechanisms. In *Single-channel recording*, Eds. SAKMANN, B. & NEHER, E., pp. 135-175. New York: Plenum Press.

COLQUHOUN, D. & HAWKES, A. G. (1987). A note on correlations in single ion channel records. *Proceedings of the Royal Society, London* **B 230**, 15-52.

COLQUHOUN, D. & SAKMANN, B. (1985). Fast events in single-channel currents activated by acetylcholine and its analogues at the frog muscle end-plate. *Journal of Physiology, London* **369**, 501-557.

COREY, D. P. & STEVENS, C. F. (1983). Science and technology of patch-recording electrodes. In *Single-channel recording*, Eds. SAKMANN, B. & NEHER, E., pp. 53-68. New York: Plenum Press.

CORONADO, R. (1987). Planar bilayer reconstitution of calcium channels: Lipid effects on single-channel kinetics. *Circulation Research* **61** (Suppl I), I46-I52.

CORONADO, R. & AFFOLTER, H. (1986). Characterization of dihydropyridine-sensitive calcium channels from purified skeletal muscle transverse tubules. In *Ion channel reconstitution*, Ed. MILLER, C., pp. 483-505. New York: Plenum Press.

CORONADO, R. & LATORRE, R. (1983). Phospholipid bilayers made from monolayers on patch-clamp pipettes. *Biophysical Journal* **43**, 231-236.

CORONADO, R. & MILLER, C. (1979). Voltage-dependent caesium blockade of a cation channel from fragmented sarcoplasmic reticulum. *Nature* **280**, 807-809.

CORONADO, R. & MILLER, C. (1980). Decamethonium and hexamethonium block of K^+ channels of sarcoplasmic reticulum. *Nature* **288**, 495-497.

CORONADO, R. & MILLER, C. (1982). Conduction and block by organic cations in a K^+-selective channel from sarcoplasmic reticulum incorporated into planar phospholipid bilayers. *Journal of General Physiology* **79**, 529-547.

CORONADO, R., ROSENBERG, R. L. & MILLER, C. (1980). Ionic selectivity, saturation and block in a K^+-selective channel from sarcoplasmic reticulum. *Journal of General Physiology* **76**, 425-446.

COUSIN, J. L. & MOTAIS, R. (1979). Inhibition of anion permeability by amphiphilic compounds in human red cell: Evidence for an interaction of niflumic acid with the band 3 protein. *Journal of Membrane Biology* **46**, 125-153.

COX, D. R. & LEWIS, P. A. W. (1966). *The statistical analysis of series of events*, 285 pages. London: Methuen and Co. Ltd.

DE MEIS, L., HASSELBACH, W. & MACHADO, R. D. (1974). Characterization of calcium oxalate and calcium phosphate deposits in sarcoplasmic reticulum vesicles. *Journal of Cell Biology* **62**, 505-509.

DE PINTO, V., BENZ, R., CAGGESE, C. & PALMIERI, F. (1989). Characterization of the mitochondrial porin from *Drosophila melanogaster*. *Biochimica et Biophysica Acta* **987**, 1-7.

DONALDSON, S. K. B. (1985). Peeled mammalian skeletal muscle fibers. Possible stimulation of Ca^{2+} release via a transverse tubule - sarcoplasmic reticulum mechanism. *Journal of General Physiology* **86**, 501-525.

DUGGAN, P. F. & MARTONOSI, A. (1970). Sarcoplasmic reticulum IX. The permeability of sarcoplasmic reticulum membranes. *Journal of General Physiology* **56**, 147-167.

DULHUNTY, A. F. (1984). Heterogenity of T-tubule geometry in vertebrate skeletal muscle fibres. *Journal of Muscle Research and Cell Motility* **5**, 333-347.

DULHUNTY, A. F. (1992). The voltage-activation of contraction in skeletal muscle. *Progress in Biophysics and Molecular Biology* **57**, 181-223.

DULHUNTY, A. F., BANYARD, M. R. C. & MEDVECZKY, C. J. (1987). Distribution of calcium ATPase in the sarcoplasmic reticulum of fast- and slow-twitch muscles determined with monoclonal antibodies. *Journal of Membrane Biology* **99**, 79-92.

DULHUNTY, A. F., JUNANKAR, P. R. & STANHOPE, C. (1992). Extra-junctional ryanodine receptors in the terminal cisternae of mammalian skeletal muscle fibres. *Proceedings of the Royal Society, London* **B 247**, 69-75.

EASTWOOD, A. B., WOOD, D. S., BOCK, K. L. & SORENSON, M. M. (1979). Chemically skinned mammalian skeletal muscle. I. The structure of skinned rabbit psoas. *Tissue and Cell* **11**, 553-566.

EBASHI, S. (1961). Calcium binding activity of vesicular relaxing factor. *Journal of Biochemistry* **50**, 236-244.

EBASHI, S. & LIPMANN, F. (1962). Adenosine triphosphate-linked concentration of calcium ions in a particulate fraction of rabbit muscle. *Journal of Cell Biology* **14**, 389-400.

ENDO, M. (1977). Calcium release from the sarcoplasmic reticulum. *Physiological Reviews* **57**, 71-108.

ENDO, M., TANAKA, M. & OGAWA, Y. (1970). Calcium induced release of calcium from the sarcoplasmic reticulum of skinned skeletal muscle fibres. *Nature* **228**, 34-36.

FERGUSON, D. G., SCHWARTZ, H. W. & FRANZINI-ARMSTRONG, C. (1984). Subunit structure of junctional feet in triads of skeletal muscle: A freeze-drying, rotary shadowing study. *Journal of Cell Biology* **99**, 1735-1741.

FINK, R. H. A. & STEPHENSON, D. G. (1987). Ca^{2+}-movements in muscle modulated by the state of K^{+}-channels in the sarcoplasmic reticulum membranes. *Pflügers Archives* **409**, 374-380.

FLEISCHER, S., OGUNBUNMI, E. M., DIXON, M. C. & FLEER, E. A. M. (1985). Localization of Ca^{2+} release channels with ryanodine in junctional terminal cisternae of sarcoplasmic reticulum of fast skeletal muscle. *Proceedings of the National Academy of Science, USA* **82**, 7256-7259.

FORD, L. E. & PODOLSKY, R. J. (1970). Regenerative calcium release within muscle cells. *Science* **167**, 58-59.

FORD, L. E. & SURDYK, M. F. (1978). Electronmicroscopy of skinned muscle cells. *Journal of General Physiology* **72**, 5a.

FRANCIOLINI, F. & NONNER, W. (1987). Anion and cation permeability of a chloride channel in rat hippocampal neurons. *Journal of General Physiology* **90**, 453-478.

FREDKIN, D. R., MONTAL, M. & RICE, J. A. (1985). Identification of aggregated Markovian models: Application to the nicotinic acetylcholine receptor. In *Proceedings of the Berkeley Conference in honor of Jerzy Neyman and Jack Kiefer*, vol. 1, Eds. LECARN, L. M. & OLSHEN, R. A., pp. 269-289. Belmont, CA: Wadsworth Publishing Co.

GAGE, P. W., GIBB, A. J. & KROUSE, M. E. (1986). Multiple subconductance states of a large conductance chloride channel in pyramidal cells dissociated from rat hippocampus. *Biophysical Journal* **49**, 414a.

GARCIA, A. M. & MILLER, C. (1984). Channel-mediated monovalent cation fluxes in isolated sarcoplasmic reticulum vesicles. *Journal of General Physiology* **83**, 819-839.

GELETYUK, V. I. & KAZACHENKO, V. N. (1985). Single Cl^- channels in molluscan neurones: Multiplicity of the conductance states. *Journal of Membrane Biology* **86**, 9-15.

GRAY, P. T. A., BEVAN, S. & RITCHIE, J. M. (1984). High conductance anion-selective channels in rat cultured Schwann cells. *Proceedings of the Royal Society, London* **B221**, 395-409.

GROSCHNER, K. & KUKOVETZ, W. R. (1992). Voltage-sensitive chloride channels of large conductance in the membrane of pig aortic endothelial cells. *Pflügers Archives* **421**, 209-217.

HALLMAN, M., MIYAI, K. & WAGNER, R. M. (1976). Isolated lamellar bodies from rat lung. Correlated ultrastructural and biochemical studies. *Laboratory Investigation* **35**, 79-86.

HALS, G. D. & PALADE, P. T. (1990). Different sites control voltage dependence and conductance of sarcoball anion channel. *Biophysical Journal* **57**, 1037-1047.

HALS, G. D., STEIN, P. G. & PALADE, P. T. (1989). Single channel characteristics of a high conductance anion channel in "sarcoballs". *Journal of General Physiology* **93**, 385-410.

HAMILL, O. P., MARTY, A., NEHER, E., SAKMANN, B. & SIGWORTH, F. J. (1981). Improved patch-clamp techniques for high-resolution current recording from cells and cell-free membrane patches. *Pflügers Archives* **391**, 85-100.

HAMILTON, S. L., ALVAREZ, R. M., FILL, M., HAWKES, M. J., BRUSH, K. L., SCHILLING, W. P. & STEFANI, E. (1989). [^{3}H]PN200-110 and [^{3}H]ryanodine binding and reconstitution of ion channel activity with skeletal muscle membranes. *Analytical Biochemistry* **183**, 31-41.

HASSELBACH, W. (1964). Relaxing factor and the relaxation of muscle. *Progress in Biophysics and Molecular Biology* **14**, 167-222.

HAYAT, M. A. (1989). *Principles and techniques of electron microscopy: biological applications*, 3rd edn., 469 pages. London: Macmillan.

HAYDON, D. A. & HLADKY, S. B. (1972). Ion transport across thin lipid membranes: a critical discussion of mechanisms in selected systems. *Quarterly Reviews of Biophysics* **5**, 187-282.

HAYNES, D. H. (1982). Relationship between H^+, anion, and monovalent cation movements and Ca^{2+} transport in sarcoplasmic reticulum: Further proof of a cation exchange mechanism for the Ca^{2+}-Mg^{2+}-ATPase pump. *Archives of Biochemistry and Biophysics* **215**, 444-461.

HEILBRUNN, L. V. & WIERCINSKI, F. J. (1947). The action of various cations on muscle protoplasm. *Journal of Cellular and Comparative Physiology* **29**, 15-32.

HILL, A. V. (1948). On the time required for diffusion and its relation to processes in muscle. *Proceedings of the Royal Society, London* **B 135**, 446-453.

HILL, A. V. (1949). The abrupt transition from rest to activity in muscle. *Proceedings of the Royal Society, London* **B 136**, 399-420.

HILLE, B. (1984). *Ionic channels of excitable membranes*, First edn., 426 pages. Sunderland, MA: Sinauer Associates, Inc.

HILLE, B. & CAMPBELL, D. T. (1976). An improved vaseline gap voltage clamp for skeletal muscle fibres. *Journal of General Physiology* **67**, 265-293.

HIRSCH, J. D., BEYER, C. F., MALKOWITZ, L., BEER, B. & BLUME, A. J. (1989). Mitochondrial benzodiazepine receptors mediate inhibition of mitochondrial respiratory control. *Molecular Pharmacology* **35**, 157-163.

HOLDEN, M. J. & COLOMBINI, M. (1988). The mitochondrial outer membrane channel, VDAC, is modulated by a soluble protein. *FEBS Letters* **241**, 105-109.

HOLLINGWORTH, S. & BAYLOR, S. M. (1990). Changes in phenol red absorbance in response to electrical stimulation of frog skeletal muscle fibers. *Journal of General Physiology* **96**, 473-491.

HUTTER, O. F. & WARNER, A. E. (1967). Action of some foreign cations and anions on the chloride permeability of frog muscle. *Journal of Physiology, London* **189**, 445-460.

HUXLEY, A. F. & NIEDERGERKE, R. (1954). Structural changes in muscle during contraction. Interference microscopy of living muscle fibres. *Nature* **173**, 971-973.

HUXLEY, A. F. & TAYLOR, R. E. (1958). Local activation of striated muscle fibres. *Journal of Physiology, London* **144**, 426-441.

HUXLEY, H. & HANSON, J. (1954). Changes in the cross-striations of muscle during contraction and stretch and their structural interpretation. *Nature* **173**, 973-976.

HYMEL, L., INUI, M., FLEISCHER, S. & SCHINDLER, H. (1988). Purified ryanodine receptor of skeletal muscle sarcoplasmic reticulum forms Ca^{2+}-activated oligomeric Ca^{2+} channels in planar bilayers. *Proceedings of the National Academy of Science, USA* **85**, 441-445.

IKEMOTO, N., RONJAT, M. & MÉSZAROS, L. G. (1989). Kinetic analysis of excitation-contraction coupling. *Journal of Bioenergetics and Biomembranes* **21**, 247-266.

INESI, G. & DE MEIS, L. (1989). Regulation of steady state filling in sarcoplasmic reticulum. Roles of back-inhibition, leakage, and slippage of the calcium pump. *Journal of Biological Chemistry* **264**, 5929-5936.

INUI, M., SAITO, A. & FLEISCHER, S. (1987). Purification of the ryanodine receptor and identity with feet structures of junctional terminal cisternae of sarcoplasmic reticulum from fast skeletal muscle. *Journal of Biological Chemistry* **262**, 1740-1747.

JACKSON, M. B., WONG, B. S., MORRIS, C. E., LECAR, H. & CHRISTIAN, C. N. (1983). Successive openings of the same acetylcholine receptor channel are correlated in open time. *Biophysical Journal* **42**, 109-114.

JALONEN, T., JOHANSSON, S., HOLOPAINEN, I., OJA, S. S. & ÅRHEM, P. (1989). A high-conductance multi-state anion channel in cultured rat astrocytes. *Acta Physiologica Scandinavica* **136**, 611-612.

JENCKS, W. P. (1989). How does a calcium pump pump calcium? *Journal of Biological Chemistry* **264**, 18855-18858.

JOHNSON, B. D. & BYERLY, L. (1993). A cytoskeletal mechanism for Ca^{2+} channel metabolic dependence and inactivation by intracellular Ca^{2+}. *Neuron* **10**, 797-804.

JÜRGENS, L., ILSEMANN, P., KRATZIN, H. D., HESSE, D., ECKART, K., THINNES, F. P. & HILSCHMANN, N. (1991). Studies on human porin. IV. The primary structures of "Porin 31HM" purified from human skeletal muscle membranes and of "Porin 31HL" derived from human B lymphocyts membranes are identical. *Biological Chemistry Hoppe-Seyler* **372**, 455-463.

JUNANKAR, P. R., CURTIS, S. M., PACE, S. M. & DULHUNTY, A. F. (1993). Immunogold localisation of the VDAC channel in mammalian skeletal and cardiac muscle. *Proceedings of the Australian Physiological and Pharmacological Society* **24**, 179P.

KASAI, M. (1981). Inhibition of the anion permeability of sarcoplasmic reticulum vesicles by some stilbene derivatives. *Journal of Biochemistry* **89**, 943-953.

KASAI, M. & KOMETANI, T. (1979). Inhibition of anion permeability of sarcoplasmic reticulum vesicles by 4-acetoamido-4'-isothiocyanostilbene-2,2'-disulfonate. *Biochimica et Biophysica Acta* **557**, 243-247.

KASAI, M. & TAGUCHI, T. (1981). Inhibition of anion permeability of sarcoplasmic reticulum vesicles by stilbene derivatives and the identification of an inhibitor-binding protein. *Biochimica et Biophysica Acta* **643**, 213-219.

KATZ, B. & MILEDI, R. (1970). Membrane noise produced by acetylcholine. *Nature* **226**, 962-963.

KAWANO, S., NAKAMURA, F., TANAKA, T. & HIRAOKA, M. (1992). Cardiac sarcoplasmic reticulum chloride channels regulated by protein kinase A. *Circulation Research* **71**, 585-589.

KAYSER, H., KRATZIN, H. D., THINNES, F. P., GÖTZ, H., SCHMIDT, W. E., ECKART, K. & HILSCHMANN, N. (1989). Zur Kenntnis der Porine des Menschen. II. Charakterisierung und Primärstruktur eines 31-kDa-Porins aus menschlichen B-Lymphozyten (Porin 31HL). *Biological Chemistry Hoppe-Seyler* **370**, 1265-1278.

KERRY, C. J., RAMSEY, R. L., SANSOM, M. S. P. & USHERWOOD, P. N. R. (1988). Glutamate receptor channel kinetics. The effect of glutamate concentration. *Biophysical Journal* **53**, 39-52.

KITAZAWA, T., SOMLYO, A. P. & SOMLYO, A. V. (1984). The effects of valinomycin on ion movements across the sarcoplasmic reticulum in frog muscle. *Journal of Physiology, London* **350**, 253-268.

KÖNIG, U., GÖTZ, H., WALTER, G., BABEL, D., HOHMEIR, H.-E., THINNES, F. P. & HILSCHMANN, N. (1991). Zur Kenntinis der Porine des Menschen. V. Die Plasmalemmständigkeit von "Porin 31HL" ist keine Folge einer Zell-Transformation. *Biological Chemistry Hoppe-Seyler* **372**, 565-572.

KOLB, H. A. & UBL, J. (1987). Activation of anion channels by zymosan particles in membranes of peritoneal macrophages. *Biochimica et Biophysica Acta* **899**, 239-246.

KOMETANI, T. & KASAI, M. (1978). Ionic permeability of sarcoplasmic reticulum vesicles measured by light scattering method. *Journal of Membrane Biology* **41**, 295-308.

KOTTKE, M., ADAM, V., RIESINGER, I., BREMM, G., BOSCH, W., BRDICZKA, D., SANDRI, G. & PANFILI, E. (1988). Mitochondrial boundary membrane contact sites in brain: points of hexokinase and creatine kinase location, and control of Ca^{2+} transport. *Biochimica et Biophysica Acta* **935**, 87-102.

KOURIE, J. I., LAVER, D. R., JUNANKAR, P. R., DULHUNTY, A. F. & GAGE, P. W. (1992). Characteristics of chloride channels from longitudinal sarcoplasmic reticulum and terminal cisternae of skeletal muscle incorporated into artificial planar bilayers. *Proceedings of the Australian Physiological and Pharmacological Society* **23**, 201P.

KOURIE, J. I., LAVER, D. R., PREMKUMAR, A., JUNANKAR, P. R. & DULHUNTY, A. F. (1993). The calcium-activation of a voltage-dependent chloride channel from the sarcoplasmic reticulum of skeletal muscle. *Proceedings of the Australian Physiological and Pharmacological Society* **24**, 138P.

KROUSE, M. E., SCHNEIDER, G. T. & GAGE, P. W. (1986). A large anion-selective channel has seven conductance levels. *Nature* **319**, 58-60.

KWOK, W. M. & BEST, P. M. (1990). Ryanodine sensitivity and multiple conductance states of the Ca release channel from native SR membrane. *Biophysical Journal* **57**, 168a.

LABARCA, P., CORONADO, R. & MILLER, C. (1980). Thermodynamic and kinetic studies of the gating behavior of a K^+-selective channel from the sarcoplasmic reticulum membrane. *Journal of General Physiology* **76**, 397-424.

LABARCA, P., RICE, J. A., FREDKIN, D. R. & MONTAL, M. (1985). Kinetic analysis of channel gating. Application to the cholinergic receptor channel and the chloride channel from *Torpedo californica*. *Biophysical Journal* **47**, 469-478.

LABARCA, P. P. & MILLER, C. (1981). A K^+-selective, three-state channel from fragmented sarcoplasmic reticulum of frog leg muscle. *Journal of Membrane Biology* **61**, 31-38.

LAI, F. A., ERICKSON, H. P., ROUSSEAU, E., LIU, Q.-Y. & MEISSNER, G. (1988). Purification and reconstitution of the calcium release channel from skeletal muscle. *Nature* **331**, 315-319.

LAVER, D. R. (1992). Divalent cation block and competition between divalent and monovalent cations in the large-conductance K^+ channel from *Chara australis*. *Journal of General Physiology* **100**, 269-300.

LAVER, D. R., KOURIE, J. I. & DULHUNTY, A. F. (1993). A model for the gating kinetics of a poly-state anion channel from the sarcoplasmic reticulum of skeletal muscle. *Proceedings of the Australian Physiological and Pharmacological Society* **24**, 139P.

LIEBOVITCH, L. S., FISCHBARG, J., KONIAREK, J. P., TODOROVA, I. & WANG, M. (1987). Fractal model of ion-channel kinetics. *Biochimica et Biophysica Acta* **896**, 173-180.

LEWIS, T. M. & BRETAG, A. H. (1991). A large conductance anion channel in a sarcoplasmic reticulum preparation from the semitendinosus muscle of the cane toad. *Proceedings of the Australian Physiological and Pharmacological Society* **22**, 19P.

LEWIS, T. M., DULHUNTY, A. F., JUNANKAR, P. R. & STANHOPE, C. (1992). Ultrastructure of sarcoballs on the surface of skinned amphibian skeletal muscle fibres. *Journal of Muscle Research and Cell Motility* **13**, 640-653.

LIU, M. & COLOMBINI, M. (1991). Voltage gating of the mitochondrial outer membrane channel VDAC is regulated by a very conserved protein. *American Journal of Physiology* **260**, C371-C374.

LIU, M. Y. & COLOMBINI, M. (1992). Regulation of mitochondrial respiration by controlling the permeability of the outer membrane through the mitochondrial channel, VDAC. *Biochimica et Biophysica Acta* **1098**, 255-260.

LIU, Q.-Y., LAI, F. A., ROUSSEAU, E., JONES, R. V. & MEISSNER, G. (1989). Multiple conductance states of the purified calcium release channel complex from skeletal sarcoplasmic reticulum. *Biophysical Journal* **55**, 415-424.

MACLENNAN, D. H. (1970). Purification and properties of an adenosine triphosphatase from sarcoplasmic reticulum. *Journal of Biological Chemistry* **245**, 4508-4518.

MACLENNAN, D. H., BRANDL, C. J., KORCZAK, B. & GREEN, N. M. (1985). Amino-acid sequence of a Ca^{2+}+Mg^{2+}-dependent ATPase from rabbit muscle sarcoplasmic reticulum, deduced from its complementary DNA sequence. *Nature* **316**, 696-700.

MACONOCHIE, D. J. & KNIGHT, D. E. (1992). Markov modelling of ensemble current relaxations: bovine adrenal nicotinic receptor currents analysed. *Journal of Physiology, London* **454**, 155-182.

MADEIRA, V. M. C. (1982). Oxalate transfer across the membranes of sarcoplasmic reticulum during the uptake of Ca^{++}. *Cell Calcium* **3**, 67-79.

MARSH, B. B. (1951). A factor modifying muscle fibre synaeresis. *Nature* **167**, 1065-1066.

MARSH, B. B. (1952). The effects of adenosine triphosphate on the fibre volume of a muscle homogenate. *Biochimica et Biophysica Acta* **9**, 247-260.

McENERY M. W. (1992). The mitochondrial benzodiazepine receptor: evidence for association with the voltage-dependent anion channel (VDAC). *Journal of Bioenergetics and Biomembranes* **24**, 63-69.

McENERY, M. W., SNOWMAN, A. M., TRIFILETTI, R. R. & SNYDER, S. H. (1992). Isolation of the mitochondrial benzodiazepine receptor: Association with the voltage-dependent anion channel and the adenine nucleotide carrier. *Proceedings of the National Academy of Science, USA* **89**, 3170-3174.

McKINLEY, D. & MEISSNER, G. (1977). Sodium and potassium ion permeability of sarcoplasmic reticulum vesicles. *FEBS Letters* **82**, 47-50.

McKINLEY, D. & MEISSNER, G. (1978). Evidence for a K^+, Na^+ permeable channel in sarcoplasmic reticulum. *Journal of Membrane Biology* **44**, 159-186.

McMANUS, O. B., SPIVAK, C. E., BLATZ, A. L., WEISS, D. S. & MAGLEBY, K. L. (1989). Fractal models, Markov models and channel kinetics. *Biophysical Journal* **55**, 383-385.

MEISSNER, G. (1975). Isolation and characterization of two types of sarcoplasmic reticulum vesicles. *Biochimica et Biophysica Acta* **389**, 51-68.

MEISSNER, G. (1983). Monovalent ion and calcium ion fluxes in sarcoplasmic reticulum. *Molecular and Cellular Biochemistry* **55**, 65-82.

MEISSNER, G. (1986). Permeability of sarcoplasmic reticulum to monovalent ions. In *Sarcoplasmic reticulum in muscle physiology*, vol. 2, Eds. ENTMAN, M. L. & VAN WINKLE, W. B., pp. 21-29. Boca Raton, FL: CRC Press Inc.

MEISSNER, G. & McKINLEY, D. (1976). Permeability of sarcoplasmic reticulum membrane. The effect of changed ionic environments on Ca^{2+} release. *Journal of Membrane Biology* **30**, 79-98.

MEISSNER, G. & YOUNG, R. C. (1980). Proton permeability of sarcoplasmic reticulum vesicles. *Journal of Biological Chemistry* **255**, 6814-6819.

MILLER, C. (1978). Voltage-gated cation conductance channel from fragmented sarcoplasmic reticulum: steady-state electrical properties. *Journal of Membrane Biology* **40**, 1-23.

MILLER, C. (1983). Integral membrane channels: studies in model membranes. *Physiological Reviews* **63**, 1209-1242.

MILLER, C. & RACKER, E. (1976). Ca^{++}-induced fusion of fragmented sarcoplasmic reticulum with artificial planar bilayers. *Journal of Membrane Biology* **30**, 283-300.

MILLER, C. & ROSENBERG, R. L. (1979a). Modification of a voltage-gated K^+ channel from sarcoplasmic reticulum by a pronase-derived specific endopeptidase. *Journal of General Physiology* **74**, 457-478.

MILLER, C. & ROSENBERG, R. L. (1979b). A voltage-gated cation conductance channel from fragmented sarcoplasmic reticulum. Effects of transition metal ions. *Biochemistry* **18**, 1138-1145.

MILLER, C., BELL, J. E. & GARCIA, A. M. (1984). The potassium channel of sarcoplasmic reticulum. *Current Topics in Membranes and Transport* **21**, 99-132.

MILLHAUSER, G. L., SALPETER, E. E. & OSWALD, R. E. (1988). Diffusion models of ion-channel gating and the origin of power-law distributions from single-channel recording. *Proceedings of the National Academy of Science, USA* **85**, 1503-1507.

MOBLEY, B. A. (1979). Chloride and osmotic contractures in skinned frog muscle fibres. *Journal of Membrane Biology* **46**, 315-329.

MOBLEY, B. A. & EISENBERG, B. R. (1975). Sizes of components in frog skeletal muscle measured by methods of stereology. *Journal of General Physiology* **66**, 31-45.

MOLNAR, E., VARGA, S., JONA, I., SEIDLER, N. W. & MARTONOSI, A. (1992). Immunological relatedness of the sarcoplasmic reticulum Ca^{2+}-ATPase and the Na^+,K^+-ATPase. *Biochimica et Biophysica Acta* **1103**, 281-295.

MORENO-SANCHEZ, R., HOGUE, B. A., BRAVO, C., NEWMAN, A. H., BASILE, A. S. & CHIANG, P. K. (1991). Inhibition of substrate oxidation in mitochondria by the peripheral-type benzodiazepine receptor ligand AHN 086. *Biochemical Pharmacology* **41**, 1479-1484.

MUELLER, P. & RUDIN, D. O. (1969a). Bimolecular lipid membranes: Techniques of formation, study of electrical properties, and induction of ionic gating phenomena. In *Laboratory techniques in membrane biophysics*, Eds. PASSOW, H. & STÄMPFLI, R., pp. 141-156. Berlin: Springer-Verlag.

MUELLER, P. & RUDIN, D. O. (1969b). Translocators in bimolecular lipid membranes: Their role in dissipative and conservative bioenergy transductions. In *Current Topics in Bioenergetics*, vol. 3, Ed. SANADI, D. R., pp. 157-249. New York: Academic Press.

NARAYANAN, N., SU, N. & BEDARD, P. (1991). Inhibitory and stimulatory effects of fluoride on the calcium pump of cardiac sarcoplasmic reticulum. *Biochimica et Biophysica Acta* **1070**, 83-91.

NATORI, R. (1954). The property and contraction process of isolated myofibrils. *Jikeikai Medical Journal* **1**, 119-126.

NEHER, E. & SAKMANN, B. (1976). Single-channel currents recorded from membrane of denervated frog muscle fibres. *Nature* **260**, 799-801.

OETLIKER, H. (1982). An appraisal of the evidence for a sarcoplasmic reticulum membrane potential and its relation to calcium release in skeletal muscle. *Journal of Muscle Research and Cell Motility* **3**, 247-272.

OLESEN, S.-P. & BUNDGAARD, M. (1992). Chloride-selective channels of large conductance in bovine aortic endothelial cells. *Acta Physiologica Scandinavica* **144**, 191-198.

ORR, I., GECHTMAN, Z. & SHOSHAN-BARMATZ, V. (1991). Characterization of Ca^{2+}-dependent endogenous phosphorylation of 160 000- and 150 000-Dalton proteins of sarcoplasmic reticulum. *Biochemical Journal* **276**, 89-96.

OWENS, K., RUTH, R. C. & WEGLICKI, W. B. (1972). Lipid composition of purified fragmented sarcoplasmic reticulum of the rabbit. *Biochimica et Biophysica Acta* **288**, 479.

PALADE, P. & VERGARA, J. (1982). Arsenazo III and antipyrylazo III calcium transients in single skeletal muscle fibers. *Journal of General Physiology* **79**, 679-707.

PALADE, P. T. & BARCHI, R. L. (1977). On the inhibition of muscle membrane chloride conductance by aromatic carboxylic acids. *Journal of General Physiology* **69**, 879-896.

PAPAHADJOPOULOS, D., NIR, S. & DUZGUNES, N. (1990). Molecular mechanisms of calcium-induced membrane fusion. *Journal of Bioenergetics and Biomembranes* **22**, 157-179.

PAPE, P. C., KONISHI, M., HOLLINGWORTH, S. & BAYLOR, S. M. (1990). Perturbation of sarcoplasmic reticulum calcium release and phenol red absorbance transients by large concentrations of Fura-2 injected into frog skeletal muscle fibers. *Journal of General Physiology* **96**, 493-516.

PATTLE, R. E. (1950). The control of foaming. I. The mode of action of chemical anti-foams. *Journal. Society of Chemical Industry* **69**, 363-368.

PESSAH, I. N., FRANCINI, A. O., SCALES, D. J., WATERHOUSE, A. L. & CASIDA, J. E. (1986). Calcium-ryanodine receptor complex. Solubilization and partial characterization from skeletal muscle junctional sarcoplasmic reticulum vesicles. *Journal of Biological Chemistry* **261**, 8643-8648.

PORTER, K. R. & PALADE, G. E. (1957). Studies on the endoplasmic reticulum III. Its form and distribution in striated muscle cells. *Journal of Biophysical and Biochemical Cytology* **3**, 269-300.

RACKER, E. (1972). Reconstitution of a calcium pump with phospholipids and a purified Ca^{++}-adenosine triphosphatase from sarcoplasmic reticulum. *Journal of Biological Chemistry* **247**, 8198-8200.

RAND, R. P., KACHAR, B. & REESE, T. S. (1985). Dynamic morphology of calcium-induced interactions between phosphatidylserine vesicles. *Biophysical Journal* **47**, 483-489.

RAYMENT, I., HOLDEN, H. M., WHITTAKER, M., YOHN, C. B., LORENZ, M., HOLMES, K. C. & MILLIGAN, R. A. (1993a). Structure of the actin-myosin complex and its implications for muscle contraction. *Science* **261**, 58-65.

RAYMENT, I., RYPNIEWSKI, W. R., SCHMIDT-BASE, K., SMITH, R., TOMCHICK, D. R., BENNING, M. M., WINKELMANN, D. A., WESENBERG, G. & HOLDEN, H. M. (1993b). Three-dimensional structure of myosin subfragments-1: a molecular motor. *Science* **261**, 50-58.

REDHEAD, C. R., EDELMAN, A. E., BROWN, D., LANDRY, D. & AL-AWQATI, Q. (1992). A ubiquitous 64-kDa protein is a component of a chloride channel of plasma and intracellular membranes. *Proceedings of the National Academy of Science, USA* **89**, 3716-3720.

ROSENMUND, C. & WESTBROOK, G. L. (1993). Calcium-induced actin depolymerization reduces NMDA channel activity. *Neuron* **10**, 805-814.

ROTH, J., TAATJES, D. J. & WARHOL, M. J. (1989). Prevention of non-specific interactions of gold-labelled reagents on tissue sections. *Histochemistry* **92**, 47-56.

ROUSSEAU, E. (1989). Single chloride-selective channel from cardiac sarcoplasmic reticulum studied in planar lipid bilayers. *Journal of Membrane Biology* **110**, 39-47.

ROUSSEAU, E., SMITH, J. S. & MEISSNER, G. (1987). Ryanodine modifies conductance and gating behaviour of single Ca^{2+} release channel. *American Journal of Physiology* **253**, C364-C368.

ROUSSEAU, E., ROBERSON, M. & MEISSNER, G. (1988). Properties of single chloride selective channel from sarcoplasmic reticulum. *European Biophysics Journal* **16**, 143-151.

ROUX, B. & SAUVÉ, R. (1985). A general solution to the time interval omission problem applied to single channel analysis. *Biophysical Journal* **48**, 149-158.

SANDOW, A. (1965). Excitation-contraction coupling in skeletal muscle. *Pharmacological Reviews* **17**, 265-320.

SANSOM, M. S. P., BALL, F. G., KERRY, C. J., McGEE, R., RAMSEY, R. L. & USHERWOOD, P. N. R. (1989). Markov, fractal, diffusion and related models of ion channel gating. A comparison with experimental data from two ion channels. *Biophysical Journal* **56**, 1229-1243.

SCHEIN, S. J., COLOMBINI, M. & FINKELSTEIN, A. (1976). Reconstitution in planar lipid bilayers of a voltage-dependent anion-selective channel obtained from Paramecium mitochondria. *Journal of Membrane Biology* **30**, 99-120.

SCHLICHTER, L. C., GRYGORCZYK, R., PAHAPILL, P. A. & GRYGORCZYK, C. (1990). A large, multiple-conductance chloride channel in normal human T lymphocytes. *Pflügers Archives* **416**, 413-421.

SCHNEIDER, G. T., COOK, D. I., GAGE, P. W. & YOUNG, J. A. (1985). Voltage sensitive, high-conductance chloride channels in the luminal membrane of cultured pulmonary alveolar (type II) cells. *Pflügers Archives* **404**, 345-357.

SCHULLERY, S. E., SCHMIDT, C. F., FELGNER, P., TILLACK, T. W. & THOMPSON, T. E. (1980). Fusion of dipalmitoylphosphatidylcholine vesicles. *Biochemistry* **19**, 3919-3923.

SCHWARZE, W. & KOLB, H.-A. (1984). Voltage-dependent kinetics of an anionic channel of large unit conductance in macrophages and myotube membranes. *Pflügers Archives* **402**, 281-291.

SELSER, J. C., YEH, Y. & BASKIN, R. J. (1976). A light-scattering measurement of membrane vesicle permeability. *Biophysical Journal* **16**, 1357-1371.

SHAMOO, A. E. & ELDEFRAWI, M. E. (1975). Carbamylcholine and acetylcholine-sensitive, cation-selective ionophore as part of the purified acetylcholine receptor. *Journal of Membrane Biology* **25**, 47-63.

SIEGEL, D. P., BURNS, J. L., CHESTNUT, M. H. & TALMON, Y. (1989). Intermediates in membrane fusion and bilayer / non-bilayer phase transitions imaged by time-resolved cryo-transmission electron microscopy. *Biophysical Journal* **56**, 161-169.

SILLÉN, L. G. & MARTELL, A. E. (1964). *Stability constants of metal-ion complexes*, 754 pages. London: The Chemical Society. (Special Publication 17)

SMITH, J. S., CORONADO, R. & MEISSNER, G. (1985). Sarcoplasmic reticulum contains adenine nucleotide-activated calcium channels. *Nature* **316**, 446-449.

SMITH, J. S., CORONADO, R. & MEISSNER, G. (1986a). Single-channel calcium and barium currents of large and small conductance from sarcoplasmic reticulum. *Biophysical Journal* **50**, 921-928.

SMITH, J. S., CORONADO, R. & MEISSNER, G. (1986b). Single channel measurements of the calcium release channel from skeletal muscle sarcoplasmic reticulum. Activation by Ca^{2+} and ATP and modulation by Mg^{2+}. *Journal of General Physiology* **88**, 573-588.

SOMLYO, A. V., GONZALEZ-SERRATOS, H., SHUMAN, H., McCLELLAN, G. & SOMLYO, A. P. (1981). Calcium release and ionic changes in the sarcoplasmic reticulum of tetanized muscle: An electron-probe study. *Journal of Cell Biology* **90**, 577-594.

SORENSON, M. M., REUBEN, J. P., EASTWOOD, A. B., ORENTLICHER, M. & KATZ, G. M. (1980). Functional heterogeneity of the sarcoplasmic reticulum within sarcomeres of skinned muscle fibers. *Journal of Membrane Biology* **53**, 1-17.

SPERELAKIS, N. (1969). Changes in conductances of frog sartorius fibers produced by CO_2, ReO_4^- and temperature. *American Journal of Physiology* **217**, 1069-1075.

SPURR, A. R. (1969). A low-viscosity epoxy resin embedding medium for electron microscopy. *Journal of Ultrastructure Research* **26**, 31-43.

STEIN, P. G. & PALADE, P. T. (1988). Sarcoballs: direct access to sarcoplasmic reticulum Ca^{2+} channels in skinned frog muscle fibers. *Biophysical Journal* **54**, 357-363.

STEIN, P. G. & PALADE, P. T. (1989). Patch clamp of sarcolemmal spheres from stretched skeletal muscle fibres. *American Journal of Physiology* **256**, C434-C440.

STEIN, P. G., NELSON, T. E. & PALADE, P. T. (1989). Mammalian sarcoplasmic reticulum K channels recorded in skinnned fibers. *Biophysical Journal* **55**, 480a.

STEPHENSON, D. G., WENDT, I. R. & FORREST, Q. G. (1981). Non-uniform ion distributions and electrical potentials in sarcoplasmic regions of skeletal muscle fibres. *Nature* **289**, 690-692.

STEPHENSON, E. W. (1981). Activation of fast skeletal muscle: contributions of studies on skinned fibers. *American Journal of Physiology* **240**, C1-C19.

STEPHENSON, E. W. (1985). Excitation of skinned muscle fibers by imposed ion gradients. I. Stimulation of ^{45}Ca efflux at constant [K].[Cl] product. *Journal of General Physiology* **86**, 971-973.

SUAREZ-ISLA, B. A., OROZOCO, C., HELLER, P. F. & FROEHLICH, J. P. (1986). Single calcium channels in native sarcoplasmic reticulum membranes from skeletal muscle. *Proceedings of the National Academy of Science, USA* **83**, 7741-7745.

SUN, X. P., SUPPLISSON, S., TORRES, R., SACHS, G. & MAYER, E. (1992). Characterization of large-conductance chloride channels in rabbit colonic smooth muscle. *Journal of Physiology, London* **448**, 355-382.

SUZUKI, M., MIYAZAKI, K., IKEDA, M., KAWAGUCHI, Y. & SAKAI, O. (1993). F-actin network may regulate a Cl^- channel in renal proximal tubule cells. *Journal of Membrane Biology* **134**, 31-39.

SZENT-GYÖRGYI, A. (1949). Free-energy relations and contractions of actomyosin. *Biological Bulletin* **96**, 140-161.

TABARES, L., MAZZANTI, M. & CLAPHAM, D., E (1991). Chloride channels in the nuclear membrane. *Journal of Membrane Biology* **123**, 49-54.

TADA, M., YAMAMOTO, T. & TONOMURA, Y. (1978). Molecular mechanism of active calcium transport by sarcoplasmic reticulum. *Physiological Reviews* **58**, 1-79.

TAKESHIMA, H., NISHIMURA, S., MATSUMOTO, T., ISHIDA, H., KANGAWA, K., MINAMINO, N., MATSUO, H., UEDA, M., HANAOKA, M., HIROSE, T. & NUMA, S. (1989). Primary structure and expression from complementary DNA of skeletal muscle ryanodine receptor. *Nature* **339**, 439-445.

TANG, J. M., WANG, J. & EISENBERG, R. S. (1987). Patch clamp of sarcoplasmic reticulum within muscle fibers. *Biophysical Journal* **51**, 106a.

TANIFUJI, M., SOKABE, M. & KASAI, M. (1987). An anion channel of sarcoplasmic reticulum incorporated into planar lipid bilayers: single-channel behavior and conductance properties. *Journal of Membrane Biology* **99**, 103-111.

THINNES, F. P. (1992). Evidence for extra-mitochondrial localization of the VDAC/porin channel in eucaryotic cells. *Journal of Bioenergetics and Biomembranes* **24**, 71-75.

THINNES, F. P., GÖTZ, H., KAYSER, H., BENZ, R., SCHMIDT, W. E., KRATZIN, H. D. & HILSCHMANN, N. (1989). Zur Kenntnis der Porine des Menschen. I. Reinigung eines Porins aus menschlichen B-Lymphozyten (Porin 31HL) und sein topochemischer Nachweis auf dem Plasmalemm der Herkunftszelle. *Biological Chemistry Hoppe-Seyler* **370**, 1253-1264.

TOURNOIS, H., GIELES, P., DEMEL, R., DE GIER, J. & DE KRUIJFF, B. (1989). Interfacial properties of gramicidin and gramicidin-lipid mixtures measured with static and dynamic monolayer techniques. *Biophysical Journal* **55**, 557-569.

VELASCO, G., PRIETO, M., ALVAREZ-RIERA, J., GASCON, S. & BARROS, F. (1989). Characteristics and regulation of a high conductance anion channel in GBK kidney epithelial cells. *Pflügers Archives* **414**, 304-310.

VIVAUDOU, M. B., SINGER, J. J. & WALSH, J. V. Jr. (1986). An automated technique for analysis of current transitions in multilevel single-channel recordings. *Pflügers Archives* **407**, 355-364.

VIVAUDOU, M. B., ARNOULT, C. & VILLAZ, M. (1989). Patch-clamp recordings of K^+ channels from membrane blebs ("sarcoballs") from skinned frog skeletal muscle fibers. *Biophysical Journal* **55**, 483a.

WAGENKNECHT, T., GRASSUCCI, R., FRANK, J., SAITO, A., INUI, M. & FLEISCHER, S. (1989). Three-dimensional architecture of the calcium channel/foot structure of sarcoplasmic reticulum. *Nature* **338**, 167-170.

WANG, J. & BEST, P. B. (1992). Inactivation of the sarcoplasmic reticulum calcium channel by protein kinase. *Nature* **359**, 739-741.

WANG, J., TANG, J. M. & EISENBERG, R. S. (1992). A calcium conducting channel akin to a calcium pump. *Journal of Membrane Biology* **130**, 163-181.

WEILER, U., RIESINGER, I., KNOLL, G. & BRDICZKA, D. (1985). The regulation of mitochondrial-bound hexokinases in the liver. *Biochemical Medicine* **33**, 223-235.

WILSCHUT, J. & HOEKSTRA, D. (1984). Membrane fusion: from liposomes to biological membranes. *Trends in Biological Science* **9**, 479-483.

WINEGRAD, S. (1965). Autoradiographic studies of intracellular calcium in frog skeletal muscle. *Journal of General Physiology* **48**, 455-479.

WINEGRAD, S. (1968). Intracellular calcium movements of frog skeletal muscle during recovery from tetanus. *Journal of General Physiology* **51**, 65-83.

WINEGRAD, S. (1970). The intracellular site of calcium activation of contraction in frog skeletal muscle. *Journal of General Physiology* **55**, 77-88.

WOLL, K. H., LEIBOWITZ, M. D., NEUMCKE, B. & HILLE, B. (1987). A high-conductance anion channel in adult amphibian skeletal muscle. *Pflügers Archives* **410**, 632-640.

WUNDER, U. R. & COLOMBINI, M. (1991). Patch clamping VDAC in liposomes containing whole mitochondrial membranes. *Journal of Membrane Biology* **123**, 83-91.

ZAHRADNIK, I., ZAHRADNIKOVA, A. & PALADE, P. (1990). Voltage and time dependent gating of frog sarcoball chloride channels. *Biophysical Journal* **57**, 497a.